Studies on the use of Nanokaolin, MWCNT and Graphene in NBR and SBR

Thesis submitted to

Cochin University of Science and Technology

in partial fulfilment of the requirements

for the award of the degree of

Doctor of Philosophy

Preetha Nair K

Department of Polymer Science and Rubber Technology
Cochin University of Science and Technology
Kochi- 682 022, Kerala, India

July **2013**

Studies on the use of Nanokaolin, MWCNT and Graphene in NBR and SBR

Ph. D Thesis

Author

Preetha Nair K
Department of Polymer Science and Rubber Technology
Cochin University of Science and Technology
Cochin- 682 022, Kerala, India
E-mail: Preethaknair@gmail.com

Supervising teachers:

Dr. Rani Joseph
Professor (Emeritus)
Department of Polymer Science and
Rubber Technology
Cochin University of Science
and Technology (CUSAT)
Cochin- 682 022, Kerala, India
E-mail: rani@cusat.ac.in

Dr. A. Mathiazhagan
Associate Professor
Department of Ship Technology
Cochin University of Science
and Technology (CUSAT)
Cochin- 682 022, Kerala, India
E-mail: alagan@cusat.ac.in

Department of Polymer Science and Rubber Technology
Cochin University of Science and Technology
Cochin- 682 022, Kerala, India

July 2013

Certificate

    This is to certify that this thesis entitled **"Studies on the use of Nanokaolin, MWCNT and Graphene in NBR and SBR"** is a report of the original work carried out by **Smt. Preetha Nair K** under our supervision and guidance in the Department of Polymer Science and Rubber Technology, Cochin University of Science and Technology, Cochin-22. No part of the work reported in this thesis has been presented for any other degree from any other institution.

Supervising teachers:

Dr. Rani Joseph
Professor (Emeritus)
Department of Polymer Science and
Rubber Technology
Cochin University of Science
and Technology (CUSAT)
Cochin- 682 022, Kerala, India

Dr. A. Mathiazhagan
Associate Professor
Department of Ship Technology
Cochin University of Science
and Technology (CUSAT)
Cochin- 682 022, Kerala, India

Cochin-22
17/07/2013

Declaration

I hereby declare that the thesis entitled **"Studies on the use of Nanokaolin, MWCNT and Graphene in NBR and SBR"** is the original work carried out by me under the supervision of **Dr. Rani Joseph** (Professor**,** Emeritus, Department of Polymer Science and Rubber Technology) and under the co-guidance of **Dr. A. Mathiazhagan** (Associate Professor, Department of Ship Technology) Cochin University of Science and Technology, Cochin-22 and has never been included in any other thesis submitted previously for the award of any degree.

Cochin-22

Preetha Nair K

17/07/2013

Acknowledgements

I am indeed fortunate to have been working with a great number of people whose contribution in assorted ways to the research and the making of the thesis deserve special mention. It is a pleasure to convey my gratitude to them all in my humble acknowledgment.

First of all, let me express my heartfelt gratitude to the Almighty for enabling my life's long cherished dream come true.

My research supervisor Prof. Dr. Rani Joseph is a unique personality, sincere, helpful and much dedicated to her work. I consider myself extremely lucky in having her as my guide. Her vast experience and limitless knowledge in the field of Rubber Technology enabled me to complete my research work successfully. My heart is full of gratitude to her for the constant encouragement and valuable advice she rendered to me.

I will be failing in my duty if I do not mention my sincere thanks to Dr. A. Mathiazhagan, (Associate Professor, Department of Ship Technology, Cochin University of Science and Technology) my co-guide, for the timely help he gave me.

With great pleasure I put on record my deep gratitude to Dr. Sunil K Narayanan Kutty (Head of the Dept. of Polymer Science and Rubber Technology) for providing necessary facilities for the completion of my research work. I am extremely thankful to Dr. Thomas Kurien. Dr. Eby Thomas Thachil, Dr. K. E. George and Dr. Philip Kurien for their encouragement and support. .

I convey my sincere thanks to Dr. Jayalata whose pertinent pieces of advice and valuable tips has helped me considerably and to Dr. Jyothish for helping me with his excellent suggestions.

I express my sincere thanks to Dr. C. K. Anandan (Head of the Department of Electronics, CUSAT) for the facilities and to Paulbert Thomas and Sreekala for the help provided to me for conducting the Microwave studies.

Preface

Elastomers have been reinforced with fillers for meeting the service requirements of the different products. Use of high concentration of particulate fillers like carbon black and silica reduces the processability and increases the weight of the final product. So the use of nanofillers is highly relevant for rubber compounding and product manufacture.

Layered silicates, nanotubes, nanosilica etc. have attracted great attention and emerged as reinforcing materials for polymer nanocomposites. But rubber nanocomposites got commercial attention only recently. Montmorillonite, hectorite and saponite are the most widely used clay minerals in polymer clay nanocomposites (PCNCs). In the past the non swellable kaolin was mainly used for rubber filling. But later kaolin modified with organosilanes is found to be successful as reinforcing filler in elastomers. The high aspect ratio, easy availability, and layered structure make nano clay good reinforcing filler in polymer nanocomposites. Carbon nanotubes and graphene have excellent combination of mechanical, thermal and electrical properties. The use of carbon nanotubes and graphene in elastomeric nanocomposites is still at its infancy.

The current research investigates the possibility of using unmodified and modified nanokaolin, multiwalled carbon nanotube (MWCNT) and graphene as fillers to impart enhancement in mechanical, thermal, and electrical properties to the elastomers. Taking advantage of latex blending method, nanoclay, MWCNT and graphene dispersions, prepared by ultra sound sonication are dispersed in polymer latices. The improvement in material properties indicated better interaction between filler and the polymer. MWCNT and graphene imparted electrical conductivity with simultaneous improvement in mechanical properties. Layered silicates prepared by microwave method also significantly improve the mechanical properties of the nanocomposites.

The thesis entitled 'Studies on the use of Nanokaolin, MWCNT and Graphene in NBR and SBR' consists of ten chapters. The first chapter is a concise introduction of nanocomposites, nanofillers, elastomeric matrices and applications of polymer nanocomposites. The state-of-art research in elastomer based nanocomposites is also presented. At the end of this chapter the main objectives of the work are mentioned.

Chapter 2 outlines the specifications of various materials used, details of experimental techniques employed for preparing and characterizing nanocomposites.

Chapter3 includes characterization of the nanofillers, optimsation of cure time of latex based composites and the methods used for the preparation of latex based and dry rubber based nanocomposites.

Chapter4 presents the reinforcing effect of the nanofillers in XNBR latex and the characterization of the nanocomposites.

Chapter5 comprises the effect of nanofillers on the properties of SBR latex and their characterization

Chapter 6 deals with the study of cure characteristics, mechanical and thermal properties and the characterization of NBR based nanocomposites.

Chapter7 is the microwave studies of MWCNT and graphene filled elastomeric nanocomposites.

Chapter 8 gives details of the preparation of layered silicates, their characterization and use in different elastomeric matrices.

Chapter 9 is the study of mechanical properties of nanoclay incorporated nitrile gloves

Chapter 10 presents the summary and conclusions of the investigation

Contents

Chapter 3
CHARACTERIZATION OF FILLERS, OPTIMIZATION OF CURING

Part 1
Characterization of fillers

Part 2
Optimization of curing parameters

Chapter 7
MICROWAVE STUDIES OF ELASTOMERIC NANOCOMPOSITES BASED ON MULTIWALLED CARBON NANOTUBES AND GRAPHENE----------------------------------- 223 - 239

Chapter 8
PREPARATION OF LAYERED SILICATES, ITS CHARACTERIZATION AND USE IN XNBR/SBR LATICES AND NBR/SBR DRY RUBBER------------------------------------- 241 - 259

Part 1
Preparation of Layered Silicates and Its Characterization

Part 2
Use of prepared layered silicates, in XNBR / SBR latices and NBR/SBR dry rubber

Chapter 9
STUDIES ON THE MECHANICAL PROPERTIES OF NANOCLAY FILLED

Chapter 10

List of Abbreviations and Symbols

List of Publications

Curriculum Vitae

.....౫౮౪.....

Chapter 1

INTRODUCTION

Rubbers also called elastomers have always fascinated the human mind. To quote Charles Goodyear (1800-1860), the inventor of vulcanization of rubber "There is probably no other inert substance, the properties of which excite in the human mind an equal amount of curiosity, surprise and admiration. Who can examine and reflect upon this property of gum elastic without adoring the wisdom of the Creator?" [1, 2].

The predominant property of elastomers include elastic behaviour after deformation, in compression or tension, great toughness under static or dynamic stresses, abrasion resistance which is higher than that of steel, impermeability to air and water, resistance to swelling in solvents and attack to chemicals [3]. There is a limit to hardness and modulus range of rubber that can be achieved by mere vulcanization [4]. So rubber industry uses a wide range of fillers to tailor the properties of elastomeric materials. Carbon black [5-8] and silica [9-11] have been used as effective reinforcing agents in rubber since the beginning of twentieth century. But the effect of these fillers and their characterization techniques were not fully understood at these times. The real starting point revealing the effect of nanofillers owe

to the invention of Nylon-6/clay nanocomposites by the Toyota Research Group of Japan. Work published by Usuki et al [12] referred Nylon-6/clay nanocomposite as 'nylon-6 clay hybrid' (NCH). First use of the term "nanocomposites" appeared in 1994 [13, 14]. Recently the new generation "nanofillers" are the main area of interest for scientists and technologists. Rubber nanocomposites reinforced with a small fraction of nanofillers have attracted great interest due to their wide range of applications.

The central theme of this thesis is the investigation of the effect of different nanofillers like layered silicates, mutiwalled carbon nanotubes and graphene nanoplatelets on the mechanical and thermal properties of polar and non polar rubbers incorporated in latex and dry rubber. Layered silicates were prepared by microwave technique and the effect of these silicates on the properties of NBR and SBR was also evaluated. A general introduction is given in the ensuing sections about nanocomposites, nanoclay, modification of clay, multiwalled carbon nanotubes, graphene, different types of synthetic rubbers, applications of polymer nanocomposites and a detailed survey on the rubber nano composites.

1.1 Nanocomposites

The term "nanocomposite" represents a new and exciting field in material science and technology. Composite is a combination of two or more materials differing in physical and chemical properties but having a distinguishable interface between the two materials. The continuous phase in a composite material is called the matrix and the other is the dispersed phase. Based on the nature of matrices, composites are divided into four classes [15]

- Polymer matrix composite

- Metal matrix composite

- Ceramic matrix composite

- Carbon matrix composite

Fillers constitute the dispersed phase. Nanoscale fillers like layered silicates, carbon nanotubes, carbon nanofibres, exfoliated graphite etc dispersed in elastomeric composites constitute rubber nanocomposite. Thus a nanocomposite is defined as a composite material where at least one of its constituents is having paricle size (1-100nm) at least in one dimension.

Classification of nanocomposites

Nanocomposites can be classified based on the nature of nanofillers [16], dimensional morphology of nanofillers [17, 18] etc.

1) Based on the nature of nanofillers

- Clay based nanocomposites

- Silica based nanocomposites

- Polyhedral oligomeric silsesquioxane (POSS) based nanocomposites

- Carbon nanotube filled nanocomposites

- Nanocomposites based on other nanofillers like metal oxide, hydroxide and carbonate.

2) Based on nanofiller's dimensional morphology

Based on the dimensional morphology nanofillers can have iso dimensional, elongated or layered structures Fig.1.1.

- Nanoparticles: When all the three dimensions of the particulates are in the nanometer range, they are isodimensional nano particles or nano granules or nano crystals e.g. Silica, Carbon black, Zinc oxide etc.

- Nanotubes: When only two dimensions are in the nanometer range and the third is larger, elongated structures as in nanotubes, whiskers or nanofibres are formed e.g. carbon nanotubes, gold or silver nanotubes, carbon nanofibres, cellulose whiskers.

- Nanolayers: When only one dimension is in the nanometer range, then layered structures having thickness of a few nanometers and length, several hundreds of nanometers are formed e.g. clay (layered silicates), layered double hydroxides (LDHs) and layered graphite flakes.
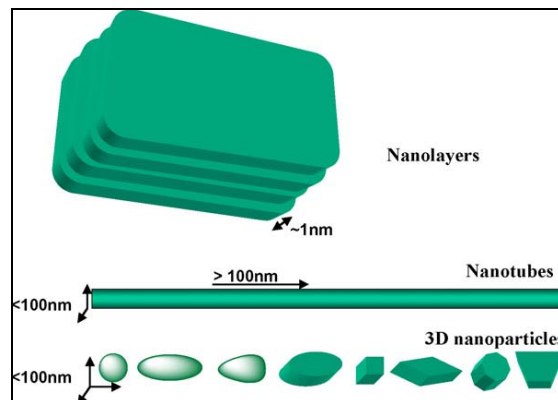
Fig. 1.1. Nanofillers dimensional morphology

Properties of polymer nanocomposites

Properties of nanocomposite depends on

- Methods of synthesis of polymer nanocomposites

- Morphology of the polymer nanocomposites

- Types of nanoparticles and their surface treatments.

- Properties of polymer matrix such as crystallinity, molecular weight, chemical structure and also whether it is a thermoplastic, thermoset or an elastomer [19].

The main advantages of nanocomposites over conventional composites are as follows

- Lighter weight due to low filler loading

- Low cost due to fewer amount of filler used

- Improved mechanical, thermal, optical, electrical, barrier properties

- Improved solvent and heat resistance

- Improved flame retardency properties

- Increased surface area, strength and toughness [20]

The main disadvantages of using nanoparticles are

- Increase in viscosity

- Optical issues

- Dispersion of fillers

- Tendency for sedimentation

- Black or grey colour formed by the use of different carbon containing nanoparticles. [21]

- Health and environmental threats caused by the production, consumption and disposal of nanoparticles

1.2   Nanofillers

1.2.1 Nanoclay

Clays are chemically hydrous silicates of Al, Mg, Fe and other less abundant elements [17]. The most important structural feature of clay mineral is that it is layered. They are made of stacked two dimensional units called 'layers' and the volume included between two successive layers are called the 'interlayer space'. In the layers the atoms are joined by ionic/ covalent bonds and in the perpendicular direction the layers are held by weaker forces. So the separation of layers requires only a small amount of energy and breaking of the layers needs more energy. Based on the electric charge of the layers, they are classified into neutral, cationic and anionic clays [22].

Fig.1.2. gives a schematic representation of neutral, cationic and anionic clays.

- Neutral calys : Layers are joined by van der Waals interactions and/or hydrogen bonds e.g. Kaolinite

- Cationic clays: Negative charge of layers are compensated by cations in the inter layer space. g: Montmorillonite

- Anionic clays: Positive layer charge is exactly compensated by anions located in the inter layer space. eg: layered double hydroxides
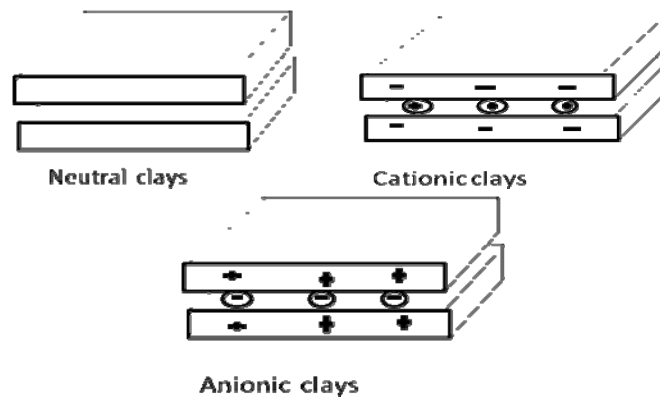
Fig. 1.2. Representation of neutral clays, cationic clays and anionic clays.

Based on the presence of octahedral and tetrahedral sheets clays are classified into 1:1 and 2:1 silicates. A layer can have tetrahedral structure, if oxygen atoms are linked to silicon atoms and octahedral structure when oxygen atoms are linked to aluminium atoms.

Thus 1:1 clay mineral contains 1 tetrahedral (T) and 1 octahedral (O) sheet per clay layer (TO type) and 2:1 clay contains 2 tetrahedral sheets with an octahedral sheet in between them (TOT). Kaolin belongs to the 1:1 type and montmorillonite belongs to 2:1 type. Fig.1.3.
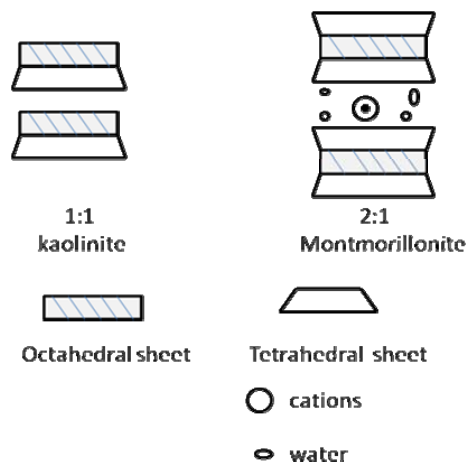
Fig. 1.3. Representation of 1:1 and 2:1 arrangement of tetrahedral and octahedral sheets in Kaolinite and Montmorillonite.

Modification of clay

Among the natural clay minerals used for preparing nanocomposites, montmorillonite takes the prime position due to its high cation exchange capacities, large surface area, good surface reactivity and surface adsorptive properties. An enhancement in the properties of the composite is achieved only when there is a good dispersion of particles in the matrix and there is adequate interaction between the nano particle and the matrix. Montmorillonite and other layered silicates are hydrophilic. To make the hydrophilic layered silicates compatible with the hydrophobic polymer matrices they haveto be modified. A popular and easy method of modifying the clay surface is by ion exchange. Most popular organic cation used for ion exchanging includes quarternary ammonium salts, alkyl imidazoles and phosphorous ionic compouds.

Kaolin

The most important mineral present in kaolin is kaolinite, $Al_4 Si_4 O_{10}$ $(OH)_8$.It consists of one layer of tetrahedrally coordinated Si (with O) and one sheet of octahedrally coordinated Al (with O and OH) [23]. Thus it belongs to the 1:1 or TO type. Neither cations nor anions are present in the interlayer space and the layers are linked by hydrogen bonds between the hydroxyl groups on octahedral sheet to the oxide arrangement of the tetrahedral sheet [24]. Fig 1.4 shows the structure of kaolinite Kaolin is a non expanding type of clay while montmorillonite belongs to the expanding type. Fig 1.5.
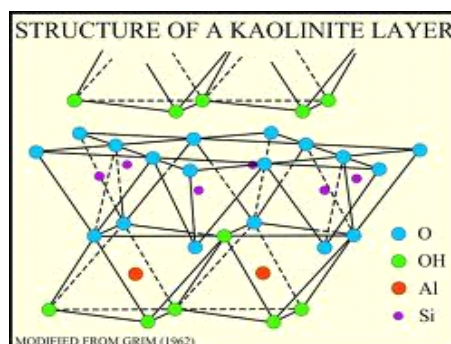
Fig. 1.4. Structure of Kaolinite
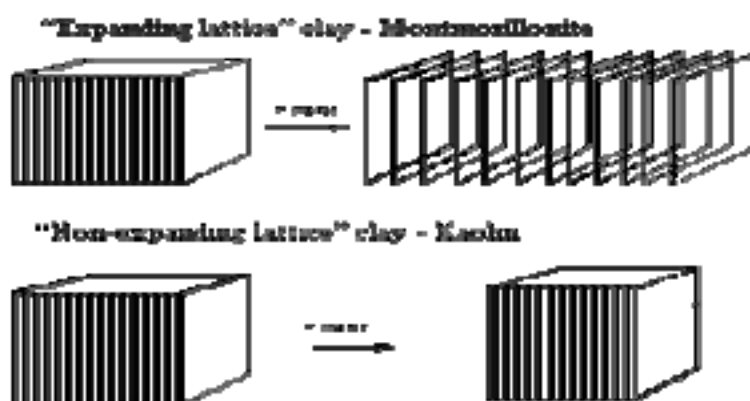
Fig. 1.5. Representation of expanding and non expanding lattice of Motmorillonite and Kaolinite

Modification in kaolin

Surface of kaolin is rather inert. Kaolin lattice is disrupted at the plate edges and at the surface ridges. This gives broken bonds with a number of OH groups, and these OH groups are the reactive sites in kaolin. The most important technique used to modify kaolin is group displacement by dipolar molecules like N-methylformamide (NMF), Dimethyl sulphoxide (DMSO), urea or salts like potassium acetate. They act as precursors for further intercalation reaction by organic molecules

and polymers. Intercalation in Kaolin is explained as a diffusion process. Driving force for the process is the strong hydrogen bonds formed between the intercalating agent and the OH of octahedral sheet [25].

Kaolin can also be modified with functional silanes [26], Methacrylic acid and poly methacrylic acid of varying molecular weight [27], rubber seed oil [28] or by water vapour plasma method [29].

A variety of organic molecules having pendant functionalities can be grafted to the interlayer surface of kaolinite. Grafting with the organic moiety makes kaolin surface organophilic.

Grafting of silanes:

Functional silanes used for grafting usually contain a hydrolytic group and a functional group. Hydrolytic group is usually an alkoxy group and functional group may be alkyl, vinyl, amino or mercapto group. Alkoxy silanes undergo hydrolysis to give silanol groups which reacts with the OH groups on the edges of kaolin either by forming hydrogen bonds or by covalent bond formation. Further the alkyl or vinyl groups can interact with the polymer matrices. This improves the interfacial adhesion and increases the mechanical properties of the composite materials [30, 31].

Fig. 1.6 is a schematic representation showing the hydrolysis of functional silanes and its reaction with OH groups on the clay surface

$$RSi(OMe)_3 \xrightarrow[-3MeOH]{Hydrolysis(3H_2O)} RSi(OH)_3 \xrightarrow[-2H_2O]{Condensation(2RSi(OH)_3)}$$
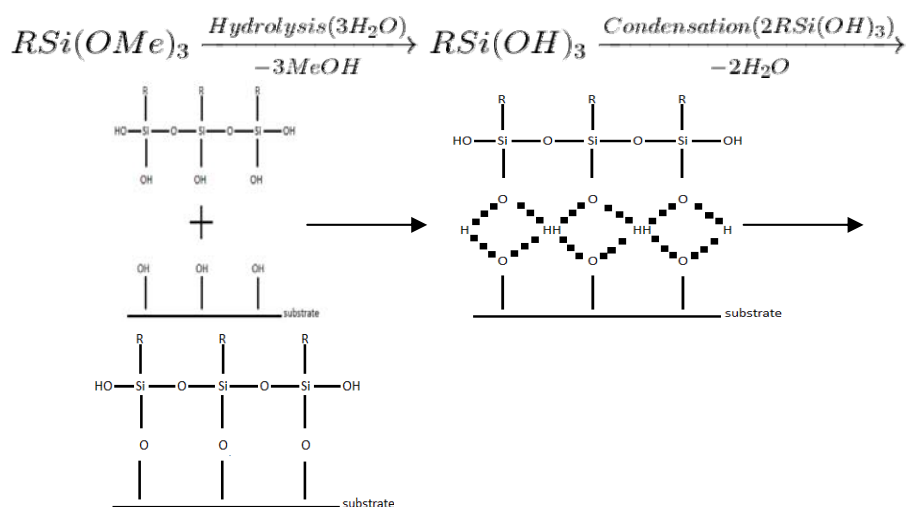
Fig. 1.6. A schematic representation showing the hydrolysis of functional silanes and its reaction with OH groups on the clay surface.

Types of polymer layered silicate nanocomposites:

Based on the interaction between the polymer matrix and layered silicate polymer layered silicate nanocomposites are classified into intercalated and exfoliated nanocomposites. [32-34]. Fig 1.7 represents the intercalated and exfoliated nanocomposites along with the conventionally filled microcomposite.

- Intercalated nanocomposites are formed when polymer chains are inserted into the layered silicates in a crystallographic regular fashion. The interlayer space expands keeping a well defined spatial relationship to each other. It is regardless of clay to polymer ratio and the distance between the layers will be of the order of a few nanometers. The remarkable properties of polymer nanocomposite are an outcome of the intercalation property.

- Exfoliated nanocomposites: When the silicate layers are totally delaminated and dispersed in the polymer matrix exfoliated

nanocomposites are formed. On exfoliation the composite loses its ordered structure and the distance between the layers is the order of radius of gyration of the polymer.

Phase separated   **Intercalated**   **exfoliated**
         (A)   **(B)**   **(C)**
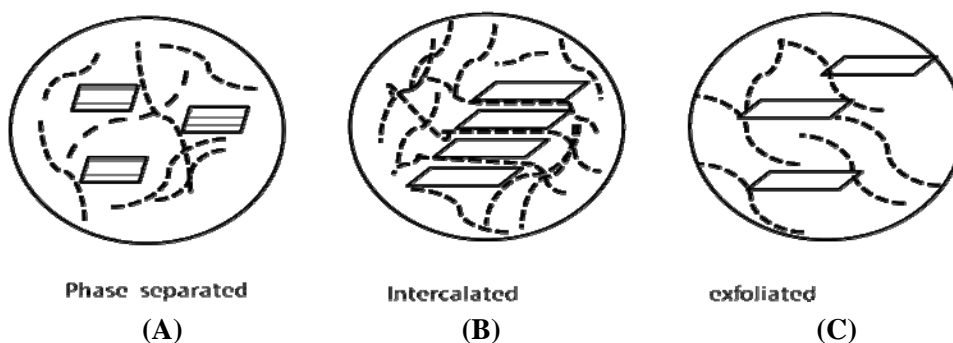
Fig. 1.7. (A) Conventionally filled polymer or microcomposite (B) polymer chains intercalated into the clay layers (C) exfoliation of the layered silicate.

Processing methods for the preparation of rubber clay nanocomposites

a)   Latex compounding:

Latex consists of sub micron sized rubber particles dispersed in water. Pristine clay being hydrophilic can be added to rubber latex either directly or in aqueous dispersion. Clay adsorbs water molecules leading to an expansion of intergallery space. Exfoliation of the clay layers takes place on stirring. Clay containing lattices may be mixed with dispersions of other rubber curatives and cast into a mould and left to dry. After drying the samples can be cured accordingly. A similar method was reported by Varghese and Karger Kocsis in preparing NR layered silicate composites. [35]. Zhang et al. [36] prepared rubber clay nanocomposites by mixing rubber latex with pristine clay suspension followed by coagulation. This approach was further applied for the preparation of a large number of composites [37-39]. Different electrolytes like dil H_2SO_4 [40-42], dil. HCl [43], $CaCl_2$ aqueous solution etc. [42] were used for coagulation.

b)   Melt compounding:

Process usually takes place in internal mixers, open mills and twin screw extruders. Method involves mixing the layered silicates with the polymer matrix and heating above the softening point of the polymer. The method usually employs the use of modified layered silicates. Organic modification of silicates reduces the hydrophilicity and assists the intercalation of rubber chains into the interlayer space. The molten polymer chains spread into the clay galleries to form either intercalated or delaminated composites according to the degree of penetration. Melt intercalation was first reported by Vaia et al. [44] in 1993. They explained the thermodynamic principles for polymer melt intercalation in organically modified clays. Melt intercalation for the preparation of rubber clay composites are also vastly investigated [45-48]. The absence of an organic solvent in the process reduces the risks of environmental hazards. The method is compatible with current industrial process such as extrusion and injection moulding**.**

c)   Solution method:

The method involves the use of a solvent system in which the polymers are soluble and the silicate layers are swellable. This method is used in the preparation of various rubber clay nanocomposites [49-51]. High cost of the solvent, selection of a suitable solvent and the enviromental impact caused by the solvents are the disadvantages of the method.

d)   In situ polymerisation method:

This process consists of inercalation of monomers as precursor species into the interlayer space of pristine clay followed by their polymerisation.

Mechanical mixing of the pretreated clay mineral with the monomer leads to the intercalation of the monomer within the interlayer space and thus promotes delamination [52, 53]. Polymerization is initiated by heat, radiation, diffusion of suitable initiator etc. Various in situ polymerization techniques include free radical polymerization [54, 55], controlled radical polymerization [56, 57], ring opening polymerization [58, 59], cationic [60] and living anionic polymerization [61].

1.2.2 Carbon nanotubes:

Carbon nanotube, considered as the stiffest and strongest man made material was discovered by Iijima in 1991. There are two basic types of carbon nanotubes viz.singlewalled carbon nanotubes (SWCNT) and multi walled carbon nanotubes (MWCNT). SWCNT consists of a single graphene sheet rolled into a seamless cylinder [62]. Fig.1.8 (A) represents the rolling of graphene sheets to form nanotubes. MWCNT consists of concentrically nested graphene cylinders arranged around a central hollow core. A special case of MWCNT called doublewalled carbon nanotubes (DWCNT) contains two concentric graphene cylinders Fig 1.8 (B).
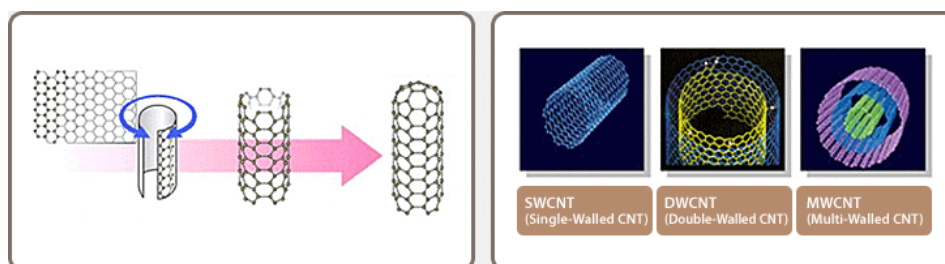
Fig. 1.8. (A).Rolling of graphene sheets in a particular direction to form naotubes   **Fig. 1.8.(B). Single, double and multiwalled carbon nanotubes**

Carbon nanotube can be synthesised by arc-discharge [63], laser ablation [64], or catalytic chemical vapour deposition (CCVD) [65] methods.

Carbon nanotubes (CNTs) have a planar hexagonal arrangement of sp^2 bonded carbon atoms, with each carbon atom joined to three neighbours, as in graphite. The end caps of nanotubes are highly reactive as compared to side walls due to the presence of defect sites like Stone Wales defects, sp^3 hybridized defects and vacancies in the nanotube lattice. [66]

These nanostructured materials have gained great importance on account of their wide range of potential applications in many areas. Their outstanding properties are a consequence of this unique bonding arrangement combined with topological defects [67]. They feature a number of extraordinary properties, like

- high electric conductivity
- high thermal conductivity
- mechanical strength
- thermal resistivity / stability
- actuational properties at low voltages
- field emission

Ajayan et al. [68] prepared the first polymer nanocomposite using CNT in 1994 .One dimensional structure of CNT, their low density, high aspect ratio and good mechanical properties make them good reinforcement in composite materials. The processing methods available for the preparation of MWCNT polymer composites include solution mixing [69, 70], bulk mixing [71, 72], insitu polymerization [73, 74], melt mixing [75, 76] and chemical modification process. Addition of a very small amount

of MWCNT in elastomers produces significant increase in electrical conductivity, mechanical stiffness and strength.

The high polarisability of the pi electron cloud leads to strong vander Waals attraction between the outer planes of neighbouring nanotubes [77]. This causes agglomeration in nanotubes and dramatically hampers the mechanical properties of the fabricated nanocomposite. So to enhance the interfacial interaction with the matrix and for the effective utilization of CNT in composite application they have to be compatible and intimately dispersed in the polymer matrix [78].

Use of surfactants is an effective way for dispersing carbon nanotubes. The surfactant molecules orient themselves in such a fashion that hydrophobic tail groups face towards the nanotube surface and the hydrophilic head groups face towards the aqueous phase producing lowering of nanotube /water interfacial tension [79]. Reports show that the outermost nanotubes in a bundle are treated more than the innermost tubes and the nanotube remains predominantly bundled even after surfactant treatment. But mechanical methods like ultrasonication can debundle the nanotubes by steric or electrostatic repulsions [80]. On sonication the high local shear will unravel the outer carbon nanotubes in a bundle and expose other sites for additional surfactant adsorption, thus the surfactant molecules gradually exfoliate the bundle in an ''unzippering'' mechanism [81]. Fig.1.9 is a schematic representation showing the attachment of surfactants on the nanotube surface, debundling of the nanotubes on sonication and, formation of latex nanotube composites.

Some of the common surfactants used for the dispersion of carbon nanotubes are sodium dodecyl benzene sulfonate (SDBS) [79], dodecyl trimethyl ammonium bromide (DTAB) [82], hexadecyl trimethyl ammonium bromide (CTAB) [83, 84], octylphenol ethoxylate (Triton X-100) [85, 86] and sodium dodecyl sulfate (SDS) [87, 88].
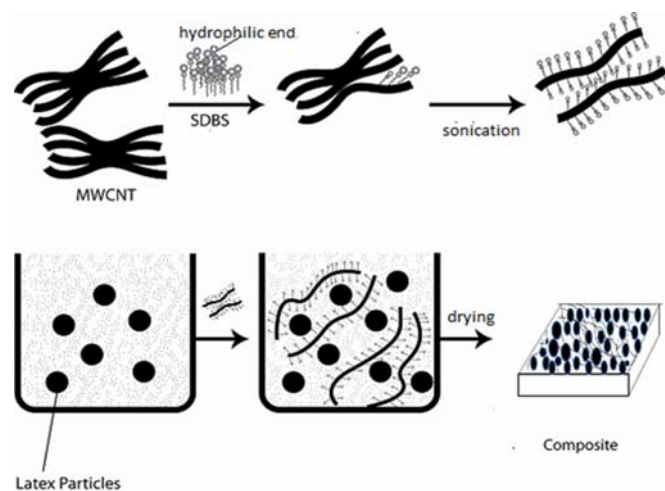
Fig.1.9. Schematic representation showing the possible attachment of surfactant on the surface of MWCNT, effect of sonication and the formation of latex nano tube composite

1.2.3 Graphene nanoplatelets

Graphene, considered as the thinnest material in the Universe is the mother of all graphitic materials like graphite, carbon nanotubes and fullerenes. Graphene as nanofiller has tremendous potential applications owing to its high surface area, aspect ratio, tensile strength, EMI shielding, thermal and electrical conductivity [89].

Graphene sheets when stacked in a honey comb like structure gives graphite. The sheets are separated by 0.334nm. The sheets can slide past one another giving its lubricating nature. Graphite on controlled oxidation

gives graphite oxide and each single sheet of graphite oxide is called graphene oxide [90]. Graphite oxides contain hydroxyl and epoxide groups on the top and bottom of the sheets and carboxyl and carbonyl groups at the sheet edges. Fig.1.10. These groups make graphene oxide hydrophilic and readily swell and disperse in water [89].

Fig. 1.10. Graphene   **Graphite**   **Graphene oxide**
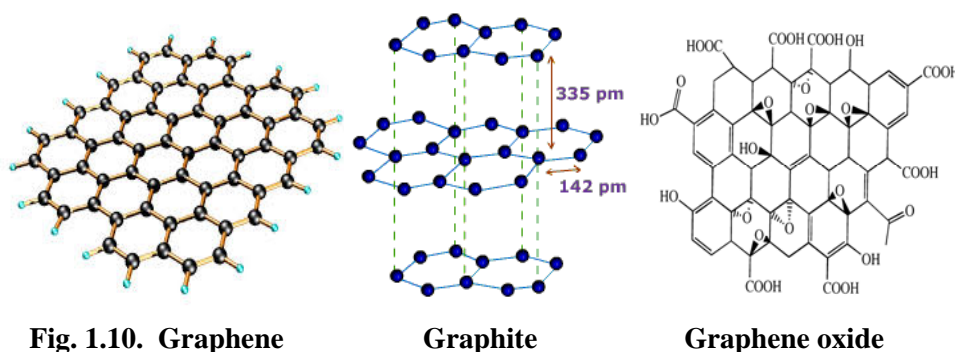
Multiple stacked graphene sheets constitute graphene nano platelets and the thickness of graphene platelets is significantly larger than an individual graphene sheet. Graphene can be prepared by chemical vapour deposition of monolayer of graphite on transitional metal surfaces. [91,92] , micromechanical exfoliation of graphite also called the "scotch tape" or "peel off '' method [93], epitaxial growth on electrically insulating surfaces such as SiC and solution based reduction of graphene oxide [94,95]. Pristine graphene is not compatible with organic polymers and is unsuitable for intercalation by polymer chains. This is because bulk graphene has a pronounced tendency to agglomerate in the polymer matrix. [95,96].

Graphene dispersions can be prepared in organic or aqueous media using either covalent or noncovalent methods of functionalisation. Noncovalent functionalisation involves wrapping of graphene sheets with

surfactants like polyethylene glycol, CTAB, SDS or through pi-pi interaction with certain organic   molecules [97].

Polymer graphene nanocomposites show improved thermal, mechanical, electrical, gas barrier and flame retardant properties when compared to the neat polymer. The increase in mechanical and electrical properties of nanotube based polymer composites is much greater than the polymer /clay or other carbon filler based polymer composites. Mechanical properties of CNT based composites are comparable with graphene based composites. On the basis of thermal and electrical properties, graphene is better filler than MWCNT [89]. The rough and wrinkled surface of graphene assists in the interlocking of graphene to the polymer chain giving better interfacial load transfer between graphene and polymer chain. Graphene sheets provide more surface area owing to its planar structure than the tube shaped CNT.The top and bottom surface of graphene sheets are in close contact with the polymer chain and also, two dimensional graphene shows higher aspect ratio than the one dimensional nanotubes.

Graphene-filled polymer composites are commonly prepared by solution mixing [98-100], melt blending, [101,102] and in situ polymerization. [103-105]. In insitu polymerization the monomer is polymerized in presence of filler and this improves the interaction between the graphitic filler and the polymer matrix. Thus composites fabricated by insitu polymerization will have high mechanical strength and lower percolation threshold. The main disadvantage of this process is that a lot of electrical energy is needed to disperse the filler in the polymeric matrix. So this method is not beneficial in the mass production of polymer composites. In solution mixing, use of a large amount of solvent and the associated environmental polution caused by the

removal of solvent are the main drawbacks. From an industrial point of view, melt blending is the preferred technique for the preparation of composites, since it is a direct, cost effective and environmentally friendly process.

Sherif Araby et al. [106] have suggested that CNT is not a proper choice for functional polymer nanocomposites, because of expensive manufacturing costs and the high viscosity caused by the 'bird's nest' structure of the entangled tubes. While graphene, a flat sheet of carbon just one atom thick, is a new class of promising filler for functional nanocomposites. Also Tapas Kuilla [89] has quoted Nicholas A. Kotov [107] in an article on recent advances in graphene based polymer nanocomposites, "When carbon fibers just won't do, but nano tubes are too expensive, where can a cost-conscious materials scientist go to find a practical conductive composite? The answer could lie with graphene sheet"

1.3 Polymeric Matrices-Elastomers

Different types of polymers are used as matrices in composites. They encompass thermoplastics, thermosets and elastomers. Selection of the polymer with a proper nanoparticle to fit the requirements and applications poses a great challenge to scientists and engineers.

Potential industrial application of elastomer based nanocomposites includes a large number of latex and dry rubber composites [108]. Latex is a stable aqueous dispersion of polymer microparticles in an aqueous medium. Latices may be natural and synthetic. Natural latex is obtained from the Hevea Brasilinesis or the "rubber" tree. Synthetic latices are produced by emulsion polymerisation. But now the term synthetic latex is defined as "any lyophobic dispersion of a polymer in a liquid phase which

is produced by a polymer reaction *ex vivo* and the term emulsion polymerisation is understood to mean *ex vivo* polymerisation reaction which produces such a polymer colloid" [109]. Synthetic latices of wide spread industrial applications include styrene butadiene copolymer latices (SBR), acrylonitrile butadiene copolymer latices (NBR), poly chloroprene latices, latices of vinyl acetate polymers, copolymers etc.

Latex is more expensive than its dry polymer counter part. Since it is a liquid it is easier to process and has better physical properties. The properties of rubber latex makes it an extremely versatile raw material for dipping and moulding purposes. The ability of rubber particles to coalesce and produce a coherent polymer film showing good barrier properties makes latex suitable for a wide range of applications. Articles produced from latex give better ageing resistance, higher strength and greater solvent resistance than those manufactured directly from dry rubber. Since a large variety of elastomers are available in dry rubber form and not as latex, dry rubber composites are more advantageous for commercial applications.

Conventional manufacturing technique for rubber composites includes mixing, forming and vulcanizing. Mixing of dry rubber compounds is usually done on a two roll mill or an internal mixer. For latex compounding all water insoluble solid ingredients are added as dispersions and water insoluble liquid ingredients as emulsions. After mixing all the ingredients, the mix is matured for 24 hrs and then it can be used for dipping and other processes.

1.3.1 Nitrile butadiene rubber (NBR)

Nitrile butadiene rubber (NBR) a copolymer of butadiene and acrylonitrile is produced by emulsion polymerisation. Structure of nitrile

rubber is given in Fig. 1.11. Nitrile rubber has characteristic properties like excellent resistance to oil, fuel and grease, good heat resistance, low level of gas permeability, high electrical conductivity, moderate tensile strength, tear strength, ozone resistance and low temperature flexiblity. Since NBR lacks self reinforcing properties incorporation of reinforcing fillers is essential to obtain vulcanizates with a reasonable level of tensile, tear and abrasion resistance.

It is considered as the workhorse of the industrial and automotive rubber products industries. In the automotive and aeronautical industry it is used in fuel and oil handling hose, seals and water handling applications.It is used to make moulded goods, foot wear, adhesives, sealants, expanded foams, floor mats etc. Its resilience makes it a useful material for making gloves.
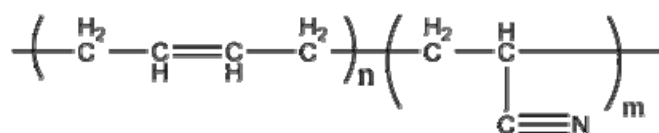
Fig. 1.11. Structure of nitrile butadiene rubber

1.3.2 Carboxylated nitrile butadiene rubber (XNBR)

Carboxylated nitrile rubber (XNBR) is a high-performance elastomer, exhibiting enhanced tensile strength, elastic modulus, hardness, and improved tear and abrasion resistance. They are produced by the inclusion of a third monomer like acrylic acid and methacrylic acid during polymerisation. Carboxylic acid groups will be distributed randomly and they will be present at levels less than 10%. Carboxyl groups can make

ionic cross links with zinc ions and this gives better properties for XNBR. These ionic crosslinks are formed along with sulphur links.

They are used in high abrasion applications such as rolls, conveyor belting, hose covers, oil well drilling parts etc.

1.3.3 Styrene butadiene rubber (SBR)

Styrene butadiene copolymer latices (SBR) comprise a large family of general purpose synthetic rubbers consisting of styrene and 1,3butadiene. Eventhough SBR is produced by emulsion (E-SBR) and solution polymerisation (S- SBR), about 85-90% of the world production of SBR is prepared by emulsion polymerisation. Fig.1.12 shows the structure of styrene butadiene rubber.

Image courtesy of Luigi Chiesa
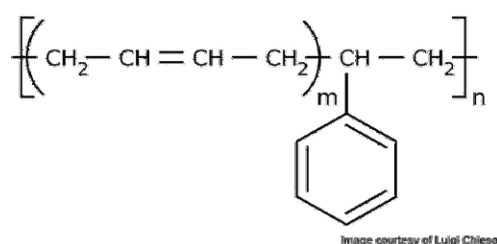
Fig.1.12. Sructure of styrene butadiene rubber

SBR is a synthetic rubber most widely used in the elastomer industry. It has good abrasion resistance, good aging resistance and low temperature properties. SBR being a non crystallising synthetic rubber lacks the self-reinforcing properties. So filler reinforcement is much pronounced with SBR. Being a non-polar polymer its vulcanizates are poor conductors of electricity. E-SBR vulcanizates are resistant to many polar solvents such as dilute acids and bases, but they swell considerably when in contact with gasoline, oils, or fats.

More than 70% of the total production of SBR is used by tyre industry. It is used in shoe heels and soles, gaskets etc. SBR latex is used in the manufacture of latex foam rubber by replacing NR latex, carpet backing and textile applications, paper coating applications, as a general purpose adhesive for paper and other fibrous materials, as a rubber to textile bonding adhesive for tyre cords etc.

1.4 Nanocomposites based on NBR, XNBR and SBR.

Rubber nanocomposites reinforced with a small volume of nanofillers have attracted attention of scientists and industrialists due to the tremendous improvement in the mechanical, thermal, dynamic mechanical, electrical, aging and flame retardancy properties of the composites. Nanoparticles considered for the preparation of rubber nanocomposites include layered silicates, nano silica, carbon nanotubes, expanded graphite etc.

Reports on the use of layered silicates as fillers in rubber industry is limited, but there are immense works reporting the enhancement in mechanical properties, thermal stability, flame retardancy, barrier properties etc. However, the most extensively used and studied layered silicate is montmorillonite (MMT) [110].

Rubber clay composites can be prepared by different processing techniques such as melt intercalation [111,112], solution blending [113], co coagulating rubber latex [38], and by mill mixing [114].

You Ping Wu et al. [115] prepared NBR, SBR, NR, and XNBR /clay nanocomposites by a cocoagulating process and introduced the concept of 'separated' rubber clay nanocomposites-as against the intercalated and exfoliated structures. Kim et al. [112] studied the effect of organo modified

montmorillonite in NBR produced by melt intercalation process. Nitrile rubber unmodified clay composites were prepared by latex blending method by Kader et al. [116].

Amit Das et al. [117] studied nanocomposites based on carboxylated nitrile rubber and organomodified clay under different mixing conditions. Remarkable improvement in properties was obtained at high temperatures. They proposed a mechanism for the interaction of layered silicate dispersion with XNBR. The same team reported the utilization of XNBR in the preparation of high performance elastomer by melt mixing. J. Fritzsche worked on carboxylated nitrile rubber (XNBR), filled with 10 phr of layered silicate and investigated the properties using dielectric and dynamic-mechanical analysis [118].

M.Salehi, produced SBR clay composite by latex coagulation method and melt intercalation method and found that better dispersion and better properties were obtained for the latex coagulated clay composite [119]. Similarly SBR/organomodified MMT composite prepared by the latex method gave better properties than the composite prepared by the compounding method [120]. Liqun Zhang also prepared SBR clay composites by mixing SBR latex with clay dispersion and coagulating the mixture [36].

Use of kaolin in the preparation of rubber nanocomposites is rarely reported. NR silane modified kaolin composites exhibited outstanding mechanical properties, gas barrier properties and good thermal stability [121]. Study of the tensile properties of unmodified kaolinite and octadecyl amine modified kaolinite on NR, prepared via latex compounding method

showed that dispersion of slicate layers is the key parameter in enhancing the physical properties of the composites [122]. NR and SBR composites containing acrylic acid and poly acrylic acid modified kaolin were prepared by Zoromba et al. [27], Tea seed oil modified kaoiln was used to prepare NR composite by Yahaya et al. [123]. Major portion of the works on kaolin are dealt with NR and its use in NBR, XNBR and SBR have not been reported so far.

High performance nitrile rubber, with a combination of excellent mechanical properties, abrasion resistance, aging resistance etc. when combined with versatile filler like MWCNT gives appreciable properties. Perez et al. [124] have suggested that the most convenient and efficient method for the preparation of MWCNT elastomer composite is melt blending. The prepared NBR/MWCNT composites showed improved properties such as resistance to solvent swelling, enhanced glass transition temperature, improved storage and loss moduli due to the strong interaction between the functional groups introduced in MWCNT surface and nitrile group of the polymer chain. Pierre Verge et al. [125] have also analysed the electrical and morphological properties of prepared NBR/ MWCNT composite by a melt blending method. The free radicals generated on the surface of NBR during heating and shear mixing assisted the grafting of polymer chain onto the CNT.

X.Chen et al. [126] prepared SBR /MWCNT composites for the first time by processing in a two roll mill and found an increase in the mechanical properties like tensile strength, tear strength, shore hardess and abrasion resistance of the composite. Xiang wen Zhou et al. [127] prepared powder SBR clay composites by spray drying of the suspension of CNT in SBR latex and Leon D Perez [124] prepared SBR/MWCNT composite by

mixing in a two roll mill. In a nouvel method SBR composites were prepared by predispersing MWCNT in ethanol and MWCNT alcohol mixture was incorporated into a 50:50 mixture of SBR/SBR blend at elevated temperature. The rubber nanocomposites prepared by such methods exhibit significantly enhanced physical properties at very low nanotube concentrations [128].

Superior mechanical and electrical properties of graphene have paved way for the preparation of advanced polymer composites. Studies on thermoplastic graphene composites are more common and the existing literature on elastomer based composite is limited. NR graphene composites were prepared by ultrasonically assisted latex mixing and insitu reduction of graphene oxide by Zhan et al.[129]. The effects of functionalized graphene sheets (FGSs) on the mechanical properties and strain-induced crystallization of natural rubber (NR) are investigated by Bulent Ozbas et al. [130]. Also Wang et al. have reported NBR/nanographite composites prepared by latex compounding technique and mechanical mixing [131].

1.5   Applications of polymer nanocomposites (PNC)

Amongst all the potential nanocomposite precursors, thermoplastic and themoset nanocomposites are most widely investigated. The development of elastomeric nanocomposites was much delayed. But once the researchers recognized the best mixing technique to disperse nanofillers in rubber matrices there was a spur in the activities in this field. Versatility of rubber makes it the most desirable material in the field of polymer nanocomposites.

Polymer nanocomposites represent a new alternative to conventionally filled polymers. Nanocomposites exhibit markedly improved mechanical

strength, thermal stability, barrier properties, good optical clarity, electrical and thermal conductivity, reduced flammability etc. Advantages of polymer nanocomposite are numerous and the possibilities for industrial application are endless

1.5.1 Polymer/Clay nanocomposites

The improvement in mechanical properties of nanocomposites resulted in major achievements in numerous automotive and other industrial applications. The most revealed application for polymer nanocomposites was for an automotive purpose by Toyota, concerning a timing belt cover [132]. The low heat build up and the enhanced wear resistance is a promising feature for tyres and technical rubber goods subject to wear. Clay incorporated tires exhibit excellent mechanical properties as compared to ordinary tires as well as improved gas barrier performance for tubeless tire applications. Generally styrene butadiene and natural rubber based clay nanocomposites are mostly used for automobile tire manufacturing and, butyl rubber find application in tubes.

Clays increase the barrier properties by creating a maze or 'tortuous path' that retards the progress of the gas molecules (CO_2, O_2, N_2) and chemicals (toluene, HNO_3, H_2SO_4, HCl, etc) through the polymeric matrix. A number of polymer matrices like butyl rubber, styrene butadiene rubber, ethylene propylene diene monomer rubber, ethylene vinyl acetate copolymer, have been used for commercial barrier applications. Due to excellent solvent barrier properties PNCs are used in the production of chemical protective and surgical gloves. PNCs are widely used in food packagings, especially proccessed meat, cheese, cereals, and dairy products, seals for blood collection tubes, stoppers for medical containers etc.

In many food packages the oxygen ingress determines the shelf life of the food in the package. Clay based polymer nanocomposites have been used in plastic bottle manufacturing industries for improving barrier, mechanical properties and shelf life of the product. The shelf-life of a clay based nanocomposite plastic beer bottle is more than 6 months. The first plastic beer bottle based on clay has been introduced by Honeywell. A recent application in sports good is in double core Wilson tennis ball. The clay nanocomposite coating of the Wilson tennis balls maintains the internal pressure for an extended period of time. This double core new tennis balls using this coating retain air longer, and is able to bounce twice as long as ordinary balls [133].

Clay incorporated polymers, when employed to coat transparent materials, enhances both toughness and hardness of these materials without sacrificing light transmission characteristics.

Nano clay based polymer coatings are used for construction purposes, pipe line coating for marine application, for decorative purposes etc. Hybrid coatings like clay and nano silver in polymer matrix improves the shelf life and anti bacterial properties in medical field.

Clay containing conducting polymers like poly pyrrole, poly thiophen etc. are used in solar cells, wind mills, micro chips transistors etc.

Flame resistance of clay finds application in cable wire jacket, car seats, packaging films, textile, surface coatings, for many steel products, paints and the most important being rocket ablative materials core manufacturing [134].

The ability of nanoclay incorporation to reduce the flammability of polymeric materials substantially improves abrasion resistance of polymer

layered silicate nanocomposites.Owing to this reason and improved optical properties it has been widely commercialized in contact lens and optical glass applications [133].

1.5.2 Polymer/CNT nanocomposites

CNTs possess remarkable mechanical, thermal and electrical properties. Based on their different application purposes, polymer/ CNT composites are classified as structural composites and functional composites. Structural composites make use of the unique mechanical properties of CNTs, while functional composites explore their high electrical and thermal conductivity. Due to the superior mechanical properties and small size of CNTs, they are used as reinforcing fibres in composites where stiffness, strength and low weight are important considerations.There are numerous applications including aerospace structural panels, sporting goods, ultra lightweight thin-walled space structures for use in space, high stiffness-to-weight space mirror substrates, automotive infrastructure and defence.

The low percolation threshold of CNT originating from the high thermal conductivity and aspect ratio, paves way for the construction of conductive composites with low CNT loading. The out standing thermal properties of CNT are made use of in temperature sensors, resistance heating and flame retardance material. CNT/polymer composites can also modify the electromagnetic interference shielding effectiveness optoelectronic properties, thermoelectric energy conversion etc.

They are also used as EMI shielding composites, antistatic materials, conductive coatings, electrode materials for super capacitors, fuel cells etc. [135].

Besides electrical and thermal properties, optical properties also need special mention. Application relating to nonlinear optics includes protection of optical sensors from high intensity laser beams. Optical and electronic properties are combined in electron emitting flat-panel displays, electro mechanical actuators, light-emitting diodes, supercapacitors, field-effect transistors etc.

1.5.3 Polymer/Graphene nanocomposites

One of the most promising aspects of graphene based polymer composites is their use in electronic application devices. Field effect transistors [136], solar cells (opto electronic) [137] and energy storage devices [138] are the three major areas where conductive composites are particularly applicable [139]. Electrical conductivity of these composites finds use in electromagnetic wave interference shielding, antistatic coatings [140].etc.

Graphene based composites incorporating PANI are used as energy storage materials. The mechanical reinforcement at low loadings of graphite oxide derived fillers, offer potential uses in weight sensitive aerospace and automotive applications such as tires. Use of graphene based materials in bio medical application is an emerging field of research. Efforts are directed towards graphene based composite biosensors application. In photo voltaics and opto electronics high transparency and electrical conductivity of graphene is considered. This makes it useful in issues related to photoexcitation and exciton mobility/diffusion as transparent conductive electrodes [139].

1.6 Objectives of the work

The present work has been undertaken to explore the potential of different types of nanofillers like nanoclay, multi walled carbon nanotube

and graphene nanoplatelets in the realm of rubber latices and dry rubber. However the use of nanokaolin and modified nanokaolin in polymeric nanocomposites is still at its infancy. Although a number of experimental studies have focussed on the preparation of nanotube and graphene dispersions and the direct determination of mechanical and conducting properties of nanotubes and graphene, the studies based on their composites is only developing. In this work, effect of very low concentration of MWCNT and graphene nanoplatelets in latex and dry rubber composites were studied with special emphasis on the mechanical, thermal and electrical properties.

The salient objectives of the research work are

- Characterization of the fillers like nanokaolin, vinyl silane grafted nanokaolin, multi walled carbon nanotube and graphene nanoplatelets

- Preparation of composites with carboxylated nitrile butadiene rubber (XNBR) and styrene butadiene rubber (SBR) lattices and dry nitrile rubber (NBR) with the above fillers.

- Characterization of the nanocomposites formed.

- Study of the mechanical and thermal properties of the nanocomposites

- Microwave studies of MWCNT/Graphene based nanocomposites

- Preparation and characterization of layered silicates and their effect on the mechanical properties of XNBR/SBR latices and NBR/SBR rubber

- Application of nanoclay and modified nanoclay in the production of gloves.

References

[1] Galimberti, M. Editor. Rubber-Clay Nanocomposites. Science, Technology and Applications. Wiley.2011.

[2] Morawetz, H. Polymers: The Origin and Growth of a Science. Dover Phoenix Editions. John Wiley&Sons .1985, 35

[3] Hofmann, W. Rubber Technology Handbook, Hanser Publishers. 1989, 1.

[4] Blow, C.M. Rubber Techology and Manufacture.2nd Edition. London. Butterworths.1975, 22.

[5] Paipetis, S. A. Melanitis, N. Kostopoulos, V. Journal of Materials Science. 1988, 23, 4282.

[6] Jovanović, V. Samaržija-Jovanović,S. Budinski-Simendić, J. Marković, G. Marinović-Cincović,M. Composites Part B: Engineering. 2013, 45, 333.

[7] Omnès, B. Thuillier, S. Pilvin, P. Grohens, Y. Gillet, S. Composites Part A: Applied Science and Manufacturing . 2008, 39, 1141.

[8] Ding, T. Wang, L. Wang, P. Journal of Polymer Science Part B: Polymer Physics. 2007, 45, 2700.

[9] Peng, Z. Kong, L. X. Li,S. Chen,Y. Huang, M. F. Composites Science and Technology. 2007, 67, 3130.

[10] Poochai, C. Pae-on, P. Pongpayoon, T. World Academy of Science, Engineering and Technology. 2010, 41,969.

[11] Bandyopadhyay, A. Bhowmick, A. K. Sarkar, M. D. Journal of Applied Polymer Science. 2004, 93, 2579.

[12] Usuki,A. Kojima, Y. Kawasumia, M. Okada, A. Fukushima, Y.Kurauchi, T. Kamigatio, O. Journal of Materials Research. 1993, 8, 1179.

[13] Lan, T. Pinnavaia, T. Clay-reinforced epoxy nanocomposites, Chemistry of Materials. 1994, 6, 2216.

[14] Okada, A. Usuki, A. The chemistry of polymer-clay hybrids. Materials Science and Engineering C. 1995, 3,109.

[15] Salavati-Niasari, M. Ghanbari, D. Advances in Diverse Industrial Applications of Nanocomposites, edited by Boreddy Reddy 2011.

[16] Bhowmick, A.K. Editor. Current Topics in Elastomers Research. CRC Press.2008.

[17] Thomas, S.Stephen, R. Editors. Rubber Nanocomposites. Preparation, Properties and Application. John Wiley&Sons. 1985.209.

[18] Kumar, A.P. Depan, D. Tomer, N .S. Singh, R. P. Progress in Polymer Science. 2009, 34 479.

[19] Koo, J.H. Polymer Nanocomposites. Processing, Characterization and Applications. McGraw- Hill, 2006. 9.

[20] Stephen, R. Ph.D Thesis.Mahatma Gandhi University.India.2005.

[21] Koo, J. H. Polymer Nanocomposites. Processing, Characterization and Applications. McGraw- Hill, 2006.10.

[22] Galimberti, M. Editor. Rubber-Clay Nanocomposites. Science, Technologyand Applications. (Chapter1). Wiley.2011, 4.

[23] Uttracki, L.A. Clay-Cotaining Polymeric Nanocomposites. Rapra Technology. 2004,1,74.

[24] Pinnavia, T. J. Beall, G.W. Polymer-Clay Nanocomposites.200,5.

[25] Jackson, M. L. Abdel-Kader, F. H. Clays and Clay Minerals, 1978, 26, 81.

[26] Braggs, B. Fornasier, D. Ralston, J. St. Smart, R. Clays and Clay Minerals, 1994, 42, 123.

[27] Zoromba, M. Sh. Belal, A. A. M. Ali, A. E. M. Helaly, F. M. Abd El-Hakim, A. A. Badran, A. S. Polymer-Plastics Technology and Engineering. 2007, 46, 529.

[28] Sukumar, R. Menon, A. R. R. Journal of Applied Polymer Science.2008, 107, 3476.

[29] Braggs, B. Ralston,J. St. Clair Smart,R. 1996, US 6071335 A.

[30] Fukushima, Y.Tani, M.J.Chem.Soc.Chem.Commun.1995, 2,241.

[31] Fukushima, Y.Tani, M. Bull.Chem.Soc.Jpn.1996, 69, 3667.

[32] Giannelis, E.P. Krishnamoorti, R. Manias, E. Adv. Polym. Sci.1999, 138,107.

[33] Alexandre, M. Dubois P. Materials Science and Engineering. 2000, 28, 1.

[34] Ray, S.S. Okamoto, M. Progr. Polym. Sci. 2003, 28, 1539.

[35] Varghese, S. Karger-Kocsis, J. Polymer. 2003, 44, 4921.

[36] Zhang, L. Wang, Y. Wang, Y. Sui, Y.Yu, D. Journal of Applied Polymer Science.2000, 78, 1873.

[37] Jia,Q. Wu ,Y. Wang ,Y. Lu,M. Zhang, L. Composites Science and Technology 2008, 68,1050.

[38] Wu,Y. Wang, Y. Zhang ,H. Wang ,Y. Yu ,D. Zhang, L. Yang,J. Composites Science and Technology. 2005, 65, 1195.

[39] Jose, L. Joseph, R. International Journal of Polymeric Materials. 2005, 54, 387.

[40] Wu, Y. Huang, H. Zhao, W. Zhang, H. Wang, Y. Zhang, L. Journal of Applied Polymer Science. 2008, 107, 3318.

[41] Ray, S. Bhowmick, A. K. Sarma, K. S. S. Majali, A. B. Tikku, V. K. Radiation Physics and Chemistry. 2002, 65, 627.

[42]   Tian M. Cheng, L. Liang, W. Zhang, L. Journal of Applied Polymer Science .2006,101, 2725.

[43]   Wang, Y. Zhang, L. Tang, C. Yu, D. J. Applied Polymer Science. 2000, 78, 1879.

[44]   Vaia, R.A. Giannelis, Macromolecules.1997, 30, 7990.

[45]   Ma,Y. Wu,Y. Wang, Y. Zhang,L. Journal of Applied Polymer Science. 2006, 99, 914.

[46]   Fritzsche, J. Das, A. Jurk, R. Stöckelhuber, K. W. Heinrich, G. Klüppel, M. eXPRESS Polymer Letters. 2008, 2,373.

[47]   Kato,M. Tsukigase, A. Tanaka, H. Usuki, A. Inai, I. Polymer Science Part A: Polymer Chemistry. 2006, 44, 1182.

[48]   Liang, Y. Cao, W. Zhang, X. Tan,Y. He, S. Zhang, L .Journal of Applied Polymer Science.2009, 112, 3087.

[49]   Pramanik, M. Srivastava, S. K. Samantaray, B.K. Bhowmick, A.K. Journal of Applied Polymer Science, 2003,87,2216.

[50]   Sadhu, S.Bhowmick, A.K.Adv.Eng.Mater.2004, 6, 738.

[51]   Sadhu, S.Bhowmick, A.K. J.Polym.Sci.Part B.Polym.Phys. 2004, 42,1573.

[52]   Qin, X. Wu, Y. Wang, K. Tan, H. Nie ,J. Applied Clay Science 2009, 45, 133.

[53]   Messersmith,P.B. Giannelis,E.P. J.Polym.Sci.A. Polym. Chem. 1995, 33, 1047.

[54]   Fu, X. Qutubuddin, S. Polymer, 2001, 42, 807.

[55]   Nese, A. Sen, S. Tasdelen, M.A. Nugay, N. Yagci, Y. Macromol. Chem. Phys. 2006, 207, 820.

[56]   Salem, N. Shipp, D.A. Polymer. 2005, 46, 8573.

[57]   Zhang, B.Q. Pan, C.Y. Hong, C.Y. Luan, B. Shi, P.J. Macromol. Rapid Commun. 2006, 27, 97

[58]   Kubies, D. Pantoustier, N. Dubois, P. Rulmont, A. Jerome, R. Macromolecules, 2002, 35, 3318.

[59]   Viville, P. Lazzaroni, R. Pollet, E. Alexandre, M. Dubois, P. J. Am. Chem. Soc. 2004, 126, 9007.

[60]   Yu, Y.H. Lin, C.Y. Yeh, J.M. J. App. Polym. Sci. 2004, 91, 1904.

[61]   Fan, X.W. Zhou, Q.Y. Xia, C.J. Cristofoli, W. Mays, J.,Advincula, R. Langmuir .2002, 18, 4511.

[62]   Moniruzzaman, M. Winey, K.I. Macromolecules 2006, 39, 5194.

[63]   Hutchison, J.L. Kiselev, N.A. Krinichnaya, E.P. Krestinin, A.V. Loufty, R.O. Morawsky, A.P. et al. Carbon. 2001, 39,761.

[64]   Zhang,Y. Iijima, S. Applied Physics Letters. 1999,75,3087.

[65]   Endo, M. Hayashi, T. Kim, Y.A. Muramatsu, H. Japanese Journal of Applied Physics 2006,45,4883.

[66]   Bose, S. Khare,R.A. Moldenaers,P. Polymer. 2010, 51, 975.

[67]   Bokobza,L. Polymer .2007,48, 4907.

[68]   Ajayan, P.M. Stephan, O. Colliex, C. Trauth, D. Science. 1994, 265,1212.

[69]   Jin, L. Bower, C. Zhou, O. Appl Phys Lett. 1998,73,1197.

[70]   Geng, H. Rosen, R. Zheng, B. Shimoda, H. Fleming, L. Liu, J et al. Adv Mater. 2002,14,1387.

[71]   Xia, H.Wang,Q. Li, K. Hu, G.H. J Appl Polym Sci. 2004, 93,378.

[72]   Ghose, S. Watson, K.A. Sun, K.J. Criss, J.M. Siochi, E.J. Connell, J.W. Compos Sci Technol. 2006,66,1995.

[73]   Fan, J. Wan, M. Zhu, D. Chang, B. Pan, Z. Xie, S. J Appl Polym Sci. 1999,74,2605

[74]   Liu, C.H, Huang, H. Wu, Y. Fan, S.S. Appl Phys Lett. 2004, 84, 4248.

[75]   Jin, Z. Pramoda, K.P. Xu, G. Goh, S.H. Chem Phys Lett. 2001,337, 43.

[76]   Potschke, P. Fornes, T. D. Paul, D.R. Polymer. 2002,43,3247.

[77]   Bose, S. Khare, R.A. Moldenaers, P. Polym. 2010, 51, 975.

[78]   Spitalsky, Z. Tasis, D. Papagelis, K. Galiotis, C. Prog Polym Sci 2010, 35, 357.

[79]   Rastogi, R. Kaushal, R. Tripathi, S. Sharma, A.L. Kaur,I. Bharadwaj, L.M. J Colloid Interface Sci. 2008, 328, 421.

[80]   Vaisman, L. Wagner, H.D. Marom, G. Adv Colloid Interface Sci. 2006, 128, 37.

[81]   Ciofani, G. Raffa, V. Pensabene, V. Menciassi, A. Dario, P. Fullerenes, Nanotubes Carbon Nanostructures. 2009,17,11.

[82]   Wang, Q. Han, Y. Wang, Y. Qin, Y. Guo, Z. J Phys Chem B. 2008, 112, 7227.

[83]   Jung, R. SikKim, H. Joon jin, H. Macromol Symp. 2007, 249, 259.

[84]   Ryabenko, A.G. Dorofeeva, T.V. Zvereva, G.I. Carbon. 2004, 42, 1523.

[85]   Islam, M. F. Rojas, E. Bergey, D. M. et al. Nano Lett. 2003,3, 269.

[86]   Liu, X. Spencer, J.L. Kaiser, A. B. Arnold, W. M. Curr. Appl. Phys. 2004, 4, 125.

[87]   Yu, J. Grossiord, N. Koning, C.E. Loos, J. Carbon. 2007, 45, 618.

[88]   Grossiord, N. van der Shoot, P.Meuldijk, J. Koning, C.E.Langmuir. 2007, 23, 3646.

[89]   Kuilla ,T. Bhadra, S. Yao,D. Kim, N.H. Bosed,S. Lee,J.H. Progress in Polymer Science.2010, 35, 1350.

[90]   Li, D. Muller, M.B. Gilje, S. Kaner, R.B. Wallac, G.G. Nat Nanotechnol. 2007,3,101

[91]   Eizenberg, M. Blakely, J.M. Surf Sci. 1979, 82, 228.

[92]   Aizawa, T. Souda, R. Otani, S. Ishizawa, Y. Oshima C. Phys Rev Lett 1990, 64,768.

[93]   Novoselov, K.S. Geim, A.K. Morozov, S.V. Jiang, D. Zhang, Y. Dubonos , S.V. Grigorieva IV, Firsov, A.A. Science. 2004,306, 666.

[94]   Berger, C. Song, Z. Li, X. Wu, X. Brown, N. Naud, C. et al. Science. 2006, 312, 1191.

[95]   Stankovich, S.Dikin, D.A. Piner, R.D. Kohlhaas, K.A. Kleinhammes, A, et al. Carbon 2007,45,1558.

[96]   Geng, Y. Wang, S.J. Kim, J.K. J Colloid Interface Sci. 2009,336, 592.

[97]   Rao, C. N. R. Sood, A. K. Voggu,R. Subrahmanyam, K. S. J. Phys. Chem. Lett. 2010, 1, 572.

[98]   Ramanathan, A. A.Abdala, S.Stankovich, D. A.Dikin, M. Herrera-Alonso, R. D.Piner, D. H. Nat.Nanotechnol. 2008, 3, 327.

[99]   Xu, Y. X. Hong, W. J. Bai, H. Li, C. Shi, G. Q. Carbon. 2009, 47, 3538

[100]   Wu, Q. Xu, Y. X. Yao, Z. Y. Liu, A. R. Shi, G. Q. ACS Nano. 2010, 4, 1963.

[101]   Kim, H. Jeong, Y. G. J. Polym. Sci., Part B: Polym. Phys. 2010, 48, 850.

[102]   Dasari, A. Yu, Z.Z .Mai, Y. W Polymer. 2009, 50, 4112.

[103] Yu, A. P. Ramesh, P. Itkis, M. E. Bekyarova E. Haddon, R. C. J. Phys. Chem. C. 2007, 111, 7565.

[104] Wang, H. L. Hao, Q. L. Yang, X. J. Lu, L. D. Wang, X. Electrochem. Commun. 2009, 11, 1158.

[105] Hu, H. Wang, X. Wang, J. Wan, L. Liu, F. Zheng, H. Chen, R. Xu, C. Chem. Phys. Lett., 2010, 484, 247.

[106] Araby,S. Zaman,I. Meng,Q.Kawashima,N. Michelmore,A. Kuan,H. Majewski,P. Ma, J. Zhang, L. Nanotechnology. 2013, 24. 165601.

[107] Kotov, N. A. Nature. 2006,442,254.

[108] Thomas, S.Stephen, R. Editors. Rubber Nanocomposites. Preparation, Properties and Application. John Wiley & Sons .1985.233

[109] Blackley, D.C.Polymer Latices.2nd Edition. 1997, 2, 138.

[110] Kim, J.K. Pal, K. Sridhar, V. Recent Advances in Elastomeric Nanocomposites V. Mittal et al. (eds.), 2011, 9.

[111] Das, A. Jurk,R. Stöckelhuber, K. W. Heinrich G. eXPRESS Polymer Letters.2007,1,717.

[112] Kim, J. Oh,T. Lee,D. Polym Int. 2003, 52, 1058.

[113] Hwang, W. Wei, K. Wu,C. Polymer Engineering and Science. 2004, 44, 2117.

[114] Thomas,P.C. Selvin, P. Thomas, George ,G. Thomas,S. Kuruvilla, J .J Polym Res. Doi. 10.1007/s10965-011-9651-1

[115] Wu,Y. Jia,Q. Yu,D. Zhang,L. Journal of Applied Polymer Science. 2003, 89, 3855.

[116] Kader, M.A. Kim, K. Lee, Y.S. Nah, C. J Mater Sci. 2006 ,41,7341.

[117] Das, A. Jurk, R. Stöckelhuber, K.W. Majumder, P.S. Engelhardt T. FritzscheJ. Klüppel, M Heinrich, G. Journal of Macromolecular Science, Part A Pure and Applied Chemistry. 2009, 46, 7.

[118] Fritzsche, J. Das, A. Jurk, R. Stöckelhuber, K. W. Heinrich, G,. Klüppel1, M eXPRESS Polymer Letters. 2008, 2, 373.

[119] Salehi, M. Razzaghi-Kashani, M.Journal of Applied Polymer Science. 2012, 126, 253.

[120] Kim ,W. Kang,B. Cho,S. Ha,C. Bae, J. Composite Interface. 2007, 14, 409.

[121] Zhang, Y. Liu,Q. Zhang,Q. Lu ,Y.Applied Clay Science .2010, 50, 255.

[122] Ruamcharoen, J. Chotisuwan, S. Ruamcharoen, P. Advanced Materials Research Vols. 2012,488,701.

[123] Yahaya1,L.E. Adebowale, K. O. Menon, A. R. R. Rugmini S, Olu-Owolabi, B. I. Chameswary J. African Journal of Pure and Applied Chemistry. 2010, 4, 198.

[124] Perez,L. Zuluaga,M.A. Kyu,T. Mark,J. E. Lopez,B.L. Polym.. Eng. Sci., 2009, 49, 866.

[125] Verge, P. Peeterbroeck, S. Bonnaud, L. Dubois, P. Composites Science and Technology 2010, doi: 10.1016/j.compscitech.2010.04.022

[126] Chen, X. H. Song, H.H .New carbon materials.2004, 19, 214.

[127] Zhou,X. Zhu,Y. Gong,Q. Liang,J. Materials Letters. 2006, 60, 3769.

[128] Das, A. Stöckelhuber, K.W, Jurk, R. Saphiannikova, M. Fritzsche, J. Lorenz,H. et al.Polym. 2008, 49, 5276.

[129] Zhan ,Y. Wu, J. Xia, H. Yan, N. Fei, G. Yuan ,G. Macromol Mater Eng. 2011,296,590.

[130] Ozbas,B Toki,S. Benjamin S. Hsiao, Chu,B. Register,R.A. Aksay,I.A. Prud'homme, Douglas,R.K. Adamson,H. Journal of Polymer Science Part B: Polymer Physics. 2012, 50, 718.

[131] Wang LL, Zhang LQ, Tian M. Wear. 2012, 276, 85.

[132] Paul, D.R. Robeson, L.M. Polymer. 2008,49,3187

[133] Anandhan, S. Bandyopadhyay, S.Polymer Nanocomposites: From Synthesis to Applications. www.intechopen.com .

[134] Koo, J.H. Polymer Nanocomposites.Processing, Characterization and Applications. McGraw- Hill. 2006, 125.

[135] Du, J.H. Bai, H. Cheng, H.M eXpress Polymer Letters.2007, 5,253

[136] Eda, G. Chhowalla, M. Nano Lett. 2009, 9,814.

[137] Spitsina, N.G. Lobach, A.S. Kaplunov, M.G. High Energy Chem. 2009, 43, 552.

[138] Tien, C.P. Teng, H.S. J Power Sources. 2010, 195, 2414.

[139] Potts, J.R. Dreyer, D.R. Bielawski C.W. Ruoff, R.S. Polymer. 2011, 52, 5.

[140] Liang,J.J. Wang, Y. Huang, Y. Ma,Y.F, Liu, Z.F. Cai, F.M. et al. Carbon. 2009, 47,922.

.....ഇരു.....

MATERIALS AND METHODS

This chapter gives a brief description of the materials used and experimental procedures used in this study.

2.1   Materials:

2.1.1 Carboxylated nitrile butadiene rubber latex (XNBR)

Chemigum CLX 530 is carboxylated acrylonitrile butadiene copolymer latex, supplied by Eliokem India Pvt. Ltd. Bombay. Specification of XNBR latex is given in Table 2.1.

Table 2.1. Characteristics of XNBR latex

Total solid content (%)	48
Brookefield viscosity(cP)	87
Surface tension (dynes/cm)	39
Average particle size (nm)	160
Bound ACN	31
pH	9

2.1.2 Styrene butadiene rubber (SBR) latex

Encord 204 latex is styrene butadiene copolymer latex, supplied by Jubilant Organosys Limited. Gujarat. Specification is given in Table 2.2.

Table 2.2. Characteristics of SBR latex

Total solid content (%)	40
Brookefield viscosity, cP	29
Surface tension (dynes/cm)	54
Specific gravity	1.00
pH	10
Total solid content (%)	40

2.1.3 Nitrile butadiene rubber (NBR)

Nitrile butadiene rubber is KNB 35L supplied by Kumho Petrochemicals. Co., Ltd. South Korea. It has acrylonitrile content 34% and Mooney viscosity (ML(1+4) at 100^0C) 41.

2.1.4 Styrene butadiene rubber (SBR)

Styrene butadiene rubber is Kumho SBR (SBR-1502) supplied by Kumho Petrochemicals.Co., Ltd. South Korea. It has Bound styrene content 24 and Mooney viscosity (ML (1+4) at 100^0C) 52.

2.2 Fillers

2.2.1 Nanoclay

Nanokaolin is Nanocaliber 100 supplied by English Indian Clays Ltd.Veli, Thiruvananthapuram.

Vinylsilane grafted nanokaolin is Nanocaliber 100V supplied by English Indian Clays Ltd.Veli, Thiruvananthapuram.

Specification of nanokaolin and vinylsilane grafted nanokaolin are given in Table 2.3.

Table 2.3. Specification of Nanokaolin and Vinylsilane grafted nanokaolin

	Nanokaolin	**Vinylsilane grafted nanokaolin**
Average Particle Size	100	100
Plate thickness (SEM)	<80 nm	<80 nm
pH (10% slurry)	8.0	7.0
Bulk density	0.3 g/cc	0.3 g/cc
BET Specific surface area	30 m^2 /g	30 m^2/g

2.2.2 Multiwalled carbon nanotube (MWCNT)

MWCNT Baytube^R 150P was supplied by Bayer Materials Science AG (Leverkusen, Germany). Table 2.4 gives the specification of MWCNT.

Table 2.4. Specification of Multiwalled carbon nanotube (MWCNT)

C-Purity	>95
Number of walls	13-15
Outer mean diameter	13-16nm
Inner mean diameter	4nm
Length	8 μm
Bulk density	150 kg/m^3

2.2.3 Graphene nanoplatelets

Purchased from Quantum materials limited, Bangalore.

2.3 Other Chemicals

Potassium oleate (10%) was used as a stabilizing agent in latex. Toluene and methyl ethyl ketone (MEK) used for swelling studies were of analytical grade.

Table 2.5. Chemicals and their suppliers

Compounding ingredients	Suppliers
ZnO (activator)	M/s Meta Zinc Ltd. Mumbai
Sulphur (cross linking agent)	M/s Standard Chemicals Co. Pvt. Ltd. Chennai
Tetra methyl thiuram disulphide (TMTD) (accelerator)	Polyolefins Industries Ltd. Mumbai
Zinc diethyl di thio carbamate (ZDC) (accelerator)	Akzo Nobel India Ltd (ICI India Ltd.)
Cyclohexyl2-benzthiazol sulphenamide (CBS) (accelerator)	Polyolefins Industries Ltd. Mumbai
Stearic acid (co- activator)	Godrej soaps pvt. Ltd. Mumbai
Vulcastab V L (Poly ethylene oxide condensate)	Akzo Nobel India Ltd (ICI India Ltd.)
Sodium do decyl benzene sulphonate($C_{18}H_{29}NaO_3S$, SDBS)	Loba Chemie
Dispersol F (Sodium methylene bis naphthalene sulphonic acid) (dispersing agent)	Indian Explosives Ltd. Kolkotta.
Vulkanox HS (1,2dihydro 2,2,4tri methyl quinoline, polymerised) (antioxidant)	M/s Bayer India Ltd.Mumbai

2.4   Experimental Methods and Characterization Techniques

2.4.1 Latex compounding

Water insoluble solid ingredients were added to latex in the form of dispersions in water. Aqueous dispersions were prepared by ball milling / sonication.

Ball Milling

Ball mill comprises of a steel cylindrical container fed with the slurry and a charge of balls as the grinding elements. The mill is operated by causing the cylindrical container to revolve slowly about its longitudinal

axis, which is horizonal. The motion of the balls against each other and also against the walls of the container causes reduction in the particle size of the material [1].

Ultra Sonication

Ultrasonicator used is a mechanical probe sonicator (13mm, Vibra Cell Processor VC 750, operating at 40% of the maximum power, 750W).

The ultrasonic power supply converts line voltage to high frequency electrical energy which in turn is converted to mechanical vibrations by a piezoelectric transducer within a converter. These vibrations are intensified by a probe thereby causing pressure waves in the liquid. This action produces millions of bubbles or cavities which expands and then collapses causing enormous shock waves in the liquid, along with an increase in temperature and pressure. The extremely high level of energy released during the process leads to the disruption of the interaction forces between the particles causing dispersion of the suspended particles in the solvent. To prevent the rise in temperature the sample container is kept in an ice water bath.

2.4.2 Rubber compounding

Compounding of rubber was done on a two roll mixing mill and brabender plasticorder

Two roll mill

Compounding of rubber was done on a two roll mill (150 mm ×300 mm). For NBR and SBR mixing was done as per ASTM D 3187-001 and 3185-99 respectively. The nip gap was set at 0.2mm and temperature maintained at $50+/-5^0$ C.

Rubber was masticated by passing through the rolls for 2 min. After the nerve has disappeared compounding ingredients were added. Finally the stock was homogenized by passing through the tight nip of the mill for six times and sheeted out at a nip gap of 3mm. Mixing time and temperature were controlled during the process.

Brabender plasticorder

Brabender plasticorder used was having a volume of 40cc (PL 3S model). There are horizontal rotors with protrusions in the mixing chamber. A dynamometer balance measures the resistance caused by the mixing and shearing of the test material against the rotating rotors. A mechanical measuring system attached to the dynamometer measures the torque. A DC thyrister controlled drive is used for controlling the speed of rotors (0 to 150 rpm). A thermocouple with a recorder is used for temperature measurements.

2.4.3 Cure characteristics

Cure studies were done in a Rubber Process Analyzer; RPA 2000 Alpha Technologies. The RPA 2000 rubber process analyzer is a new dynamic mechanical rheological tester (DMRT) designed to measure the dynamic properties of raw polymers, uncured compounds and final cured compounds. It investigates the physicomechanical properties of polymers before, after or during the process of curing.

It has two directly heated opposed biconical dies. Approximately 5g of the sample is placed in the lower die, and is oscillated through a small deformation angle at a frequency of 50 cycles per minute (cpm). The torque transducer on the upper die senses the force transmitted through the rubber

sample. The measurements made by the torque transducer are fed into the computer. The selected properties are measured and the results are calculated and displayed. Data obtained from a torque-time curve is given in Table 2.6.

Table 2.6. Data obtained from the torque-time curve

Data obtained	Description
Minimum torque M_L	Torque obtained for the homogenized mix at the test temperature before the onset of cure
Maximum torque M_H	Maximum torque obtained during curing
Torque M_T	Torque at a given time.
Induction time T_5	Time taken for 5% vulcanization.
Scorch time T_{10}	Time for obtaining 10% of the maximum torque.
Optimum cure time T_{90}	Time taken for reaching 90% of the maximum torque

Cure rate index (CRI) can be calculated from the equation

$$CRI = 100/T_{90} - T_{10}$$ ---(1)

Where T_{90} and T_{10} are the optimum cure time and scorch time respectively.

Cure charecteristics of the samples were determined using RPA 2000 at a temperature of 160^0C as per ASTMD 2084-01

2.4.4 Moulding

The test specimens were moulded in standard moulds by compression moulding on an electrically heated hydraulic press having 45 cm × 45cm platen at a pressure of 200 kg /cm^2 at 160^0C for an optimum cure time. After curing the mouldings were cooled by dipping in cold water and conditioned for 24 hrs before testing.

2.4.5 Physical tests

Tensile properties

Tensile strength is the force per unit area of cross section, which is required to break the test specimen, provided the stress is substantially uniform over whole of the cross section.

Tensile strength=load (N) /area of cross section (mm^2) -------------(2)

Elongation at break is the maximum value of elongation, expressed as a percentage of the original length.

Elongation a break= $(L-L_0)100/L_0$ -------------------------------------(3)

L_0 and L are the initial and final length of the sample.

The value of tensile stress (force/unit area) required to stretch the test piece from the unstrained condition to a given elongation is called modulus or tensile stress at a given strain.

It is expressed in the unit of stress (MPa or N/mm^2)

These Tests were carried as per ASTM D 412-2002 on a Shimadzu Model AGI Universal Testing Machine using test specimens punched out from the molded sheet using the C-type die. The measurements were carried out at a cross head speed of 500 mm/min.

Tear strength

Tear strength or tear resistance is, how well a material resists the growth of any cut when under tension. It is expressed in N/mm.

Tear strength = Load (N) / Thickness (mm) --------------------------(4)

Tear strength of the samples were tested on Shimadzu Model AGI Universal Testing Machine according to ASTM D 624–2000 using un-nicked 90^0 angle test specimens that were punched out from the moulded sheets, along the mill grain direction. The measurements were carried out at a crosshead speed of 500 mm per minute.

2.4.6 Swelling studies

Known weights of circular specimens, 20mm in diameter, punched out from the vulcanized sheets were immersed in suitable solvents. For NBR, methyl ethyl ketone (MEK) and for SBR, toluene was taken as the solvent. Samples were periodically taken out from the solvent, quickly dried using a filter paper and weighed. The weights of the swelled samples were determined at regular intervals until no further increase in solvent uptake was noted.

Swelling index and Solvent uptake were computed according to the following equation.

$$\text{Swelling index} = W_S\text{-}W_i/W_i \times 100 \text{ -------------------------------------}(5)$$

Where W_S is the weight of the swollen sample and W_i is the initial weight of the sample i.e. the weight of the sample before swelling.

$$\text{Solvent uptake Qt \%} = \frac{\text{Mass of solvent sorbed/Molar mass of solvent}}{\text{Mass of polymer}} \times 100 \text{ --}(6)$$

2.4.7 Strain sweep studies

Strain sweep studies were conducted on unvulcanized samples to study rubber filler interaction. The RPA 2000 rubber process analyzer is a

new dynamic mechanical rheological tester (DMRT) designed to measure the dynamic properties of raw polymers, uncured compounds and final cured compounds. The instrument reads strain and torque signals through appropriate softwares. RPA performs strain sweep tests in which variation of storage modulus (G'), loss modulus (G") and complex modulus (G*) with the change in strain amplitude are measured.

The procedure involves loading the RPA cavity with an excess volume of test material. As per, ASTM D 5289, about 5 gm (4.4 cc) of a standard filled rubber compound with specific gravity 1.14g/cc is recommended.The samples were prepared by die cutting 46mm diameter disks from a 2mm thick sheets of test material. Testing temperature was selected as 100^0 C and the shear strain was varied from 0.5% to 40% keeping the frequency of measurements at 0.5 Hz.

2.4.8 Thermogravimetric analysis (TGA)

Thermogravimetric analysis is a thermal analysis technique available for understanding the thermo-physical properties of materials. TGA aims at the investigation of pyrolysis and thermal degradation behaviour of solids [2]. It monitors the mass of a sample as a function of temperature or time while the substance is subjected to a controlled temperature programme [3]. The integral (TGA) and derivative (DTG) thermogravimetric curves give information about thermal stability and extent of degradation of the polymeric material. The heating process brings a lot of changes in the material and finally leaves behind the inorganic filler as the inert residue. TGA studies were carried out on a Q50 (TA Instrument). The analyzer comprises of a high precision balance with a pan to load the sample. The loaded pan is placed in an electrically heated oven with a

thermocouple to measure temperature. The sample weight should be about 8-10 mg. TGA scans are recorded at a constant heating rate in the temperature range ambient to 800^0C at a heating rate of 10^0C/min in nitrogen atmosphere.

2.4.9 Differential scanning calorimetry (DSC)

Differential scanning calorimetry is also a thermal analysis technique for measuring the energy necessary to establish nearly zero temperature difference between a substance and a reference material whilst the two specimens are subjected to controlled temperature programme. One of the major applications of DSC is the measurement of glass transition temperature. Physical properties of the polymer undergo dramatic changes at T_g, where the material undergoes a change from glass to rubbery state.

DSC measurements were conducted using a DSC, Q-100 (TA instrument) calorimeter having a temperature accuracy of $+/-1^0$ C. The samples were heated at a rate of 10^0C /min from ambient to 100^0C. ·

2.4.10 X- **ray diffraction (XRD)**

X-ray diffraction studies are used for the characterization of crystalline materials and their structure determination. X-ray diffraction is based on constructive interference of monochromatic X-rays and a crystalline sample. Each crystalline solid has its unique characteristic X-ray powder pattern which may be used as a "fingerprint" for its identification [4].

From the diffractogram particle size are calculated using the Debye-Scherrer equation.

$$D = 0.9 \lambda / \beta \cos \theta \quad \text{---(7)}$$

where D is the particle size, λ is the wavelength of the incident x-ray beam, β is the full width at half maximum (FWHM) of an hkl X-ray diffraction peak at θ value, and θ is half of the diffraction angle 2θ corresponding to the peak. By using Braggs law $n\lambda = 2d\sin\theta$, the crystallographic spacing (d) for clay could be computed. Increase or decrease of spacing gives information about the type of polymer composite formed. Immiscible will show no change in d spacing, for intercalated composites d spacing increases, for deintercalated, d spacing decreases and for exfoliated the spacing may be so expansive and disordered to give a signal [5].

Xray diffractograms were recorded using Bruker AXS D8 Advance Diffractometer with CuKα radiation of wavelength 1.54 A°, tube voltage 40KV and tube current of 25 mA. XRD results were obtained in the range $2\theta = 3$ to 80^0 at a scan rate of 4^0/min.

2.4.11 Fourier transform infrared spectroscopy (FTIR)

FTIR is a good analytical tool used to determine the structure and functional groups in a molecule. FTIR aims at determining the molecular structure by detecting the characteristic vibrational frequencies of molecules. For a vibrational mode in a molecule to be IR active, it must be associated with changes in the permanent dipole FTIR analysis was conducted using Thermo Nicolet, Avatar 370 model IR spectrometer, in 4000-400cm^{-1} spectral range with a resolution of 4cm^{-1}. Here transmittance % is presented as the function of wave number (cm^{-1}).

2.4.12 High resolution transmission electron microscopy (HRTEM)

Direct imaging of individual nano particles is made possible by TEM. TEM is unique since it provides a real space image on the atom distribution in the nanocrystal and on its surface. The JEOL JEM 2100 High Resolution Transmission Electron operating at 200 kV acceleration voltages was used for the study.

2.4.13 Scanning electron microscopy (SEM)

Scanning electron microscopy is a method for high-resolution imaging of surfaces. The method uses a focused beam of high-energy electrons to generate a variety of signals at the surface of solid specimens. These signals include secondary electrons, back scattered electrons, diffracted backscattered electrons, photons, visible light, and heat. Of these, the signals produced by secondary electrons are the most important for studying the morphology and topography of the samples.

Morphology of the samples were studied using a scaning electron microscope JEOL Model JSM - 6390LV. Gold coated samples were used for analysis

Field Emission Scanning Electron Microscope (FESEM) of Hitachi SU6600 Model was also used for the study.

2.4.14 Electron dispersive spectrometer (EDS)

Qualitative elemental analysis, standardless quantitatve analysis, Xray line scans and mapping are performed with SEM-EDS combination. EDS has the specification JEOL Model, JED-2300.

2.4.15 Inductively coupled plasma atomic emission spectrometer (ICP-AES)

Elemental composition of a sample can be determined from the emission of atomic spectrum. The element can be identified by the wavelength at which emission occurs and the concentration can be detected by the intensity of the emitted radiation.

ICPAES analysis is done using Thermo Electron IRIS INTREPID II XSP DUO, with a resolution of 0.005nm to 200 nm.

2.4.16 Atomic force microscopy (AFM)

AFM permits resolution of individual atoms on both conducting and insulating surfaces [6]. AFM consists of a cantilever with a sharp tip at its end that is used to scan the specimen surface. The performance of an AFM critically depends on the physical characteristics of the cantilever and tip. Three modes are commoly used in AFM (1) Contact mode when the tip is in costant contact with the surface of the sample (2) The tapping mode when the tip periodically contacts the surface for only a brief time and then is removed from the surface (3) The non contact mode when the tip hovers a few nanometers above the sample surface.

AFM images were obtained by using a Park Model XE 100 in non contacting mode. Anisotropic silicon probes with 125 μm × 40 μm × 4 μm mounted on a rectangular beam with a spring constant of 40 N/m and a resonance frequency of 200-300 kHz with a scan rate of 1Hz were used for the measurements. Fig.2.1. gives the block diagram of AFM.
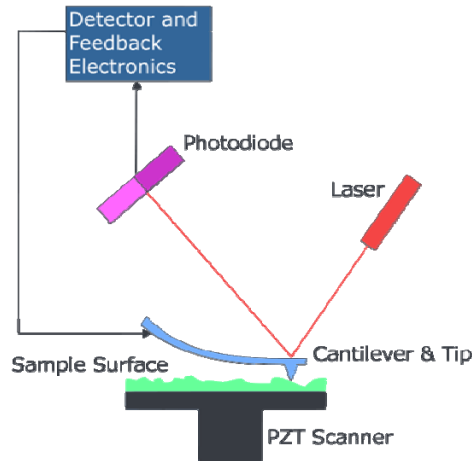
Fig.2.1. Block diagram of Atomic Force Microscope

2.5 Conductivity studies

2.5.1 DC electrical conducivity

DC electrical conducivity of nanotube and graphene filled samples were measured by a standard two probe electrode configuration using a Keithley Nanovolmeter at room temperature. Rectangular strips of the sample ($4\times 2\times 2$ mm) were placed between two electrodes through which current was passed. Resistance was measured directly from the instrument and conductivity was calculated using the formula

$$\sigma \text{ (S/cm)} = (I/V) \times l/A \quad \text{---(8)}$$

where σ is the electrical conductivity I is the current (amperes), V is the voltage (volts), l is the thickness of the sample (cm) and A is the area of contact of electrodes with sample (cm^2).

2.5.2 Microwave studies using cavity perturbation technique

Cavity perturbation technique was used for studying the dielectric properties of materials at microwave frequencies. When a dielectric material

is inserted into a cavity resonator the resonant frequencies of the cavity are perturbed at the position of maximum electric field. At this position the contribution of magnetic field for perturbation is minimum [7, 8].

The basic idea of the cavity perturbation is the change in the overall geometric configuration of the elecromagnetic fields with the insertion of a small sample. So from the measurement of perturbation of the sample, the dielectric parameters like dielectric permittivity, dielectric loss, skin depth and AC conductivty were calculated. The measurements were done using Agilent Performance Network Analyzer E8362B in the S band (2-4GHz) frequency region.

Design of cavity resonators

Cavity resonators are made of brass or copper wave-guides.They are either rectangular or cylindrical. The inner walls of the cavity are coated with silver. The S band rectangular wave guides have a dimension of 34.5cm×7.2cm×3.4cm.

Theory

The introduction of a dielectric material into the resonant cavity will produce a field perturbation given by Kupfer et al. as

$$-\frac{d\Omega}{\Omega} \approx \frac{(\varepsilon^* - 1)\int\limits_{V_s} EE_0^* dV}{2\int\limits_{V_c} |E_0|^2 dV} \quad \text{---(9)}$$

$d\Omega$ - Complex frequency shift
Vs   - Volume of sample
V_c - Volume of cavity

E_0 - Electric field in the unperturbed cavity

E - Electric field in the perturbed cavity

$\varepsilon*$ - Relative complex permittivity of the sample

$\varepsilon* = \varepsilon' - j\varepsilon''$

ε' - Real part of complex permittivity

ε'' - Imaginary part of complex permittivity

The real part of complex permittivity known as dielectric constant or dielectric permittivity gives the amount of induced and permanent alignment.

Dielectric constant $\varepsilon' = 1 + V_c./V_s \; f_0 - f_s/2f_s$ -------------------------- (10)

Dielectric loss is the energy required to align dipoles or move ions.

Dielectric loss $\varepsilon'' = V_c / 4V_s . \; (Q_0 — Q_s)/ Q_0 \, Q_s$ ----------------- (11)

Skin depth or penetration depth δf gives the effective distance of penetration of an electromagnetic wave into the material [10] .

$\delta f = 1/\alpha f$ -- (12)

αf is the absorption coefficient. It gives the absorption of electromagnetic waves when it passes through the medium.

AC conductivity σe is given as, $\sigma e = 2\pi \; f \, \varepsilon_0 \, \varepsilon''$ ----------------- (13)

Method

Resonance frequency f_0 and the quality factor Q_0 of the cavity in the unperturbed conditions are measured initially. Then the sample is inserted into the cavity and positioned at the maximum electric field. Resonance frequency fs and quality factor Qs after loading the samples are again measured. From this, the permittivity values are calculated.

References

[1]   Blackley, D.C. Polymer Latices Science and Technology, Chapman and Hall, London, UK. 1997,3,12.

[2]   Flynn, J. H. Thermochim. Acta. 1974, 8, 69.

[3]   Neil,C.M. Editors Allen, Sir Geoffrey and Bevington, J.C. Comprehen. Polym. Sci. Pergamon Press, New York. 1989,15.

[4]   Chandran, S.Ph.D Thesis, Cochin University of Science and Technology, India, 2008.

[5]   Koo, J.H. Polymer nano composites, Processing, Characterization and Applications, McGraw-Hill. 2006, 81.

[6]   Skoog, Hooler, Crouch. Instrumental analysis, India Edition. CENGAGE learning.2007, 677.

[7]   Meng, B. Booske, J. Cooper, R. IEEE Transactions on Microwave Theory and Techniques. 1995,437.

[8]   Santra, M. Limaye, K. U. IEEE Transactions on Microwave Theory and Techniques. 2005, 53.

[9]   Kupfer, K. Kraszewski, Knochel, R. Sensors UpdateVol 7 and Microwave sensing of moist materials, food and other dielectrics. Wiley- VCH, Germany, 2000, 186-209.

[10]   Stephen, C.W. Frederic, H.L. Microwave made simple: Principles and applications. United States, Brookcrafters, Chelesa. 1985.

.....೧೧೩.....

Chapter 3

CHARACTERIZATION OF FILLERS, OPTIMIZATION OF CURING PARAMETERS AND PREPARATION OF COMPOSITES

Contents

CHARACTERIZATION OF FILLERS

3.1 Introduction

The term 'filler' in rubber technology is used as a misnomer for materials primarily intended to reduce the cost of the more costly rubber. But for scientists and researchers, fillers are the most important materials available for improving the properties of elastomers. They occupy a prime position because of their significant contribution to reinforcement and processabiliy. Traditional fillers like carbon black and silica are now replaced by nano scale fillers like layered silicates, carbon nanotubes, graphene etc.

Layered silicates, belonging to the family of phyllosilicates are most often used in the preparation of polymer layered silicate nanocomposites. Carbon nanotubes and graphene, because of their unique potential uses for structural, electrical and mechanical properties are also of immense interest to the scientific society.

Part I of this chapter deals with characterization of the fillers used - nanokaolin, vinyl silane grafted nanokaolin, mullti walled carbon nanotubes and graphene nanoplatelets. Fillers were characterized by XRD, FTIR and SEM analysis.

3.2 Experimental

Materials

Nanokaolin and vinyl silane grafted nanokaolin were obtained from English Indian Clays Ltd. Veli, Thiruvananthapuram.Specification is given in Table 2.3

Multi walled carbon nanotube (MWCNT) was obtained from Baeyer Materials Science AG (Leverkusen Germany). Specificaion is given in Table 2.4. Graphene nanoplatelet was purchased from Quantum materials limited, Bangalore.

Nanokaolin is designated as 'C' and Vinyl silane grafted nanokaolin as 'V'. Multi walled carbon nanotubes are referred as 'MWCNT' and Graphene nano platelets as 'graphene'

Characterization Techniques

Fillers used in this study were characterized by XRD, FTIR and SEM analysis.

Xray diffractograms were recorded using Bruker AXS D8 Advance Diffractometer with CuKα radiation of wavelength 1.54 A°. FTIR analysis was conducted using Thermo Nicolet, Avatar 370 model IR spectrometer. SEM morphology of the samples were studied using a scaning electron microscope JEOL Model JSM - 6390LV. Details of XRD, FTIR and SEM analysis are given in Sections 2.4.10, 2.4.11 and 2.4.13 respectively.

3.3   Results and Discussion
3.3.1 Nanokaolin
3.3.1.1 X-ray diffraction analysis (XRD)

Fig.3.1 shows the Xray diffraction pattern of nanokaolin (C). The characteristic peaks of nanokaolin are seen around $2\theta = 12.5^0$ (d=7.05A^0), $2\theta= 20^0$ (d= 4.41A^0), and $2\theta= 25^0$ (d=3.55A^0) [1, 2]. Using Debye-Scherrer equation the particle size of nanokaolin was calculated as 16nm.

Fig. 3.1. X-ray diffraction pattern of nanokaolin('C')

3.3.1.2 Fourier transform infrared spectroscopy (FTIR)

Fig. 3.2. shows the FTIR spectrum of nanokaolin.The characteristic stretching vibration of nanokaolin at 3695, 3670, 3650 and 3625cm^{-1} are seen in the figure. These are attributed to the surface hydroxyl groups.The band at 3625cm^{-1}is due to the inner hydroxyl groups and are not affected by intercalation [3].
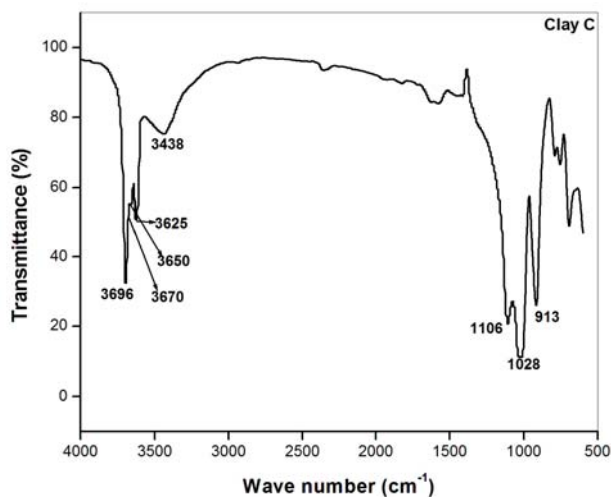
Fig. 3.2. FTIR spectrum of nanokaolin ('C')

Strong bands at 1106 cm^{-1} represents the perpendicular Si-O vibrations and the absorption peaks at 1028 cm^{-1} and 913 cm^{-1} gives the Si-O-Si stretching and Al-OH bending vibration respectively.

3.3.1.3 Scanning electron microscopy (SEM)

Fig.3.3 and Fig.3.4 show the SEM images of ball milled nanokaolin and sonicated nanokaolin respectively under different magnification. In ball milled nanokaolin large flakes are stacked together to form agglomerates. On sonication the size of the clay platelets were reduced and agglomeration was less due to stacking of smaller kaolin platelets.
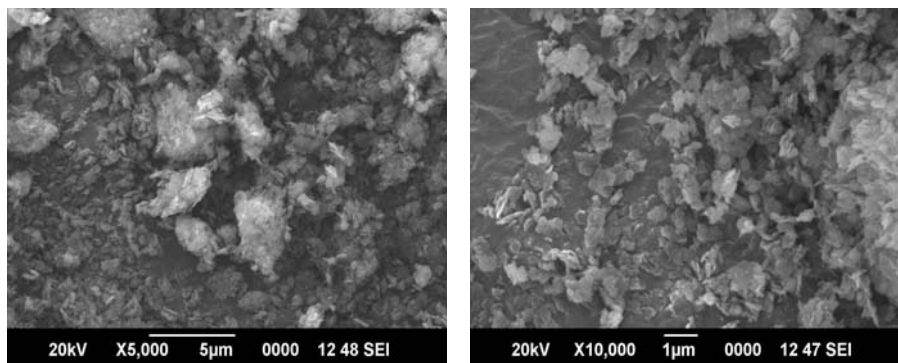
Fig. 3.3. SEM images of ball milled nanokaolin
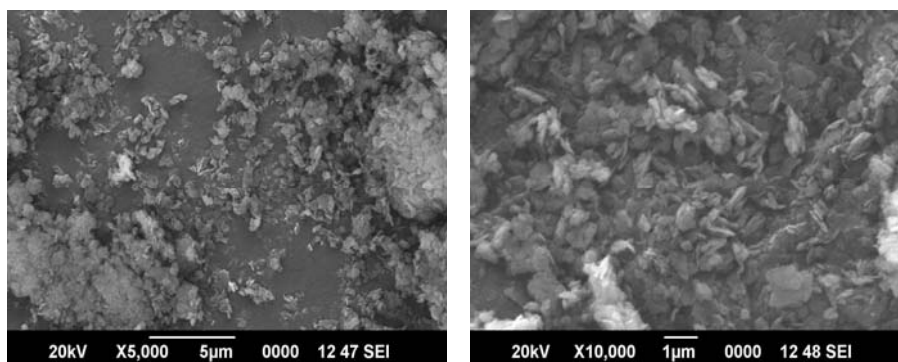
Fig. 3.4. SEM images of sonicated nanokaolin

3.3.2 Vinyl silane grafted nanokaolin

3.3.2.1 X-ray diffraction analysis (XRD)

Fig. 3.5 gives the XRD pattern of vinylsilane grafted nanokaolin.

Vinylsilane grafted nanokaolin showed diffraction peaks at $2\theta=12^0$(d=7.1A^0), 20.09^0(d=4.41A^0) and 25^0(d=3.55 A^0). The decreased intensity of the peak at $2\theta=20.09^0$ was an indication that the number of clay particles having spacing 4.41 A^0 was very small. Since the d values of 'C' and 'V' are almost the same, it might be inferred that grafting had taken place only in some of the OH groups on the edge surface of nanokaolin and that grafting of vinylsilane on nanokaolin had not increased the inter layer spacing. Particle size as determined from Debye-Scherrer equation was 21 nm.
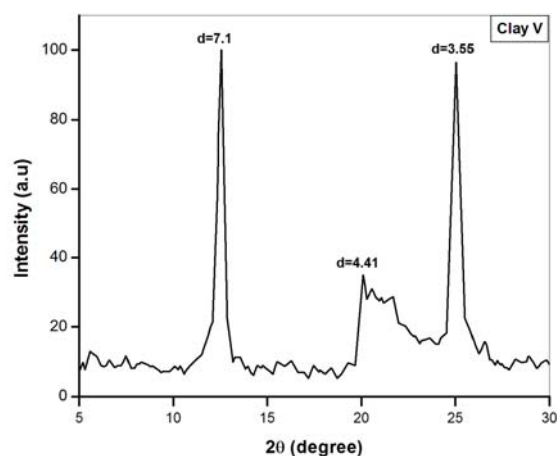
Fig. 3.5. X-ray diffraction pattern of vinylsilane grafted nano kaolin ('V')

3.3.2.2 Fourier transform infrared spectroscopy (FTIR)

Fig 3.6 shows the FTIR spectrum of vinylsilane grafted nanokaolin. The characteristic stretching vibration of OH groups of kaolin at 3698, 3676, 3652 and 3624 cm^{-1} were seen in the modified nanokaolin ('V') also. The band at

3624 cm^{-1} was the stretching band of internal hydroxyl group. The other three bands were attributed to inner surface hydroxyl groups [4]. Band at 2925cm^{-1} was the symmetric C- H vibration of Si-O-CH$_3$ [5] and the band at 2855cm^{-1} was the aliphatic C-H stretching vibration.Water molecules coordinated on octahedral Al ions were characterized by the band at 1580 cm^{-1}[6]. At 1418 cm^{-1} CH$_2$ groups and vinyl groups merged together [5]. Perpendicular Si-O vibrations were found at 1111cm^{-1}[4]. 1031cm^{-1} was the in plane Si-O-Si stretching vibration. 915cm^{-1} represented the Al-OH bending and the bands at 700cm^{-1},753cm^{-1} were the OH bend (out of plane) of alcohols.
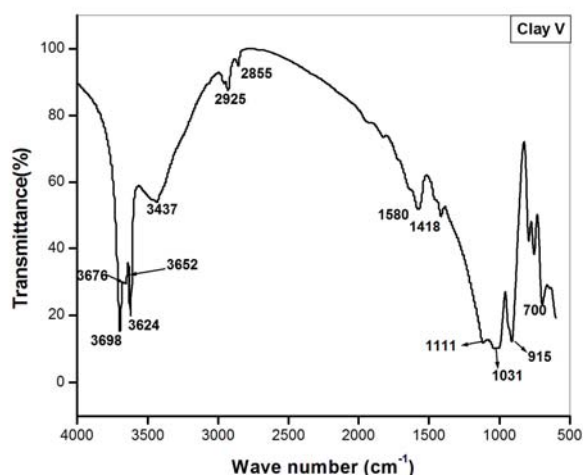
Fig. 3.6. FTIR spectrum of vinylsilane grafted nanokaolin ('V')

3.3.2.3 Scanning electron microscopy (SEM)

Fig.3.7 and Fig. 3.8 shows the SEM photographs of the ball milled and sonicated vinylsilane grafted nanokaolin under different magnification. It was seen that sonication reduced the size and agglomeration of clay particles. Clay flakes seemed to have angular edges with size in the range 40 nm. The particle size was greater than that determined from Debye-Scherrer equation, due to agglomeration of particles.
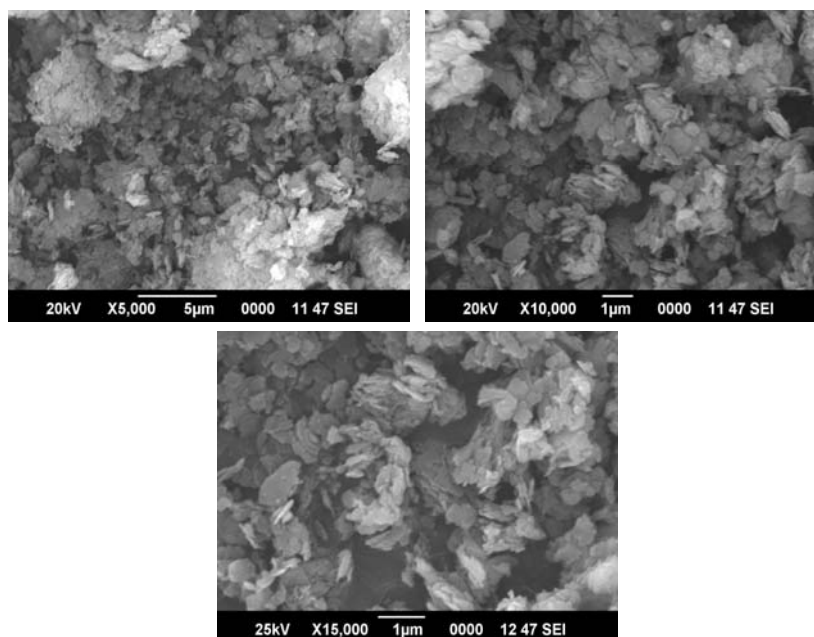
Fig. 3.7. SEM images of ball milled clay 'V'
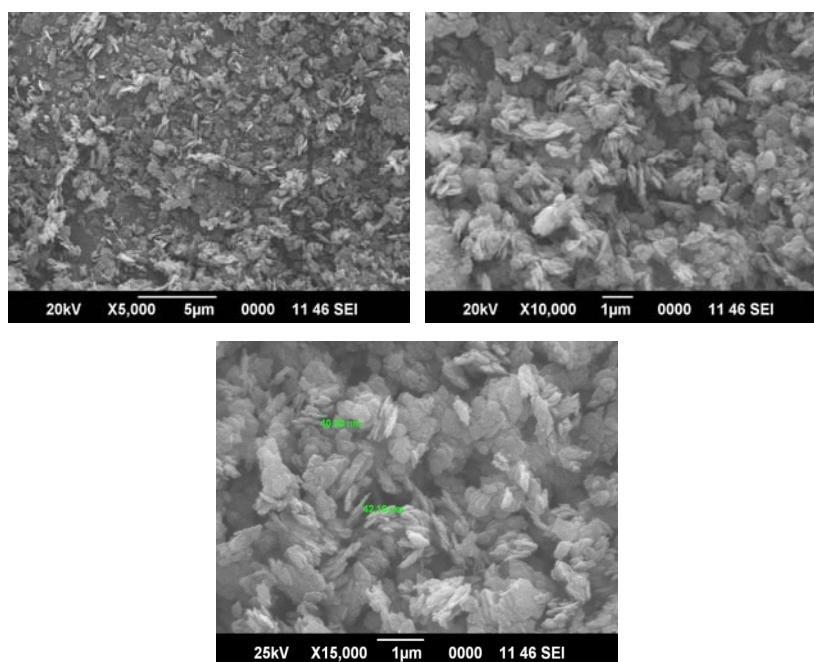
Fig 3.8. SEM images of sonicated clay 'V'

3.3.3 Multi walled carbon nanotube
3.3.3.1 X-ray diffraction analysis (XRD)

Fig.3.9 shows the Xray diffraction pattern of MWCNT.

MWCNT displayed one diffraction peak at $2\theta = 25.7^0$ corresponding to a basal spacing of 3.5 A^0. This is the characteristic peak of MWCNT. Particle size was found to be 40 nm.
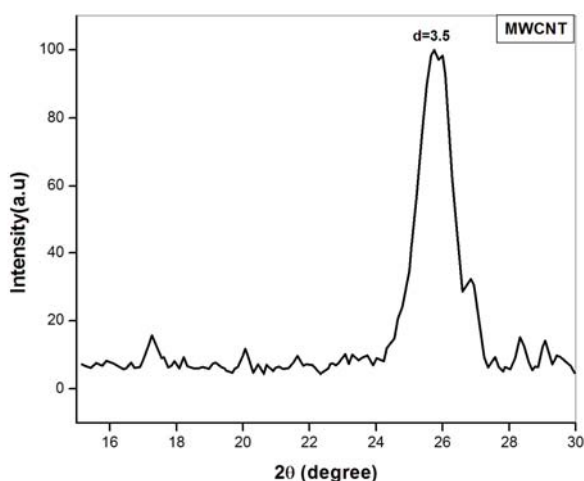
Fig. 3.9. X ray diffraction pattern of MWCNT

3.3.3.2 Fourier transform infrared spectroscopy (FTIR)

Fig.3.10 shows the FTIR spectrum of MWCNT. It did not show any characteristic peak in the spectrum. The as obtained MWCNT was further purified by refluxing with HCl for 24 hrs. Fig.3.11 shows the FTIR spectrum of acid treated MWCNT. The spectrum of MWCNT after acid treatment showed bands at 3430cm-^{1} and 1640cm,-^{1} attributed to hydroxyl groups and carbonyl groups respectively [7]. The two bands at 2850 cm^{-1} and 2930cm^{-1} were assigned to the CH stretching vibrations. The peak at 1558cm^{-1} correspond to the stretching mode of C=C bond that formed the frame work of carbon nanotube sidewall [8].

Results indicate that oxygen containing functional groups such as hydroxyl and carbonyl groups were introduced on the naotube surface due to the elimination of part of catalytic metallic nanoparticles, during purification process [9]. Introduction of these hydrophilic groups on nanotube surface might have helped MWCNT to disperse easily in aqueous medium.
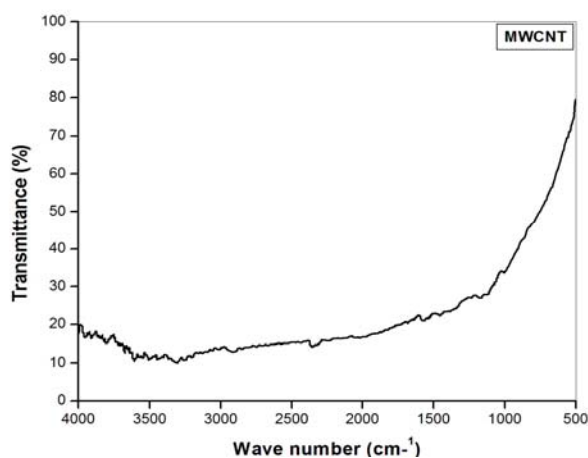
Fig. 3.10. FTIR spectrum of MWCNT before purification
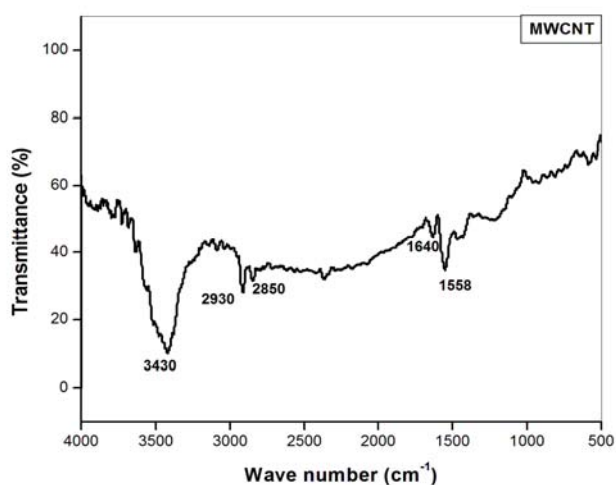
Fig.3.11. FTIR spectrum of acid treated MWCNT

3.3.3.3 Scanning electron microscopy (SEM)

Fig.3.12 (A) shows the SEM image of MWCNT before purification. It showed low purity and the samples remained as bundles. Fig.3.12 (B) and (C) shows the SEM images of MWCNT after purification. On purification they unbundle but remain entangled and appear as loose curly thread like entities. The entanglement was due to van der Waals effect arising from sp^2 C-C bonding [10]. Their diameter as seen from the SEM image was in the range 60-80nm. It was difficult to make out the accurate length of the nanotubes due to twisting of the tubes.
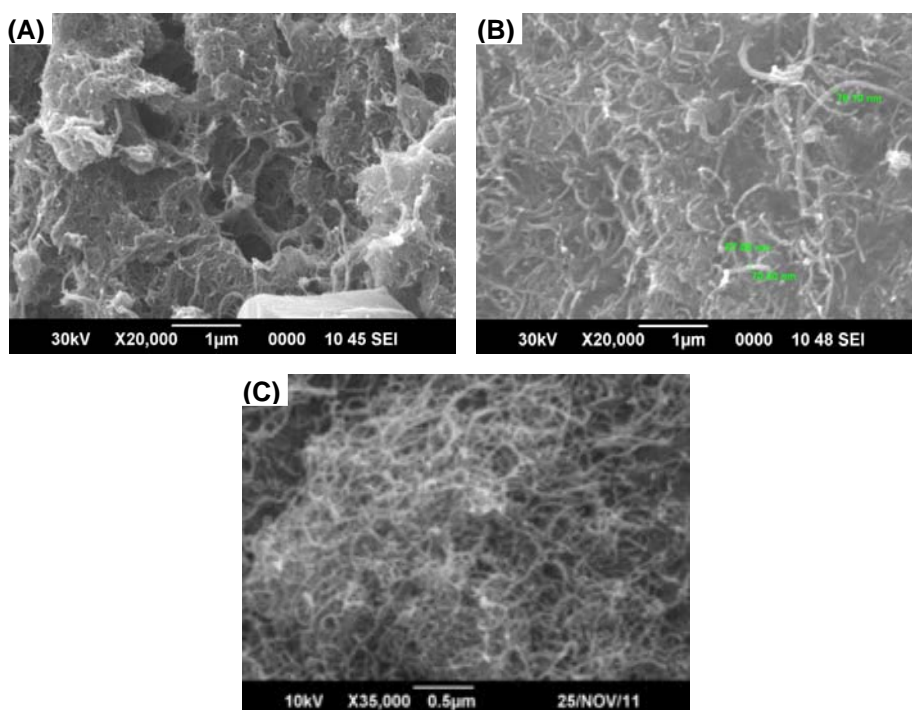
Fig.3.12. SEM images of MWCNT (A) before purification (B) and (C) after purification

3.3.4 Graphene
3.3.4.1 X-ray diffraction analysis (XRD)

Fig.3.13 shows the XRD pattern of graphene. Literature reports the 2θ value of graphite as 26^0 with an interlayer spacing of $3.4A^0$ and the XRD of pure graphene to be devoid of any peak [11, 12, 13].

The diffraction peak obtained for graphene sample at $2\theta=26^0$ with an interlayer spacing of $3.4A^0$ was consistent with the layer spacing of graphite. So the interlayer spacing of the graphene sheets might have a structure similar to that of graphite [11]. Also it is reported that graphene nanoplatelets are not a single graphene layer but rather consists of a number of graphene sheets [14].
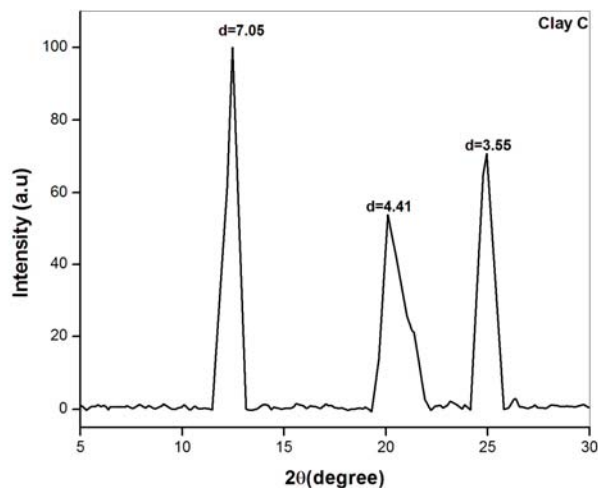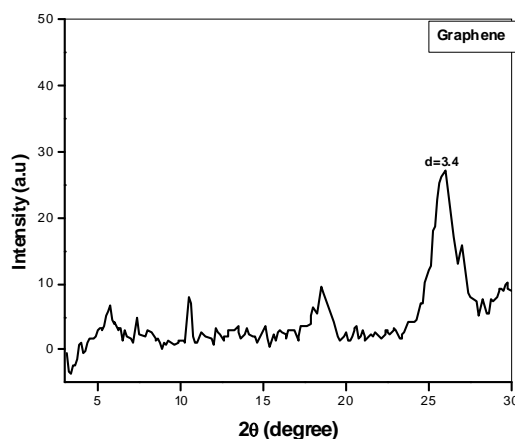

Fig.3.13. Xray diffraction pattern of graphene

3.3.4.2 Fourier transform infrared spectroscopy (FTIR)

Fig.3.14 shows the FTIR spectrum of graphene. The peak at $3696cm^{-1}$ could be attributed to the stretching vibration of adsorbed water molecules and the peak at $1546cm^{-1}$ gave the skeletal vibrations of graphene sheets.The peak at $1442cm^{-1}$ gave the aliphatic CH bending [13] of graphene.
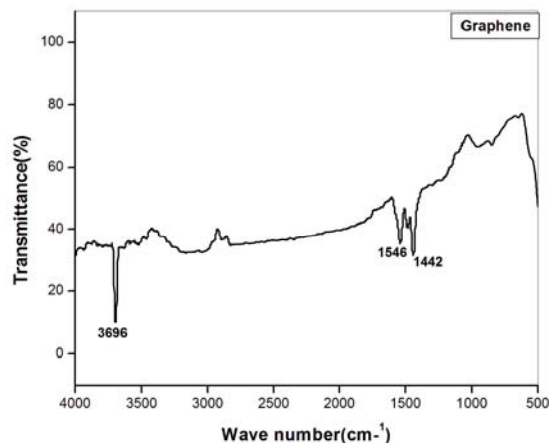
Fig. 3.14. FTIR spectrum of Graphene nanoplatelet

3.3.4.3 Scanning electron microscopy (SEM)

Fig.3.15 shows the SEM images of graphene. The anisometric shape of graphene caused coplanar alignment of sheets into layered aggregates. The surface of aggregated sheets were fairly smooth and seemed to consist of thin stacks anchored with each other at the edge of the platelets. Thus the graphene nanoplatelets actually consisted of several layers of graphene sheets.
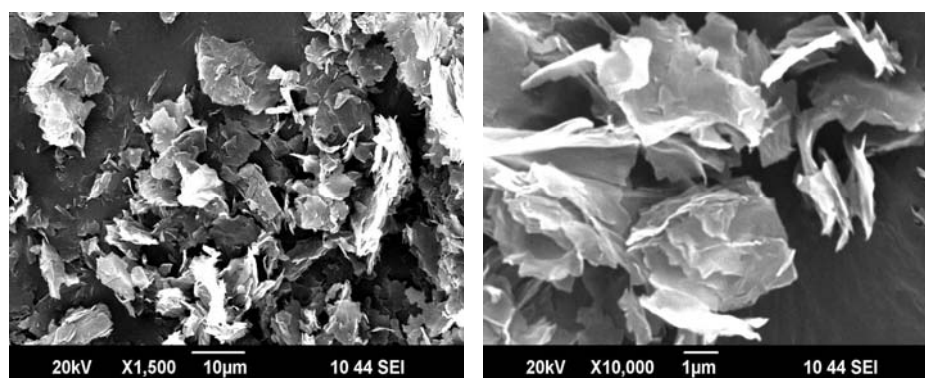
Fig. 3.15. SEM images of graphene nanoplatelets

3.4 Conclusions

XRD analysis gave the characteristic peaks of nanokaolin at $2\theta=12^0$, 20^0 and 25^0. Grafting of vinyl silane did not increase the interlayer spacing of modified clay. MWCNT had diffraction peak at $2\theta =25.7^0$ corresponding to a basal spacing of 3.5 A^0.

From XRD analysis, particle sizes of nanokaolin, vinylsilane grafted nanokaolin, MWCNT and graphene were found to be 16, 21, 40 and 15 nm respectively.

FTIR spectrum of nanokaolin gave the characteristic stretching vibration of hydroxyl groups and the stretching and bending vibrations of Si-O-Si and Al-OH groups. In vinyl modified clay there was no decrease in the absorbance of OH stretching frequency. This showed that silanes have reacted only with some of the OH groups of kaolin, preferably with OH groups on the edge surface, due to steric hinderance. MWCNTshowed no characteristic peak for virgin material. But on purification with acid, polar hydroxyl and carbonyl groups were introduced on the surface of MWCNT.

SEM images showed, sonication of clay reduced the size and agglomeration of the clay particles. Acid treatment of MWCNT reduced bundling of nanotubes and they appeared as loose, curly thread like entities. A smooth layered structure of graphene was visible in the SEM image.

Part 2

OPTIMIZATION OF CURING PARAMETERS

Until recently, most of the studies on polymer clay composites were dealt in detail with thermoplastic [15-20] and thermosetting matrices [21-24]. Relatively very little attention has been paid to rubber composites. Among the various nanoclays used for composite preparation, montmorillonite takes prime position. Polymer clay nanocomposites derived from organically modified montmorillonite have been extensively studied, as shown by a large number of publications on the subject [25-28]. Studies on kaolin polymer nanocomposites are at its infancy. Rubber/modified kaolin composites are prepared by Zoromba et al.[1] and Sukumar [29]. Nanokaolin and nanosized hydroxyl aluminium oxalate (nano-HAO) were used in low density polyethylene (LDPE)/ethylene propylene diene rubber (EPDM) blends by Zhi-Hong Chang [30].

Cure characteristics of dry rubber composites are usually determined based on studies from rubber process analyzer (RPA). But for latex composites this is not possible. Cure time of the latex composites are optimised by studying the mechanical properties of the composites. Hence based on literature and experimental investigation a preliminary work was done to optimise the cure time of latex based composites and to find the reinforcing effect of nanokaolin on the mechanical properties of XNBR and SBR latices.

3.5 Experimental

Materials:

XNBR Latex- CLX 530 supplied by Eliokem India Pvt. Ltd.Bombay

SBR latex- Encord 204 supplied by Jubilant Organosys Limited. Gujarat.

Nanokaolin-English Indian Clays Ltd.Veli, Thiruvananthapuram.

Calcium nitrate tetrahydrate supplied by Alpha chemicals, Ernakulam.

All other chemicals are of commercial grade.

Preparation of nanocomposites

Formulation used for the preparation of latex vulcanizates is given in Table 3.1. Dispersion of nanokaolin was made by (1) ball milling for 24 hrs and (2) by sonication for 30min.Compounding of latices was done using 5phr each of ball milled and sonicated nanokaolin. All the ingredients were added to latex in the same sequence as given in the Table 3.1. The addition of each ingredient to the latex was followed by vigorous stirring with a glass rod. After their complete addition the compounded latex was ball milled for 1 hr. It was then kept overnight for maturation.Well cleaned glass plates (10×10cm) were used as formers and calcium nitrate tetrahydrate solution as the coarcervant.

Table 3.1. Formulation for the preparation of latex vulcanisates

Ingredients	XNBR latex mix Dry weight (gms)	SBR latex mix Dry weight (gms)
XNBR latex 50%	100	-
SBR latex 50%	-	100
Wingstay L dispersion 50%	0.75	-
Pot. oleate10%		0.25
Nanokaolin 50% (Ball milled and sonicated)	5	5
ZnO dispersion 50%	3.5	1.5
ZDC dispersion 50%	2.0	1.5
TMTDdispersion 50%	0.5	1.5
S dispersion 50%	1	1.5

Initially the cleaned glass plate was dipped in $Ca(NO_3)_2.4H_2O$ solution and then in the compounded latex. When the latex deposit was partially dry it was again immersed in the $Ca(NO_3)_2$ solution. The process was repeated until a thin latex film of uniform thickness was formed on the glass plate. The glass plates were dried at room temperature. When the film became dry and transparent it was kept in air circulated oven at 100^0C. Sheets were cured for different time intervals (20, 25, 30 and 35 min).

Methods

Vulcanized latex films containing 5phr ball milled nanokaolin and 5phr sonicated nanokaolin were prepared separately and their mechanical properties were studied using Shimadzu Model AGI Universal Testing Machine. Sonication of nanokaolin was done in mechanical probe sonicator (13mm, Vibra Cell Processor VC 750, operating at 40% of the maximum power, 750W).

3.6 Results and Discussion

Fig.3.16. (A)-(D) shows the variation in tensile strength,elongation at break, modulus at 300% elongation and tear strength of the composites plotted against cure time, for XNBR without filler and XNBR containing 5phr each of ball milled and sonicated nanokaolin. From the figure it is clear that the mechanical properties increased by the incorporation of both ball milled and sonicated nanokaolin.
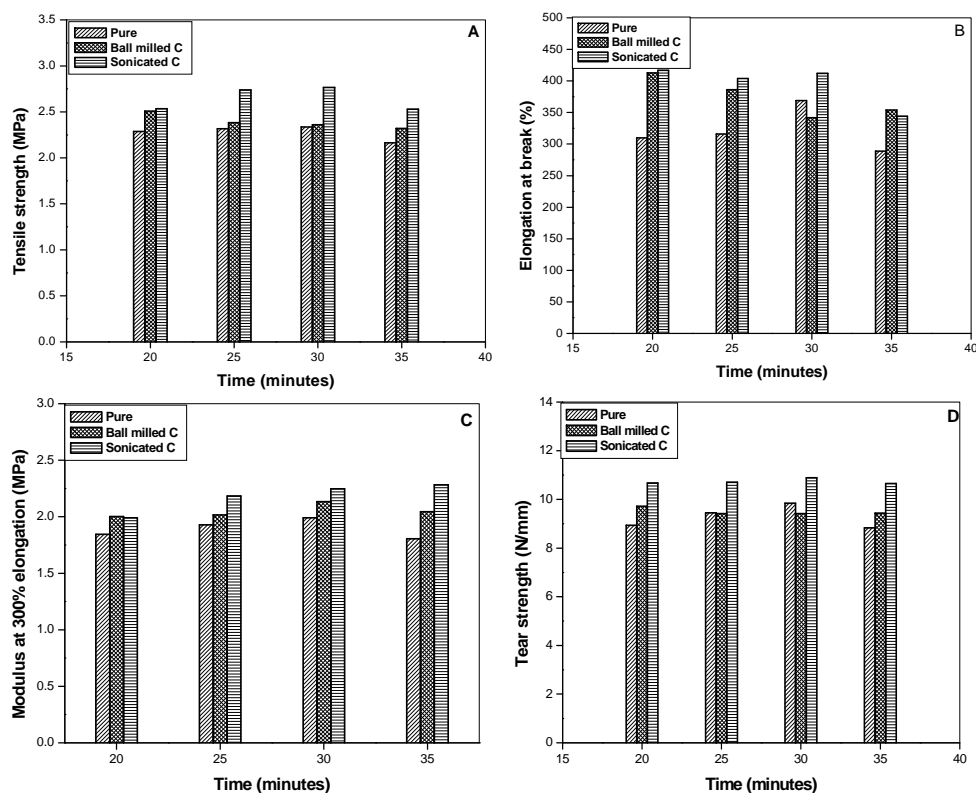
Fig. 3.16. Variation of (A) Tensile strength (B) Elongation at break (C) Modulus and (D)Tear strength against time of vulcanization.

It was seen that the sonicated nanokaolin showed better improvement in mechanical properties than the ball milled sample. SEM images of ball milled and sonicated nanokaolin given in Fig.3.3 and Fig.3.4 show the reduction in agglomeration and size of nanokaolin on sonication. Further Fig. 3.17. shows the ball milled nanokaolin has a greater tendency to settle down when stored for a long period compared to the sonicated sample. All these contributes to the better dispersion of nanokaolin in the polymeric marix leading to the enhancement in mechanical properties of sonicated nanokaolin in XNBR. There was no conspicuous effect in the variation of

curing time on the mechanical properties of the two composites. So the optimum cure time was taken as 30 min.

Fig. 3.17. Dispersions of clay made by sonication (left) and ball milling (right) after 5weeks of preparation

A similar procedure was adopted for preparing SBR nanokaolin films.Here also sonicated and ballmilled nanokalolin were used. Sonicated nanokaolin gave better results and the optimum cure time for SBR latex sheets were taken as 40 min. at 110^0C.

3.7 Conclusion

Both, ball milled and sonicated nanokaolin showed a reinforcing effect in XNBR. But sonicated nanokaolin was found to be much more reinforcing than ball milled sample. After comparing the tensile properties of the latex films, cured at different time intervals, the cure time was optimised as 30min at100^0C for XNBR latex composites and 40 min at 110^0C for SBR latex composites.

Part 3

PREPARATION OF LATEX (XNBR & SBR) AND DRY RUBBER (NBR) BASED NANOCOMPOSITES

Polymer nanocomposites are prepared by different methods like melt compounding [31-33], solution intercalation [31, 34, 35] and latex stage compounding [36, 37]. In melt blending the filler is mixed directly with rubber in the molten state. In solution blending, polymer is dissolved in a suitable solvent along with nanofiller followed by evaporation of solvent to obtain the nanocomposite. For latex composites the method usually employed is mixing of latex and nanofiller followed by coagulation and drying [38-40]. Karger-Kocsis and co-workers [41] prepared NR latex /layered silicate composites by mixing layered silicates and compounding ingredients with rubber latex and then casting on raised glass plates. It was allowed to dry in air till it became transparent and then vulcanized in air circulated oven. Compounding ingredients are added to latices as aqueous solutions if they are water soluble solids or liquids, as dispersions if they are water insoluble solids and as emulsions if they are water insoluble liquids [42].

This part deals with the preparation of dispersions for latex compounding, preparation of filler dispersions, formulations used in the preparation of mixes and preparation of latex based and dry rubber based nanocomposites.

3.8 Experimental

Materials

Materials employed for the preparation of composites include XNBRlatex, SBR latex and NBR (dry rubber) as polymer matrices. Nanokaolin, vinyl silane grafted nanokaolin, MWCNT and graphene were

used as fillers. SDBS and VulcastabVL were used for preparing MWCNT and graphene dispersions. Other compounding ingredients include ZnO, S, TMTD, ZDC, Stearic acid, HS, CBS and wingstay L. The details of all these materials are given in Chapter2.

Methods

Methods for preparing dispersions include ball milling and ultra sonication. For dry rubber composites mixing in two-roll mill and brabender plasticorder are made use of. Cure time of the mixes were determined by RPA and the test specimens were compression moulded. Description of these methods are given in Chapter 2.

3.9   Results and Discussion
3.9.1 Preparation of dispersions for latex compounding:

The compounding ingredients were added to latex in the form of dispersion/emulsion/solution. Table3.2 gives the formulation for preparing dispersions of the latex compounding ingredients.

Table 3.2. Formulation of dispersion

Dispersion (50%)	Dispersol F	Deionized water	Time ball milled (hrs)
Sulphur (100parts)	3	97	72
Zinc Oxide (100parts)	2	98	24
ZDC (100parts)	2	98	48
TMTD (100parts)	2	98	48
Wingstay L (100parts)	2	98	48

3.9.2 Preparation of filler dispersions:

3.9.2.1 Dispersion of clay

Clay dispersion was made by ball milling and ultra sonication. Ball milled clay had a greater tendency to settle down than the sonicated sample,

when kept for a long time. Vials containing dispersions of ball milled and sonicated clay are given in Fig 3.17 and the SEM images of the ball milled and sonicated clays are given in Fig. 3.3. Fig.3.4, Fig.3.7 and Fig. 3.8. Addition of sonicated clay gave better properties to the composite. So sonicated clay was used in the course of the study. Thus nanokaolin ('C') and vinylsilane grafed nanokaolin ('V') obtained as dispersions were sonicated for half an hour before adding to the latex.

3.9.2.2 Dispersion of multiwalled carbon nanotube and graphene

MWCNT and graphene are not easily dispersed in water. Common methods employed for the preparation of dispersions of MWCNT and graphene include chemical modification and noncovalent modification. Chemical modification often leads to destroying their structure while noncovalent modification is simple and convenient. Noncovalent approach involves adsorption of surfactants and polymers on the surface of nanotube and graphene rendering them dispersible in aqueous and organic media. But adsorption of polymers may not be a proper choice for electronic device applications, as polymer itself can participate in electrical events [43]. Use of surfactants reduces this anomaly since they can be washed out easily.

Surfactants or surface active agents when present in low concentration get adsorbed on to the surface of a system and orient in such a fashion that the hydrophobic tail groups face towards the system and the hydrophilic head groups face towards the aqueous phase. This reduces the interfacial tension facilitating the solubility of nanotube and graphene.

Here a range of surfactants were used to evaluate the competing sabilization of MWCNT /graphene dispersions. The dispersing power of

cationic surfactant CTAB (hexadecyltrimethyl ammonium bromide), anonic surfactant SDBS (sodiumdodecyl benzene sulphonate), and non ionic surfactants Tween 80 (Polyethylene sorbitol ester), and Vulcastab VL (Polyethyleneoxide condensate) were explored. Fig.3.18 gives a representation of the surfactants used.
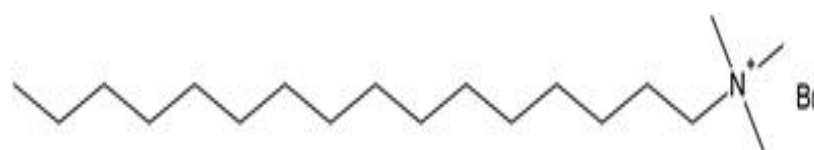
(A) CTAB
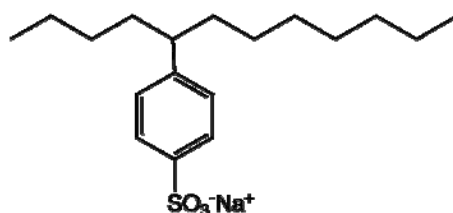
(B) SDBS
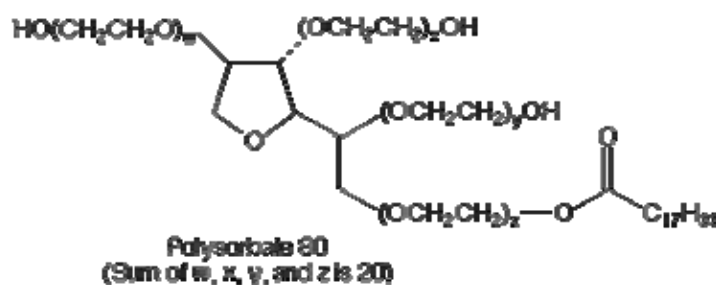
(C) Tween 80

(D) Non ionic surfactant

Fig. 3.18. Representation of (A)CTAB (B) SDBS,(C) Tween 80 (D) a non ionic surfactant

Carbon nanotube dispersions were prepared by sonicating an aqueous suspension of nanotube with the surfactant SDBS for 30 mts. A suitable concentration ratio of MWCNT to surfactant was found out by suspending nanotube in water with various concentrations of different surfactants and sonicating for 30 minutes. The concentration ratio was varied from 1:2 to 1:10 by weight for the different surfactants. The most stable dispersion was obtained for 1:5 ratio in the case of SDBS. The dispersion remained stable for more than five weeks
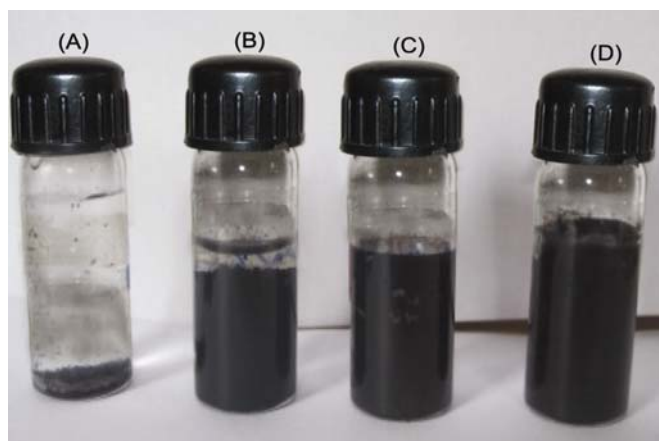
Fig. 3.19. Vials showing the dispersion of MWCNT in (A) pure water (B) water containing CTAB (C) Tween 80 (D) SDBS

Fig.3.19 shows the photographs of vials containing dispersion of MWCNT in water, CTAB, Tween 80 and SDBS. In the absence of a surfactant MWCNT settled at the bottom. Even though the dispersion in Tween 80 was good, the best dispersion was obtained in SDBS. The trend for the dispersing power of surfactants could be explained on the basis of their chemical structure. The presence of a benzene ring structure in SDBS led to greater adsorption to the graphitic surface due to π–π stacking type interaction [44-46]. The tail length of the surfactant also contributed to the dispersing power of the

surfactant. Longer tails means high spatial volume and more steric hindrance, thus providing greater repulsive forces between individual carbon nanotubes [47]. But it is evident that whenever "tail length factor" and "benzene ring factor" compete, the latter contributes more to the formation of dispersion.

Dispersing power of graphene was studied in Vulcastab VL and CTAB. Fig.3.20 shows the vials containing graphene dispersions. VulcastabVL gave a better dispersion. Dispersion in CTAB was also good but it showed a slow tendency to settle down. Graphene dispersions were prepared by sonicating an aqueous suspension of graphene with vulcastabVL for 30 min. Graphene and 20% Vulcastab were taken in the ratio 1:7. The dispersion remained stable for more than 5 weeks.
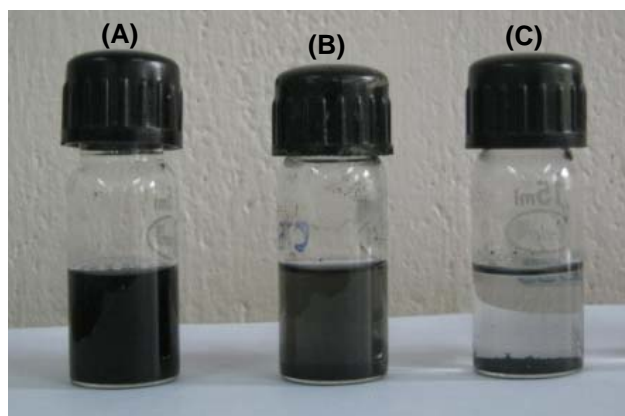
Fig. 3.20. Vials containing the dispersion of graphene in (A) Vulcastab V L (B) CTAB and (C) water.

VulcastabVL is a nonionic surfactant that contains active molecules with no electric charge. They are formed by the condensation of ehylene oxide (hydrophilic part) with an organic hydrophobic compound.

Use of Vulcastab as a dispersing agent for graphene has not been reported so far.

Unlike cationic and anionic surfactants the non ionic surfactant has a low toxicity profile. They are also good latex stabilizer. In the biomedical field poly ethylene oxide is a preferred solubility polymer [48].

3.10 Formulations used in the preparation of compounds

Formulations used in the preparation of XNBR latex compounds, SBR latex compounds, NBR(dry) rubber compounds and SBR (dry)compounds are given in Table3.3,3.4,3.5 and 3.6 respectively.

Table 3.3. Formulation for XNBR latex compounds

Ingredients	Dry Weight (g)
XNBR latex 50%	100
Wingstay L dispersion 50%	0.75
Filler	varying concentration
ZnO dispersion 50%	3.5
ZDC dispersion 50%	2.0
TMTDdispersion 50%	0.5
S dispersion 50%	1

Table 3.4. Formulation for SBR latex compounds

Ingredients	Dry Weight (g)
50% SBR latex	100
10% Pot. Oleate	0.25
Filler	varying concentration
50% ZnO dispersion	1.5
50% ZDC dispersion	1.5
50%TMTD dispersion	1.5
50% S dispersion	1.5

Table 3.5. Formulation for NBR (dry) compounds

Ingredients	Weight (g)
NBR	100
S	1.5
ZnO	4.5
Stearic acid	2.0
Filler	varying concentration
HS	1
CBS	1
TMTD	0.25

Table 3.6. Formulation for SBR (dry) compounds

Ingredients	Weight (g)
SBR	100
ZnO	4.5
Stearic acid	2
HS	1
Filler	varying concentration
CBS	0.8
TMTD	0.1
S	2

3.11 Preparation of nanocomposites

3.11.1 Preparation of rubber latex (XNBR/SBR) clay nanocomposite by latex blending technique.

Clay slurry was sonicated for 30 min. Compounding ingredients were added to XNBR and SBR latex in the same sequence as given in Tables 3.2. & Table 3.3 respectively. The addition of each ingredient to the latex was followed by stirring with a glass rod. After their complete

addition the compounded latex was ball milled for 1 hr. It was then kept overnight for maturation.Then it was poured into glass trays (15×15cm) as per ASTM D 1076-88. About 30-35 ml of the compounded latex was taken in each tray, slowly tilted so that a film of uniform thickness (1-1.5mm) was obtained. The glass trays containing the compounded latex were kept on levelled table and dried at room temperature. The transparent dried films were cured in air circulated oven. XNBR sheets were cured at 30 min (100^0C) and SBR sheets were cured for 40 min (110^0C).

3.11.2 Purification of MWCNT

The as received MWCNT was purified before composite preparation. About 5g of MWCNT was refluxed with 500ml 2MHCl for 24 hours. Washed with water, filtered and dried at 80^0C.

3.11.3 Preparation of rubber(XNBR/SBR) latex MWCNT/graphene nanocomposite by latex blending technique

Stabilizing agent was first added to the latex, followed by the addition of MWCNT/Graphene dispersion. The dispersion was added drop by drop with continuous stirring. After that other ingredients were added to XNBR and SBR latex in the same order as given in theTables 3.2 and 3.3. respectively. The compounded latex was again stirred for 1 hr, kept overnight for maturation and then poured into glass trays (15×15cm). The dried NBR sheets were cured at 100^0 C for 30 min. and SBR sheets at 110^0C for 40 min.

3.11.4 Preparation of rubber clay nanocomposite by mixing in a two roll mill.

Compounding of rubber with clay was done on a two roll mill (150 mm ×300 mm). For NBR and SBR mixing was done as per ASTM D

3187-001 and 3185-99 respectively. The nip gap was set at 0.2mm and temperature maintained at $50+/-5^0$ C.

Rubber was masticated by passing through the rolls for 2 min. After the nerve has disappeared the compounding ingredients were added in the same order as mentioned in Table 3(4) and 3(5). After mixing the stock was homogenized by passing through the tight nip of the mill for six times and sheeted out at a nip gap of 3mm. Mixing time and temperature was controlled during the process.

3.11.5 Preparation of rubber MWCNT/graphene nanocomposite by mixing in a Brabender Plasticorder

Compounding of rubber with MWCNT/graphene was done in a brabender plasticorder. Further, homogenisation of the compound was carried out on a laboratory (15×33 cm) two roll mill at a friction raio of 1:1.25. The temperaure of the roll was maintained at $60+/-5^0$C and the compound was homogenised by passing 6 times endwise through a tight nip and finally sheeted out at nip gap of 3mm.

3.12 Determination of cure characteristics

Cure characteristics of the mixed compounds were determined using a rubber process analyzer (RPA), at a temperature of 160^0C. Cure parameters like cure time, scorch time, minimum torque and maximum torque were obtained from RPA

3.13 Moulding

The test specimens for determining the physical properties were prepared in standard moulds by compression moulding on an electrically

heated press having 45×45 cm platens at a pressure of 200 Kg cm^{-2} to the respective optimum cure time at 160^{0}C. After curing the mouldings were cooled by dipping in cold water and conditioned for 24 hrs before testing.

3.14 Conclusion

Ball milled clay showed greater tendency to settle than the sonicated sample.SDBS was found to be a good dispersing agent for MWCNT and Vulcastab VL for graphene. Latex blending method seemed to be a good method for preparing latex composites

References

[1] Zoromba, M. Sh. Belal, A. A. M. Ali, A. E. M. Helaly, F. M. Abd El-Hakim, A. A. Badran, A. S. Polymer-Plastics Technology and Engineering. 2007, 46, 529.

[2] González, J. A. Carreras, A. C. Ruiz, M. del C. Lat. Am. Appl. 2007,37.

[3] Ebokl, T.A. Detellier,C. Journal of Physics ad Chemistryof Solids. 2006, 67,950.

[4] Xuening,L. Hongtao, Z. Zhizhong,Y. Chengyong,H.A. Chinese Science Bulletin. 2005, 50, 1320.

[5] Matinlinna, J.P. Mutlu O¨zcan. Lassila, L.V.J. Vallittua, P. K. Dental Materials, 2004, 20, 804. .

[6] Noda,I. Dowrey, A.E. Haynes, J.L. Colloids and Surfaces.1989,36, 427

[7] Perez L.D. Zuluaga, M .A. Kyu,T. Mark, J.E. Lopez,B.L. Polymer Engineering and Science. 2009, 866.

[8] Tahermansouri,H. Chobfrosh khoei, D. Meskinfam, M. Int.J.Nano. Dim. 2010, 1, 153.

[9] Abuilaiwi, F.A. Laoui, T. Al-Harthi, M. Ali, M. The Arabian Journal for Science and Engineering. 2010, 35, 37.

[10] Vaisman, L. Wagner,H. D, Marom, G. Advances in Colloid and Interface Science. 2006, 37,128.

[11] Park, S. An, J. Potts, J.R. Velamakanni,A. Murali,S. Ruoff, R.S.Carbon, 2011,49,3019.

[12] Wu, Y. Wang, B. Ma, Y. Huang,Y. Li,N. Zhang,F. Chen,Y. Nano Res. 2010, 3, 661.

[13]   Lian,P. Zhu,X. Liang,S. LI, Z. Yang ,W. Wanga,H. Electrochimica Acta. 2010, 55, 3909.

[14]   Das,A. Kasaliwal ,G.R. Jurk, R. Boldt R , Fischer D , Stöckelhuber K W, Heinrich, Klaus Werner. Composites Science and Technology. 2012, 72, 1961.

[15]   Pinnavaia, T.J Beall, G.W.Eds., Polymer Clay Nanocomposites, Wiley, New York. 2000.

[16]   Gloaguen, J.M. Lefebvre, J.M. Polymer. 2001, 42, 5841.

[17]   Pramanik, M . Srivastava, S. K. Samantaray, B. K. Bhowmick, A. K. Journal of Polymer Science Part B: Polymer Physics. 2002, 40, 2065.

[18]   Dennis, H.R. Hunter, D.L. Chang, D. Kim, S. White, J.L. Cho, J.W. Paul, D.R. Polymer.2001, 42, 9513.

[19]   Ray,S.S. Okamoto,M. Prog. Polym. Sci. 2003,28, 1539.

[20]   Hasegawa,N. Okamoto,H. Kato,M. Usuki,A. Journal of Applied Polymer Science. 2000,78,1918.

[21]   Yeh,J. Huang,H. Chen,C. Sua,W. Yub,Y.   Surface and Coatings Technology.2006, 200, 2753.

[22]   Leia,H. Dub,G. Pizzic,A. Celzardd,A. Fange,Q.Journal   of   Adhesion Science and Technology.2010,24.

[23]   Wang, Z. Lan, T. Pinnavaia, T. J. Chem. Mater.1996, 8 , 2200.

[24]   Wang, Z. & Pinnavaia, T. J. Chem. Mater. 1998,10, 3769.

[25]   Liang, Y. Cao,W. Zhang,X.   Tan,Y. He,S. Zhang,L. Journal ofApplied Polymer Science. 2009, 112, 3087.

[26]   Liu,L. Luo, Y. Jia,D. Fu,W.   Guo,B. Journal of   Elastomers and Plastics. 2006, 38.

[27]   Liu,L. Jia,D. Luo,Y. Guo,B. Journal of Applied Polymer Science. 2006, 100, 1905.

[28]   Ahmadi,S.J. G'Sell,C. Huang,Y. Ren,N. Jean,A.M. Hiver,M. Composites Science and Technology. 2009, 69, 2566.

[29]   Sukumar,R. Menon,A.R.R. Journal of Applied Polymer Science. 2008, 107,3476.

[30]   Chang,Z.Guo,F.Chen,J.Yu,J.Wang,G.Polymer Degradation and Stability. 2007,92,1204.

[31]   Liang,Y. Wang,Y. Wu, Y. Lu,Y. Zhang,H. Zhang,L. Polymer Testing . 2005, 24, 12.

[32]   Kato, M. Tsukigas, A. Tanaka,H. Usuki,A. Inai, I. Journal of Polymer Science Part A: Polymer Chemistry. 2006, 44, 1182.

[33]   Das,A. Jurk,R. Stöckelhuber, K. W. Heinrich G. eXPRESS Polymer Letters. 2007,1, 717.

[34]   Hwang,W.Wei,K.Polymer Engineering and Science. 2004,44.

[35]   López-Manchado,M.A. Herrero, B. Arroyo M, Polymer International. 2004, 53, 1766.

[36]   Ma,J. Xiang, P. Mai,Y. Zhang, L. Clay Macromolecular Rapid Communications. 2004, 25, 1692.

[37]   Jia, Q. Wu, Y. Wang, Y. Lu, M. Yang,J. Zhang, L. Journal of Applied Polymer Science. 2007, 103, 1826.

[38]   Rahmatpoura, A. Abdollahia,M. Shojaee.M. Journal of Macromolecular Science, Part B: Physics. 2008,47, 523.

[39]   Abdollahi,M. Khanli,H.H. Aalaie,J. Yousefi,M.R. Polymer Science Series. A. 2011 53, 1175.

[40]   Wu,Y. Wang, Y.Zhanga,H. Wang,Y. Yu,D. Zhang,L. Yang,J. Composites Science and Technology. 2005,65, 1195.

[41]   Varghese, S. Karger-Kocsis, J. Polymer. 2003, 44, 4921.

[42]   Blackley,D.C. Polymer Latices. Application of latices. 1997,3,1.

[43]   Rastogi,R. Kaushal,R. Tripathi, S.K. Sharma,A.L. Kaur,I. Bharadwaj, L.M. Journal of Colloid and Interface Science. 2008, 328, 421.

[44]   M.F. Islam, E. Rojas, D.M. Bergey, A.T. Johnson, A.G. Yodh, Nano Lett. 2003,3,269.

[45]   J.F. Liu, W.A. Ducker, Langmuir. 2000,16,3467.

[46]   Ciofani, G. Raffa, V. Pensabene,V. Menciassi, A. Dario, P. Fullerenes, Nanotubes Carbon Nanostruct. 2009,17,11.

[47]   Napper, D.H. Napper, Polymeric Stabilization of Colloidal Dispersion, Academic Press, London. 1983.

[48]   Moore,V.C. Strano,M.S. Haroz, E.H. Hauge,R.H.Smalley,R.E. Nano letters. 2003, 3, 1379.

.....�⋇.....

Chapter 4

CARBOXYLATED NITRILE RUBBER LATEX (XNBR) BASED NANOCOMPOSITES

4.1 Introduction

Polymer nanocomposites (PNCs) have opened a new dimension in the field of material science because of the wide spectrum of applications of the nanofillers in polymeric systems. Elastomer nanocomposites reinforced with low volume of nanofillers significantly improve the mechanical, thermal, barrier and flame retardant properties.

Carboxylated nitrile rubber (XNBR) is a terpolymer of acrylonitrile, butadiene and a carboxyl group containing monomer such as acrylic or methacrylic acid. Incorporation of carboxyl groups increases inter and intra molecular interactions, resulting in improved properties of the polymer. Owing to the high polarity of carboxyl groups present, they are regarded as polar rubbers.

Reinforcing effect of silica [1], ZnO [2], organic filler from olive husk powder (OHP) [3], short jute fibre [4], hydrotalcites [5] and hygro thermally decomposed polyurethane on XNBR [6] are reported. Only few reports regarding the utilization of layered silicate in XNBR are available

[7-9]. Moreover, studies on multiwalled carbon nanotubes and graphene filled XNBR composites are so far not reported in literature and hence the study is the first one of its kind.

This chapter deals with the study of the effect of nano kaolin, vinylsilane grafted nanokaolin, multiwalled carbon nanotubes (MWCNT) and graphene nano platelets in the mechanical and thermal properties of the nanocomposites and the different methods used for characterization of the nanocomposites.

4.2 Experimental
4.2.1 Materials

Carboxylated nitrile butadiene rubber latex (XNBR) is CLX 530 purchased from Eliokem India Pvt. Ltd. Bombay. Specification is given in Table 2.1.

Nanokaolin (Nanocaliber100) and Vinylsilane grafted nanokaolin (Nanocaliber 100V) were supplied by English Indian Clays Ltd., Veli, Thiruvananthapuram. Specification is given in Table 2. 3.

Multiwalled carbon nanotube (MWCNT) - Baytube[R] 150P was obtained from Baeyer Materials Science AG (Leverkusen Germany). Specification is given in Table.2.4. Graphene nanoplatelets were purchased from Quantum materials Ltd., Bangalore.

Nanokaolin is designated as 'C' and XNBR containing 1,5,10 phr nanokaolin is referred as XNBR-1C, XNBR-5C and XNBR-10C. Vinylsilane grafted nanokaolin is represented as 'V'and XNBR containing 1, 5, 10, phr vinylsilane grafted nanokaolin as XNBR-1V, XNBR-5V and XNBR-10V.

Also, Graphene nanoplateletes are referred as graphene.

4.2.2 Preparation of XNBR based nanocomposites

Formulation used for the preparation of dispersions for latex compounding is given in Table 3.2. Preparation of filler dispersions are dealt in Sections 3.9.2.1 and 3.9.2.2. Formulation used for the preparation of XNBR compounds is given in Table 3.3 and the methods for the preparation of XNBR/clay nanocomposites and XBR/MWCNT/graphene nanocomposites are given in Section 3.11.1 and 3.11.3.respectively

4.2.3 Methods

Tensile strength, elongation at break, modulus and tear strength of the nanocomposites were determined as per the respective ASTM standards using a Universal Testing Machine (UTM, Shimadzu, model AG1). Swelling studies were done in methyl ethyl ketone as solvent and strain sweep analysis was performed using Rubber Process Analyzer (RPA 2000). Thermal analysis of the composites were carried on TGA (TGA Q-50)) and DSC (DSC Q100) TA instruments. Xray diffraction studies were done using Bruker AXS D8 Advance Diffractometer with CuKα radiation of wavelength 1.54 A°. FTIR analysis was conducted using Thermo Nicolet, Avatar 370 model IR spectrometer. The morphology of tear fractured surfaces of XNBR based nanocomposites were studied using JEOL model JSM 6390 LV. AFM images were obtained by using a Park Model XE 100 in non contacting mode. A detailed description of the methods employed is given in Chapter 2.

4.3 Results and Discussion
4.3.A Nanokaolin in XNBR Latex

Carboxylated nitrile butadiene rubber (XNBR) based nanocomposites with varying amounts of nanokaolin were prepared by latex stage mixing.

Sonication of nanokaolin and the technique adopted for the preparation of the nanocomposite helped to get a uniform dispersion of clay in XNBR latex. Proper dispersion of clay particles, partial exfoliation/ intercalation of clay and interaction of clay with the polar rubber latex made nanokaolin a good reinforcing filler in XNBR latex.

4.3A.1 Mechanical properties

Variation of tensile strength, elongation at break, modulus at 300% elongation and tear strength of the nanocomposites were studied at different loadings of nanokaolin. Fig.4.1 shows the variation of these properties with clay loading. It was seen that the mechanical properties increased with clay loading, reached a maximum value and then decreased.Thus tensile strength increased by 110%, elongation at break by 168% and modulus by 30% at 25 phr concentration of nanokaolin. Tear strength increased continuously with the increase in concentration of nano kaolin.
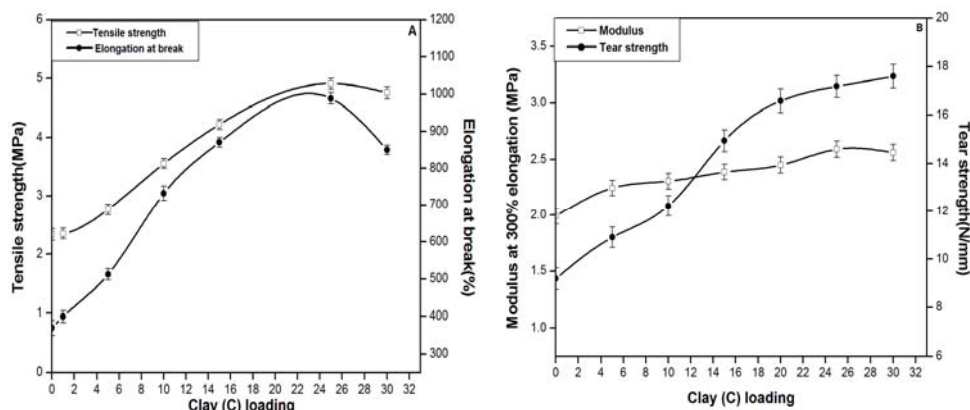
Fig.4.1. Variation of (A) Tensile strength and Elongation at break (B) Modulus and Tear strength of XNBR-C nanocomposite

There was no significant increase in the mechanical properties of the nanocomposites at low filler loading. This might be due to the lack of

proper dispersion of the filler. As the filler loading increased, the surface interaction with the polymer increased, resulting in better properties [10]. At still higher loadings, aggregation of filler might have reduced the interfacial area between the polymer and clay and thus weakened the available reinforcing links [11].

Kaolin particles are in the form of hexagonal plates closely packed resembling the pages of a closed book. The external surface of kaolin comprises of hydroxyl groups on one side, oxygen on the other side and the edges of all the layers called the "broken bonds surfaces" [12]. There is an abundance of OH groups on the plate edges and these are considered as the major reactive sites of clay particles [13]. The clay platelets are held together by weak hydrogen bonds between the hydroxyl groups of the octahedral sheet and basal oxygen of the adjacent layer tetrahedral sheet.

Polar interaction between CN and COOH group of XNBR with OH group of clay led to the increase in tensile strength of the nanocomposite. Generally rigid fillers cause a significant reduction in elongation at break, but the presence of nanokaolin increased the elongation at break. The clay particles in the form of platelets provide more interfacial contact for rubber molecules, and greater slippage of the clay layers led to higher elongation at break. The increase in modulus with the addition of clay was due to the intercalation/exfoliation behaviour of the clay layers in the nanocomposite. XRD analysis confirmed the extent of intercalation. Since there was no chemical interaction between the clay layers and rubber matrix, the increase in modulus was not very high. The uniformly dispersed clay layers blocked

the propagation of cracks imparting more resistance to tear propogation resulting in increased tear strength.

Sonication of nanokaolin helped to loosen the close packing of the clay platelets. During compounding and ball milling, intercalation of rubber chains into the clay galleries had taken place. The interaction between the polar hydroxyl group in clay and polar CN and COOH groups on XNBR helped in intercalation. A schematic representation of clay before and after sonication and the intercalation of polymer chain into the intergallery space is represented schematically in Fig 4.2
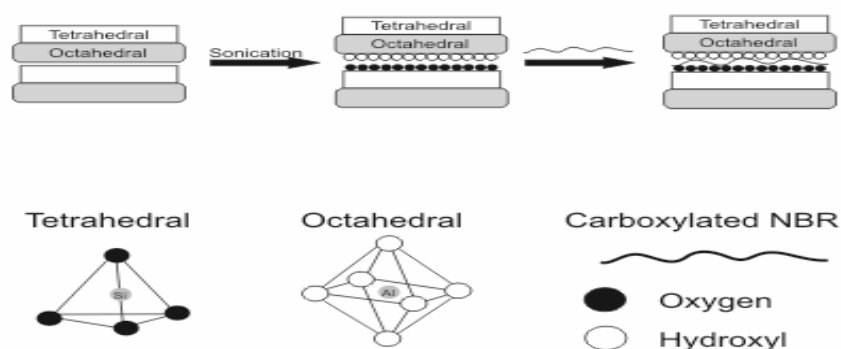
Fig. 4.2. Schematic representation of clay before and after sonication and the intercalation of polymer chain into the intergallery space

4.3A.2 Swelling studies

Swelling of the vulcanized samples was carried out by immersing circular specimens of 20mm diameter and 1mm thickness in methyl ethyl ketone (MEK) until equilibrium was reached. Fig.4.3 shows the change in MEK uptake with time of filled XNBR for different concentration of nanokaolin. Absorption took place in two distiguished zones. The first zone represented initial solvent uptake. Here the swelling rate was very high due to a large concentration gradient and the polymer sample was under severe

solvent stress. In the second zone the swelling rate was reduced due to a decrease in the concentration gradient and finally an equilibrium state with zero concentration gradient was reached [14]. Swelling rate decreased with the increase in filler loading. This was because the platelet like morphology of nanokaolin embedded in the matrix enhanced the tortuosity of the path. But it was found that at 30 phr the solvent uptake was more than that at 25 phr loading. This might be due to the aggregation of filler at the high concentration. Due to aggregation the clay platelets might not be completely available in the rubber matrix to enhance the tortuosity of the path.

Fig.4.4 shows the variation of swelling index with concentration of nanokaolin.Swelling index is inversely proportional to the extent of cross linking. With the addition of clay swelling index decreased due to clay rubber interaction.
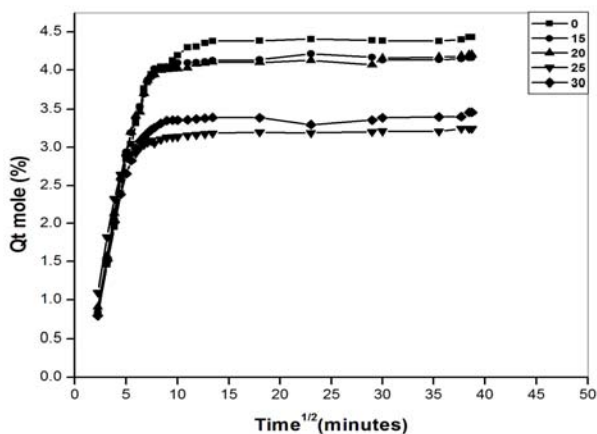
Fig. 4.3. Sorption curves of XNBR- C nanocomposites
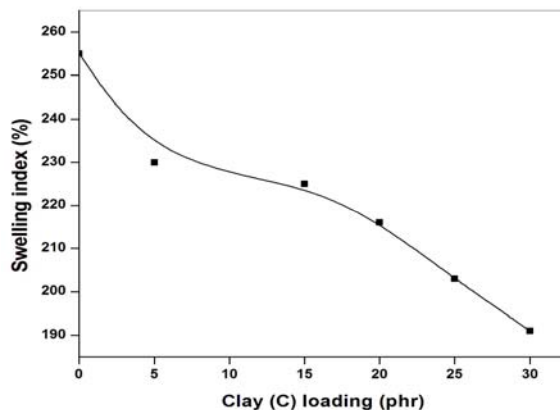
Fig. 4.4. Variation of swelling index with clay loading

4.3A.3 Strain sweep analysis

Strain sweep studies were conducted to study the rubber filler interactions. The variations of complex modulus with strain for XNBR latex clay nanocomposite are shown in Fig.4.5. The complex modulus values at low strains were a measure of filler polymer interaction, the high values of modulus were due to higher filler-filler or filler polymer interactions. The decrease in modulus with increase in strain was due to the disentanglement of uncured rubber molecules and the breakdown of filler rubber network produced by filler-filler interaction and filler-rubber interaction. The reason why XNBR clay nanocomposite possessed high modulii was that although both the clay-rubber interaction and the compatibility between the clay and XNBR are weak in it, the filler-filler interaction was very strong due to filler aggregates. The complex modulus value increased with clay content indicating better rubber filler interaction. The increase in modulus was due to the inclusion of rigid filler particles in the soft rubber matrix
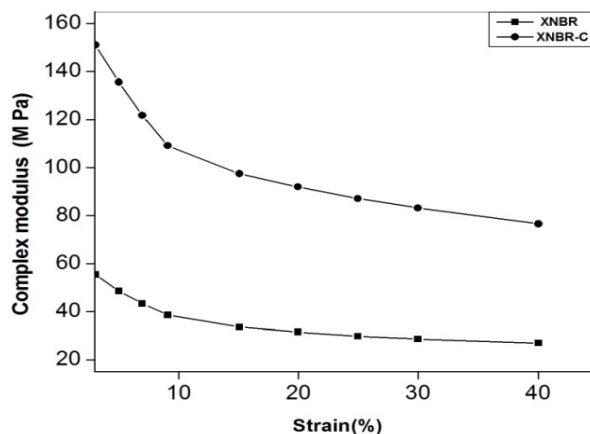
Fig. 4.5. Variation of Complex modulus with strain for XNBR-C nanocomposite

4.3A.4 Thermogravimetric analysis (TGA)

Fig.4.6 shows the TGA curves of XNBR and XNBR-25C. Table 4.1 gives the thermal analysis data of XNBR and XNBR-25C. Major degradation of XNBR began at 350^0C and completed around 500^0C. Hence XNBR was stable upto 350^0C in nitrogen atmosphere. The peak of DTG curve gives the temperature corresponding to the maximum degradation (T_{max}). XNBR degraded in two steps with Tmax at 432^0C and 456^0C. The two major peaks corresponded to the multiple degradation steps of the butadiene part present in XNBR. This involved the elimination of acrylonitrile and butadiene part followed by the main chain scission [15]. The high residue formed might be due to the formation of stable structures through probable cyclisation reaction that acrylonitrile could undergo at elevated temperature [16].

The degradation of the nanocomposites also took place in two steps. Incorporation of clay had marked increase in onset temperature, temperatures for maximum degradation (T_1 and T_2) and temperature for 10%, 25% and 50% weight loss. Residue remaining for the nanocomposite was much higher than

in XNBR without filler. All these indicated the enhancement in the thermal stability of the nanocomposite on addition of nanokaolin.

Table 4.1. Thermal analysis results of XNBR and XNBR-25C nanocomposite

Samples	On set temp (^{0}C)	Tmax(^{0}C)		Temp. at 10% wt.loss(^{0}C)	Temp. at 25% wt.loss (^{0}C)	Temp. at 50%wt.loss (^{0}C)	Residue (%)
		T1	T2				
XNBR	326	432	456	386	430	450	13.67
XBR-25C	334	441	465	396	438	465	25.72
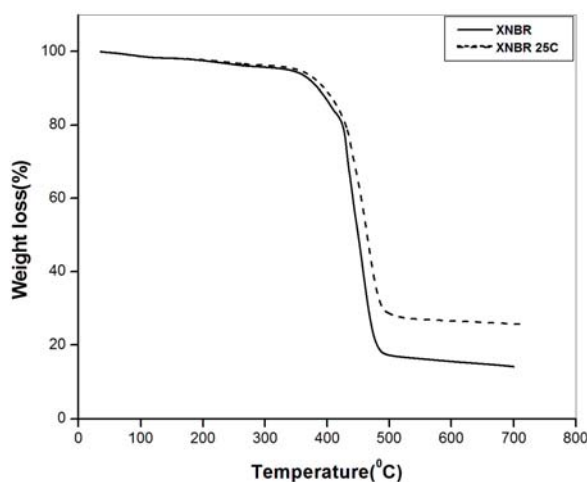
Fig. 4.6. TGA curves of XNBR and XNBR-25C nanocomposite

4.3A.5 Differential scanning calorimetry (DSC)

DSC studies of XNBR showed T_g at -25.13^{0}C. Incorporation of nano kaolin showed a marginal increase in T_g as given in the Table 4.2. The effect of dispersed clay layers on the free volume of rubber influenced the Tg of rubber. This might be attributed to the interaction between the organic and inorganic phases. These interactions increased the rigidity of the soft matrix and limited the movement or motion of the polymer chain.

<div align="center">**Table 4.2. T_g values of XNBR and XNBR-25Cnanocomposite**</div>

Sample	T_g
XNBR	-25.13C
XNBR-25C	-25.5 C

4.3A.6 X-ray diffraction analysis (XRD)

Fig.4.7 shows the XRD pattern of XNBR, nanokaolin ('C') and XNBR-25C nanocomposite. No peak was observed for pure XNBR suggesting its amorphous nature. Characteristic peaks of nanokaolin shifted from 25^0 to 23.93^0 and 12.5^0 to 10.93^0. This increased d spacing from 3.56 to 3.71 A^0 and 7.05 to 8.08 A^0. The peak at 20^0 collapsed, showing that exfoliation had taken place to some extent. The dispersion of clay layers in XNBR could be considered as a bimodal structure representing both intercalated and exfoliated state [17]. The reduction in the width of the peak of the composite suggested a well ordered intercalated structure.
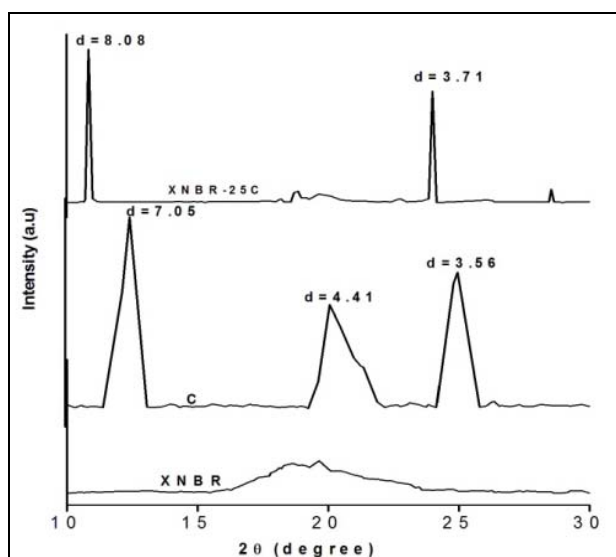
<div align="center">**Fig 4.7. X-ray diffraction pattern of XNBR, 'C' and XNBR-25C**</div>

Similar results were reported in literature when montmorillonite (MMT) was used as the reinforcing filler. Amit et al. [18] worked on carboxylated NBR/organomodified MMT composites and showed that intercalation is a common process from 2.5 to 10 phr organo clay mixed at 160^0C. In an NBR-organically modified MMT nanocomposite a decrease in d spacing after curing was observed [19]. S.Sadhu and A.K. Bhowmick [20] have dealt with unmodified MMT on SBR with varying styrene content and using dicumyl peroxide as the curing agent and suggested that exfoliation had taken place in all these composites.

4.3A.7 Fourier transform infrared spectroscopy (FTIR)

Fig.4.8. shows the IR spectrum of XNBR, nanokaolin ('C') and XNBR-C nanocomposite. Appearance of peaks at 2930cm^{-1} and 2852cm^{-1} in the nanocomposite corresponds to the C-H stretching vibration of CH$_2$ groups [3000-2700 cm^{-1}] in the rubber back bone. This showed the intercalation of polymer chain in the interlayer space of nanokaolin. Reduction of OH stretching vibration of nanokaolin (3696cm^{-1}, 3625cm^{-1} and 3438cm^{-1}) [21], disappearance of CN peak of XNBR (2238cm^{-1}) and the appearace of a peak at 1640cm^{-1} in the composite was an indication of the formation of an amide linkage. In the formation of the nanocomposite CN group of XNBR might have undergone partial hydrolysis giving the amide. Intensity of the peak at 1440cm^{-1} corresponding to the OH bend in carboxylic acid of XNBR was very much reduced in the composite. This showed the interaction of OH group of clay with COOH group of XNBR. The disappearance of the sharp peak at 969cm^{-1} corresponding to the stretching of butadiene double bond in XNBR confirmed the decrease in unsaturation of the composite.The slight shift of the peaks in the range 900-

1200 cm^{-1} corresponding to the bending of Si-OH and Al-OH group of clay showed the interaction of Si-OH and Al-OH groups of nanokaolin with COOH group of XNBR.
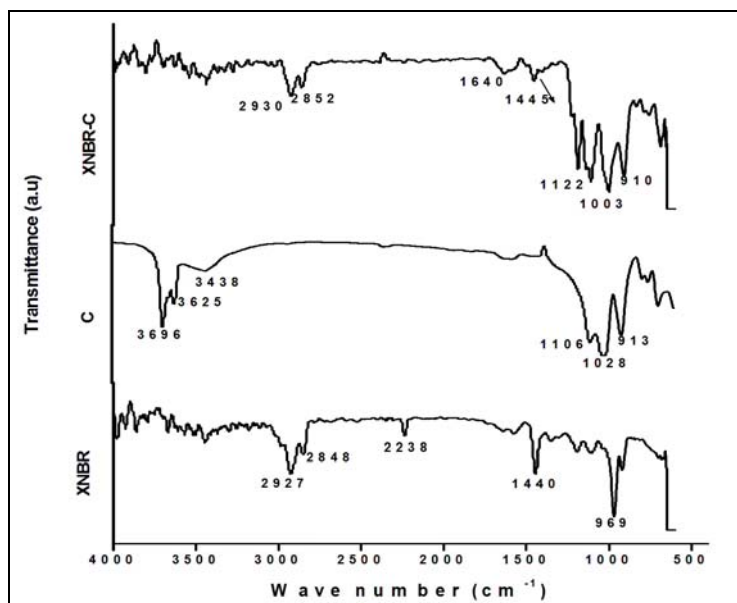
Fig. 4.8. FTIR spectrum of XNBR, nano kaolin ('C') and XNBR-C nanocomposite

4.3A.8 Scanning electron microscopy (SEM)

Fig.4.9 shows the SEM photographs of the tear fractured surface of XNBR (A) without filler and (B) XNBR-25C nanocomposite. Particles seen scattered in the image of XNBR without filler might be due to ZnO. In the nanocomposite the clay platelets are thickly and uniformly dispersed in the marix. Latex blending technique for the preparation of the nanocomposite followed by ball milling of the compounded latex led to homogeneity in mixing. The interaction of filler with XNBR gave greater rubber-filler adhesion leading to decrease in the tendency of the filler particles to agglomerate. From the figure it is seen that clay platelets are

uniformly dispersed in matrix. This uniformity in dispersion led to the reinforcement in properties of the nanocomposite.

(A)

(B)
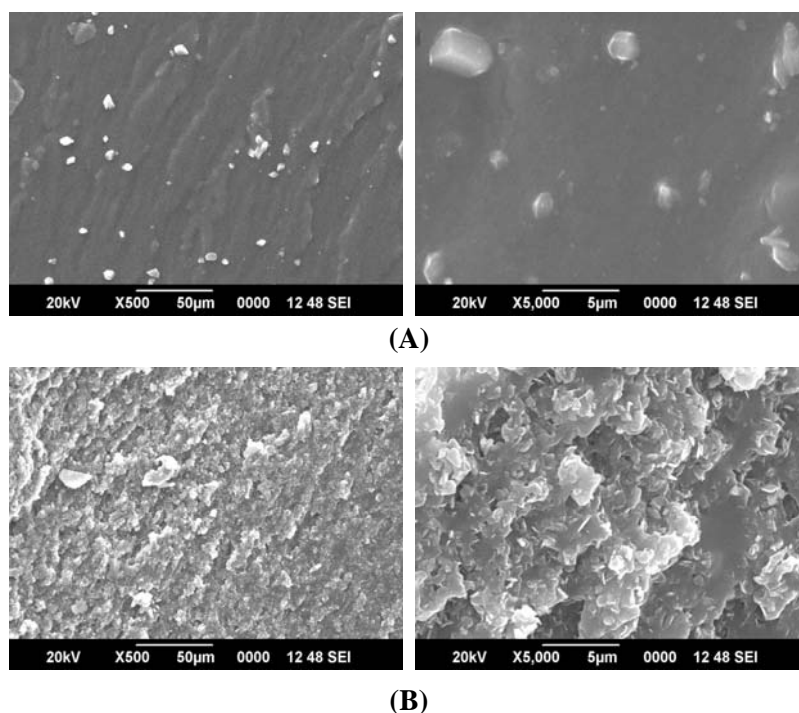
Fig. 4.9. SEM images of (A) XNBR and (B) XNBR -25C nanocomposite

4.3A.9 Atomic force microscopy (AFM)

Fig.4.10 shows the AFM images of XNBR-25C composite. This shows the homogeneous distribution of clay particles in the matrix. The homogeneously dispersed regions have different phase contrast. The light regions are the dispersed clay particles and the dark regions are the soft rubber matrix. Some aggregated clay particles are also seen in the image.

File Name	111013Topography001
Head Mode	NC-AFM
Source	Topography
Data Width	256 (pxl)
Data Height	256 (pxl)
X Scan Size	30 (µm)
Y Scan Size	30 (µm)
Scan Rate	0.8 (Hz)
Z Servo Gain	3.31
Set Point	884.5 (nm)
Amplitude	1.233E3 (nm)
Sel. Frequency	299.36E3 (Hz)
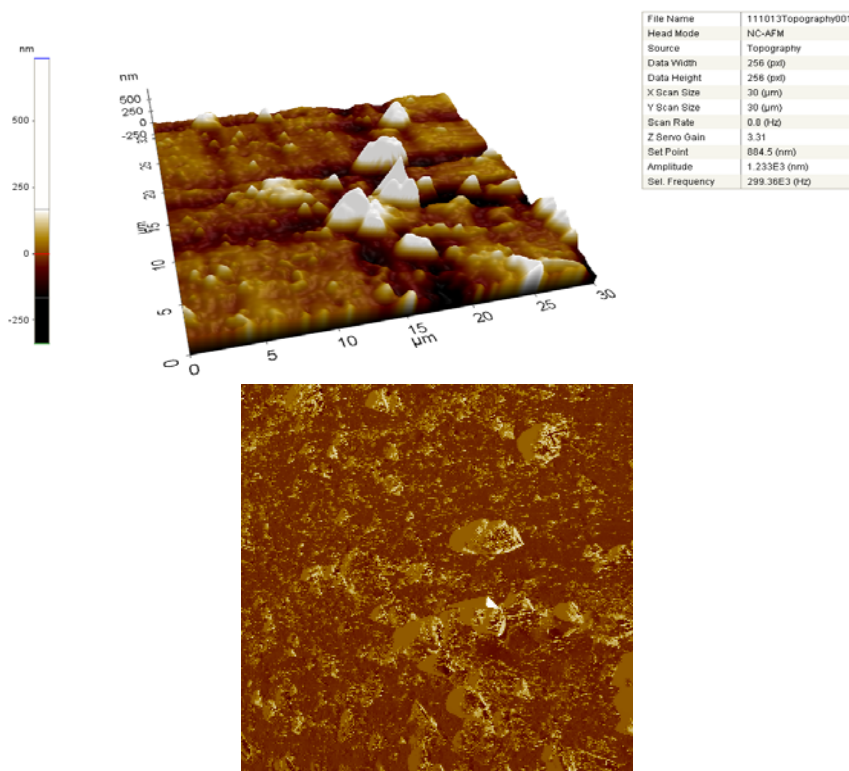
Fig. 4.10. AFM images of XNBR-C nanocomposite

4.3A.10 Conclusions

Inclusion of nanokaolin in XNBR enhanced the mechanical properties of the nanocomposite.Tensile strength increased by 110%, elongation at break by 168% and modulus at 300% elongation by 30%. Maximum improvement in properties was obtained at 25 phr concentration of nanokaolin showing the nanoeffect was not much pronounced in the composite. Tear strength increased continuously with the increase in concentration of nano kaolin. Thermal stability of the nanocomposite increased with the incorporation of nanokaolin, but T_g remained constant. XRD analysis confirmed the intercalation of polymer chain into the inerlayer space of nanokaolin. FTIR sudy confirmed the interaction of Si-OH and Al-OH groups of nanokaolin

with COOH group of XNBR. SEM and AFM analysis showed uniform dispersion of nanokaolin in XNBR.

4.3B Vinylsilane Grafted Nanokaolin in XNBR Latex

Effect of vinylsilane grafted nanokaolin ('V') on the physico mechanical properties of XNBR vulcanizates are investigated. Studies prove that silane treated nanokaolin is good at imparting reinforcement to carboxylated nitrile butadiene rubber (XNBR). On grafting, silanes react mainly with some of the OH groups on the edge surface of nanokaolin. Free hydroxyl groups on the kaolin surface forms hydrogen bonds with carboxyl (COOH) and cyano (CN) groups present in the rubber chain. The polymer chain can intercalate inside the clay galleries and the butadiene part can interact with the vinyl group through van der Waals forces. The extent of hydrogen bond formation depends on the number of hydroxyl groups available at the edges of clay surface and the number of cyano and carboxyl groups in XNBR. A schematic representation of grafting of vinyl silanes on the surface of kaolin and the interaction with the polymer chain is shown in Fig. 4. 11.
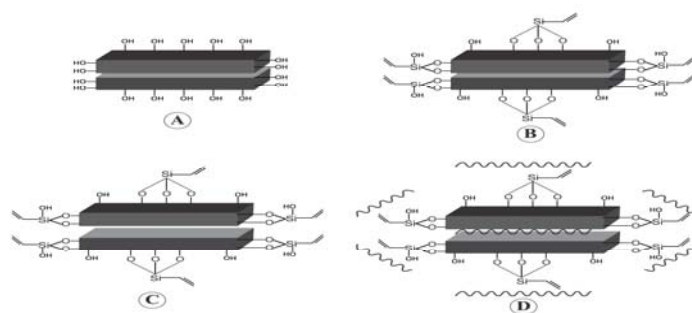
Fig. 4.11. Plausible mechanism showing the grafting of vinyl silanes on the surface of kaolin and its interaction with the polymer chain.

A - Kaolin containing OH groups on the edge surface.
B - Grafting of vinyl silane on kaolin
C - Increase in inter layer space on sonication
D - Intercalation of polymer chain into the interlayer space.

4.3B.1 Mechanical properties

Fig.4.12.(A) gives the variation in tensile strength/elongation at break and (B) gives the variation in modulus at 300% elongation/tear srength, of XNBR/V nanocomposite with increase in 'V' loading.

Tensile strength, elongation at break and modulus increased by 92%, 157% and 44% respectively at 15phr loading. Incorporation of clay minerals usually improves the tensile strength of polymers [22-25]. Intercalation of rubber molecules into the inter layer space of clay resulted in the increase of d spacing. High interfacial area and good interfacial adhesion led to an increase in tensile strength. Interaction between clay and polymer occurs through the interaction of OH group of clay and polar groups of XNBR. At a concentration greater than 15phr, agglomeration of clay particles resulted in filler-filler interaction leading to a decrease in the tensile strength. Elongation at break (EB) for polymer/clay nanocomposites depend on the interfacial interactions of polymer/clay system. Polar polymers have stronger interfacial interactions with clays and their composites show better elongation at break than the pure polymer [26]. There are instances where EB decreases with the filler loading [25,27, 28]. Kader et al. [17] have reported an increase of EB in NBR/MMT composite. Sodium salt of rubber seed oil (SRSO) modified kaolin gave only 22% increase in EB in NR composite [29]. Here, vinylsilane grafted nanokaolin gave 157% increase in EB. The interaction of CN and COOH groups of the polymer with OH groups on clay and the interaction of the unsaturated vinyl groups with the double bonds of the polymer facilitated the intercalation of polymer chains in between the clay platelets. At higher clay concentration non exfoliated aggregates were

present and this made the composite stiffer, with reduced elongation at break.

The modulus at 300% elongation increased with filler loading upto 15 phr and then decreased. The increase was due to the higher cross link density and good distribution of filler in the matrix. The increase in tear strength with concentration showed the filler could resist the growth of crack in the nanocomposite.
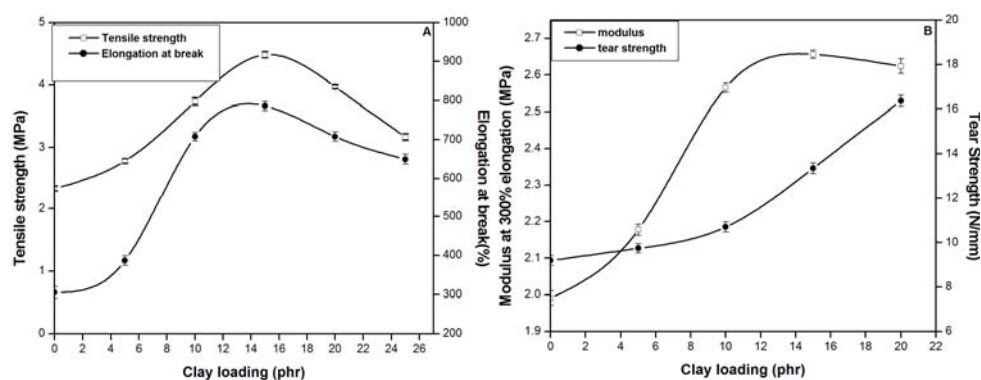
Fig.4.12. Variation of (A) Tensile strength and Elongation at break (B) Modulus and Tear strength of XNBR-V nanocomposite

4.3B.2 Swelling studies

Fig.4.13 shows the sorption curves of vulcanisates obtained by plotting Q_t, mole (%) uptake per 100 g of the solvent, against time. As the clay loading increased the equilibrium solvent uptake decreased. This was due to the increased hindrance exerted by the clay particles at higher loading. The interaction of polymer and clay developed a strong interface which restricted the entry of solvent [30].

Gum had the maximum solvent uptake at equilibrium swelling. Q_t value decreased drastically with the addition of clay. The swelling uptake

was high at the initial zone. This was because of the large concentration gradient [14]. After this the sorption rate reached a plateau corresponding to the equilibrium swelling where the concentration gradient was zero. The solvent uptake was lowest for 15 phr nanocomposite. The presence of the uniformly dispersed impermeable clay layers increased the average diffusion path and thus decreased the rate of transportation [31]. Due to aggregation of clay particles at higher concentration (20 and 25 phr) some voids were formed as seen in the SEM image (Fig.4.17) of the nanocomposite with 20phr loading. This increased the solvent absorption for the nanocomposite with 20phr and 25phr clay loading.
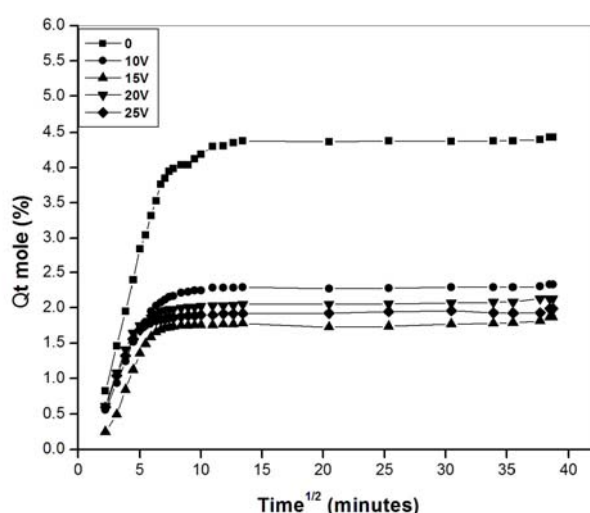
Fig. 4.13. Sorption curves of XNBR and XNBR-V nanocomposites

4.3B.3 Thermo gravimetric analysis (TGA)

Table 4.3 gives the thermal analysis data and Fig. 4.14 gives the TGA curves of XNBR, XNBR-15V and XNBR-25V. Onset temperature, peak maximum (T_{max}) and temperature at 50% weight loss increased with the

addition of 'V'.This indicated an increase in the thermal stability of the nanocomposite. Thermal decomposition of clay in the nanocomposite created a char layer and thus delayed the degradation [32].

At 25 phr the maximum degradation temperature (T_2) was lower and residue higher than that of 15phr nanocomposite. This showed that the morphology of the nanocomposite at higher concentration did not allow for maintaining a good thermal stability [33].

Table 4.3 Thermal analysis results of XNBR and XNBR-V nanocomposites

Samples	On set temp. (^{0}C)	Tmax (^{0}C)		Temp. at 50%wt.loss(^{0}C)	Residue %
		T_1	T_2		
XNBR	326	432	456	450	13.67
XNBR -15V	334	434	460	455	17.30
XNBR- 25V	334	434	458	457	21.11
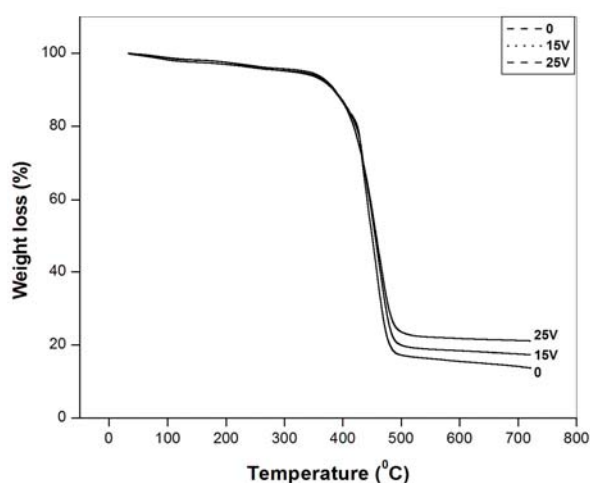
Fig. 4.14 TGA curves of XNBR and XNBR-V nanocomposites

4.3B.4 Differential scanning calorimetry (DSC)

Usually the interaction of polymer chains with the clay particles affects the segmental mobility of polymer matrix.

The confinement of the intercalated polymer chains between the clay layers reduce the segmental mobility of the matrix and increase the glass transition temperature (T_g) of the polymer. Good rubber–filler interaction shifts the glass transition temperature towards higher temperatures compared to the unfilled rubber matrix [34-36]. Table 4.4 gives the T_g values of XNBR and XNBR-15V. Here T_g of the nanocomposite was almost the same as that of pure XNBR. This showed that there was only a weak interaction between the less hydrophilic organomodified clay and the rubber latex. So the confinement of the intercalated polymer chain in the clay galleries did not affect the segmental mobility of the polymer matrix.

Table 4.4. T_g values of XNBR and XNBR-15 Vnanocomposite

Sample	T_g
XNBR	-25.13
XNBR -15 V	-25.80

4.3B.5 Xray diffraction analysis (XRD)

X-ray diffraction patterns in the 2θ range 10-30^0 for XNBR, 'V' and the composite with 1 phr and 15 phr 'V' are given in Fig.4.15. Vinylsilane grafted nanokaolin had diffraction peaks at 12^0 (d=7.1 A^0), 20.09^0 (d=4.41A^0) and 25^0 (d=3.56A^0) while XNBR being amorphous did not show a diffraction pattern in this range. The diffraction pattern for XNBR-1V had a number of strong peaks at higher angles indicating the introduction of

stacked layers of clay with a crystallographic order in the XNBR matrix [37]. At a low clay concentration the viscosity of the composite might not be enough to create adequate shearing force to intercalate the rubber molecules into the gallery space [38]. At higher loading the dispersion of clay layers in XNBR matrix might be considered as a bimodal structure representing both intercalated and exfoliated structure [17]. The peak shifted to a smaller angle side with a slight increase in d spacing to 7.8 A^0. This showed intercalation of polymer chains into the clay galleries. The position of the other two peaks remained the same. The peak at 20.09^0 had become broader and extended to the lower 2θ value in the composite. Such broadening of diffraction peak suggested partial exfoliation. The decrease in the intensity of the peak at 25^0 showed uniform distribution of rubber particles in the inter gallery space.

Literature has cited examples where introduction of hexa decyl trimethyl ammonium bromide modified montmorillonite (MMT) in NBR has increased d spacing from 2.6 nm to 3.9 nm [39]. Similar increase in d spacing by the introduction of MMT in XNBR was reported by Das, A. [18]. Partial exfoliation/intercalation in NBR/layered silicate composite was reported by Thomas,P [40] .

The modified clay gave a hydrophobic environment. Sonication of clay dispersion helped in the expansion of clay layers and the polar polymer chain intercalated into the inter gallery space. Hydrogen bonding between the CN and COOH group of XNBR and OH group of clay favoured the intercalation of the polymer chain
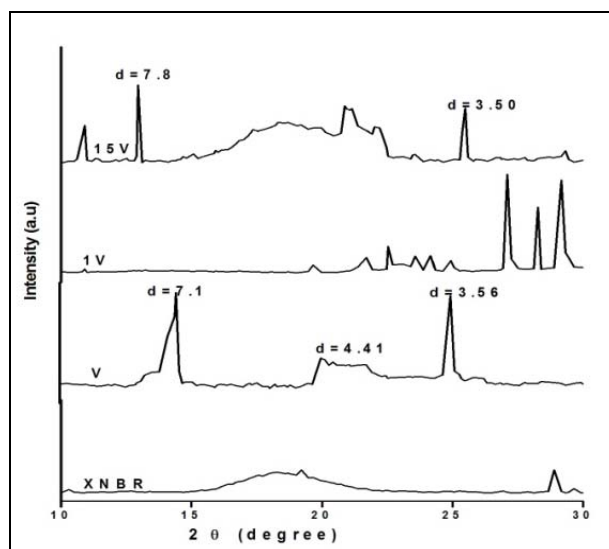
Fig. 4.15. X-ray diffraction pattern of XNBR, 'V' and XNBR-V nanocomposites

4.3B.6 Fourier transform infrared spectroscopy (FTIR)

Fig.4.16 shows the IR spectrum of XNBR and XNBR-V nanocomposite. In XNBR-V the characteristic OH stretching vibration at 3624cm^{-1} attributed to the inner surface hydroxyl groups of kaolin was shifted to 3612cm.[-1] This gave evidence for the keying in of the polar polymer chain into the inter gallery space of vinyl grafted nano kaolin.The formation of new bands at 3200-3550 cm^{-1} range also showed the presence of hydrogen bonded OH groups in the nanocomposite.

XNBR-V nanocomposite showed a stronger band at 2926cm^{-1} and 2848 cm^{-1} compared to that of XNBR. This might be due to the superimposition of OH band of carboxylic acid [3300-2500] on the CH stretching bands. The band at 2238 cm^{-1} remained unchanged showing there was no reaction of modified kaolin with the CN group of XNBR. The sharp peak at 1596 cm^{-1} gave the stretching vibration of a carboxylate ion

in the composite. The carboxylate may be zinc carboxylate formed by the reaction of the COOH group in the latex with ZnO. The peak at $1445 cm^{-1}$ might be due to the merging of CH_2 groups with the vinyl groups from the modified clay. Peaks in the range 1000-1110 cm^{-1} showed Si-OR bonds. 1031 cm^{-1} and $1111 cm^{-1}$ peaks seen in clay were shifted to 1017 cm^{-1} and 1104 cm^{-1} respectively. The bending vibration of Al-OH in modified nanokaolin also shifted from 915 cm^{-1} to $909 cm^{-1}$.The interaction of COOH group on XNBR with the Si-OH group and Al-OH group on the clay surface which, was already bonded to the silica tetrahedral alumina octahedral of kaolin, might have caused this shift of the Si-O and Al-OH band in the composite [18]. Corresponding to the strong peak at $970 cm^{-1}$ in XNBR there was only a weak band at 965 cm^{-1}in the composite showing a reduction in the stretching of butadiene double bond.This might be due to the interaction of butadiene double bond with vinyl group of clay.
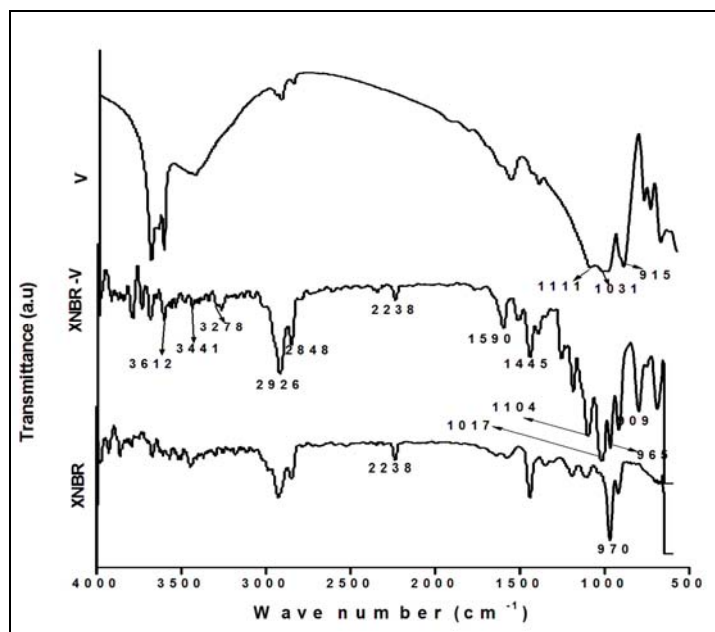
Fig.4. 16. FTIR spectrum of XNBR, XNBR-Vnanocomposite and 'V'

4.3B.7 Scanning electron microscopy (SEM)

Fig.4.17(A),(B) and (C) shows the SEM micrographs of the tensile fractured surfaces of unfilled XNBR and composites containing 15phr and 25 phr vinyl grafted nanokaolin. In the figure the dark phase represents XNBR matrix and the bright phase corresponds to the clay particles. Clay particles are seen in the shape of platelets. At 15phr filler loading the dispersed clay particles seem to be fully encapsulated in the matrix. There was no obvious phase separation observed between clay and the matrix. This indicated better clay NBR adhesion. The uniform dispersion led to the reinforcement in the properties of the nanocomposite. At higher concentration (25phr) aggregation of clay particles created voids, due to improper dispersion of particles as seen in Fig. 4 .17(C).
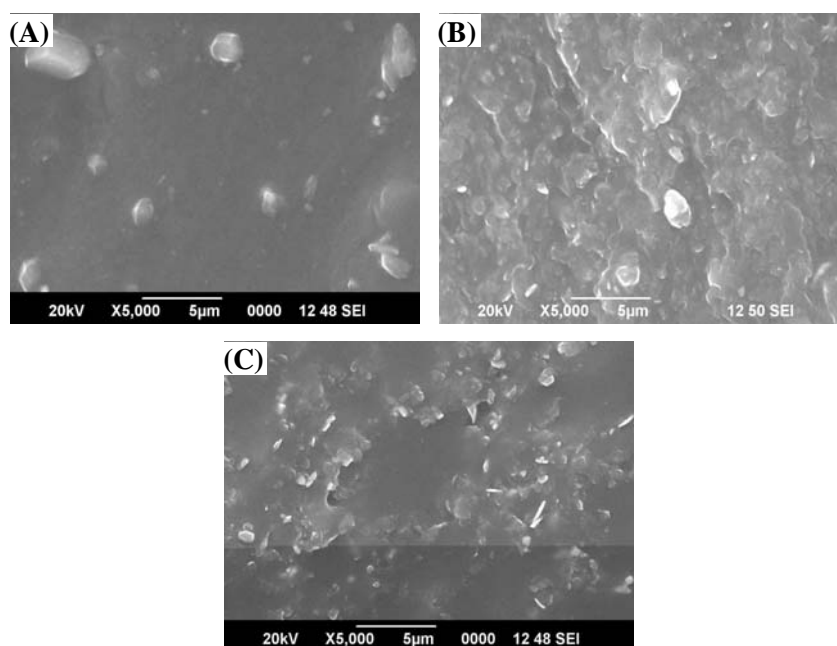
Fig.4.17. SEM images of (A) XNBR (B) XNBR-15V (C) XNBR-25V

4.3B.8 Conclusions

Vinyl silane grafted nano kaolin enhanced the mechanical properties of XNBR.Tensile strength increased by 92%, elongation at break by 157% and modulus by 44%. Maximum reinforcment was obtained at 15 phr concentration of the modified nanokaolin (15V). Swelling studies also showed solvent uptake was minimum for XNBR-15V nanocomposite. Greater reduction in swelling rate was observed for XNBR-V, when compared to XNBR- C nanocomposite. This might be due to the presence of bulky vinyl groups which caused greater hindrance to the flow of solvent. Eventhough T_g remained a constant, there was slight increase in the thermal stability of the nanocomposite.Slight increase in interlayer spacing as evidenced by XRD analysis indicated intercalation, of polymer chains into the clay galleries. SEM analysis showed a uniform dispersion of the clay particles, at lower concentration and agglomeration of clay particles at a higher concentration.

4.3C Multiwalled Carbon Nanotube in XNBR Latex

The unique mechanical properties and extremely large surface area per unit volume of carbon nanotubes makes it an intriguing reinforcement for polymers. Since the discovery of carbon nanotubes, extensive research has been done by incorporating different types of carbon nanotubes as nanoreinforcements into polymeric materials, to form new nanocomposites that possess high mechanical strength, electrical and thermal conductivity.

Here, MWCNT was dispersed in sodium dodecyl benzene sulphonate (SDBS) by sonication. The dispersed MWCNT (0.05-0.3 gm) was

incorporated in XNBR latex. Mechanical, electrical and thermal properties of these nano composites were studied. Nanocomposites were characterised by Fourier transform infrared spectroscopy (FTIR), X-ray diffraction (XRD) and Scanning electron microscope (SEM) analysis.

4.3C.1. Mechanical properties

The mechanical properties (tensile strength, elongation at break, modulus at 300% elongation and tear strength) versus MWCNT concentration are graphically plotted in Fig. 4.18.(A) and (B). It was seen that tensile strength, elongation at break, modulus and tear strength of the nano composites increased with increase in the loading of nanotube, reached a maximum value and then decreased. Even at a very low concentration of 0.15 phr tensile strength increased by 78% and elongation at break by 86%. Modulus and tear strength increased by 31% and 19% respectively at 0.1 phr.
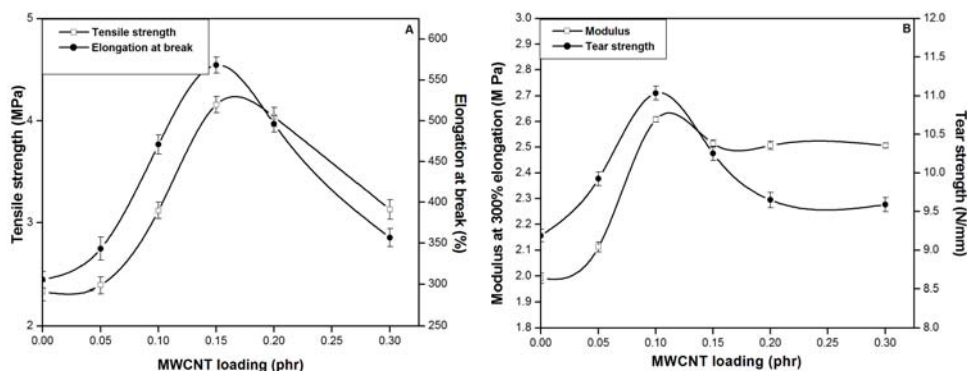
Fig.4.18. Variation of (A) Tensile strength and Elongation at break (B) Modulus and Tear strength of XNBR-MWCNT nanocomposite

An efficient dispersion of nanotube and a good interphase between nanotube and the matrix led to reinforcement in properties.

Sonication of nanotube dispersion in SDBS followed by latex stage mixing contributed to the uniform dispersion of nanotube in the matrix [41]. There was strong interfacial interaction between the polar nitrile (CN) group and carboxylic (COOH) group on the surface of XNBR with the π electron cloud of the nanotube. The good rubber filler interaction would increase the effectiveness of stress transfer from rubber matrix to filler particles dispersed in rubber matrix. This led to an increase in the tensile strength of the nano composite. The increase in elongation at break might be due to the fact that XNBR matrix allowed more rheological flow due to good rubber filler interaction [42]. Increase in tear resistance and modulus of the nanocomposite might be due to the reinforcement of the well dispersed MWCNT with high Young's modulus and strength in XNBR matrix [43]. Formation of aggregates at higher concentration led to reduction in the mechanical properties of the nano composite.

Significant improvement in mechanical properties of polymeric matrices by carbon nanotube addition has been reported. Weerachai et al. [44] observed an increase of 55% and 14% in tensile strength and elongation at break of NR-MWCNT nanocomposites at 5 phr loading. Tear resistance and modulus also increased with the increase in MWCNT loading. Bokobza, has reported an increase of 45% in elastic modulus and 70% in tensile strength by the incorporation of MWCNT in SBR.

4.3C.2 Swelling studies

Fig.4.19 shows the sorption curves of the vulcanizates in MEK obtained by plotting Qt (mole percentage uptake for 100g of the solvent)

against Time$^{1/2}$ at room temperature. XNBR without filler showed the maximum uptake at equilibrium, since there was no restriction for the solvent to diffuse into the vulcanizate.

The reduction in the equilibrium swelling is a measure of the degree of adhesion between the polymer chains and the filler particles. The presence of elecron acceptor groups in XNBR can interact strongly with the electron donating hydroxyl groups on the MWCNT surfaces [46] (IR spectrum of MWCNT, (Fig.3.11) shows the presence of OH group in it). On interaction of the polymer with the filler, a single macromolecular chain covers sizable number of active sites on the filler surface.Thus only a small number of chains are anchored on the surface of the filler [47]. It is likely that unanchored NBR chains are contributing to the swelling of the elastomeric nanocomposite network. Fig.4.20 depicts the decrease in swelling index with increase in the concentration of MWCNT.

Swelling percentage is a measure of the degree of cross-linking. Reduction in swelling indicated increase of cross-link density. The effect of increase in cross link density was further confirmed by the small increase in glass transition temperatures [48] (refer Table 4.6).Weerachai Sangchay et al. have referred to the decrease in swelling in NR/MWCNT nano composite as due to the decrease in NR content by the addition of non swellable solid MWCNT[43].
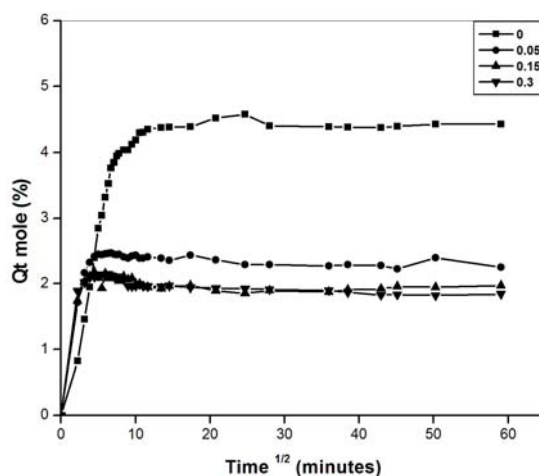
Fig. 4.19. Sorption curves of XNBR- MWCNT nanocomposites
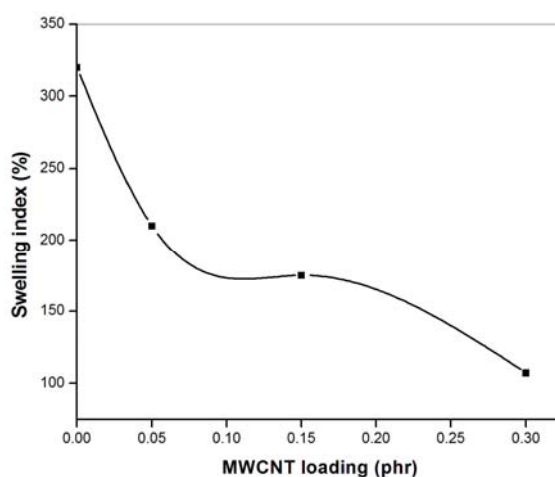
Fig. 4.20. Variation of swelling index with MWCNT loading

4.3C.3 Thermogravimetric analysis (TGA)

By comparing the weight loss as a function of temperature the effect of MWCNT on the thermal stability of XNBR could be analysed. Fig.4.21 shows the TGA curves of pure XNBR and XNBR–MWCNT nano composites containing 0.05 and 0.15phr MWCNT. The samples displayed similar behaviour. Thermal analysis results of XNBR and the nano composites

are given in Table 4.5. There was an increase in the onset temperature and a shift of maximum peak (T_2) to higher temperature on adding MWCNT. Small increase in T_{50} and T_{75} also showed slight increase in the thermal stability of the nanocomposites. Percentage of residual weight increased with the increase in concentration of nanotube. The presence of residue beyond 500^0C in the TGA curve might be due to the presence of other compounding ingredients in the mix. Eventhough nanotube was added in very small quantity it could impose restriction to the mobilization of rubber macromolecules and conduct heat homogeneously and avoid heat concentration [49].

Leon D.Perez et al. [46] studied the thermal stability of MWCNT/ NBR and MWCNT/ SBR nano composites at high filler loading up to 15 phr. They suggested that the ability of MWCNT to suppress thermal degradation of the elastomer might be attributed to barrier effects as in the case of clay fillers or a reduction of the pyrolysis rate, due to the decrease of the polymer global mobility.

Table 4.5. Thermal analysis results of XNBR and XNBR-MWCNT nano composite

Samples	On set temp(^{0}C)	Tmax(^{0}C)		Temp. at 50% wt.loss(^{0}C)	Temp. at 75% wt.loss(^{0}C)	Residue%
		T1	T2			
XNBR	326	432	456	450	471	13.67
XNBR 0.05MWCNT	333	431	458	450	471	15.91
XNBR 0.15MWCNT	334	432	459	453	475	16.54
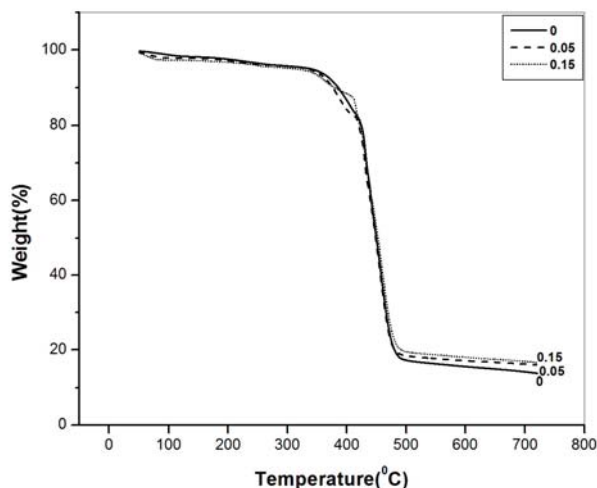
Fig. 4.21. TGA curves of XNBR and XNBR-MWCNT nanocomposites

4.3C.4 Differential scanning calorimetry (DSC)

DSC analysis results of XNBR and its nano composites are given in Table 4.6. DSC analysis was performed in order to determine the effect of MWCNTon the glass transition temperature of XNBR. There was a small increase in T_g on the addition of nanotube. This was due to the high interfacial area of interaction between the nanotube and the matrix which reduced the mobility of the polymer chain segments. This was a sign of compatibility between carbon nanotube and XNBR matrix. It is understood that the loading of MWCNT used were too small to produce a more significant change in T_g.

Table 4.6. T_g values of XNBR and XNBR-MWCNTnanocomposites

Samples	T_g
XNBR	-25.13
XNBR .05 MWCNT	-23.33
XNBR 0.15MWCNT	-23.19

4.3C.5 X- ray diffraction analysis (XRD)

XRD patterns of MWCNT, XNBR-MWCNT nano composite and XNBR are shown in Fig.4 .22. MWCNT displayed one diffraction peak at $2\theta=25.7^0$ corressponding to a basal spacing of 0.35 nm. This is the characterestic peak of MWCNT. Amorphous nature of XNBR was evident from its XRD pattern. The characteristic peak of MWCNT was absent in the nano composite.This showed exfoliation of nanotube and indicated efficient mixing of nanotube with the polymer matrix.
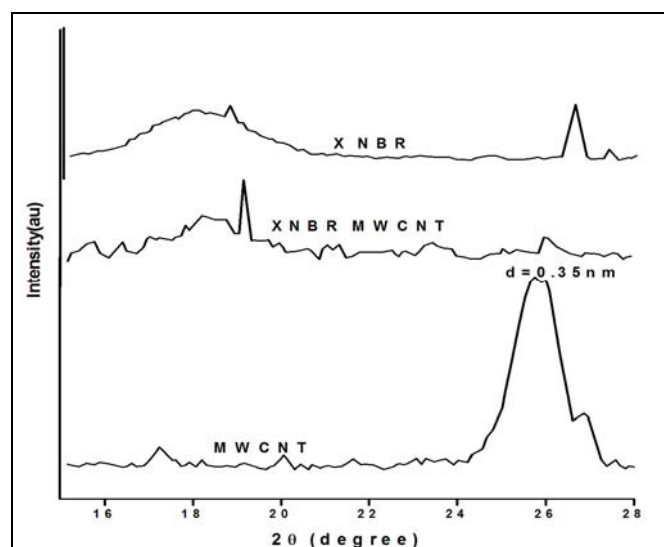
Fig.4.22. X-raydiffraction pattern of MWCNT, XNBR-MWCNT nano composite and XNBR

4.3C.6 Fourier transform infrared spectroscopy (FTIR)

Fig.4.23 shows the FTIR of XNBR, XNBR–MWCNT nano composite and MWCNT. Almost all the bands associated with the stretching of CH_2 groups were shifted to lower wave number in the nano composite. The peak at $969cm^{-1}$ attributed to stretching of butadiene double bond in XNBR was shifted to $964cm^{-1}$. The absorption band at $1440cm^{-1}$ due to OH bend in

carboxylic acid in XNBR was shifted to 1436cm^{-1}. These shifts might be due to the interaction between polymer chain and nanotube surface.The characteristic peak of CN at 2238cm^{-1} remained intact. The broad band due to OH stretch of hydroxyl group in MWCNT disappeared in the nano composite. In the IR spectrum of MWCNT the peak at 1558cm^{-1} corresponded to the stretching mode of C=C bond that formed the frame work of carbon nanotube sidewall [50]. This peak was present in the nano composite also but with a reduced intensity. This showed the interaction of the polymer chain with the C=C bonds in the nanotube.
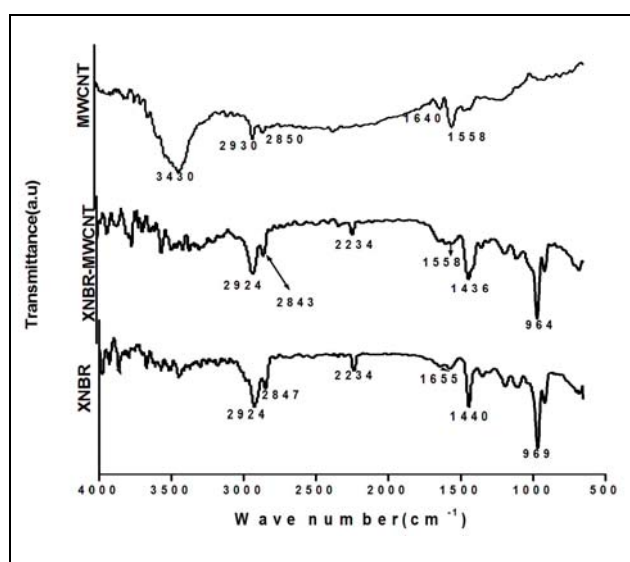
Fig.4.23. FTIR spectrum of XNBR, XNBR–MWCNT nanocomposite and MWCNT

4.3C.7 Scanning electron microscopy (SEM)

Fig. 4.24 (A), shows the SEM images of the MWCNT dispersed on the surface of the nano composite. Latex blending had given a homogeneous and uniform dispersion of nanotubes abundantly on the surface.

Fig.4.24 (B), (C) and (D) show the tear fractured surface of XNBR-MWCNTnanocomposites at different magnification. Absence of any agglomerates and void spaces in the rubber matrix, as seen at low magnification is a clear evidence of the good dispersion of nanotube in rubber. Because of the strong interaction between MWCNT and XNBR, the nanotubes were deeply embedded in XNBR. Thus MWCNT can carry stress throughout the rubber matrix leading to an effective reinforcement in the properties. Under high magnification short length of the nanotubes were visible. This might be due to the curved structure of the nanotube with one or both ends sunk in the matrix.
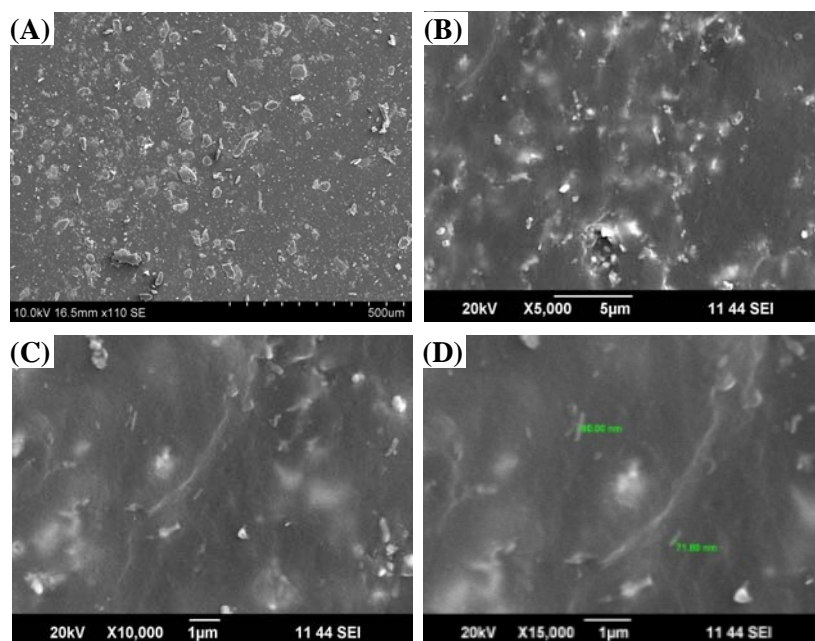
Fig.4.24. SEM images of (A) surface of the nano composite (B, C, D) tear fractured surface of the nano composite

4.3C.8 Conductivity studies

Fig.4.25 shows the variation of log of DC electrical conductivity of the nano composites against MWCNT loading. Conductivity of pure XNBR was of the order $10.^{-7}$ With increase of MWCNT loading conductivity value also increased and became 10^{-2} ie orders of magnitude higher than that of pure XNBR. At low filler concentration the conductivity remained very close to the conductivity of the pure, electrically insulating polymer marix, since the fillers occur only individually or in small clusters throughout the matrix [51]. Percolation threshold and drastic increase in electric conductivity was a result of continuous network of MWCNT in the polymer matrix. The conducting CNTs were either making physical contact between themselves or were separated by small gaps [52] across which 'hoping or tunneling' [53] of electrons took place.

Lorraine et al. [54] have dealt with the electrical conductivity of nano composites prepared from aqueous dispersion of conductive nanofillers (carbon black, antimony doped zinc oxide and carbon nanotubes) and latex [poly (vinyl acetate-co-acrylic) polydisperse latex/a poly(vinyl acetate) polydisperse latex/monodisperse poly(vinyl acetate) latex.] When the conducting carbon nanotubes in aqueous dispersion were mixed with the latex and allowed to dry a series of microstructure changes took place and the conductive particles became trapped in the polymer matrix. The micro structure of the matrix could force percolation to occur at a lower value by segregating the conductive particles to a restricted volume within the microstructure [54].
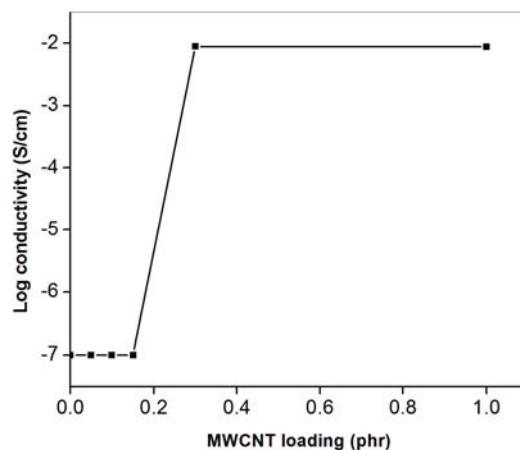
Fig.4.25. Variation of DC conductivity with MWCNT loading.

4.3C.9 Conclusions

MWCNT is good reinforcing filler in XNBR. Preparation of the nano composite by sonication of purified MWCNT in SDBS and latex blending technique gave a uniform dispersion of MWCNT in XNBR. This was observed in the SEM images of the nano composites. Absence of new peaks in the IR spectrum indicated there was only a strong interaction between the matrix and filler and no new bonds were formed in the nano composite. In XRD analysis the characteristic peak of MWCNT at 25.8^0 was absent in the nano composite, showing exfoliation in the nano composite and confirmed the strong interaction between nanotube and matrix.

Mechanical properties of the nano composite increased with a very small concentration of MWCNT. Tensile strength increased by 78%, elongation at break by 86%, modulus by 31% and tear strength by 19%. The incorporation of MWCNT in rubber matrix produced small enhancement in thermal properties. Electrical conductivity experiments revealed the presence of a percolation network at low filler loading, as low as 0.15 phr.

4.3D Graphene Nanoplatelets in XNBR Latex

Compared to carbon nanotubes, graphene nanoplatelets are cheaper and possess higher functionalities due to their high structural integrity[55] The two dimensional platelet geometry of graphene and graphene based materials offer certain property improvements which even single walled nanotubes cannot provide when dispersed in a polymer marix [56] Their high thermal conductivity, mechanical stiffness, fracture strength, electronic transport properties etc.can be harnessed when they are incorporated in a composite material [57].

Graphene based nanocomposites were prepared in XNBR latex. Graphene dispersion was made in a non ionic surfactant vulcastab VL. Graphene was added in small concentration ranging from 0-0.5phr. Mechanical properties of the nanocomposites increased even with the very low concentration of graphene.There were increase in the thermal stability and glass transition temperature of the nanocomposites. FTIR, XRD and FESEM analysis were used in the characterization of the nanocomposites.

4.3D.1 Mechanical properties

Mechanical properties of XNBR-graphene nanocomposites are shown in Fig.4.26. Fig. 4.26(A) gives the variation of tensile strength and elongation at break while Fig.4.26(B) gives the variation of modulus at 300% elongation and tear srength of the nanocomposite at various concentrations. It is seen that tensile strength, elongation at break, modulus and tear strength of XNBR increased significantly, reached an optimum value and then decreased.The tensile strength of the nanocomposite increased by 38%, elongation at break by 73% and tear strength by 27%, with a graphene concentration as low as 0.15 phr.

Strong interfacial adhesion between the platelets and polymer matrix was crucial for effective reinforcement [58-60]. Improved nanofiller dispersion, and alignment of the filler in the matrix also enhanced the mechanical properties of the nanocomposites.

The tensile modulus of the nanocomposite showed an increase of 21% at 0.2 phr concentration. When dispersed in a polymer matrix, the thin platelets would adopt wavy or wrinkled structures. Under the influence of an applied tensile stress these crumpled platelets would tend to unfold, rather than stretch in-plane and this reduced the modulus value [61].
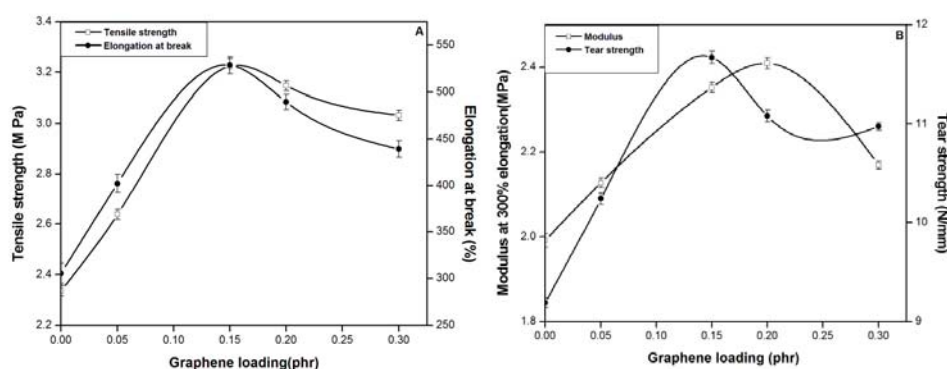
Fig.4.26.Variation of (A) Tensile strength and Elongation at break (B) Modulus and Tear strength of XNBR-graphene nanocomposite

4.3D.2 Swelling studies

Swelling studies were done in methyl ethyl ketone. The variation of solvent sorption Qt% against $time^{1/2}$ and swelling index (%) with concentration of graphene are shown in Fig.4.27 and 4.28 respectively.

With the addition of filler the swelling rate decreased. This can be ascribed in terms of the polar nature of XNBR matrix. Polar-polar interaction between polymer and filler reduced agglomeration of filler

particles. The swelling of 0.05 and 0.3 phr nanocomposites followed the same trend. Swelling was rapid at the beginning and then the swelling rate reached equilibrium.
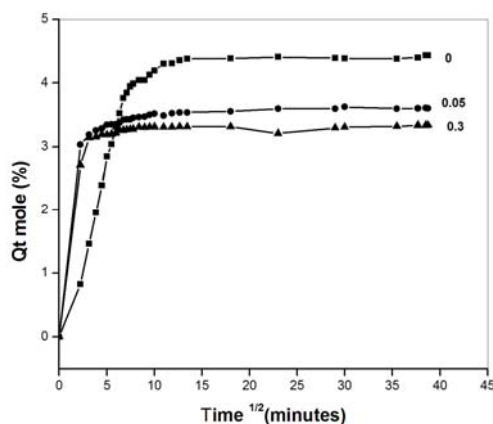
Fig. 4.27. Sorption curves of XNBR- graphene nanocomposites
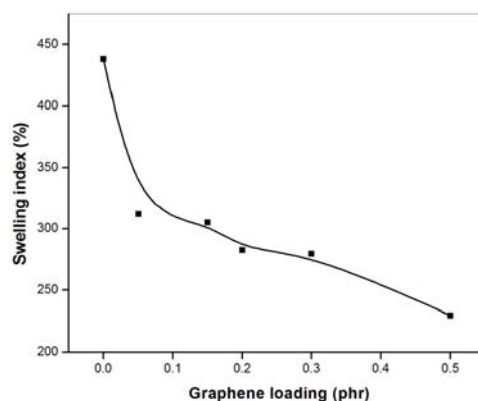
Fig. 4.28. Variation of swelling index with graphene loading

4.3D.3 Thermogravimetric analysis (TGA)

TGA curves of XNBR and nanocomposite containing 0.15 phr graphene are shown in the Fig.4.29 and thermal degradation results are given in Table 4.7.The data revealed that there was an increase of 7^0C in the onset temperature by the addition of 0.15 phr graphene. Temperature of maximum weight loss (T_2), temperature at 5% and 50% weight loss

were higher in the nanocomposite. Thus the addition of a very low concentration of graphene increased the thermal stability of the nanocomposite. The residual value of the nanocomposite was almost the same as that of XNBR.
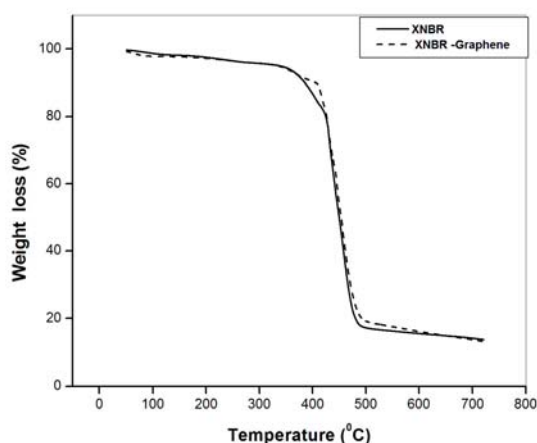
Fig.4.29. TGA curves of XNBR and XNBR-0.15 graphene nanocomposite

Table 4.7. Thermal analysis results of XNBR and XNBR-0.15 graphene

Samples	On set temp. (^{0}C)	Tmax (^{0}C)		Temp. at 5%wt.loss(^{0}C)	Temp.at 50%wt.loss	Residue
		T_1	T_2			%
XNBR	326	432	456	337	450	13.67
XBR- 0.15 Graphene	333	432	463	339	451	14.37

4.3D.4 Differential scanning calorimetry (DSC)

Table 4.8 gives the T_g of XNBR and the nanocomposites containing different graphene loadings. T_g of XNBR without filler was at -25.13^0C. There was a gradual increase in T_g with the addition of graphene. Thus with 1phr loading of graphene T_g increased to -23.79 ^{0}C. This showed the incorporation of graphene even in very small concentration increased the stiffness of the composite and restricted the mobility of XNBR chain.

Table 4.8. T$_g$ values of XNBR and XNBR graphene nanocomposites

Sample	T$_g$ (^{0}C)
XNBR	-25.13
XNBR-0.05graphene	-25.05
XNBR-0.15graphene	-24.75
XNBR-0.2graphene	-24.14
XNBR-1graphene	-23.79

4.3D.5 X- ray diffraction analysis (XRD)

X-ray diffraction pattern of graphene and XNBR-0.15 graphene nanocomposite is shown in Fig.4.30.The broad peak of nanocomposite indicated exfoliation of graphene platelets by the intercalation of ploymer chain.
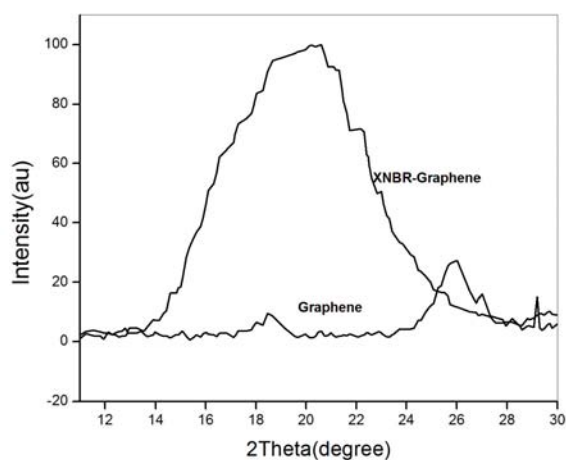
Fig.4.30. X-ray diffraction pattern of graphene and XNBR-0.15 graphene nanocomposite

4.3D.6 Fourier transform infrared spectroscopy (FTIR)

Fig.4.31 shows the IR spectrum of graphene, XNBR-0.15graphene nanocomposite and XNBR. The peaks corresponding to the CH stretch vibration and CN group of XNBR were seen in the composite also. The

peaks at 1539 cm^{-1} and 1437cm^{-1} giving the skeletal vibrations and the aliphatic CH bending [62] respectively of graphene sheets were seen to be more pronounced in the nanocomposite with a slight shift to a higher wave number. This showed the interaction of π electrons of graphene platelets with the polymer chain.
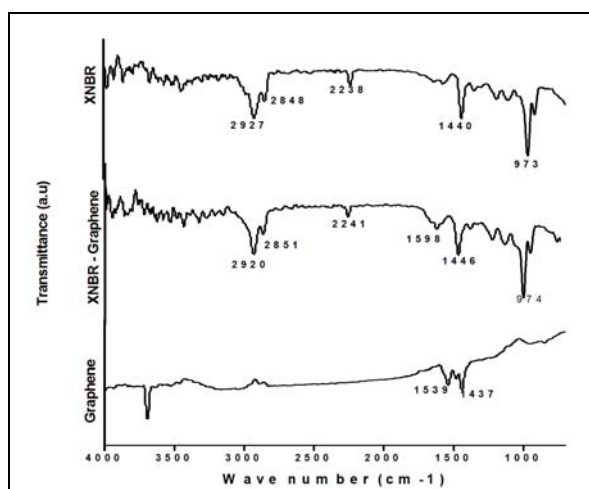
Fig.4.31. FTIR spectrum of graphene, XNBR-0.15 graphene nanocomposite and XNBR

4.3D.7 Field emission scanning electron microscopy (FESEM)

Fig. 4.32 shows the FESEM images of XNBR-graphene nanocomposite surface and Fig.4.33 represent the FESEM images of the tear fractured surfaces of the nanocomposite. A uniform distribution of graphene with clear particle profiles and clear interface boundary were seen on the surface of XNBR. While photographs of the tear fractured surface gave information on the interfacial adhesion between the filler particles and rubber matrix. In the tear fractured surface, the interface profile was indistinct showing good adhesion between filler and matrix [63].
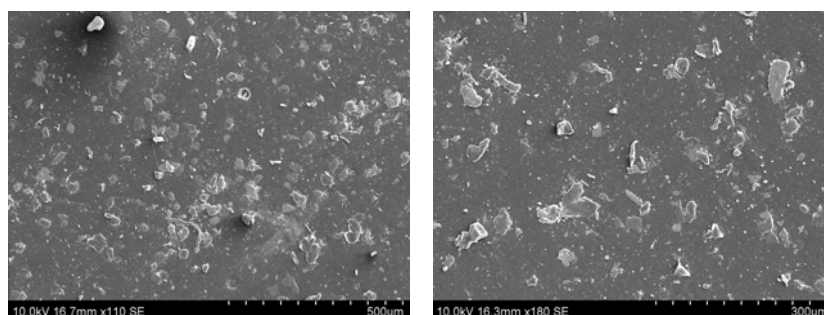
Fig.4.32. FESEM images of the surface of XNBR-graphene nanocomposite
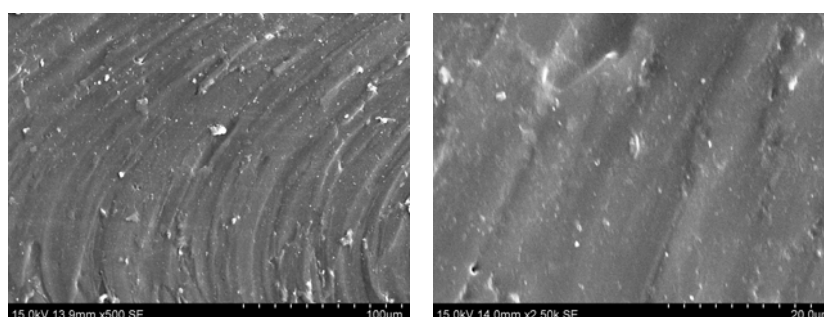
Fig.4.33. FESEM images of the tear fractured surface of XNBR-graphene nanocomposite

4.3D.8 Conductivity studies.

The DC electrical conductivity of XNBR-graphene nanocomposites are plotted in Fig.4.34 as a function of graphene loading. A sharp rise in conductivity was observed at 0.1phr concentration of graphene, indicating a filler network formation. The high aspect ratio of graphene enabled a good network formation in the matrix at such a low concentration of graphene. Generally percolation threshold and drastic increase in electrical conductivity results when the concentration of filler is sufficient to provide continuous electrical paths through the polymer matrix. The conducting elements should either make contact between themselves or should be separated by very small distances across which electrons could tunnel. The percolation threshold varies considerably with the shape and agglomeration of the filler

as well as the type of polymer used. Below the percolation threshold the conductivities of the composites were approximately the same and close to that of the pure, electrically insulating polymer matrix.
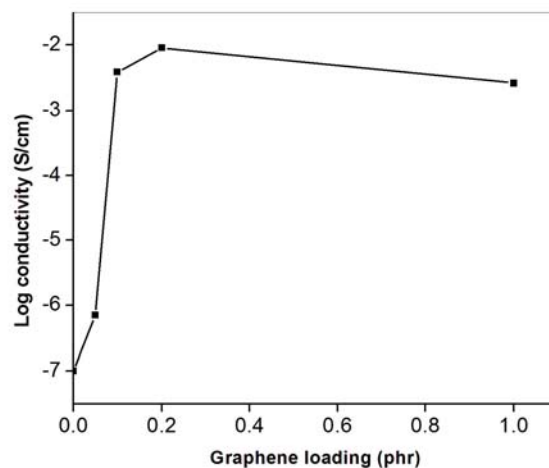
Fig.4.34. Variation of DC conductivity with graphene loading

4.3D.9 Conclusions

Preparation of graphene dispersion in a non ionic surfactant, Vulcastab VL and the method employed for the preparation of the nanocomposite contributed to the reinforcing effect of the graphene in XNBR latex. Inclusion of graphene nanoplatelets in a very low concentration (0-0.5 phr), increased tensile strength by 38%, elongation at break by 73%, tear strength by 27% and modulus by 21%. T_g and thermal stability of the nanocomposite increased with the increase in concentration of graphene platelets. FTIR analysis showed the interaction of π electrons of graphene with the polymer chain. SEM analysis of the tear fractured surface of the nanocomposite showed good interaction between graphene platelets and XNBR latex.

References

[1]   Mahaling, R.N. Jana, G.K. Das, C.K. Macromolecular Research. 2005, 13, 306.

[2]   Przybyszewska, M. Zaborski, M. eXPRESS Polymer Letters. 2009, 3, 542.

[3]   Mousa, A. Heinrich, G. Wagenknecht, U. Polymer-Plastics Technology and Engineering. 2011, 50, 1388.

[4]   Chakraborty, S. K. Setua, D. K. De, S. K. Rubber Chemistry and Technology. 1982, 55, 1286.

[5]   Laskowska, A. Lipińska, M. Zaborski. Academy Publish.org - Journal of Engineering   and Technology 2, 24.

[6]   Kumar, R. Karger–Kocsis J. European Polymer Journal. 2002, 38, 2231.

[7]   Ibarra, L. Rodríguez, A. Mora, I. European Polymer Journal. 2007, 43, 753–761.

[8]   Fritzsche, J. Das, A. Jurk, R. Stöckelhuber. K.W. Heinrich, G. Klüppel, M. eXPRESS Polymer Letters. 2008, 2, 373.

[9]   Wu,Y. Wang,Y. Zhang,H. Wang,Y. Yu,D. Zhang,L.Yang,J. Composites Science and Technology. 2005, 65, 1195.

[10]   Sadhu, S. Bhowmick, A. K. Journal of Applied Polymer Science. 2004, 92, 698.

[11]   Li, H. Wang, L. Song, G. Li, Z.G.P. Zhang, C. Gao, L. Iranian Polymer Journal. 2010, 19, 39.

[12]   Ou, R. Zhang, J. Deng, Y. Ragauskas, A.J. Journal of Applied Polymer Science. 2007, 102, 1987.

[13] Braggs, B. Fornasiero, D. Ralston,J. ST.Smart,R. Clays and Clay Minerals. 1994,42,123.

[14] Stephen, R. Joseph, K. Oommen,Z.Thomas,S.Composites Science and Technology. 2007, 67, 1187.

[15] Markovic, G. Radovanović, B. Vodnik,V. Marinović-Cincović, M.Beograd, Budinski- Simendić, J. Novi Sad. Testing and measuring. KGK März, 2009, 103.

[16] Soares, B.G. de Oliveira, M. Zaioncz, S. Scielo. doi: 10.1590/S0104-14282010005000055

[17] Kader, M. A. Kim, K. Lee, Y.S. Nah, C. J Mater Sci. 2006, 41, 7341.

[18] Das,A. Jurk,R. Stockelhuber,K.W. Majumder,P.S. Engelhardt,T. Fritzsche,J. Klu¨ppel,M. Heinrich, G. Journal of Macromolecular Science Part A: Pure and Applied Chemistry. 2009,46,7.

[19] Choi, M.D. Kader, A. Cho, B.H. Huh, Y. Nah, C.Journal of Applied Poly mer Science.2005, 98, 1688

[20] Sadhu, S, Bhowmick, K. A. Journal of Polymer Science Part B: Polymer Physics. 2004. 42, 1573.

[21] Xuening, L. Hongtao, Z. Zhizhong,Y. Chengyong,H.A. Chinese Science Bulletin.2005,50 1320.

[22] Fornes, T.D. Yoon, P.J. Keskkula, H. Paul, D.R. Polymer. 2001, 42, 9929.

[23] Shelley, J.S. Mather, P.T. DeVries, K.L. Polymer. 2002, 42, 5849.

[24] Kojima, Y. Usuki, A. Kawasumi, M. Okada, A. Kurauchi, T. Kamigaito.O. J. Appl. Polym. Sci. 1993, 49, 1259.

[25] Shojaeia, A. Faghihia, M. Polym. Adv. Technol. 2010, 21, 356.

[26] 26.Wang, S.J. Long, C.F. Wang, X.Y. Li, Q. Qi, Z.N. Journal of Applied Polymer Science. 1998, 69, 1557.

[27] Sadhu, S. Bhowmick, A.K. Rubber chemistry and technology. 2003, 76.

[28] Patra, S. P. Prusty, G. Swain, S.K. Bull. Mater. Sci. 2012, 35, 27.

[29] Sukumar, R. Menon, A.R.R. Journal of Applied Polymer Science. 2008,107, 3476.

[30] Mathew, L. Joseph, K.U. Joseph,R. Bull. Mater. Sci., 2006, 29, 91.

[31] Vijayalekshmi, V. Ph.D Thesis. Cochin University of Science and Technology.India.2009.

[32] Koo,J.K. Ezekoye,O.A. Lee,J.C. Ho,W.K. Bruns,M.C. Rubber –Clay Nanocomposites, Science, Technology and Applications Edited by Galimberti, M. Wiley.2011,489.

[33] Alexandre, M. Dubois, P. Materials Science and Engineering, 2000, 28, 1.

[34] Das, A. Stöckelhuber, K.W. Jurk, R. Jehnichen, D. Heinrich, G. Applied Clay Science.2011, 51,117.

[35] Chowdhury, R. Journal of Applied Polymer Science. 2007,103, 1206.

[36] Kim, J. Oh, T. Lee, D. Polym Int. 2003,52,1058.

[37] Nah, C. Ryu, H.J. Kim, W.D. Chang,Y. Polymer International Polym Int. 2003,52,1359.

[38] Hwang, W. Wei, K. Wu,C.Polymer Engineering and Science. 2004,44, 2117.

[39] Liu, L. Jia, D. Luo,Y. Guo,B. Journal of Applied Polymer Science. 2006, 100, 1905.

[40]   Thomas, P. C. Selvin, P. Thomas. George, G. Thomas,S. Kuruvilla, J. J Polym Res. 2011 DOI 10.1007/s10965-011-9651-1.

[41]   Anand. A.K. Jose, S. T. Alex, R. Joseph, R. Int J Polym Mater. 2010, 59, 33.

[42]   EI-Nashar, D.E. Ward, A.A. Abd-EI-Messieh, S.L. Elastomers and Plastics. 2009, 434.

[43]   Sangchay, W. Sikong, L. Kooptarnond, K. CMU.J.Nat.Sci. 2008, 7, 137.

[44]   Sangchay, W. Sikong, L. Kooptarnond, K. Technology and Innovation for Sustainable Development Conference (TISD2008) 2008.

[45]   Bokobza, L. A review. Polymer. 2007, 48, 4907.

[46]   Perez, L.D. Zuluaga, M.A. Kyu, T. Mark,J.E. Lopez,B.L. Polymer Engineering and Science. 2009,866.

[47]   Lipatov, Y.S. Polymer Reinforcement, ChemTec Publishing, Canada .1995.

[48]   Montazeri, A. Montazeri, N. Materials and Design. 2011, 32, 2301.

[49]   Sui, G. Zhong, W. H. Yang, X. P. Yu, Y. H. Zhao, S. H. Polym.Adv. Technol.2008, 19, 1543.

[50]   Tahermansouri,H. Chobfrosh khoei,D. Meskinfam,M. Int.J.Nano. Dim.2010,1, 153.

[51]   Bose, S. Khare, R. A. Moldenaers, P. Polymer. 2010, 51, 975.

[52]   Reffaee, A.S.A. El Nashar D.E. Abd-EI-Messieh, S. L. Abd-El Nour, K. N. Mater Des .2009, 30, 3760.

[53]   Lorenz, H. Fritzsche, J. Das, A. Sto¨ckelhuber, K.W. Jurk, R. Heinrich, G. Klu¨ ppel, M. Composites Science and Technology. 2009, 69, 2135.

[54]   Francis, L.F. Grunlan, J.C. Sun, J. Gerberich, W.W.   Colloids and Surfaces A: Physicochem. Eng. Aspect. 2007, 311, 48.

[55]   Araby, S. Zama, I. Meng,Q. Kawashima, N. Michelmore, A. Kuan, H. Majewski, P. Ma, J. Zhang, L. Nanotechnology.2013, 24, 1.

[56]   Potts, J.R. Dreyer, D.R. Bielawski, B.C.W. Ruoff, R.S. Polymer. 2011, 52 , 5.

[57]   Stankovich, S. Dikin, D.A. Geoffrey, H. B. Dommett. Kohlhaas, K.M. Zimney, E.J Stach, E.A. Piner, R. D. Nguyen, S.T. Ruoff, R.S. Nature.2006, 442, 282.

[58]   Paul, D.R. Robeson, L.M. Polymer. 2008, 49, 3187.

[59]   Kluppel M, editor. The role of disorder in filler reinforcement of elastomers on various length scales. Springer. 2003,164,86

[60]   Pukánszky, B. Fekete, E. editors.Adhesion and surface modification. Springer. 1999, 139,109.

[61]   Wakabayashi, K. Pierre, C. Dikin, D.A. Ruoff, R.S. Ramanathan,T. Brinson, L.C et al. Macromolecules. 2008, 41, 1905.

[62]   Liana, P. Zhub, X. Lianga, S. Li, Z. Yang,W. Wang, H. Electrochimica Acta. 2010, 55 , 3909.

[63]   Yang,J. Tian,M. Jia,Q. Zhang,L. Li,X. Journal of Applied Polymer Science.2006, 102, 4007.

.....৪০৫.....

Chapter 5

SBR LATEX BASED NANOCOMPOSITES

5.1 Introduction

Styrene butadiene rubber (SBR) is one of the most versatile synthetic rubber compounds, produced by the copolymerisation of styrene and butadiene. The important limitations of SBR are poor strength, low resilience, low tear strength and poor tack. For amorphous polymers like SBR which does not undergo strain induced crystallisation, the use of fillers can improve the processability and mechanical properties and thus reduce the cost of rubber articles [1].

Among the vast nanofillers available for fabricating polymer nanocomposites, clay has been focussed and studied the most due to its easy availability, low cost, special stratified structure, high surface area, high aspect ratio etc.

SBR based nanoclay composites have been reported by several authors [2-6]. Wonho Kim et al. [4] used octadecyl amine modified MMT to prepare SBR composites by latex coagulating and melt mixing methods.

According to Kim, though compounding by melt mixing is an environmentally friendly method, it is very difficult to intercalate rubbery materials into the clay galleries. While in the latex method swellable clays like MMT are easily exfoliated by dispersing in deionized water and the high molecular weight polymer chain need not penetrate the galleries of the silicate. Other benefits include easy use of rubber in the form of latex and maximum dispersing effect of MMT in solution and the use of water as solvent.

Composites based on carbon nanotube have attracted great interest due to their unique mechanical, surface, electrical and multi functional properties. The improvement in properties is observed due to the nano-scale microstructure and extremely large interfacial area of the nanotubes [7]. The most common methods employed to prepare nanotube/polymer composites are solution blending, melt blending and insitu polymerisation. Of these, solution blending is most amenable to small sample sizes and is an effective method [8].

Studies of elastomeric composites with MWCNT include MWCNT/ NBR/SBR composites prepared by melt mixing on a two roll mill [9], MWCNT/NR composites prepared by solvent mixing method using toluene as the solvent [10] and MWCNT/methyl vinyl silicone rubber composites prepared by solution method [11].

The major challenges encountered in devoloping high performance polymer/carbon nanotube composites are, homogeneous dispersion of carbon nanotubes and strong interfacial interactions to ensure efficient load transfer from the polymeric matrix to the carbon nanoubes. Carbon nanotubes usually exist as bundles with vander Waals forces holding the

tubes together [12]. The yield strength of the composite is related to the morphology, domain size, and size homogeneity of the nanotube in the matrix [13].

A review on recent advances in graphene based polymer nanocomposites discusses the effectiveness of graphene as nanofiller in various polymeric matrices like epoxy, polystyrene, polyaniline, polyurethane, poly (vinylidinefluoride), polycarbonate, PET etc. [14]. Reports on elastomer based graphene composites are limited. Zhan et al. [15] prepared NR/graphene composites by a latex stage mixing method, and in situ reduction process of the graphene oxide. Graphite powder with different forms and sizes were mixed in NBR using a twin roller by Jian Yang [16]. Wang et al. [17] prepared NBR composites with expanded graphite by latex compounding and mechanical mixing. Amit Das et al. [18] mixed solution of styrene butadiene rubber with graphene nanoplatelets, expanded graphite and carbon nanotubes using an internal mixer. Kim et al. [19] prepared SBR based graphene nanocomposites by solution mixing method

Pristine graphene as a bulk material has a tendency to agglomerate in a polymer matrix, so they are unsuitable as such for intercalation by polymer materials. But they can be easily dispersed in suitable solvents like water, acetone, chloroform, tetrahydrofuran (THF), dimethylformamide (DMF) etc. owing to their weak forces that stack the layers together.

Graphite is composed of stacks of parallel two dimensional graphene sheets with sp^2 hybridized carbon atoms tightly bonded in hexagonal rings. The adjacent graphene sheets are held together by weak van der Waals forces [20]. Graphene nanoplatelet is not an individual graphene sheet but comprises

of multiple graphene sheets that are stacked together [21, 18]. Thus, the thickness of the platelets is significantly larger than individual graphene sheet.

In this chapter the effect of addition of different nanofillers like nanokaolin, vinylsilane grafted nanokaolin, multiwalled carbon nanotube and graphene nanoplatelets in SBR latex are discussed. SBR based nanocomposites were prepared by a latex blending technique. SBR latex was mixed with aqueous dispersion of nanofillers and other compounding ingredients and cast in glass trays. The casting was allowed to dry in air and then vulcanized in air circulated oven.

5.2 Experimental
5.2.1 Materials

SBR latex - Encord 204, supplied by Jubilant Organosys Ltd., Gujarat. Specification of SBR latex is given in Table2.2. Nanokaolin (Nanocaliber100) and Vinylsilane grafted nanokaolin (Nanocaliber 100V), were supplied by English Indian Clays Ltd., Veli, Thiruvananthapuram. Specification is given in Table 2. 3. Multiwalled carbon nanotube (MWCNT) - Baytube ^{R} 150P was obtained from Baeyer Materials Science AG (Leverkusen Germany). Specification is given in Table 2.4. Graphene nanoplatelets were purchased from Quantum materials Ltd., Bangalore.

Nanokaolin is designated as 'C'and SBR composites containing 1, 5, 10 phr 'C' are referred as SBR-1C, SBR-5C, SBR-10C etc. Vinylsilane grafted nanokaolin is designated as 'V' and SBR containing 1, 5,10 phr V are represented as SBR-1V, SBR-5V, SBR-10V etc and graphene nanoplateles are referred as graphene.

5.2.2 Preparation of SBR based nanocomposites

Formulations used for making SBR latex compounds are given in Table 3.4. Preparation of SBR latex/clay nanocomposites and SBR/ MWCNT/graphene nanocomposites are given in Section 3.11.1. and Section 3.11.3 respectively.

5.2.3 Methods

Detailed description of the methods used for the study of the mechanical properties (Section 2.4.5), swelling studies (Section 2.4.6), TGA (Section 2.4.8), DSC (Section 2.4.9), XRD (Section 2.4.10), FTIR (Section 2.4.11), SEM (Section 2.4.13) and AFM (Section 2.4.16) are included in Chapter 2.

5.3   Results and Discussion
5.3A Nanokaolin in SBR Latex

Aqueous dispersion of nanokaolin was sonicated for 30min and added to SBR latex in concentrations ranging from 0-20phr. Latex stage blending technique adopted for the preparation of XNBR-C nanocomposites resulted in good interaction of hydrophilic clay with SBR latex. There was an appreciable increase in tensile strength, elongation at break, modulus and tear strength of the nanocomposites. Thermal stability and T_g increased by increasing the concentration of nanokaolin. SBR/nanokaolin composites were characterized by XRD, FTIR, SEM and AFM analysis.

5.3A.1 Mechanical properties

Tensile properties of polymer–clay composite vulcanizates depend on several factors, including the extent of clay dispersion, the degree of

interfacial adhesion between the clay platelets and the polymer matrix as well as the extent of crosslink density [22].

For SBR- nanokaolin composites, tensile strength, elongation at break and modulus at 300% elongation increased with increase in the concentration of nanokaolin reached a maximum value and then decreased. Fig.5.1 shows the variation of mechanical properties with clay loading.

Strong interaction of hydrophilic clay with SBR latex resulted in the reinforcement in properties. When the concentration of clay was above a critical level, aggregates were formed resulting in poor dispersion of clay. This led to degradation in mechanical properties of the nanocomposite at higher concentration [23]. Tear strength continuously increased with the concentration of clay. The special layer structure of the clay in the composites led to interfacial sliding between the clay layers and SBR matrix. This could decrease the energy of expansion of the crack, resulting in an increase in tear strength with concentration [5, 6]. The maximum % increase in the tensile properties along with their composition is given in Table.5.1.

Table 5.1. Percentage increase in mechanical properties of SBR-C nanocomposites

Properties	Maximum % increase	Composition of nanokaolin (phr)
Tensile strength	87	15
Elongation at break	47	15
Modulus	55	15
Tear strength	119	20
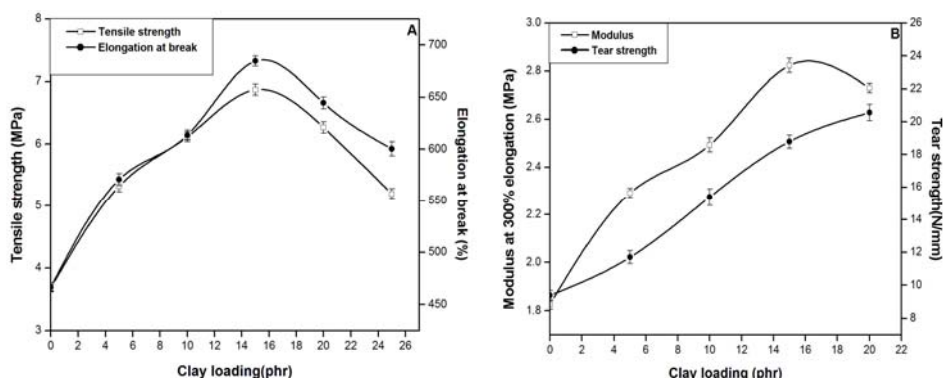
Fig. 5.1. Variation of (A) Tensile strength Elongation at break and (B) Modulus /Tear strength of the nanocomposite with clay (C) loading.

5.3A.2 Swelling studies

The variation in solvent uptake with increase in concentration of naokaolin was studied using toluene as the solvent. The diffusion curves were plotted as Q_t, mole % uptake per 100g of the solvent against time. From Fig.5.2 it is found that gum has the maximum up take at equilibrium. Swelling rate of the nanocomposites decreased with increase in concentration of clay. The clay platelets were distributed in the polymer matrix in multiple parallel layers. These impenetrable clay layers forced the solvent molecules to flow through the polymer in a "torturous path", forming complex barriers to the solvent molecules [24].
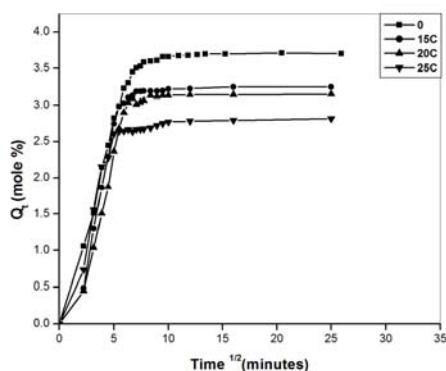
Fig.5.2. Sorption curves of SBR-C nanocomposites

5.3A.3 Thermogravimetric analysis (TGA)

Fig.5.3 shows the TGA curve and Table.5.2 gives the thermal analysis data of unfilled and filled SBR. The temperature of onset of degradation of SBR shifted from 320^0C to 337^0C by the addition of 15phr nanokaolin. Maximum degradation temperature, Tmax and the temperature at 10% (T_{10}), 25% (T_{25}) and 50% (T_{50}) weight loss were shifted to higher temperature in SBR-15C nanocomposite. This showed the thermal stabiliy of the composite increased by the addition of nanoclay. It is generally observed that the inclusion of inorganic components into organic materials improves the thermal stability of the polymer [25]. The observed increase in the thermal stability of SBR-15C nanocomposite was due to the high thermal stability of nanoclay and good interaction between the clay layers and polymer matrix through intercalation/exfoliation. The intercalated polymer chains were covered by clay layers which prevents the direct exposure of the chains to thermal influence.

Table.5.2 Thermal analysis results of SBR and SBR-15C nanocomposite

Name	Onset temp.(^{0}C)	Peak max. T_{max} (^{0}C)	T_{10} (^{0}C)	T_{25} (^{0}C)	T_{50} (^{0}C)	Residue %
SBR	320	441	365	398	426	3.08
SBR-15C	337	444	372	402	432	13.92
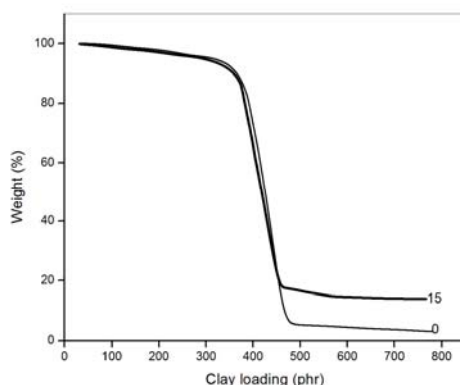
Fig.5.3. TGA curve of SBRand SBR-15C nanocomposite

5.3A.4 Differential scanning calorimetry (DSC)

Glass transition temperature of SBR and SBR-15C nanocomposite is given in Table.5.3. DSC curve of SBR latex showed Tg at -16^0C whereas the composite showed a small increase in Tg. The increase in Tg might be due to the effect of dispersed clay on the free volume of the polymer and the confinement of intercalated/exfoliated polymer chains within the clay galleries which resist the segmental motion of the polymer chains [26]

Table 5.3. T$_g$values of SBR and SBR-15C nanocomposite

Sample	T$_g$ (^{0}C)
SBR	-16
SBR- 15C	-14

5.3A.5 X- ray diffraction analysis (XRD)

XRD spectra of nanokaolin ('C') and SBR-15C nanocomposite are given in Fig.5.4. The presence of a broad peak in the composite is an indication of exfoliation. Due to the greater compatibility of the hydrophilic nanokaolin with SBR latex, the polymer chain is more effective in causing exfoliation of clay. A very small peak with a larger spacing   (d=9.22A^0) was also seen in the nanocomposite, which confirmed intercalation in a very small number of clay particles.
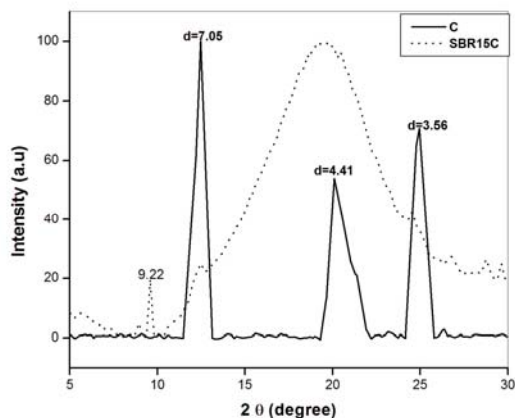
Fig. 5.4. X-ray diffraction pattern of nanokaolin ('C') and SBR-15C nanocomposite

5.3A.6 Fourier transform infrared spectroscopy (FTIR)

FTIR spectrum of SBR-15C and SBR is given in Fig 5.5 and Fig.5.6 respectively. The intensities of the peaks at 2916 and 2844 cm^{-1} attributed to the CH stretching of aromatic rings in SBR and the peaks in the range 1400-1600cm^{-1} and 699 cm^{-1} referring to the styrene units, [27] had become sharper in the nanocomposite. The peak corresponding to the trans 1, 4 butadiene of the styrene unit at 968cm^{-1} remained with almost the same intensity. Peaks at 1100, 1028 and 913 cm-^{1} in the composite correspond to the Si-O-Si, Al-O-Si units in nanokaolin. Intensity of characteristic OH stretching vibration of nanokaolin was reduced in the composite (FTIR spectrum of nanokaolin is given in Fig.3.2). Reduction in the intensity of OH band in nanokaolin, and strengthening of bands due to styrene units showed the interaction of OH group of nanokaolin with the bulky styrene units of SBR.
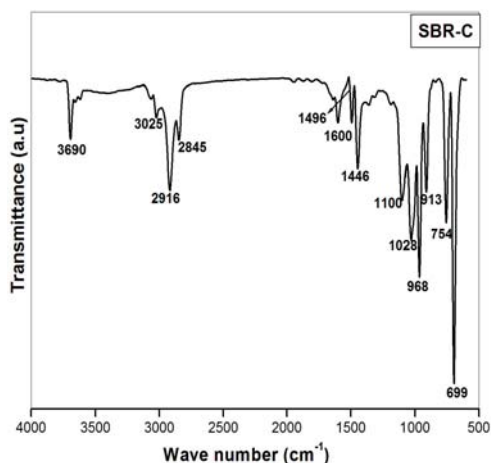
Fig. 5.5. FTIR spectrum of SBR-15C nanocomposite
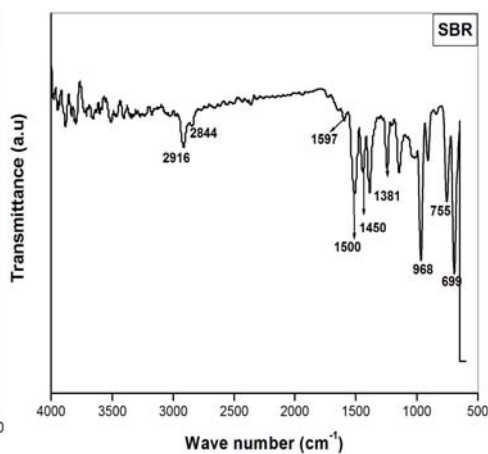
Fig. 5.6. FTIR spectrum of SBR

5.3A.7 Scanning electron microscopy (SEM)

Fig. 5.7 (A) and (B) show the SEM images of SBR-15C nanocomposite at different magnification. From the SEM images it is seen that the clay platelets are well embedded in the marix. At a still higher magnification a homogeneous dispersion having a continuous phase was visible (Fig 5.7(B)). This showed good compatibility and adhesion of clay with SBR latex.
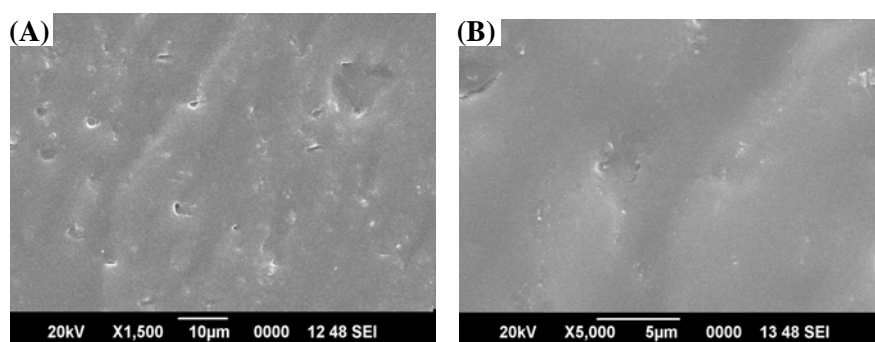
Fig.5.7. (A) and (B) SEM images of SBR-15C nanocomposite

5.3A.8 Atomic force microscopy (AFM)

Fig.5.8 displays the AFM image of SBR-15C nanocomposite. A smooth surface with clay particles embedded in it and some clay aggregates locally confined in some areas are visible in the image.
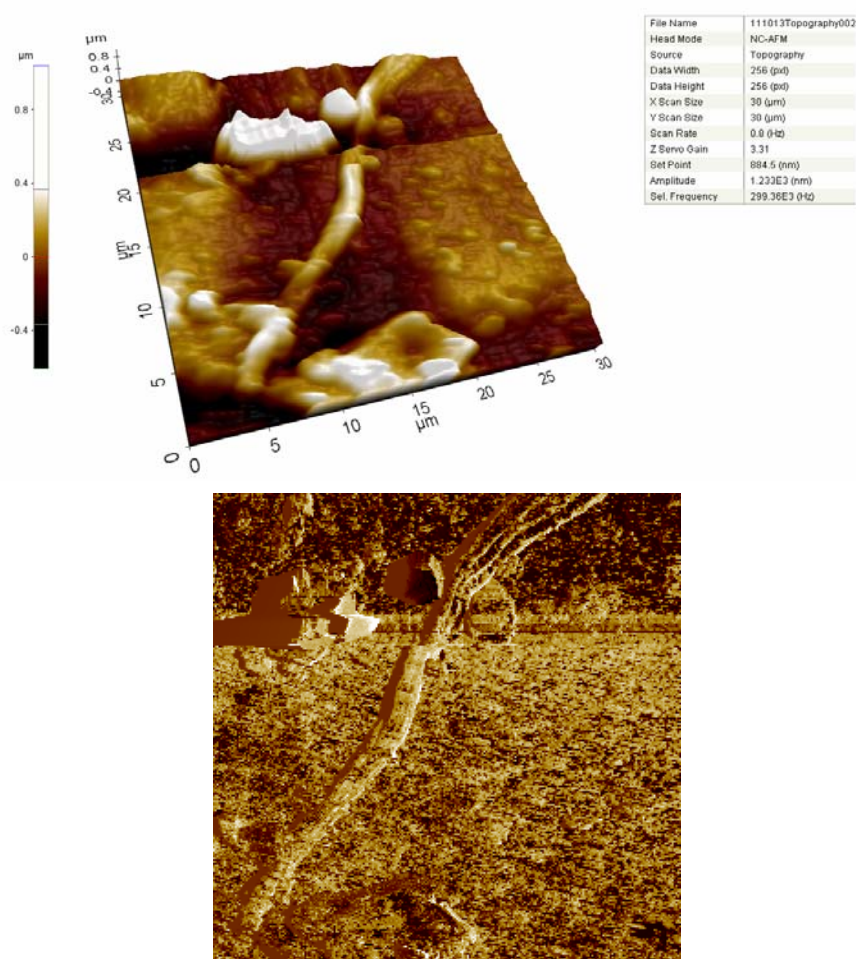
Fig. 5.8. AFM image of SBR-15C nanocomposite.

5.3A.9 Conclusions

SBR/nanokaolin composites prepared by the latex stage blending showed good improvement in mechanical properties owing to the improved

dispersion of clay platelets. Intercalation/exfoliation of clay layers took place during latex stage blending as observed by XRD analysis. The composite showed improved thermal stability.

5.3B Vinylsilane Grafted Nanokaolin in SBR Latex

Vinylsilane modified nanokaolin (V) was incorporated in SBR latex in concentrations varying from 0-25 phr. Vinylsilanes usually used for the treatment of clay are vinyl triethoxy silane and vinyl trimethoxy silane.The alkoxy groups are hydrolytic groups which are hydrolyzed to silanol groups in presence of water or moisture [28-30]. These silanol groups can form covalent bonds with some of the OH groups on the edge surface of clay by a condensation mechanism, or they can form hydrogen bonds with the OH groups in clay, while the vinyl groups can interact with the polymer chains. This is schematically represented in Fig.1.6. This interaction will give a reinforcing effect for the modified clay in SBR latex. SBR latex/ vinylsilane grafted nanokaolin composites have not been reported so far. Mechanical/thermal properties and characterization of SBR latex/vinyl silane grafted nanokaolin composites are discussed here.

5.3B.1 Mechanical Properties

Fig.5.9 (A) and (B) shows the variation of tensile strength/elongation at break and modulus/tear strength of the nanocomposite with clay ('V') loading (0-25 phr). Table5.4 gives the percentage increase in the mechanical properties of the nanocomposite at various filler loading. The addition of clay at lower loading did not produce any significant increase in tensile strength due to the lack of proper dispersion of the filler. Tensile srength of SBR-V nanocomposite was found to be smaller

than that of SBR-C nanocomposite. This is because organic modification of nanokaolin had made it organophilic and hydrophobic. This decreased the compatability of clay with SBR latex, causing a reduction in the tensile strength.

The decrease in elongation at break by the inclusion of rigid filler in a soft marix is a common observation [31, 32]. Incorporation of fillers with poor adhesion to the polymer matrix weakens interfacial regions between filler surfaces and rubber matrix causing a reduction in the elongation at break.

An increase in modulus was expected due to the decrease in elongation at break. Although compatability between modified clay and rubber latex was low, there was interaction between the non polar SBR and the vinyl group of clay. This led to an increase in modulus value.

Tear strength of SBR-V nanocomposite increased with the modified clay loading. This was attributed to the layer structure of nanoclay [33].
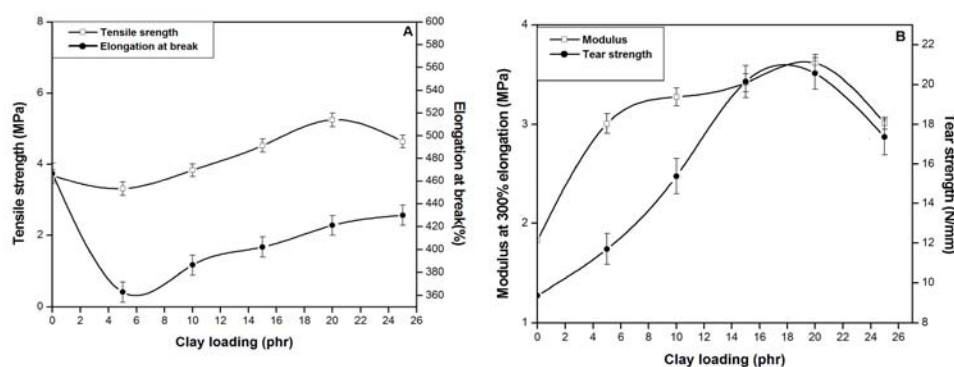
Fig. 5.9. Variation of (A) Tensile strength/Elongation at break and (B) Modulus/Tear strength of the nanocomposite with clay 'V' loading

Table 5.4. Percentage increase in mechanical properties of SBR-V nanocomposite

Properties	%increase	Composition of V (phr)
Tensile strength(MPa)	43	20
Modulus(MPa)	98	20
Tear strength (%)	119	20

5.3B.2 Swelling studies

Fig.5.10 gives the variation of Q_t, mole % with Time$^{1/2}$. When compared to SBR-C nanocomposites, SBR-V nanocomposites showed greater swelling rate. This is because the compatability of the organophilic clay in SBR latex was less than that of unmodified clay. So there was more filler–filler interaction and more chances to form filler aggregates. As a result the clay platelets might not be fully available in the matrix to enhace the tortuosity of the path
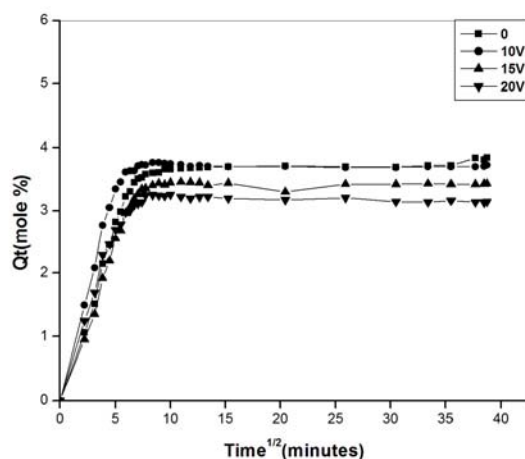
Fig. 5.10. Sorption curves of SBR-V nanocomposites

5.3B.3 Thermogravimetric analysis (TGA)

TGA curves for SBR and its composites containing 10 phr and 20 phr vinylsilane grafted nanokaolin are given in Fig. 5.11 and their thermal analysis

data are given in Table 5.5. Onset temperature increased with increase in clay loading. T_{10}, T_{25} and T_{50} showed gradual increase with the addition of clay, while T_{max} remained a constant. The thermal stability obtained by the addition of modified clay in SBR was less than that obtained by the addition of unmodified clay. This might be due to the reduction in the polymer filler interaction in SBR/modified clay nanocomposite. Percentage of residue remaining at 700^0C increased with the increase in clay loading. At higher clay loading the interaction between clay and SBR increased and the matrix became stiffer and thus the diffusion of heat and gases through the bulk became more difficult. This prevented the complete degradation of the nanocomposite.

Table 5.5. Thermal analysis results of SBR and SBR-15V nanocomposites

Sample	Onset temp. (^0C)	Peak max. (^0C)	Residue (%)	T_{10} (^0C)	T_{25} (^0C)	T_{50} (^0C)
SBR	320	441	3.08	365	398	426
SBR -10V	328	438	9.32	366	400	430
SBR- 20V	330	440	12.67	371	402	433
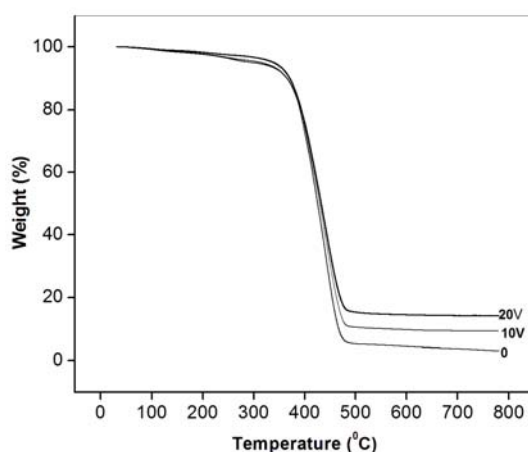
Fig. 5.11. TGA curves of SBR-V nanocomposite

5.3B.4 Differential scanning calorimetry (DSC)

DSC analysis data of SBR and SBR-V nanocomposite is given in Tabla5.6. SBR-V nanocomposite gave a very small increase in T_g with the incorporation of modified clay, showing that the SBR chain mobility was restricted in the nanocomposite.

Table 5.6. Glass transition temperature of SBR and SBR-20V nanocomposite

Sample	T_g
SBR	-16
SBR- 20V	-15

5.3B.5 X- ray diffraction analysis (XRD)

Insertion of polymer chains in the interlayer space of clay causes an increase in the interlayer volume and a shift in the diffraction peaks to lower angles. Diffraction peaks will be absent in case of exfoliation, when the clay layers are completely and uniformly dispersed in the polymer matrix [34].

Fig.5.12 gives the XRD patterns of 'V' and SBR-20Vnanocomposite. The nanocomposite showed only a slight shift in the 2θ angle with a small increase in d spacing.The d spacing increased from 7.1 to $7.5A^0$ and from 3.56 to 3.58 A^0in the nanocomposite.The peak at 2θ value 20^0 was also very much reduced in the nanocomposite formed.The presence of bulky styrene ring in the polymer chain would have slightly restricted the intercalation of polymer chain into the interlayer space of clay.This showed the intercalation of SBR into the clay layers was insignificant. The reduced compatibility between the hydrophobic organo modified clay and the hydrophilic SBR latex prevented the exfoliation of clay.
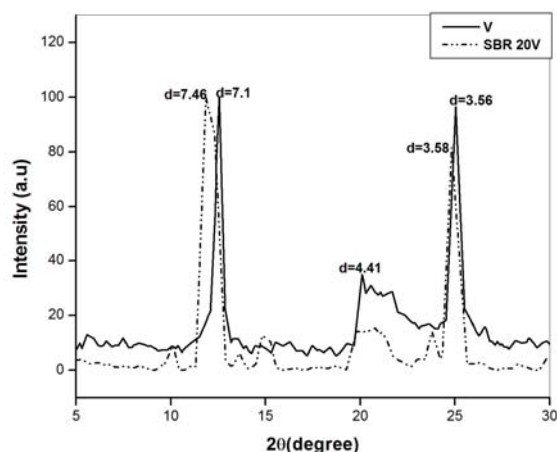
Fig.5.12. X-ray diffraction pattern of vinylsilane grafted nanokaolin (V) and SBR-20V nanocomposite

5.3B.6 Fourier transform infrared spectroscopy (FTIR)

IR spectrum of SBR-20V nanocomposite is given in Fig 5.13. The charecteristic OH stretching bands of nanokaolin (Fig 3.6) in the range 3600-3690cm^{-1} were seen in the nanocomposite also. Peaks due to CH$_2$ symmetric and asymmetric stretching (2916 and 2844cm^{-1}) in SBR (Fig.5.6) had become sharper in the nanocomposite due to the interaction of vinyl group of clay with the CH$_2$ group of rubber back bone. A medium peak at 1447cm^{-1} represented the merging of CH$_2$ groups of rubber with the vinyl groups of clay. The peak at 1095cm^{-1} showed the C-O stretch of alcoholic groups in clay. Appearance of a very strong band at 1023cm^{-1} was due to Si-O-Si (siloxane network) stretching vibration of clay [35]. The peak due to butadiene double bond in SBR at 963cm^{-1} was very much reduced in the nanocomposite. This might be due to the interaction of butadiene double bond with the double bonds of vinyl group in the modified clay.
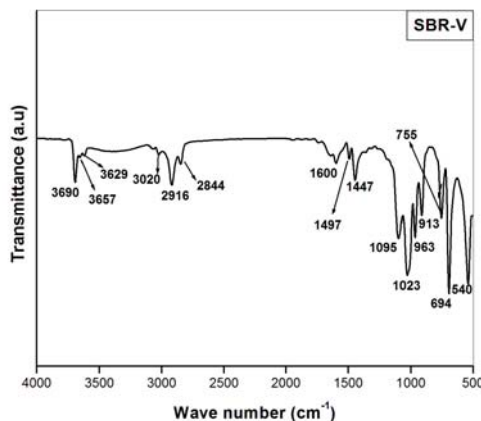
Fig.5.13. FTIR spectrum of SBR-20V nanocomposite

5.3B.7 Scanning electron microscopy (SEM)

Fig.5.14 shows the SEM photograph of SBR-V nanocomposite. The particles seem to project out from the matrix showing less compatibility of modified clay particles with the matrix.
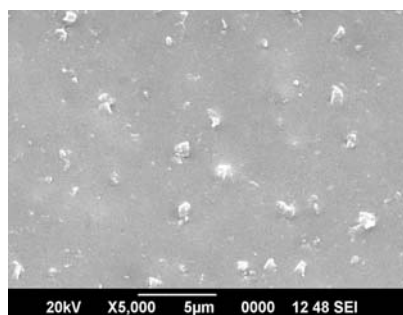
Fig.5.14. SEM image of SBR-V nanocomposite

5.3B.8 Conclusions

Vinylsilane grafted nanokaolin enhanced the tensile strength, modulus and tear strength of SBR. Enhancement in properties were less in SBR-V compared to SBR-C nanocomposite. XRD data showed that the intercalation of polymer chain with the bulky styrene group led to an

insignificant increase in the interlayer spacing. SEM images also proved the low compatability of modified clay with SBR latex. Thermal studies showed an improvement in the thermal stability of the nanocomposite and a slight increase in the glass transition temperature. FTIR analysis showed the interaction of vinyl groups in clay with the butadiene double bonds of the polymer chains.

5.3C MWCNT in SBR Latex

When mixed with rubber, carbon nanotubes usually give a poor dispersion, due to agglomeration of nanotubes by van der Waals forces. Any agglomeration results in the reduction of properties of the composite as it prevents efficient stress transfer to individual nanotubes. Here, an efficient dispersion of MWCNT was made by sonication in presence of a cationic surfactant SDBS. Introduction of functional groups on the nanotube surface during purification process improved the affinity to water and was beneficial for the preparation of MWCNT dispersion in SDBS. Moreover the functional groups loaded on the nanotube surface assisted in the interfacial bonding between carbon nanotube and SBR latex causing enhancement in the mechanical properies of the composite. MWCNT was added only in very small concentration to SBR latex. The nanocomposites prepared were characterized and their properties studied in detail.

5.3C.1 Mechanical Properties

Fig.5.15 (A) and (B) shows the variation in mechanical properties of SBR by the addition of MWCNT and Table5.7 gives the percentage increase in the mechanical properties. The addition of MWCNT brought about remarkable increase in tensile strength, elongation at break, modulus and tear

strength. This confirmed that MWCNT carried stress throughout the rubber matrix and played an effective role in the reinforcement of the nanocomposite.

MWCNT was added to SBR latex only in very small concentration ranging from 0-1.5 phr. Even with the very small concentration, tensile strength increased by 65%, elongation at break by 41%, modulus by 95% and tear strength by 68%. Well dispersed nanotube and good interface between the nanotube and SBR matrix led to the increase in tensile strength of the nanocomposite [36]. High Young's modulus and strength of the well dispersed nanotubes led to the increase in tear strength and modulus of the nanocomposite [7].

Fig.5.15.Variation of (A) Tensile strength and Elongation at break (B) Modulus and Tear strength of SBR-MWCNT nanocomposite

Table.5.7. Percentage increase in mechanical properties of SBR-MWCNT nanocomposites

Properties	% increase	Composition of MWCNT (phr)
Tensile strength	65	1.5
Elongation at break	41	1
Modulus	95	1.5
Tear strength	68	1

5.3C.2 Swelling studies

Fig 5.16 gives the variation of Qt (%) with $T^{1/2}$.The swelling rate of the nanocomposite containing 0.5 phr MWCNT was found to be greater than SBR without filler.This might be because the surfactant SDBS used for the preparation of MWCNT dispersion might have created a weak interface at the low cocentration of nanotube and must have assisted in the penetration of the solvent. But with the increase in concentration of MWCNT, the effect of the interphase diminished and the distribution of MWCNT in the matrix prevented the penetration of the solvent leading to a decrease inn the swellig rate.
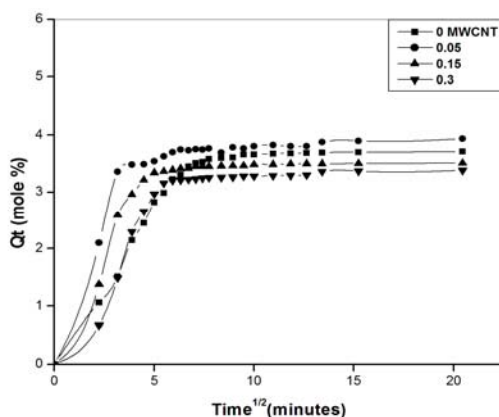
Fig. 5.16. Sorption curves of SBR-MWCNT nanocomposites

5.3C.3 Thermogravimetric analysis (TGA)

TGA trace of the nanocomposite containing 0.15phr MWCNT and SBR are shown in Fig.5.17. From Table 5.8 it is seen that the onset degradation temperature, Tmax and temperature at 5% and 50% weight loss are higher for the nanocomposite, showing that it is thermally more stable. As suggested by M. Moniruzzaman in a review on 'Polymer nanocomposites containing carbon nanotubes' the dispersed nanotubes might hinder the flux of degradation product

and thereby delay the onset of degradation. Polymers near the nanotube degrade more slowly which would shift the Tmax to higher temperature and the effect of higher thermal conductivity in the nanotube/polymer composites facilitates heat dissipation within the composite. All these factors might have contributed to the thermal stability of the SBR-MWCNT nanocomposite [8].

Table 5.8. Thermal analysis results of SBR and SBR-0.15MWCNT

Samples	On set temp. (^{0}C)	Tmax (^{0}C)	Temp. At 5%wt.loss (^{0}C)	Temp.at 50%wt.loss (^{0}C)	Residue %
		T_1			
SBR	320	441	313	426	3.08
SBR-0.15MWCNT	331	450	325	430	4.65
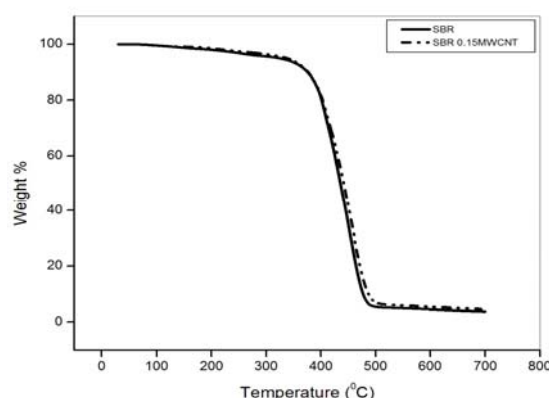
Fig. 5.17. TGA curves of SBR and SBR-0.15MWCNT nanocomposite

5.3C.4 Differential scanning calorimetry (DSC)

Table 5.9 gives the T_g of SBR and SBR containing 0.15phr MWCNT. T_g of the nanocomposite decreased with the addition of MWCNT. The decrease in Tg showed the labile nature of polymer chains and the weak interaction among SBR molecular chains in the nanocomposite. Lipatov has suggested that the chain mobility depends on the polymer cohesive forces. In

non polar elastomers, the cohesive forces are low and therefore only minor changes in T_g were expected for carbon nanotube SBR composites [9]

Table 5.9. T_g values of SBR and SBR-0.15MWCNT nanocomposite

Sample	T_g (^{0}C)
SBR	-16
SBR-0.15 MWCNT	-17

5.3C.5 Fourier transform infrared spectroscopy (FTIR)

IR spectrum of the SBR-MWCNT nanocomposite (Fig.5.18) showed strong peaks at 2916 cm^{-1} and 2849cm^{-1}.This might be due to a synergetic effect of CH stretch on SBR by the addition of MWCNT.The medium peak at 1546cm^{-1} is the stretching mode of C=C of MWCNT.The sharp, strong peak at 699cm^{-1} showed the interaction of styrene units of SBR with MWCNT. (FTIR of SBR is given in Fig 5.6 and MWCNT is given in Fig.3.11)
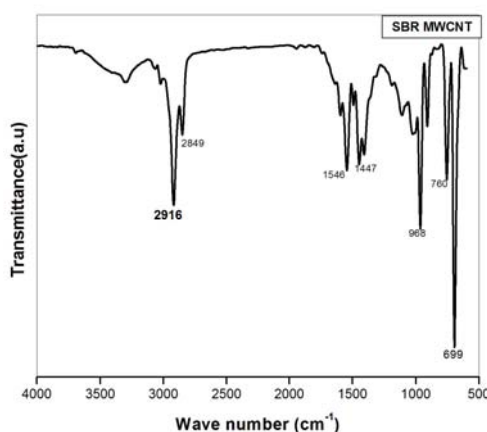
Fig.5.18. FTIR spectrum of SBR-MWCNT nanocomposite

5.3C.6 Scanning electron microscopy (SEM)

The tear fractured surface of the nanocomposite is shown in Fig.5.19. The surface seems to be rough with a number of ridge lines indicating the direction of crack propogation.These ridgelines of reinforcement indicate good compatability of MWCNT and polymer matrix
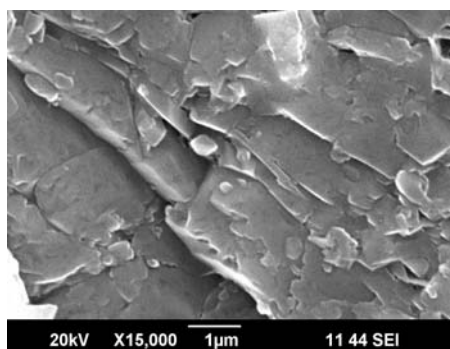
Fig.5.19. SEM images of SBR-MWCNT nanocomposite

5.3C.7 Conclusions

There was remarkable improvement in mechanical properties of SBR with the addition of nanotube at a loading as low as 1.5phr.Tensile strength showed 65% increase while modulus and tear strength gave 95% and 68% increase respectively. Thermal sability of the nanocomposite increased by the addition of MWCNT .

5.3D Graphene Nanoplatelets in SBR Latex

Naturally occuring graphite being a source material for graphene nanoplatelets, is gaining prominence as an ideal reinforcing material to improve polymer properties. 2D confinement of graphene platelets to polymer matrix and its high surface area makes it a superior nanofiller in the field of material science. Graphene nanoplatelet is not an individual

graphene sheet but comprises multiple graphene sheets that are stacked together [18, 21]. Thus, the thickness of the platelets is significantly larger than an individual graphene sheet.

Effect of graphene on the mechanical and thermal properties of SBR latex is discussed. The composites are characterized by XRD, FTIR and SEM analysis.

5.3D.1 Mechanical properties

Fig.5.20 gives the variation of tensile strength/elongation at break and modulus/tear strength of SBR/graphene nanocomposite. Table 5.10 gives the % increase in the mechanical properties of the nanocomposites.Tensile strength increased by 66% and modulus by 110% by the addition of 1phr graphene. Improvement in the mechanical properties of graphene containing nanocomposite depends on the distribution of graphene layers in the polymer matrix, interfacial bonding between the graphene layers and polymeric matrix [14] and the alignment of graphene in the matrix [37].

Graphene dispersion prepared in vulcastab might be considered as comprising of graphene platelets surrounded by an interphase [37]. From the SEM images it appears that graphene platelets are enveloped by a fine glazing, fur like covering (Fig.5.24)

Formation of an interphase around the platelets might enhance stress tranfer [38]. So even in the absence of a covalent bonding between the filler and the matrix the presence of the interphase assisted in the reinforcement in properties. The SEM images also showed a uniform distribution of graphene. Increase in elongation at break might be attributed to the sliding effect of graphene platelets, which could be taken as a plasticization effect

[39]. All these contributed to the enhancement in the mechanical properties of the composite.
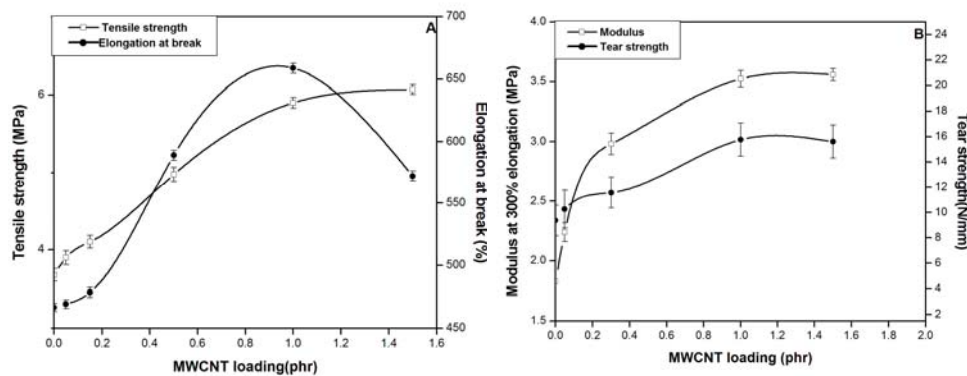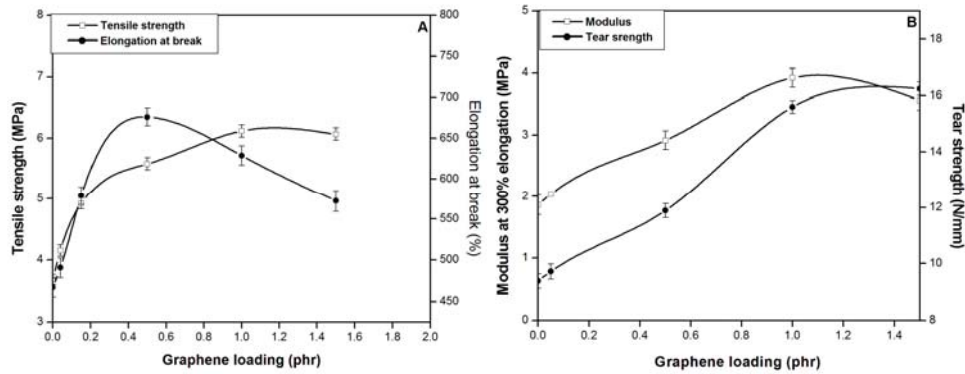

Fig.5.20. Variation of (A) Tensile strength and Elongation at break (B) Modulus and Tear strength of SBR-graphene nanocomposite

Table5.10. Percentage increase in mechanical properties of SBR-graphene nanocomposites

Properties	% increase	Composition of graphene (phr)
Tensile strength	66	1
Elongation at break	45	0.5
Modulus	110	1
Tear strength	66	1.5

5.3D.2 Swelling studies

Fig.5.21shows the sorption curves of SBR graphene nanocomposites Here the swelling rate of nanocomposites was found to be higher than that of SBR without filler. Similar abnormal behaviour was reported in blends of NR/XSBR [40]. The presence of vulcastab envelopping the graphene platelets might have created a weak interphase which assisted in the penetration of the solvent resulting in an increase in the swelling rate.
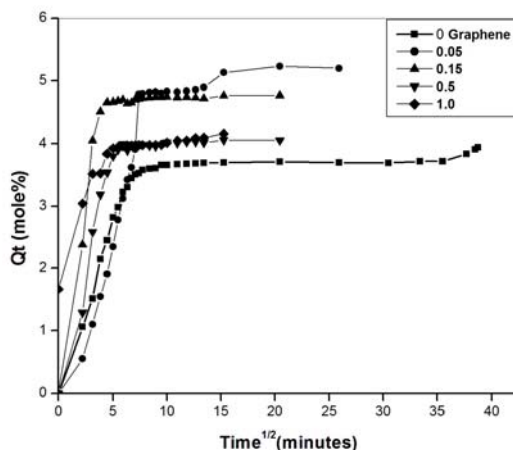
Fig. 5.21. Sorption curves of SBR-graphene nanocomposites

5.3D.3 Thermogravimetric analysis (TGA)

T_{max}, T_{10}, T_{25} and T_{50} values decreased showing that the graphene platelets could not transfer heat properly. The small decrease of thermal resistance is an evidence for the heterogenity and lack of filler protective action [41] in the nanocomposite.

Table 5.11. Thermal analysis results of SBR and SBR-0.05graphene

Samples	On set temp. (^{0}C)	Tmax (^{0}C)	Temp. at wt.loss (^{0}C)			Residue%
			T_{10}	T_{25}	T_{50}	
SBR	320	441	365	398	426	3.08
SBR-0.05Graphene	322	436	355	391	421	4.54

5.3D.4 Differential scanning calorimetry (DSC)

Two competing effects on the chain mobility of the polymer matrix, at the interface of a nanofiller/polymer composite are (1) enhancement in

mobility caused by a larger free volume and (2) restriction in mobility caused by physical or chemical interaction with the filler. Free volume reduces T_g while interaction with the filler produces an opposite effect [42].

From Table 5.12 it is seen that with the addition of graphene, T_g of the nanocomposite first increased and then decreased. At low concentration there might be greater interaction between polymer chain and filler particles which restricted the mobility of the polymer chains leading to an increase in T_g. But when concentration of graphene increased, aggregation might have taken place leading to an increase in the free volume available in the composite. This led to the increasein the mobility of polymer chain and consequent decrease in T_g

Table 5.12 Tg values of SBR and SBR-graphene nancomposites

Sample	T_g (^{0}C)
SBR	-16
SBR-0.3Graphene	-14
SBR-0.5Graphene	-16
SBR-1.0Graphene	-19

5.3D.5 X- ray diffraction analysis (XRD)

Fig 5.22 gives the XRD diffraction pattern of graphene and SBR-graphene nanocomposite. Absence of peak in the nanocomposite is an indication of the complete exfoliation of graphene platelets.
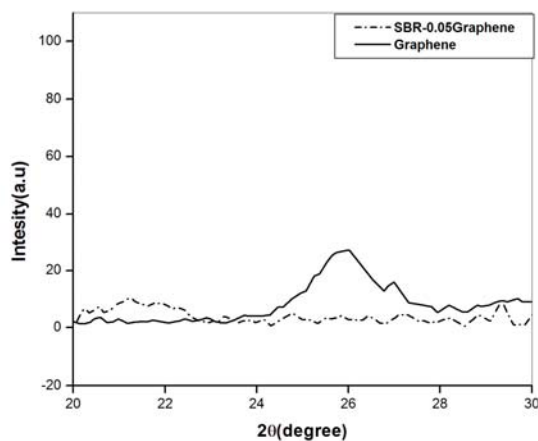
Fig. 5.22. X-ray diffraction pattern of graphene and SBR-0.05 graphene

5.3D.6 Fourier transform infrared spectroscopy (FTIR)

Fig.5.23 shows the IR spectrum of SBR/graphene nanocomposite.. Peaks at 2918 cm^{-1} and 2844 cm^{-1} represented the C-H stretch of aromatic rings, peak at 1590cm^{-1} showed the presence of C=C and the peaks at 962 and 695 cm-^{1} gave the styrene units present in the nanocomposite.
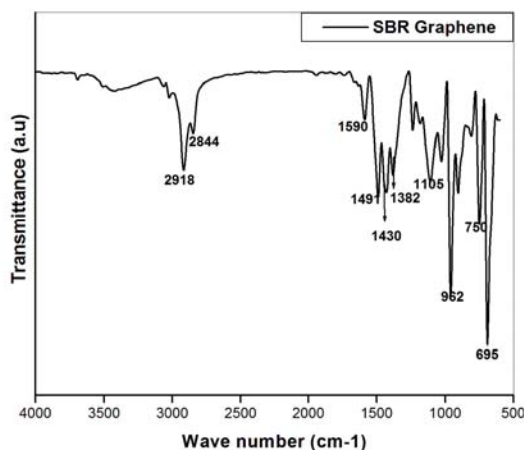
Fig.5.23. FTIR spectrum of SBR-graphene nanocomposite

Greater intensity of these peaks in the nanocomposite showed the interaction of pi electrons of graphene with the unsaturated sites in SBR.

(FTIR of SBR and graphene are shown in Fig.3.14 and Fig.5.6 respectively). The appearance of a new peak at 1105 cm^{-1} might be assigned to the C-O-C stretching (dialkyl) of ether group from the surfactant vulkastab (polyetyhleneoxide condensate).

5.3D.7 Scanning electron microscopy (SEM)

Fig.5.24 gives the SEM photographs of SBR-graphene nanocomposite. Graphene nanoplatelets were seen to be uniformly dispersed in the matrix. A shining glaze and a very fine feathery sheath was seen surrouding the graphene platelets. This might be the envelope created by the non ionic surfactant vulcastab around the graphene particles.
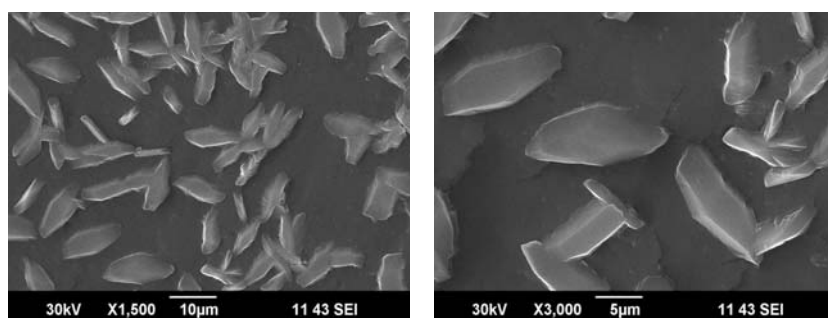
Fig.5.24. SEM images of SBR-graphene nanocomposite

5.3D.8 Conclusions

An aqueous dispersion of graphene was prepared using a novel surfacant vulcastab.The composite showed remarkable improvement in mechanical properties. Proper dispersion of graphene platelets in SBR might have enhanced stress transfer leading to reinforcement in properties. Increase in swelling rate by the penetration of the solvent might be attributed to the presence of a weak interface caused by the surfactant. FTIR spectrum showed the interaction of graphene platelets with the unsaturated sites in SBR matrix.

References

[1] Renukappa, R.D. Sudhaker, S.J. Journal of Reinforced Plastics and Composites.2006, 25, 1173.

[2] Susmita, S. Bhowmick, A.K. Journal of applied polymer science. 2004, 92,698.

[3] Ma, J. Mai, P.X. Z hang, L. Macromol, Rapid Commun. 2004, 25, 1692.

[4] Kim, W. Kang, B. Cho, S. Ha, C. Bae, J. Composite Interfaces. 2007, 14, 409.

[5] Jia, Q. Wu,Y. Wang,Y. Lu,M. Yang,J. Zhang,L. Journal of applied polymer science. 2007, 103,1826.

[6] Zhang,L. Wang,Y. Wang,Y. Sui,Y. Yu,D. Journal of Applied Polymer Science. 2000,78,1873.

[7] Zhou,X. Zhu,Y. Gong,Q. Liang, J. Materials Letters. 2006,60, 3769.

[8] Moniruzzaman, M. Winey, K.I. Macromolecules. 2006, 39, 5194.

[9] Perez, L.D. Zuluaga, M.A. Kyu, T. Mark, J.E. Lopez, B.L. Polymer Engineering and Science. 2009, 866.

[10] Sui, G. Zhong,W.H. Yang, X. P. Yu, Y. H. Zhao, S. H. Polym. Adv.Technol.2008, 19, 1543.

[11] Jiang, M. Dang, Z. Xu F, H. European Polymer Journal. 2007, 43, 4924.

[12] Liu, X. Yang, W. Xie,B. Yang, M. Materials and Design. 2012, 34,355.

[13] Shokoohi, S. Arefazar, A. Naderi, G. Mater Des. 2011,32,1697.

[14] Kuilla,T. Bhadra,S. Yao, D. Kim,N.H. Bose,S. Lee,J.H. Progress in Polymer Science. 2010,35, 1350.

[15] Zhan, Y. Wu, J. Xia, H. Yan, N. Fei, G. Yuan, G. Macromol Mater Eng. 2011,296,590.

[16] Yang, J. Tian, M. Jia, Q.X. Zhang, L.Q. Li, X.L. J Appl Polym Sci. 2006,102,4007.

[17] Wang, L.L. Zhang, L.Q. Tian, M. Wear. 2012,276,85.

[18] Das, A. Kasaliwal, G.R. Jurk, R. Boldt, R. Fischer, D. Stöckelhuber, K.W. Heinrich,G. Composites Science and Technology. 2012, 72, 1961.

[19] Kim, J.S. Hong, S. Park, D.W. Shim, S.E. Macromol Res. 2010, 18, 558.

[20] Sengupta, R. Bhattacharya, M. Bandyopadhyay, S. Bhowmick, A.K. Prog Polym Sci. 2011, 36,638.

[21] Rafiee, M.A. Rafiee, J. Wang, Z. Song, H. Yu, Z-Z. Koratkar, N. ACS Nano. 2009, 3, 3884

[22] Pal, K. Rajasekar, R. Kang, D.J. Zhang, Z.X. Pal, S.K. Das, C.K. Kim, J.K. Mater Design. 2010, 31.

[23] Li,H. Sun,J. Song ,Y. Zheng,Q. J Mater Sci. 2009, 44,1881.

[24] Katoch, S. Sharma, V. Kundu, P. P.org 13. 2010, 1, 1-31.

[25] Wen J, Wilkes, G L.Chem Mater.1996, 8, 1667.

[26] Kader M. A,. Kim, K. Lee Y.S. Nah, C. J Mater Sci. 2006, 41,7341.

[27] Wang,C. Huang, X. Yang,J. European Polymer Journal.2001, 37, 1895.

[28] Kerner, D. Kleinschmit,P. Surface modified synthetic silicate filler,a process for its production and its use. United States 4,704,414.A, 1987.

[29] Johansson, U. Holmgren, A. Forsling,W.Frost,R.L. Clay minerals. 1994, 34, 239.

[30]   Braggs et al Surface modification of kaolinite USP 6,07,1335,2000.

[31]   Ismail, H. Jaffri, R.M. Polymer Testing. 1999, 18, 381.

[32]   Poh, B. T. Ismail, H. Tan, K. S. Polym Test. 2002, 21, 801.

[33]   Wu, Y. Huang, H. Zhao, W. Zhang, H. Wang, Y.Zhang, L. J Appl Polym Sci. 2008, 107, 3318.

[34]   Stephen, R. Alex,R. Cherian,T. Varghese,S. Joseph,K. Thomas,S. Journal of Applied Polymer Science. 2006, 101, 2355.

[35]   Matinlinna,J.P. Mutlu O¨ zcan. Lassila,L.V.J. Vallittua,P.K. Dental materials. 2004, 20, 804.

[36]   Sangchay, W. Sikong, L. Kooptarnond, K. CMU. J.Nat.Sci. Special. Issue on Nanotechnology. 2008, 7.

[37]   Deng, F. Vliet, K.J.V. Nanonotechnology.2011, 22,165703.

[38]   Potts J.R. Dreyer, D.R. Bielawski, C.W. Ruoff, R.S. Graphene-based polymer nanocomposites.Polymer. 2011,52, 5.

[39]   Ismail, M.N. Khalaf A. I. Journal of Applied Polymer Science. 2011, 120, 298.

[40]   Stephen, R. Joseph, K. Oommen, Z.Thomas,S. Composites Science and Technology. 2007, 67,1187.

[41]   Kaczmare K,H. Podgorski,A.Polymer degradation and stability. 2007, 92,939.

[42]   Oh,S.M. Oh,K.M. Dao,T.D. Lee,H. Jeong,H.M. Kim,B.K. Polym. Int.2013, 62, 54.

.....ജരോ.....

Chapter 6

NBR BASED NANOCOMPOSITES

6.1 Introduction

In unvulcanized raw rubber the polymer chains are long and flexible with an entangled and kinked structure. An uncured rubber cannot be used to make articles with a good degree of elasticity. Transformation of uncured rubber to useful rubber with unique physical and chemical properties is achieved by the process of vulcanization. On vulcanization physical and chemical cross links are formed between the polymer chains giving a three dimensional net work structure. The inclusion of rigid entities increases stiffness and resistance to fracture due to interaction between the elastomer and filler surface. The properties and performance of the elastomeric nanocomposites depend on the structure of the polymer matrix, the cross linking chemistry of rubber, nature of nanofillers, the physical and chemical interaction of the fillers with the rubber matrix, the degree of filler dispersion in the rubber matrix and the methods by which they are prepared [1]. NBR because of its good processability, resistance to oils, fuel and chemicals, as well as excellent mechanical properties after vulcanization, is a good candidate for elastomer based nanocomposites

Significant improvement in mechanical and barrier properties are obtained by the inclusion of nanosized silicates in elastomeric matrices. Efficiency of the silicates in modifying the properties of rubber depends on the degree of their dispersion and the extent of exfoliation in rubber. One advantage of rubber silicate nanocomposite is that the high shear stress generated locally during compounding of the very high molecular weight rubber material is beneficial to the delamination of the layered silcate [2].

Recently carbon nanotubes (CNTs) have become increasingly attractive due to the possiblities of large scale production of these materials. Multiwalled carbon nanotubes are widely used in industrial applications, because their production is less complex and more cost effective due to the consumption in low loading to achieve comparable composite properties [3]. The intrinsic potential of carbon nanotubes as reinforcing filler in elastomeric materials is given by Liliane Bokobza in a review on "Multiwall carbon nanotube elastomeric composites"[4].

Since high purity graphene can be obtained from plentiful resource of natural graphite by relatively convenient approaches [5], this cost effective nanofiller even replaces carbon nanotubes in many key applications [6].

In this Chapter NBR based nanocomposites were prepared using different fillers like nanokaolin, vinylsilane grafted nanokaolin, MWCNT and graphene nanoplatelets. Mixing of nanoclay in two roll mill and MWCNT/ graphene in brabender plasticorder helped to get a uniform dispersion of filler in NBR. The effect of these nanofillers on the cure behaviour, mechanical properties and thermal properties were studied in detail. The composites formed were characterized by XRD, FTIR and SEM analysis

6.2 Experimental
6.2.1 Materials

NBR: Nitrile rubber is Kumho NBR (KNB 35L) supplied by Kumho Petrochemicals Co., Ltd. South Korea. It has acrylonitrile content (% by weight) 34 and Mooney viscosity ML (1+4) at $100^0C=41$

Nanokaolin is Nanocaliber100 and vinylsilane grafted nano kaolin is Nanocaliber 100V supplied by English Indian Clays Ltd.Veli, Thiruvananthapuram. Specification given in Table 2. 3. Multiwalled carbon nanotube (MWCNT) - Baytube^R 150P obtained from Bayer Materials Science AG (Leverkusen Germany). Specification given in Table 2.4. Graphene nanoplatelets were purchased from Quantum materials Ltd. Bangalore.

Nanokaolin is designated as 'C' and NBR compounds cotaining 1,5,10 phr naokaolin is represented as NBR-1C, NBR-5C, NBR-10C etc. Vinylsilane grafted nanokaolin is represented as 'V' and the compounds containing 1,5, and 10phr vinylsilane grafted nanokaolin are designated as NBR-1V, NBR-5V, NBR-10V etc. Graphene nanoplatelets used are referred as graphene.

6.2.2 Preparation of NBR based nanocomposites

Formulation used for the preparation of NBR compounds is given in Table 3.5. Mixing and homogenization of the rubber compounds were done in a two roll mill and brabender plasticorder. Details for the preparation of NBR/clay nanocomposite, by mixing in a two roll mill is given in Section 3.11.4. Preparation of NBR/MWCNT/graphene nanocomposites by mixing in brabender plasticorder is given in Section 3.11.5. Cure characteristic of

the mixes were determined using Rubber Process Analyser (R PA 2000-Alpha Technologies) as per ASTM D 2084-1995B. Details of the cure study are given in Secion 2.4.3. The test samples were further vulcanized in an electrically heated hydraulic press having 45 cm × 45cm platen at 160^0C at a pressure of 200Kg/cm^2 on the mould upto an optimum cure time. Moulded samples were conditioned for 24 hrs before testing.

6.2.3 Methods

Methods used for the study of mechanical properties are given in Section 2.4.5 and Swelling studies in Section 2.4.6. Thermal analysis were done in TA instuments (Section 2.4.8 &2.4.9) and the characterization methods included XRD (Section 2.4.10), FTIR (Section 2.4.11) and SEM analysis (Section 2.4.13)

6.3 Results and Discussion
6.3A. Nanokaolin in NBR

Nanokaolin provides excellent reinforcement in rubber. Liu et al. [7] incorporated nanokaolin in SBR, NR, BR and EPDM and compared their reinforcing effect with that of precipitated silica (PS). Malicka-Soczka [8] studied the effect of both modified and unmodified kaolin in butadiene–styrene rubber (KER 1500). No further works on unmodified nanokaolin/ elastomer composites were reported.

This part deals with the study of the reinforcing effect of nanokaolin (C) on the mechanical properties of NBR. Cure characteristics, swelling studies, strain sweep studies, thermal studies were also considered. The composites were characterized by XRD, FTIR and SEM analysis.

6.3A.1 Curing Studies

Fig. 6.1 shows the cure graphs of NBR-C nanocomposites containing different concentrations of nanokaolin (0, 1, 10 and 20 phr) at 160^0C. As a general trend torque initially decreases, then increases and finally levels off. The initial decrease is due to the softening of the rubber matrix, the increase in torque value is due to the cross linking of rubber and the levelling off is an indication of completion of curing.

Vulcanization characteristics expressed in terms of minimum and maxium torque, optimum cure time (T_{90}), scorch time (T_{10}) and cure rate index (CRI) of NBR and nanokaolin filled NBR are given in Table.6.1. The increase in cure time, scorch time and decrease in CRI values were an indication of the cure retarding effect of nanokaolin. The adsorption of curatives on the surface OH groups of nanokaolin decreased the effective concentration of curatives leading to an increase in the optimum cure time. The increase in scorch time denoted the processing safety of the vulcanizate.

Maximum torque M_H is a measure of shear modulus [9]. It gives the extent of cross linking reaction and a measure of filler polymer interaction. Increase in M_H with filler loading showed improved interaction behaviour and good interfacial adhesion between matrix and filler.

Minimum torque is related to the viscosity of the compound. It measures the stiffness of the unvulcanized compound.The decrease in M_L value suggested that the incorporation of filler did not impose any restriction to the molecular motion of the macromolecular polymer chain.
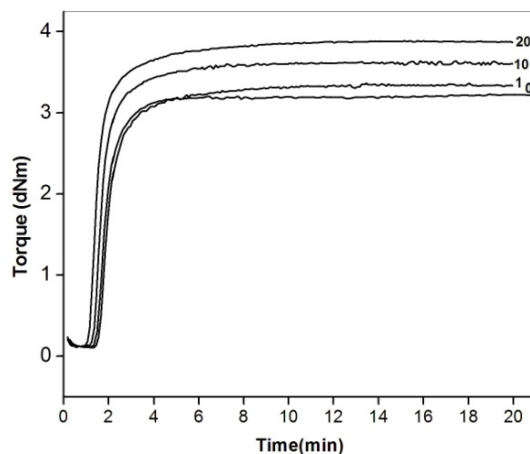
Fig.6.1. Rheographic curves of NBR-C nanocomposites

Table.6.1. Cure properties of NBR-C nanocomposites

Concentration of nanokaolin (phr)	Min.Torque M_L (dNm)	Max.Torque M_H (dNm)	Opt. cure time T_{90} (min)	Scorch time T_{10} (min)	Cure Rate Index CRI
0	0.160	2.673	1.30	0.49	124
1	0.101	3.54	3.16	1.44	58.14
10	0.101	3.644	3.04	1.39	60.60
15	0.124	3.680	3.13	1.42	58.48
20	0.104	3.896	2.97	1.19	56.18

6.3A.2 Mechanical properties

Variation of tensile strength and elongation at break of NBR-C nanocomposites at different concentration of nanokaolin are shown in Fig. 6.2(A).The variations of modulus and tear strength of the composites are given in Fig. 6.2(B). A remarkable increase in the mechanical properties of nanocomposites was observed. Tensile strength, elongation at break, modulus at 300% elongation and tear strength increased by 56%, 30%, 17% and 49% respectively at 15 phr nanokaolin.

Interaction between clay platelets having large surface area and the polymer chains facilitated stress transfer, resulting in improved tensile properties [10]. Tensile strength and elongation at break were found to reach a maximum at 15 phr loading and after that properties declined with increase in concentration of the filler. The increase in tensile strength might be due to the increase in interfacial bonding of clay platelets and good interaction between the clay platelets and NBR. Increase in interfacial bonding arose by intercalation or possible exfoliation of clay layers, as evidenced by XRD analysis. The nanokaolin layers are linked through hydrogen bonding between hydroxyl groups on the octahedral sheet and oxide arrangement of tetrahedral sheet. Even though the intercalation reactivity of kaolin was low due to hydrogen bonding between the layers, the free OH groups on kaolin could interact with the CN groups of NBR. Decrease in tensile strength at higher loading might be due to agglomeration of clay tactoids, leading to stress concentration.

In contrast to other conventional fillers elongation at break of NBR-C nanocomposite was found to increase with clay concentration upto 15 phr. Better filler dispersion and strong rubber-filler interaction led to an increase in elongation at break. With the increase in rubber-filler interaction, decoiling of rubber chain might have taken place, leading to greater adsorption of energy by rubber molecules and slippage of clay particles. At higher loading the elongation at break decreased because of filler aggregation.Aggregation of filler weakens the number of available reinforcing links. The formation of non exfoliated aggregates at higher clay content made these composites much more brittle.

Modulus and tear strength of the nanocomposite increased upto 15 phr and then remained a constant upto 25 phr. There was only 11% increase in the modulus. Lack of strong interfacial bonding between nanokaolin and NBR matrix reduced the load transfer efficiency leading to the small improvement in modulus. The dispersed clay layers restricted the rubber chains and resisted the development of cracks, leading to an increase in tear strength.
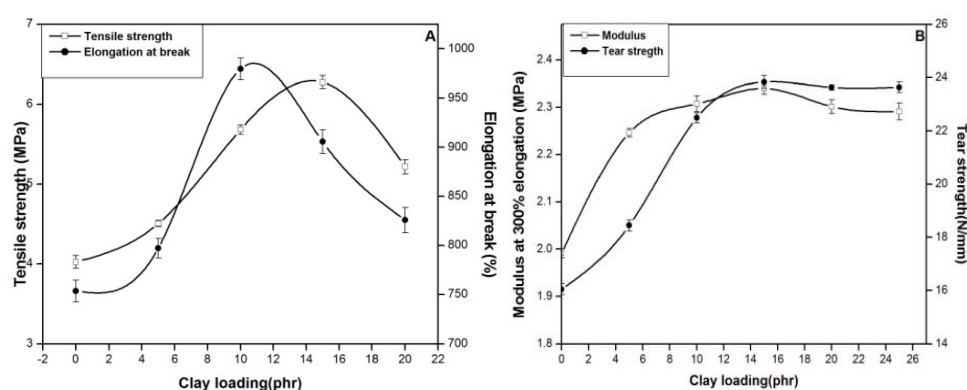
Fig.6.2. Variation of (A) Tensile strength/Elongation at break and (B) Modulus /Tear strength of the nanocomposite with clay 'C' loading.

6.3A.3 Strain sweep analysis

Fig. 6.3 shows the variation of complex modulus with strain % for uncured compounds containing different concentrations (0, 1, 5, 10, 15 phr) of nanokaolin. Complex modulus increased with increase in clay loading. At high concentration, the filler particles formed agglomerates leading to the formation of a filler network. This filler network resulted in the interaction of polymer chain with the filler particles leading to an increase in the complex modulus. At low strain the complex modulus would be high, but with the increase in strain destruction of network resulted in the reduction of complex modulus.
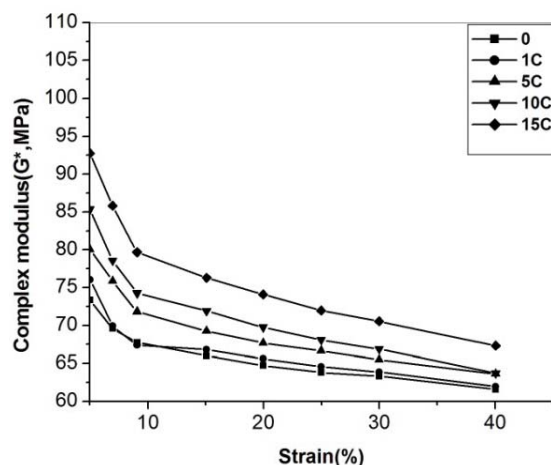
Fig. 6.3. Variation of complex modulus with strain for NBR-C nanocomposite

6.3A.4 Thermogravimetric analysis (TGA)

TGA thermograms of NBR and NBR containing 5phr and 15 phr nanokaolin are given in Fig.6.4 (A) and (B) respectively. DTG curve of NBR showed that degradation takes place in two steps with a shoulder at 428^0C and a major peak at 456^0C.This was due to the multiple degradation of the butadiene component present in raw rubber [1, 11, 12]. The degradation pattern of the nanocomposites also followed the same trend. Thermal degradation characteristic of NBR based nanocomposites are given in Table 6.2.The initiation temperaure and the peak maxima showed a small increase by adding nanokaolin in NBR. Inclusion of an inorganic component to organic material improved the thermal stability [13]. High values of T_{10}, T_{25} and T_{50} showed increase in the thermal stability of the nanocomposite. Clay acted as an insulation and mass transport barrier against the volatile components produced during the thermal degradation of polymer [14]. Clay also formed a layered carbonaceous char during degradation of the nanocomposite and increased the thermal stability of the polymer [15].

Clay minerals are inorganic materials which are stable in the temperature range at which the polymer degrades and clay remains as residue after the heating programme [16].

Table.6.2. Thermal analysis results of NBR and NBR-C nanocomposites

Sample	Onset temp.(^{0}C)	Peak max.(^{0}C)	Residue %	T_{10}.(^{0}C)	T_{25}.(^{0}C)	T_{50}.(^{0}C)
NBR	340	428, 456	6.783	376	420	445
NBR- 5C	341	427, 455	15.45	379	423	449
NBR-15C	341	428, 458	16.69	380	425	452
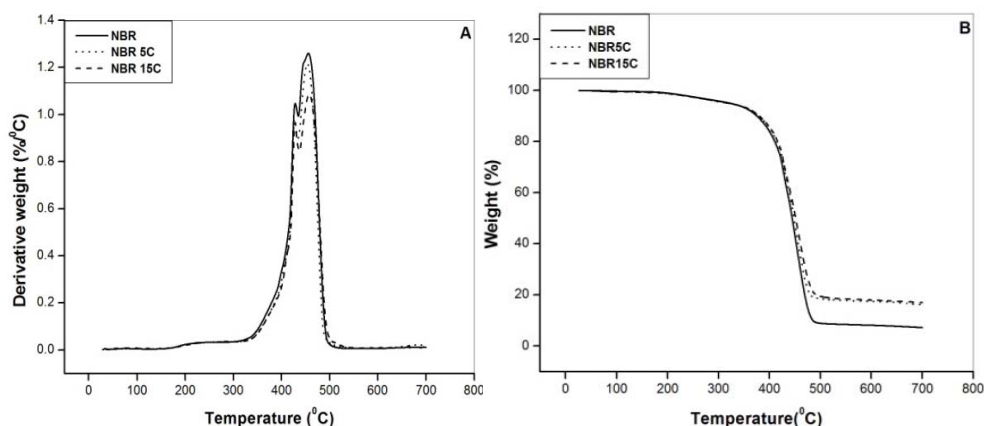
Fig.6.4. (A) DTG and (B) TGA curves of NBR and NBR-C nanocomposites

6.3A.5 Differential scanning calorimetry (DSC)

T_g of NBR and NBR-15 C nanocomposites are summarized in Table 6.3. T_g of NBR and its composite was almost the same, showing that the clay layers did not impose any restriction to the movemet of polymer chains.

Usually, when polymer chain network gets adsorbed strongly on to the filler surface, effective degree of cross linking increases.The cross linking may be stronger if the filler contains some reactive surface groups that may cross

link to the polymer chain. Either chemisorption or physisorption may take place at the filler surface. When chemisorption take place there will be permanent chemical bonding between filler particles and polymer chains.This severely restrict the movement of polymer chains relative to the filler surface, when high stresses are applied. While, physisorption arising from long range van der Waals forces between the surface of the filler and the polymer does not impose any hinderance to the chain mobility [17]. This might be the reason for the decrease in T_g of NBR-C nanocomposite.

Table 6.3. T_g of NBR and NBR-15C nanocomposite

Sample	T_g
NBR	-22.71
NBR-15C	-23.91

6.3A.6 X-ray diffraction analysis (XRD)

Fig.6.5.gives the typical Xray diffraction patterns of nanokaolin and NBR/nanokaolin composite.The characteristic peaks of nanokaolin with spacing 7.05 ($2\theta=12.5^0$), 4.41($2\theta=20^0$) and 3.56 A^0 ($2\theta=25^0$) [18, 19] are shown in the figure. XRD peak at 12.5^0 corresponding to the interlayer space of 7.05A^0 was shifted to a lower angle in the nanocomposite, with a corresponding increase in the interlayer spacing. Shift to lower angle indicated intercalation of NBR into the clay galleries. The disappearance of the peaks between 13^0 and 25^0 in the nanocomposite showed exfoliation had taken place to some extent. Peak at a higher 2θ value for the nanocomposite indicated collapse of some intercalated structure. Similar results were reported when montmorillonite was used as reinforcing filler. For NBR /sodium montmorillonite composite a peak appeared with a decrease in intensity compared to pristine Na-Mt [10]. S.Sadhu and Bhowmick, A. K.

[20] have dealt with unmodified montmorillonite on SBR with varying styrene content and using di cumyl peroxide as the curing agent and suggested that exfoliation had taken place in all the nanocomposites.
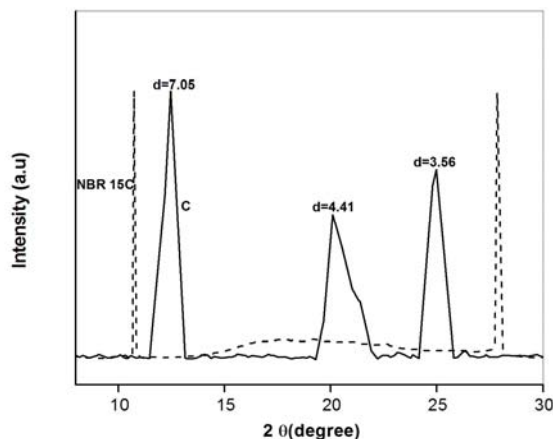
Fig. 6.5. X-ray diffraction pattern of 'C'and NBR-15C nanocomposite

6.3A.7 Fourier transform infrared spectroscopy (FTIR)

Fig.6.6. gives the IR spectrum of NBR and NBR-15C nanocomposite. The characteristic stretching vibration of nanokaolin, in the range 3600cm^{-1} was observed in the composite. The closely spaced peaks were due to the surface and inner hydroxyl groups in nanokaolin.The peaks at 2916 cm^{-1} and 2844 cm,$^{-1}$ due to CH stretching vibration of CH$_2$ groups of NBR remained with the same intensity in the nanocomposite.The peak at 2237cm,$^{-1}$ characteristic of CN group in NBR had no change in the nanocomposite, showing CN group had not involved in any chemical reaction. The strong peak at 1535 cm^{-1} due to the presence of zinc stearate and the small peak at 1735 cm^{-1} attributed to the CO stretching of the carboxyl group of zinc stearate were seen in the nanocomposite also. The difference in the IR spectrum of NBR and its nanokaolin composite lies in the range 1400-700cm^{-1}. The CH$_2$ stretch vibration at 1256cm^{-1} had become

sharper in the nanocomposite. New peaks seen at 1094cm,$^{-1}$ 1023cm^{-1} and 913 cm^{-1} correspond to the stretching and bending vibrations of Si-O-Si and Al-OH groups in nanokaolin. The introduction of these sharp peaks in the nanocomposite showed there was strong interaction between the Si-OH and Al-OH groups in nanokaolin with the butadiene double bonds in NBR.
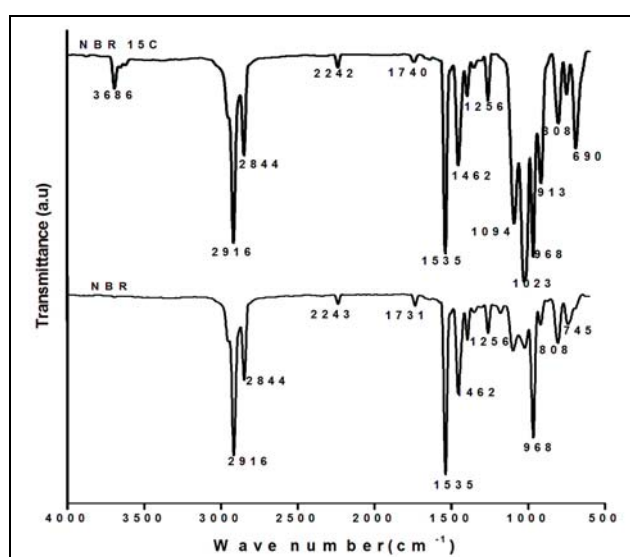
Fig.6.6. IR spectrum of NBR and NBR-15C nanocomposite

6.3A.8 Scanning electron microscopy (SEM)

Fig. 6.7(A) and (B) shows the SEM photographs of the tear fractured surface of NBR-C nanocomposite containing 15 phr nanokaolin. A uniform dispersion of clay particles were seen in the SEM images. Most of the clay particles were well embedded in the polymer marix.This strong adhesion and good dispersion of clay paricles in NBR matrix contributed to the reinforcing property of nanokaolin in NBR matrix.
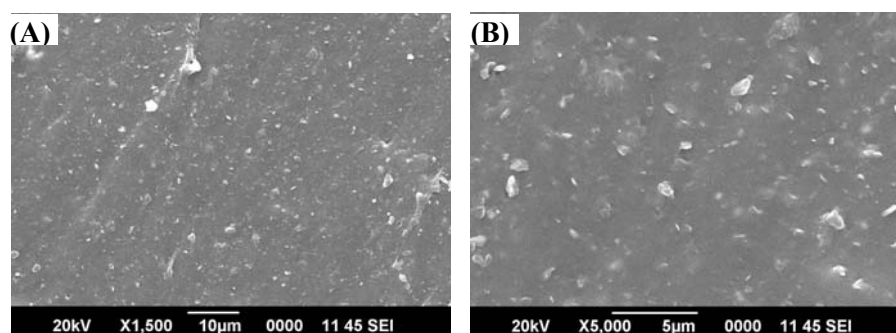
Fig. 6.7. (A)and (B) SEM images of tear fractured surfaces of NBR-15C nanocomposite

6.3A.9 Conclusions

NBR nanokaolin composite showed good improvement in mechanical properties compared to the gum. Uniform dispersion of nanokaolin and the interaction of the OH groups of clay wih the polar nitrile rubber led to the enhancement in mechanical properties of the nanocomposite. TGA studies showed that there was an increase in the thermal stability of the nanocomposite. The decrease in T_g of the nanocomposite was an indication that the chain mobility is unaffected by the presence of clay. XRD results showed the inercalation of polymer into the intergallery space of clay. Analysis of the IR spectrum showed that there was only strong interaction between the Si-OH and Al-OH groups in nanokaolin with the double bonds in NBR.

6.3B. VinylSilane Grafted Nanokaolin in NBR

Silane treated clays are used as reinforcing fillers in natural and synthetic rubbers. The functional silanes usually employed for modification are vinyl or sulphur fuctional silanes.Vinyl functional silane treated clays are used in elastomeric applications where good compression set is required. This part deals with the study of the effect of vinylsilane grafted nanokaolin (V) in NBR. This modified nanokaolin gave good reinforcement in

properties when incorporated in NBR.The nanocomposites formed were characterized and their reinforcing effect was studied.

6.3B.1 Curing studies

Fig 6.8.shows the cure graphs of the compounds and the cure parameters are presented in Table 6.4.The addition of vinylsilane grafted nanokaolin retarded curing, as indicated by the increase in scorch time and optimum cure time and by decrease in CRI. Removal of some accelerator free radicals, formed by the interaction of the modified silicate with accelerator, during the cross linking reaction, retarded the curing reaction [2, 21]. Increase in M_H and ΔM value gave the extent of cross linking reaction and the strong influence of the organoclay on the cross linking density of the rubber compound. The unsaturated sites of vinyl group gets cross linked with butadiene part of NBR in the vulcanization process. Moreover the polar low molecular mass vulcanization curatives like ZnO, ZDC, stearic acid and sulphur might easily penetrated between the clay layers resulting in rubber cross linking inside the clay galleries [21].

Table 6.4. Cure properties of NBR-V nanocomposites

Concentration of 'V'(phr)	MinTorque M_L (dNm)	MaxTorque M_H(dNm)	$\Delta M=M_H-M_L$ (dNm)	Opt.cure time T_{90} (min)	Scorch time T_{10} (min)	Cure Rate Index CRI
0	0.160	2.673	2.513	1.30	0.498	124
1	0.098	3.455	3.357	3.05	1.44	58.14
3	0.088	3.351	3.263	3.35	1.39	60.60
5	0.09	3.540	3.45	2.96	1.42	58.48
7	0.088	3.425	3.337	2.99	1.19	56.18
10	0.124	3.680	3.556	3.13	1.42	58.48
15	0.104	3.729	3.625	2.99	1.38	62.11
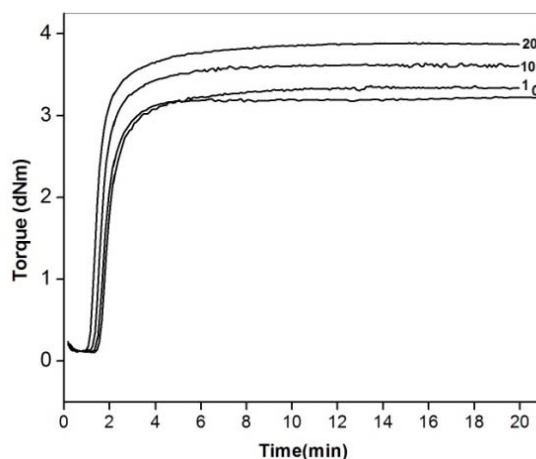
Fig.6.8. Rheographic curves of NBR-V nanocomposites

6.3B.2 Mechanical Properties

Mechanical properties of the nanocomposites are shown in Fig. 6.9 (A) and (B). From Fig 6.9 (A) it is clear the tensile strength and elongation at break of the nanocomposite increased with the clay loading upto 5 phr and then decreased.Tensile strength increased by 32% and elongation at break by 13%. Since tensile strength and elongation are properties that correlate with the interfacial phase adhesion it can be concluded that there was uniform dispersion and strong interfacial adhesion between the dispersed clay and polymer matrix.
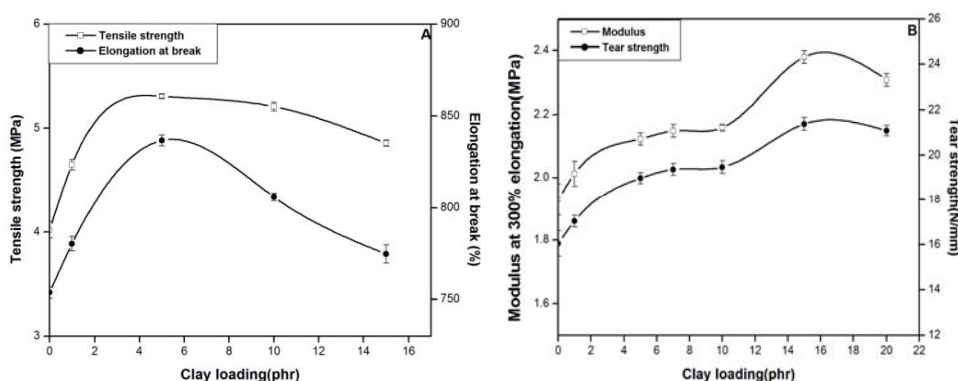
Fig .6.9. Variation of (A) Tensile strength/Elongation at break and (B) Modulus /Tear strength of the nanocomposite with clay (V) loading

Modulus and tear strength increased with concentration of vinylsilane grafted nanokaolin as shown in Fig.6.9 (B). At 15 phr there was 24% increase in modulus and 33% increase in tear strength. The high shear stress generated during compounding helped in the delamination of the layered clays and the intercalation of rubber molecules into the gallery space.

6.3B.3 Strain sweep analysis

Fig.6.10. shows the variation in complex modulus with the addition of vinyl grafted nanokaolin (1, 5, 10 and 15 phr) in NBR. At low strain the complex modulus values of the nanocomposites was very high. But with increase in strain, complex modulus decreased. Formation of filler networks, i.e., either filler-filler or filler-polymer networks leads to the increase in complex modulus at low strain. In NBR-V nanocomposites, increase in complex modulus might be due to the interaction of polymer chains with the organic groups present in vinyl grafted nanokaolin. Destruction of network structure at high strain resulted in the decrease in complex modulus.
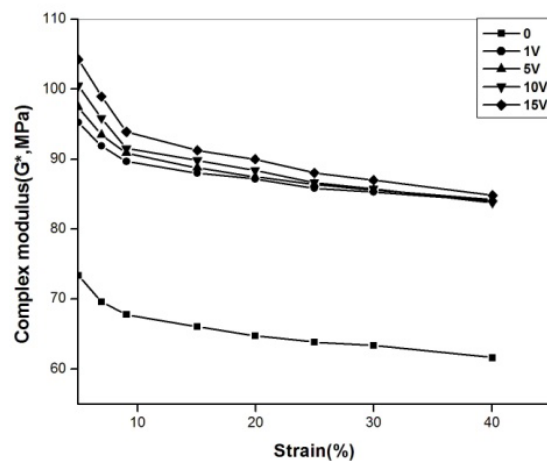
Fig. 6.10. Variation of complex modulus with strain for NBR-V nanocomposite

6.3B.4 Thermogravimetric analysis (TGA)

The thermal properties of NBR-V nanocomposites were studied by thermogravimetric analysis. Table.6.5. shows the thermal degradation data for NBR and NBR containing 7 phr and 15 phr modified nanokaolin (V). The TGA and DTG curves of pure NBR and the composites are shown in Fig.6.11 (A) & (B). The DTG curves showed multiple degradation steps in nitrogen atmosphere [1]. Onset of degradation started around 340^0C for all the vulcanizates. Hence the samples might be considered thermally stable upto 340^0C in nitrogen atmosphere. There was slight increase in peak max.T_2, T_{25} and T_{50}. So the thermal sability of the nanocomposites increased by the addition of modified nanokaolin.The improvement in the thermal stability was due to the presence of intercalated/exfoliated clay layers. The hydrogen bonding interaction between the polar polymer chains with the OH groups of clay, along with vander Waals interaction improved the thermal stability of the nanocomposite. Alex and Nah [22] reported the thermal degradation temperature of NR/organoclay nanocomposite was independent of the presence and concentration of organoclay.

(A)   (B)
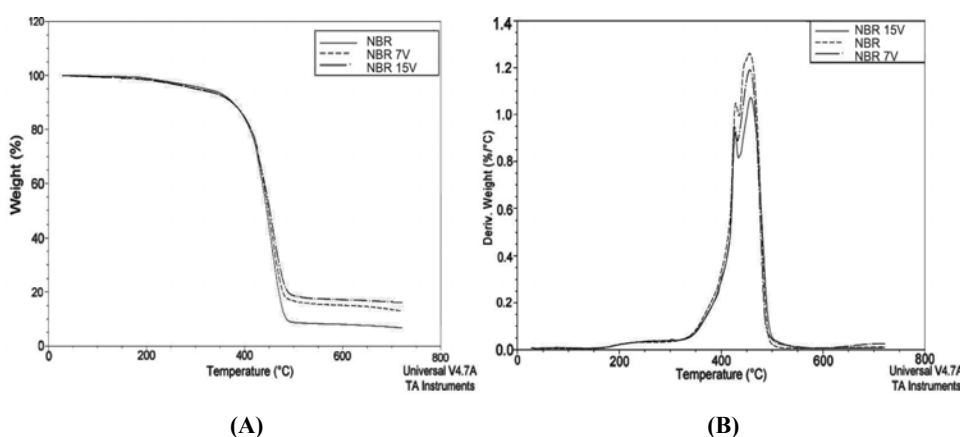
Fig. 6.11 (A) TGA and (B) DTG curves of NBR and NBR-V nanocomposites

It was also observed that the amount of residue increased with the increase in clay content. The residual materials were mainly due to zinc salts and inorganic fillers.

Table 6.5. Thermal analysis results of NBR and NBR -Vnanocomposites

Sample	Onset temp. (^{0}C)	Peak max. (^{0}C)		Residue %	T_{25} (^{0}C)	T_{50}(^{0}C)
		T_1	T_2			
NBR	340	428	456	6.783	420	445
NBR 7V	339	427	456	12.98	422.44	448
NBR 15V	340	427	458	16.23	422.87	451

6.3B.5 Differential scanning calorimetry (DSC)

Table.6.6. gives the glass transition temperature (T_g) of NBR and NBR-V nanocomposite.The addition of modified clay did not produce any change in T_g indicating there was no restriction to polymer chain mobility. The interaction between the filler and polymer was only physisorption as against to chemisorption. Both physisorption and chemisorption leads to reinforcement in properties but the absence of chemical bond between the filler and polymer surface did not pose any restriction to the polymer chain mobility.

Table 6.6. T_g of NBR and NBR-15Vnanocomposite

Sample	T_g
NBR	-22.71
NBR-15 V	-23.23

6.3B.6 X-ray diffraction analysis (XRD)

Fig.6.12 shows the XRD pattern of 'V' and NBR-15V nanocomposite. The peak corresponding to the interlayer spacing 7.1A^0 in vinylgrafted

nanokaolin was slightly shifted to a smaller angle making a very small increase in the inter layer spacing. This showed the intercalation of rubber molecules into the inter layer space of the vinyl grafted moieties. Other characteristic diffraction peak of 'V' between 2θ, 20^0-25^0 was absent in the nanocomposite. This showed the special directional and parallel arrangement of clay platelets in the rubber matrix. The SEM images (Fig.6.14) also confirmed the particular arrangement of the clay platelets.

On grafting silanes react mainly with some of the OH groups on the edge surface. Then only the lateral surface of clay particles will be organophilized. So there will not be any clay exfoliation in the presence of polymer and it will even be less effective than intercalation by ion exchange [21].
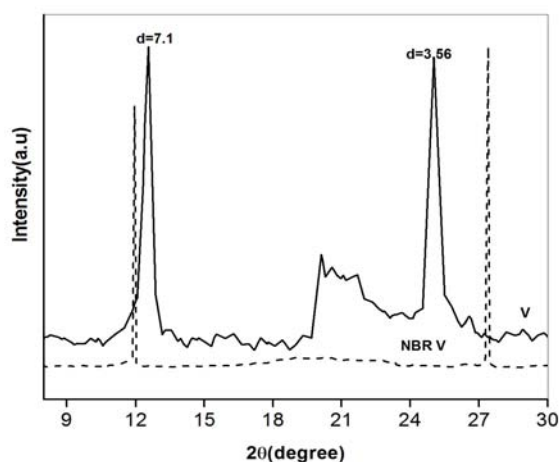
Fig .6.12. Xray diffraction pattern of V and NBR-15Vnanocomposite

6.3B.7 Fourier transform infrared spectroscopy (FTIR)

Fig.6.13 shows the IR spectrum of NBR and NBR-15V nanocomposite. IR spectrum for unfilled and clay filled specimens did not show a significant difference in the range 3000-1500cm^{-1}. So there seemed to be no change in the

chemical arrangement. The peaks due to the OH groups (the closely spaced peaks around 3600 cm^{-1}) in nanokaolin were very much reduced (IR of vinylgrafted nanokaolin, Fig.3.6) in the nanocomposite. Peak at 1535cm^{-1} showing the presence of zinc stearate and the small peak at 1731 showing CO stretch of carboxyl group of zinc stearate were seen in NBR as well as NBR-V nanocomposite. The peak at 1463cm^{-1} in the nanocomposite might be formed by the merging of - CH$_2$- groups of NBR and vinyl group of modified clay. The peaks at 1103cm^{-1} and 1031cm^{-1} gave the perpendicular Si-O vibrations and Si-O-Si stretching vibrations respectively of the modified clay.The intensity of the peak at 968 cm^{-1}due to the butadiene double bond of NBR was reduced in the composite. This might be due to the interaction of butadiene double bond with the vinyl group of clay.
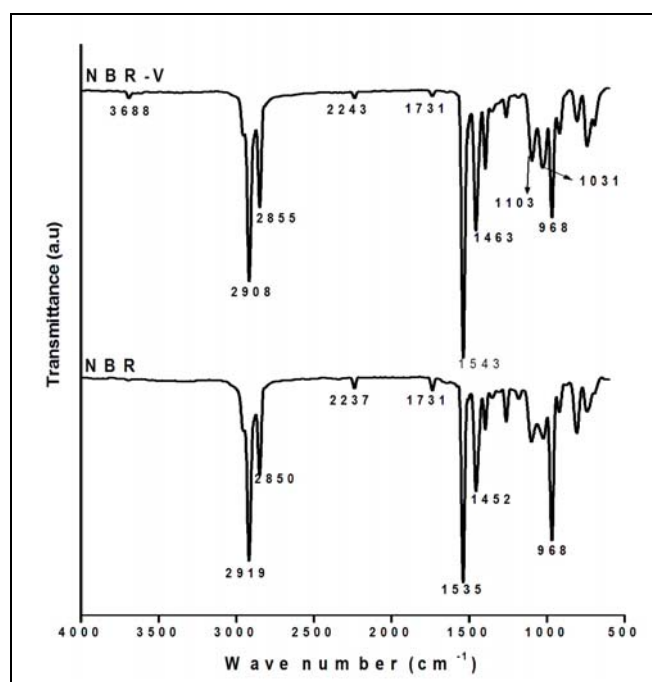
Fig. 6.13. FTIR of NBR and NBR-15 Vnanocomposite

6.3B.8 Scanning electron microscopy (SEM)

Fig.6.14 shows the SEM images of NBR-V nanocomposite under different magnification. Directional and parallel arrangement of clay platelets are seen in the SEM images.
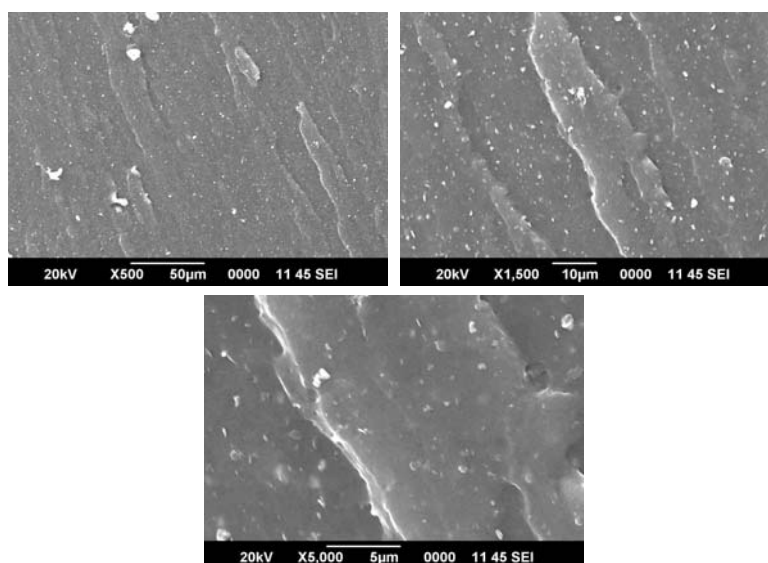
Fig.6.14. SEM images of tear fractured surface of NBR-15 Vnanocomposite

6.3B.9 Conclusions

Good dispersion of modified clay in NBR resulted in the improvement in mechanical properties of the nanocomposite. Tensile strength increased by 32% and elongation at break by 13% at 5phr concentration. Modulus and tear strength of the nanocomposite increased with increase in the concentration of the filler. Modified clay got a cure retardation effect in NBR. Thermal analysis showed a slight increase in the thermal stability and no chage in the glass transition temperature of the nanocomposite. Grafting with vinyl silanes caused organophilization only to the lateral surface of clay and so a complete exfoliation could not be expected in the presence of

the polymer. IR analysis confirmed interaction of the vinyl group of clay with the buadiene double bond of the polymer chain. SEM photographs revealed the directional and parallel arrangment of the clay layers in NBR matrix.

6.3C. MWCNT in NBR

Carbon nanotubes show properties of both diamond and graphite. They are strong and thermally conductive like diamond, electrically conductive like graphite and also they are light and flexible [22]. In spite of the exceptional, thermal, electrical and mechanical properties of carbon nanotubes the expected reinforcement is not usually obtained by their incorporation in polymeric matrices. Nanotubes when mixed in rubber usually results in poor dispersion due to the attractive vander Waals bonds between the outer planes of neighbouring nanotubes resulting in their agglomeration [23]. Proper dispersion and distribution of these anisotropic filler is a challenging task. Dispersing nanotubes in polymer matrices can be achieved either by the formation of covalent bonds or by the establishment of a non covalent interaction between the polymer chain and nanotube surface [24]. Covalent modification involves reactive coupling between the functional moieties on the CNT surface with the available functional groups of the polymer.This significantly improves the structural properties of the nanocomposites. But studies have shown that covalent modification can perturb the extended π conjugation system of CNT and adversely affect the intrinsic electronic characteristics of the nanotubes [25]. Noncovalent treatment is characterized by the adsorption of different hierarchical structures on the nanotube surface through various specific interactions. This method preserves the integrity of nanotubes, gives significant improvement

in the structural properties of the composite and shows a positive influence on the electrical conductivity of the nanocomposite [25].

Here the as received carbon nanotubes were first purified by refluxing with 500ml 2M HCl for 24 hours. This resulted in the introduction of hydroxyl and carbonyl groups on the surface of nanotubes, caused by the elimination of metallic nanoparticles during the purification process, cutting the nanotube caps [26, 27]. The purified nanotubes were incorporated in NBR, in very low concentrations. The composites were characterized and their mechanical, thermal and electrical properties were studied.

6.3C.1 Curing Studies

Cure parameters obtained during the curing process are reported in Table 6.7. Minimum torque is a measure of viscosity of the compound. The increase in minimum torque on the addition of MWCNT indicated an increase in viscosity and a reduction in the mobility of rubber chains [28]. The highest value of minimum torque was obtained at 0.3 phr MWCNT concentration. This is because at higher concentration occlusion of rubber takes place within and between the filler aggregates. This increased the immobility of the elastomer layers and thus led to an increase in the minimum torque value

Maximum torque of the nanocomposites was very close to that of gum. Maximum torque is a measure of the extent of cross linking between the rubber chains and it gives the extent of filler polymer interaction. The very small concentration of MWCNT used might be insufficient to produce a considerable change in the torque value.

Scorch time is a measure of premature vulcanization or scorch safety of the rubber compound. Scorch time decreased with the addition of MWCNT. Similar behaviour was reported when MWCNT was added to NR [29]. Addition of thermally conducting MWCNT could improve the conductivity of NBR and thus help in vulcanization. Cure time which is the time required to reach maximum torque also decreased slightly with filler loading. Thus MWCNT had an accelerating effect on the cure reaction.

Cure rate index is a measure of rate of cure reaction. The rate of cure reaction increased initially and then decreased. Increase in cure rate index at low concentration might be due to the presence of crosslinks formed between MWCNT and NBR. When concentration of MWCNT increased the cross links were reduced due to agglomeration of MWCNT.

Table 6.7. Cure charecteristics of NBR- MWCNT nanocomposite

MWCNT laoding	Min Torque M_L (dNm)	Max Torque M_H (dNm)	$\Delta M = M_H - M_L$ (dNm)	Opt. cure T_{90} (min)	Scorch time T_{10}(min)	Cure Rate Index CRI
0	0 .160	2.673	2.513	1.30	0.49	124
0.02	0.425	2.644	2.475	1.03	0.293	125.156
0.05	0.222	2.697	2.219	1.18	0.381	135.685
0.15	0.849	2.494	1.645	1.07	0.213	116.686
0.3	1.121	2.869	1.748	1.11	0.199	110

6.3C.2 Mechanical Properties

Fig.6.15(A) and (B) shows the variation of tensile strength/elongation at break and modulus/tear strength respectively of NBR-MWCNT nanocomposites. Tensile strength increased by 36% (0.05phr), modulus by 24% (0.3phr) and tear strength by 32% (0.02phr). After attaining an optimum value the mechanical properties decreased with higher loading.

A.M. Shanmugharaj et al. [30] have reported that the increase in tensile strength and modulus in polymer multiwalled carbon nanotube composites were not remarkable due to poor adhesion and weak van der Waals forces, which gave rise to lower stress transfer ability in the composites. But here even wih a very low concentration of MWCNT there was considerable increase in tensile strength, modulus at 300% elongation and tear srength. This might be due to the interfacial bonding between the polar NBR matrix and the functional groups loaded on the surface of MWCNT during purification. Elongation at break of the nanocomposite decreased with the incorporation of MWCNT. Cracks are usually initiated at the in-homogenities like voids, and nanotube agglomerates act as stress concentrators or weak spots of cross link density [23]. So the decrease in elongation might be attributed to an insufficient dispersion of CNT agglomerates.
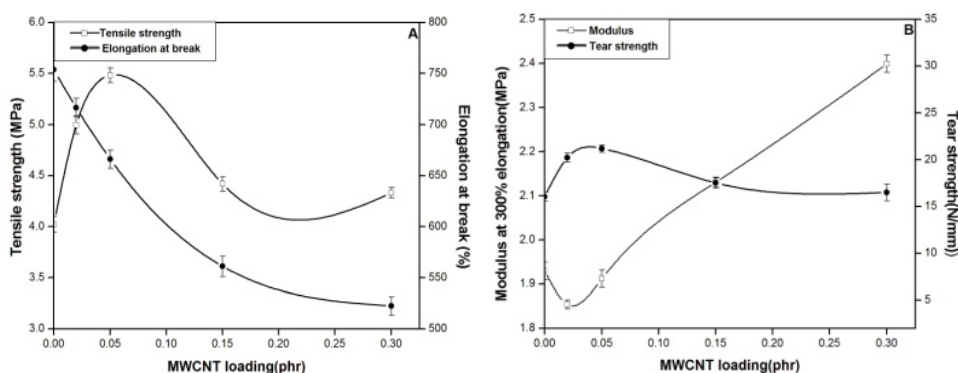
Fig 6.15. Variation of (A) tensile strength and elongation at break (B) modulus and tear strength of NBR-MWCNT nanocomposites

6.3C.3 Swelling studies

Swelling studies of the vulcanizates containing different concentration of MWCNT were done in MEK at room temperature. Fig.6.16 shows the decrease in swelling index with the addition of MWCNT. As the filler loading increased

the solvent uptake decreased due to the increased hinderance exerted by nanotubes at higher loadings. Contribution to reinforcement effect arose from molecular interaction between rubber and filler. This interaction led to an increase in the effective degree of cross linking and could be evaluated from equilibrium swelling. As the cross linking increased the swelling ratio decreased.

The entangled structure of nanotubes having nanometer scale diameters and micrometer scale lengths can themselves provide physical cross links. This will result in more cross link in the composite than in unfilled NBR, eventhough the chances for a chemical reaction between MWCNT and NBR are negligible.

Sorption curves of the vulcanizate were obtained by plotting Qt % against time as given in Fig.6 17. The uptake of the solvent was rapid initially but soon reached an equilibrium state. The unfilled vulcanizate had the maximum uptake at equilibrium swelling. The curves showed two distinct regions-an initial steeper region with high sorption rates due to large concentration gradient and a second region exhibiting reduced sorption rates that ultimately reached equilibrium. The value decreased with increase in filler loading.
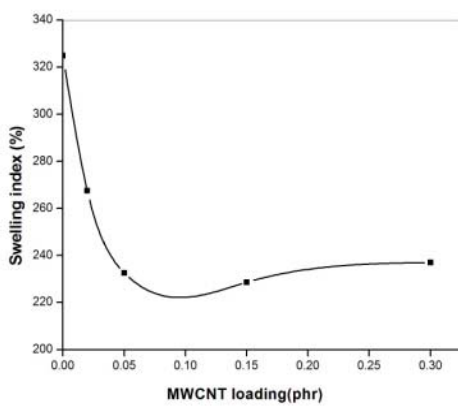
Fig.6. 16. Variation of swelling index (%) MWCNT loading
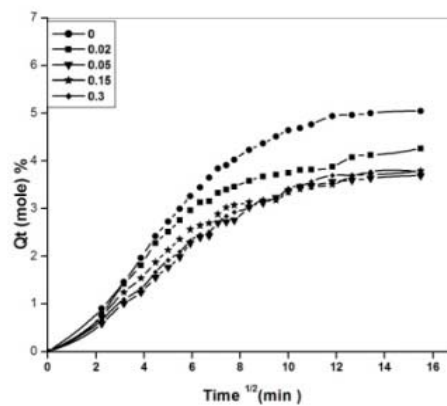
Fig. 6.17. Sorption curves of NBR and with NBR- MWCNT nanocomposites

6.3C.4 Thermogravimetric analysis (TGA)

The thermal behaviour at the heating range of 30^0C to $700\ ^0$C of the neat polymer and the MWCNT filled samples are shown in Fig.6.18. (A) and (B). Thermal analysis data is given in Table 6.8. Due to the multiple degradation steps of the butadiene component present in raw rubber, unfilled NBR degraded in two steps with one minor peak at 428^0C and a major peak at 456^0C. The nanocomposite also followed the same pattern. Temperature at 10%, 25% and 50% weight losses for the nanocomposite were the same as that of gum. Peak maxima were also, almost the same. So the inclusion of nanotube in such a small concentration did not affect the thermal stability of the nanocomposite.
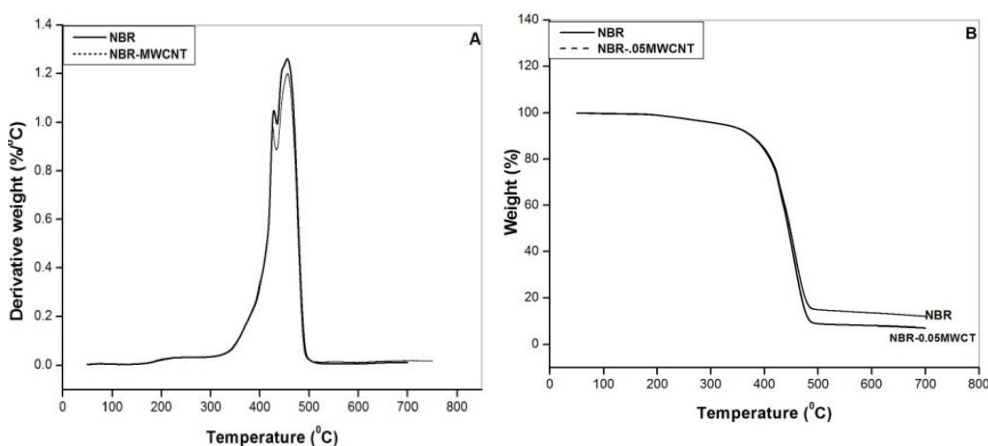
Fig 6.18 (A) DTG and (B) TGA curves of NBR and NBR 0.05MWCNT

Table 6.8.Thermal analysis results of NBR and NBR-0.05 MWCNT

Sample	Onset temp. (^{0}C)	Peak max.(^{0}C)		Residue %	T_{10} (min)	T_{25} (min)	T_{50} (min)
		T_1	T_2				
NBR	340	428	456	6.783	375	420	445
NBR-0.05 MWCNT	334.31	425.31	456.58	11.22	375.51	420.98	447.03

6.3C.5 Differential scanning calorimetry (DSC)

The glass transition temperatures of NBR and NBR-MWCNT naocomposites are given in Table 6.9. In conventional composites due to the interaction between filler and rubber molecules the molecular motion of rubber molecules will be affected and the influence can be reflected in thermoanalysis curve. Loss in mobility of the chain would result in an increase in T_g and most probably in a change of the thermal expansion of the free volume. Here it is believed that the amount of carbon nanotubes used were too small to produce any change in the chain flexiblity/T_g

Table 6.9. T_g of NBR and NBR-MWCNTnanocomposites

Samples	T_g
NBR	-22.57
NBR -0.05 MWCNT	-22.57
NBR-0.3 MWCNT	-23.42

6.3C.6 X-ray diffraction analysis (XRD)

Fig.6.19 shows the XRD diffractograms of MWCNT, NBR and NBR-MWCNT nanocomposite. The characteristic peak of MWCNT is at $25.7^0.$ The nanocomposite did not show any peak in this range. This showed the absence of an ordered intercalated or rather an exfoliated structure of the nanocomposite.
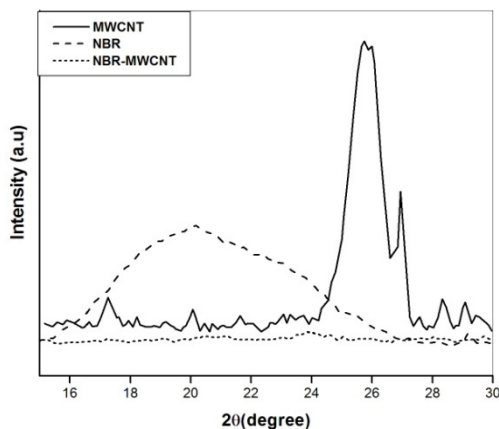
Fig.6.19. Xray diffraction pattern of MWCNT, NBR and NBR-0.05MWCNT

6.3C.7 Fourier transform infrared spectroscopy (FTIR)

Fig.6.20 shows the IR spectrum of NBR and NBR-0.05MWCNT nanocomposite. The increase in the intensity of the band at 969cm^{-1} confirmed the interaction of the π electrons of the nanotube with the butadiene double bond. The introduction of the peak at 1594cm^{-1} might be due to C=C from the MWCNT. The increase in the intensity of the band at 2235 cm^{-1} might be due to the polar interaction of the carboxylic group of nanotube with the CN group of NBR.
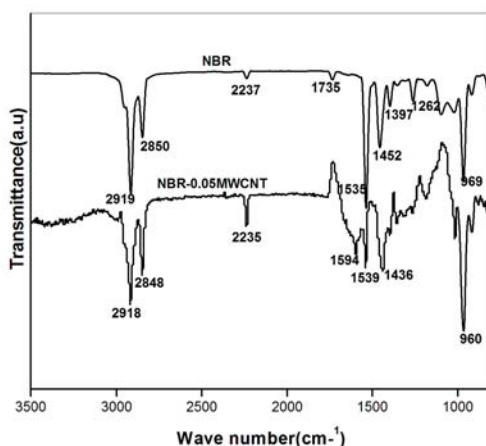
Fig. 6.20.FTIR spectrum of NBR and NBR-0.05MWCNTnanocomposite

6.3C.8 Scanning electron microscopy (SEM)

SEM images of the tear fractured surface of the nanocomposite are shown in Fig. 6.21. The rough surface of the nanocomposite showed typical brittle fracture behaviour with a lot of agglomerates. It seemed that the nanotubes having weak interface are pulled out of the matrix showing that the interfacial bonding between the CNTs and the rubber matrix need to be improved.
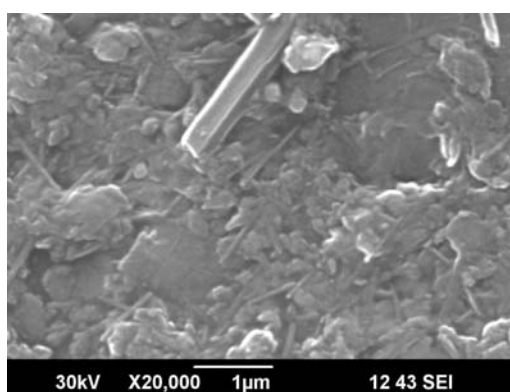
Fig. 6.21. SEM imagesof NBR -0.05 MWCNT nanocomposite

6.3C.9 Conductivity

The electrical conductivity of polymer nanocomposite with carbon nanotubes depend on several factors, like nanotube concentration, polymer matrix, filler-matrix interaction, filler orientation and the processing techniques intended to improve the dispersion of carbon nanotubes in the host marix [31] .

In general, the electrical conductivity of a particulate composite reveals a non-linear increase with the filler concentration, passing through a percolation threshold, as shown in Fig.6.22. At low filler concentrations, the conductive particles are separated from each other and the electrical

properties of the nanocomposite are dominated by the matrix. With increasing filler concentration local clusters of particles are formed. At the percolation threshold, these clusters form a connected three-dimensional network through the component, resulting in a jump in the electrical conductivity.
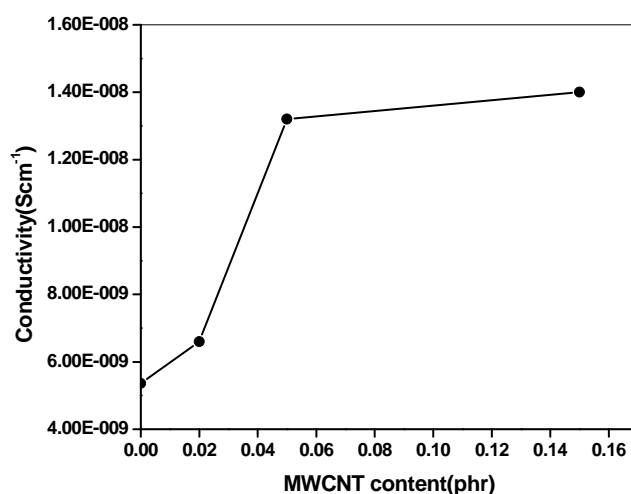
Fig. 6.22. Electrical conductivity of NBR/MWCNT nanocomposites

6.3C10 Conclusions

Purification of MWCNT by refluxing with HCl introduced OH and CO groups in it. Mechanical properties of NBR increased with the addition of MWCNT. Presence of nanotube restricted the solvent swelling capacity of the nanocomposite. There were no appreciable changes in the thermal stability and glass transition temperature of the nanocomposites. IR spectrum confirmed the absence of a chemical bond between NBR and MWCNT. SEM images showed pull out of MWCNT which might be due to the poor interaction of MWCNT in NBR. MWCNTs increased electrical coductivity of NBR.

6.3D Graphene Nanoplateles in NBR

Graphene nanoplatelets were incorporated in NBR at very low concentration. Cure characteristics, mechanical and thermal properties of the nanocomposites were studied. They were further characterized by XRD, FTIR and SEM analysis.

6.3D.1 Curing studies

The cure characteristics of graphene loaded NBR is given in Table 6.10. Minimum torque of the nanocomposite was almost equal to that of gum. The addition of graphene in small concentration did not affect the viscosity or mobility of rubber chains. Certain nanostructures when dispersed in various polymers can form net work structures that could constrain the motion of polymer chains. Another reason for the low viscosity might be the lubricant property of graphene [32]

Maximum torque M_H and ΔM (M_H-M_L) showed a slight increase on the addition of graphene.The increase in M_H and ΔM are usually the effect of an increase in cross link density. Here the physical interaction of the graphene platelets with NBR and the wrinkled topology of graphene platelets would have enhanced mechanical locking and adhesion and have slightly accelerated the curing reaction.

A small increase in modulus (6%) of the nanocomposite also indicated the reinforcement is not due to the increase in cross linking, but it is an effect of the physical interaction and nanofiller geometry [33]. Optimum cure time i.e. the time taken for obtaining 90% of the maximum torque was almost a constant and there was increase in the scorch time showing a better processing safety fot the nanocomposite.The

inclusion of graphene increased the rate of curing reaction by participating in the cure reaction as observed by the increase in the CRI value.

Table 6.10. Cure characteristics of NBR/ graphene nanocomposite

Graphene Loading (phr)	Min. Torque M_L (dNm)	Max. Torque M_H(dNm)	$\Delta M= M_H - M_L$	Opt. cure T_{90} (min)	Scorch time T_{10} (min)	Cure Rate Index CRI
0	0.160	2.673	2.513	1.30	0.49	124
0.05	0.167	3.040	2.873	1.34	0.69	153
0.15	0.160	2.954	2.794	1.32	0.60	138
0.3	0.157	2.899	2.742	1.25	0.56	147

6.3D.2 Mechanical properties

The variation in mechanical properties of graphene filled NBR are given in Fig 6.23 (A) and (B).The addition of graphene platelets showed marked increase in tensile strength and elongation at break. The addition of 0.3 phr graphene increased the tensile strength to 162% and elongation at break to 47%.

The intrinsic properties of graphene, their wrinkled structure and the physical interaction with the host polymer might have enhanced the mechanical interlocking and adhesion of graphene to the polymer marix. This strengthened the interaction and load transfer between graphene and NBR leading to reinforcement in properties [33,34].

The dispersed graphene platelets with the wavy and wrinkled structure would unfold rather than stretch inplane under an applied tensile stress leading to a small increase in modulus (6%) and tear strength (16%).

Incomplete exfoliation and restacking of platelets also led to lowering of modulus values due to decreased aspect ratios [34].
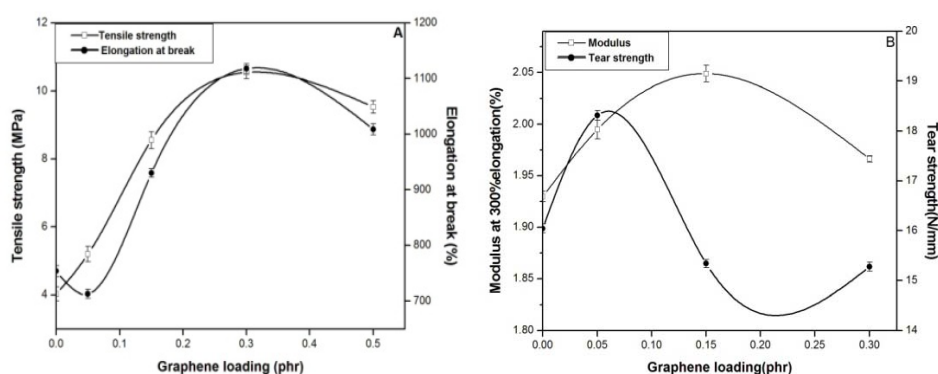
Fig 6.23. Variation of (A) Tensile strength and Elongation at break (B) Modulus and Tear strength of the NBR-graphene nanocomposite

6.3D.3 Swelling studies

Fig.6.24. shows the plot of MEK up take, Q_t mole (%) against time, of graphene reinforced NBR. On the addition of graphene, swelling rate showed a rapid decrease. All the samples showed regular increase in swelling with time. The rate of uptake increased at first, but later became constant as final equilibrium is approached. These curves are often referred to as sigmoid sorption curves [35]. At 0.05 phr graphene concentration swelling was least and cross link density maximum. Fig. 6.25 gives the variation of swelling index with concentration of graphene. As the filler concentration increased the solvent uptake decreased.
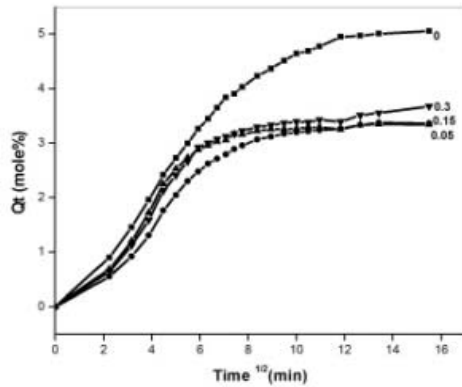
Fig.6.24. Sorption curves of NBR-Grapheme nanocomposites
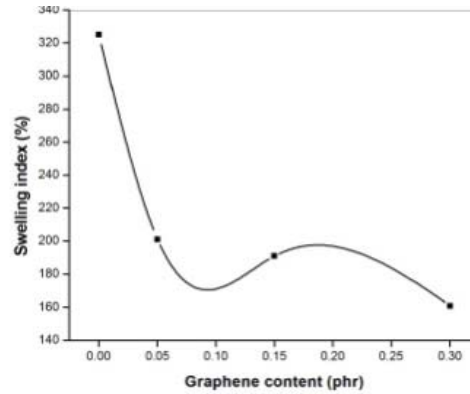
Fig.6.25. Variation of swelling index with clay loading

6.3D.4 Thermogravimetric analysis (TGA)

Fig.6.26 (A) and (B) gives the DTG and TGA curves of non oxidative thermal degradation (under nitrogen flow) of NBR and NBR containing 0.15 phr graphene. Their thermal stability data is given in Table 6.11 .It is seen that very low concentration of graphene did not affect the thermal stability of the nanocomposite. There was no change in the on set degradation temperature, peak maximum, temperature at 10%,25% and 50% weight loss for the nanocomposite .
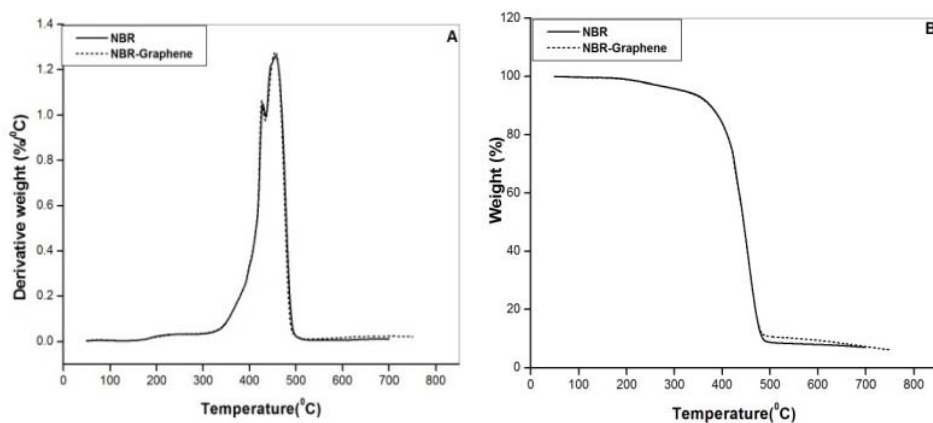
Fig.6.26 (A) DTG and (B) TGA curves of NBR and NBR -0.15 graphene

Table 6.11. Thermal analysis results of NBR and NBR-0.15 graphene

Sample	Onset temp. (^{0}C)	Peak max.(^{0}C)		Residue %	T_{10} (min)	T_{25} (min)	T_{50} (min)
		T_1	T_2				
NBR	340.6	428.49	455.91	6.783	375.60	420.24	444.79
0.15G	341.2	427.75	455.56	5.873	374.78	419.67	444.49

6.3D.5 Differential scanning calorimetry (DSC)

Table 6.12 gives the glass transition temperature of NBR and NBR-graphene nanocomposites. At 0.05 and 0.15 phr concentration of graphene, there was no change in the glass transition temperature. But when concentration was increased to 0.3phr, a slight increase in Tg was observed. Thus the mobility of NBR chain was restricted when the concentration of graphene platelets increased.

Table 6.12. Tg values of NBR and NBR-0.15graphene

Sample	T_g (^{0} C)
NBR	-22.57
NBR-0.05Graphene	-23.07
NBR-0.15 Graphene	-22.37
NBR-0.3 Graphene	-21.57

6.3D.6 X-ray diffraction analysis (XRD)

Like nanoclays graphene also has a layered structure, so when dispersed in a polymer matrix graphene exhibits similar states of dispersion like stacked, inercalated or exfoliated depending on their processing techniques and affinity between the plates. Fig.6.27 gives the XRD diffractograms of graphene, NBR and NBR-0.15 graphene nanocomposite

in the 2θ range 0-30^0.The characteristic broad peak of graphene was found at 26 ^{0}. The composite was devoid of any peaks in this 2θ range.So the polymer molecules must have exfoliated the graphene layers.
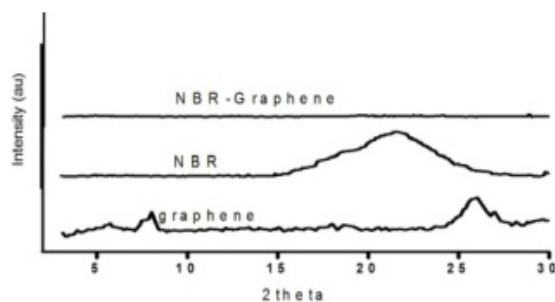
Fig. 6.27. X-ray diffraction pattern of graphene, NBR and NBR-0.15 graphene

6.3D.7 Fourier transform infrared spectroscopy (FTIR)

Fig.6.28 shows the IR spectrum of NBR and NBR-0.15gaphene.The peaks in the range 2900 and 2850cm^{-1} attributed to the CH stretch vibration are seen in the unfilled and filled polymer. The characteristic peak of CN remained intact in the nanocomposite, showing there is no interaction of graphene platelets with the CN group of NBR. The peak in the range 1530cm^{-1}, representing the zinc carboxylate ion was seen in the composite also. The butadiene stretch at 969cm^{-1} had become sharper and intense. This might be due to the interaction of butadiene double bond with the pi electrons of graphene. The peaks due to CH$_2$ deformation at 1452, 1397 and 1262 cm^{-1} have reduced in the composite. So from the IR spectra it can be inferred that in the composite there is only interaction of CH$_2$ groups and pi electrons of graphene with the butadiene double bond of NBR.
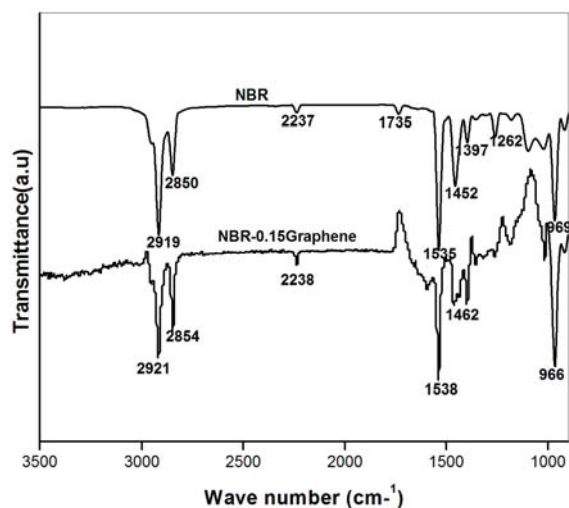
Fig.6.28. FTIR of NBR, and NBR-0.15 graphene

6.3D.8 Scanning electron microscopy (SEM)

Fig 6.29 gives the SEM images of NBR-graphene nanocomposites. Graphene platelets do not appear flat,but have a curved wrinkled structure.This structure might be due to the intrinsic flexiblity of the atomically thin sheets.This structure helped in the dispersion of the graphene platelets and minimized restacking of the platelets. The graphene platelets seemed to be well embedded in the polymeric matrix showing the adhesion of the filler with the matrix.
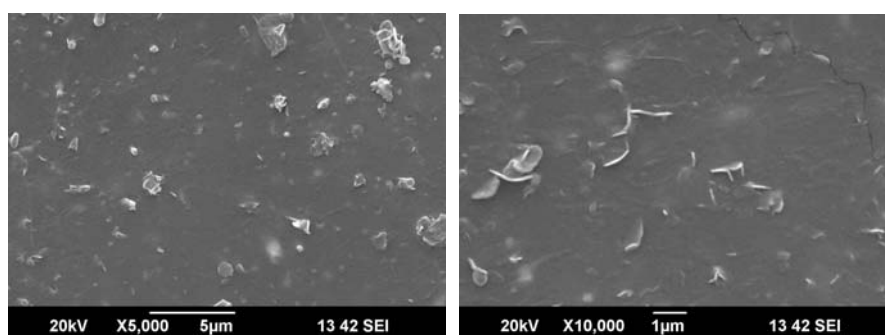
Fig.6.29. SEM imagesof NBR-graphene nanocomposite

6.3D.9 Conclusions

NBR /graphene nanoplatelet composites prepared by the simple mill mixing method had shown good improvement in tensile strength and elongation at break. Thermal stability of the nanocomposite was unaffected by the incorporation of a small amount of graphene.There was a small improvement in the glass transition temperature of the nanocomposite at a higher concentration. XRD analysis showed the exfoliation of graphene layers in the nanocomposite. From IR spectrum it was clear that there was no chemical bonding between graphene platelets and NBR.

References

[1]   Bhowmick, A. K. Bhattacharya, M. Mitra, S. Dinesh Kumar, K. Maji, P.K. Choudhury, A. George, J.J. Basak, G.C. Adv Polym Sci. 2011, 239. 1.

[2]   Hwang, W. Wei, K. Polymer Engineering and Science. 2004, 44, 2117.

[3]   Moniruzzaman, M. Winey, K.I. Macromolecules. 2006, 39, 5194.

[4]   Bokobza, L. Polymer. 2007, 48, 4907.

[5]   Cho, D. Lee, S. Yang, G. Fukushima, H. Drzal, L.T. Macromol Mater Eng. 2005, 290,179.

[6]   6 Li, B. Zhong, W. J Mater Sci. 2011, 46, 5595.

[7]   Liu,Q. Zhang,Y. Xu,H. Applied Clay Science. 2008, 42.

[8]   8. Malicka-Soczka, A. Domka, L. Kozak , A. Physicochem. Probl. Miner. Process .2010, 44, 151.

[9]   Mohamad, N. Muchtar,A. Jameelah,M. Ghazali Dahlan Hj. Mohd Che Husna European Journal of Scientific Research. 2008, 24, 538.

[10]   Kader, M. A. Kim, K. Lee Y.S, Nah C. J Mater Sci. 2006, 41,7341.

[11]   Mathew,L. Ph.D Thesis. Cochin University of Sciece and Techology 2009, 246.

[12]   Thermal Analysis Application No. HB 427.   Application published in METTLER TOLEDO TA Application Handbook Elastomers Volume 2 .

[13]   Wen, J. Wilkes, G. L. Chem Mater. 1996, 8, 1667.

[14]   Zhu, J. Uhl, F.M. Morgan, A.B. Wilkie, C.A. Chem. Mater. 2001, 13,4649.

[15]   Ray, S.S. Okamoto, M. Prog. Polym. Sci.2003, 28, 1539.

[16]   Gilman, J.W. Appl. Clay Sci.1999, 15, 31.

[17]   Mark, J. E. J. Phys. Chem. B. 2003, 107, 903.

[18]   Zoromba,M.Sh. Belal, A.A.M. Ali, A.E.M. Helaly, F.M. Abd EI-
        Hakim, A.A. Badran A.S.   Polymer. Plastics Technology and
        Engineering. 2007, 46, 529.

[19]   Zhenbang, P.I. Zhuoqin, L. Chao, Y. Xike,T. Jinbo, F.E.I. Jianhua,Z.
        Front Earth Sci.China. 2007,1,26.

[20]   Sadhu, S. Bhowmick, A.K. Journal of polymer science part B:polymer
        Physics. 2004, 42, 1573.

[21]   Galimberti,M. Rubber-Clay Nanocomposites Science,Techology and
        Applications. Wiley. 2011, 285.

[22]   Alex,R. Nah,C. Journal of Applied Polymer Science. 2006,102, 3277.

[23]   Esawi , A.M.K. Farag,M.M. Materials and Design. 2007, 28, 2394.

[24]   Lorenz,H. . Fritzsche, J.   Das, A. . Stöckelhuber, K.W.   Jurk, R.
        Heinrich, G. Klüppel, M. Composites Science and Technology. 2009,
        69, 2135.

[25]   Verge,P. Peeterbroeck ,S. Bonnaud ,L. Dubois,P. Composites Science
        and Technology. 2010, 70, 1453.

[26]   Bose, S. Khare , R.A. Moldenaers,P. Polymer. 2010,51, 975.

[27]   Faraj,A. Abuilaiwi1, Tahar Laoui1, Mamdouh Al-Harthi and Muataz
        Ali Atieh. The Arabian Journal for Science and Engineering. 2010, 35.

[28]   Yuca,N. Karatepe,N. Yakuphanoğlu,N. World Academy of Science,
        Engineering and Technology. 2011,79 ,611.

[29]   Nair, A.B. Kurian,P. Joseph,R.European Polymer Journal 2013,49, 247.

[30]   Sui,G. Zhong,W. Yang,X. Zhao,S. Macromol. Mater. Eng. 2007, 292, 1020.

[31]   Shanmugharaj, A.M. Bae, J.H. Lee, K.Y. Noh,W.H. Lee,S.H. Ryu, S.H. Composites Science and   Technology. 2007, 67 1813.

[32]   Bokobza,L. eXPRESS Polymer Letters .2012, 6, 213.

[33]   Li,B. Zhong, W. J Mater Sci. 2011, 46, 5595.

[34]   Ozbas,B. O'Neill,C.D. Register,R.A.   Aksay,I.A. Prud'homme, R.K. Adamson,D.H. Journal of Polymer Science Part B: Polymer Physics. 2012,50,910.

[35]   Potts, J.R. Dreyer, D. R. Bielawski,C.W. Ruoff,R.S. Polymer. 2011, 52, 5.

.....ೞಃ.....

Chapter 7

MICROWAVE STUDIES OF ELASTOMERIC NANOCOMPOSITES BASED ON MULTIWALLED CARBON NANOTUBES AND GRAPHENE

7.1 Introduction

Polymer composites filled with electrically conducting particles exhibit a broad spectrum of properties useful for a variety of applications in science and technology.Their unique electric and dielectric properties together with the mechanical and chemical stability are made use of in the production of various components for electronic applications [1].The most important application being protection against radiation, as in microwave absorbers for electromagnetic interference shielding of various devices [2]. Polymer composites containing conductive fillers like carbon black, carbon fiber and metal fibers have been extensively studied, particularly for electromagnetic interference shielding, radar absorption, electronic packaging etc. But the high filler volume used in these cases deteriorates their overall mechanical properties. Thus carbon nanotubes and graphene replaced these conventional fillers in polymer composites [3].

Dielectric and microwave properties of graphene filled and nanotube filled NR composites were studied by Al-Hartomy, O.A.et al. [4-6].

Microwave measurement techniques used for the study of dielectric properties fall under two categories (1) resonance technique and (2) transmission technique. Dielectric property measurement by resonant technique has higher accuracy than measurement by transmission technique especially for dielectric loss [7]. Resonance techniques can further be divided into dielectric resonance technique and perturbation technique.

Cavity perturbation technique has been extensively used for measuring dielectric parameters of materials at microwave frequency [8]. The main advantages of cavity perturbation technique are

1) There is no tolerance limit on the shape and dimension of measured specimen.

2) Specimen is usually a small piece of rod, sheet or bar of 1mm^2 cross section. For thin rod shaped samples the perturbation technique is the most suitable method for the measuremet of dielectric properties at microwave frequencies.

The basic concept of perturbation technique is that the presence of a small piece of the dielectric sample in the resonant cavity will result in a shift of resonant frequency and a decrease of the quality factor of the cavity. Rectangular or cylindrical wave guide resonators are used in this technique.The volume of the sample is much smaller than the volume of the resonant cavity. The sample is introduced into the cavity resonator at the position of maximum electric field, where the contribution of magnetic field for the perturbation is minimum [9]. From the measurement of perturbation due to sample, the dielectric parameters can be determined.

7.2   Experimental

Materials

XNBR latex: Chemigum CLX 530 was supplied by Eliokem India Pvt. Ltd.Bombay.

SBR latex: Encord 204 was supplied by Jubilant Organosys Limited. Gujarat.

NBR: Kumho NBR, KNB 35L manufactured supplied by Kumho Petrochemicals

SBR: Kumho SBR (SBR-1502) supplied by Kumho Petrochemicals

MWCNT: MWCNT Baytube^R 150P was obtained from Baeyer Materials Science AG (Leverkusen Germany)

Graphene: Graphene nanoplatelets, supplied by Quantum Materials Limited, Bangalore.

Preparation of nanocomposites:

Forrmulation used in the preparation of XNBR latex compound (Table 3.3), SBR latex compound (Table 3.4), NBR(dry) compound (Table3.5) and SBR (dry) compound (Table 3.6)   are given in Chapter 3. A detailed description for the methods of preparation of latex (XNBR /SBR) based MWCNT/graphene nanocomposites are given in Section 3.11.3. Preparation of dry rubber (NBR/SBR) based MWCNT/graphene nanocomposites are given in Section 3.11.5.

MWCNTand graphene were added in concentration ranging from 0-0.3 phr

Methods

The dielectric properties in the microwave frequency (S band 2-4 GHz) of the prepared nanocomposites (XNBR/MWCNT, XNBR/graphene, SBR/MWCNT, SBR/graphene, NBR(dry)/MWCNT, NBR(dry)/graphene, SBR(dry)/MWCNT, SBR(dry)/graphene were evaluated by Cavity Perturbation Technique [10,11] using Agilent Performance Network Analyzer E8362B (Section 2.5.2).

The resonant frequency f_0 and the corresponding quality factor Q_0 of each resonant peak for the empty cavity were first determined. Then a particular resonant frequency in the S band region was selected. The dielectric sample was introduced into the cavity and the position adjusted for maximum perturbation. At this position there was maximum shift of resonant frequency towards the low frequency region with minimum amplitude of the peak. The new resonant frequency f_s and the quality factor Q_s were observed.The procedure was repeated for other frequencies and measurements were done [12]. From the volume of the sample and the cavity resonator the dielectric parameters were evaluated [13, 14].

The parameters were calculated using the following formula

Dielectric constant $\varepsilon' = 1 + V_c/V_s . f_0 - f_s/2f_s$ ----------------------------(1)

Dielectric loss $\varepsilon'' = V_c / 4V_s . (Q_0 — Q_s)/ Q_0 Q_s$ --------------------(2)

Skin depth $\delta f = 1/\alpha f$ --(3)

AC conductivity $\sigma e = 2\pi f \varepsilon_0 \varepsilon''$. ---(4)

Here f_0 and Q_0 are the resonant frequency and quality factor of the empty cavity resonator, f_s and Q_s are the corresponding parameters of the cavity loaded with the sample .Vc and Vs are the volumes of the cavity and sample respectively. αf is the absorption coefficent.

7.3   Results and Discussion

Dielectric constant

The dielectric constant is a measure of the ability of the material to be polarized or it is a measure of how much energy from an external electric field is stored in the material [15]. Generally the dielectric constant of a material arises due to the polarization of molecules. The different types of polarization possible in a material are (1) electronic polarization (2) atomic polarization and (3) orientation polarization. Higher the polarizability of the material greater will be the dielectric constant [12].

Fig. 7.1. (A) and (B), shows the frequency dependence of real part of permittivity of MWCNT and graphene filled XNBR in the S band frequency region (2-4GHz). From the figure it is seen that the dielectric constant of the nanocomposites are enhanced by the incorporation of MWCNT and graphene. Since it is a measure of polarization, the interaction of XNBR containing polar CN and COOH groups with MWCNT and graphene containing pi electrons were more pronounced. E' value also increased with frequency, although a small dip was seen at the intermediate frequency. Thus XNBR-MWCNT and XNBR-graphene nanocomposites had values 4.09 and 3.6 respectively at 3.9 GHz.

Fig.7.1(C) and (D), shows the variation of dielectric constant with frequency of SBR-MWCNT and SBR-graphene nanocomposites. At higher

concentrations of MWCNT and graphene, E' value decreased with increase in frequency. The decrease in permittivity with increase in frequency revealed that the system exhibited strong interfacial interaction only at low frequency. The composites prepared might be considered as a heterogeneous system where conducting nanotube and graphene were covered with the insulating SBR. In such cases interfacial polarization arises from the difference in the conductivities of the two phases. This was analogous to Maxwell-Wagner double layer structure [16, 17]. High dielectric constant at low frequency might be due to induction polarization and migration of charge carriers. But at higher frequency, the migration of charge carriers lags behind the applied field decreasing the dielectric constant.

Fig.7.1(E),(F) and (G), (H) gave the variation of E' with frequency for NBR (dry)/MWCNT, NBR(dry)/graphene and SBR(dry)/MWCNT, SBR(dry)/graphene nanocomposites respectively. E' value increased with loading of nanotube and graphene as well as with increase in frequency. Polar NBR gave higher values of E' than non polar SBR. Table 7.1 gives the values of dielectric constants of gum rubber at the highest frequency (4GHz). The low values for SBR was characteristic of its non polar nature.

Table.7.1. Values of dielectric constants of unfilled rubber at a frequency of 4GHz

Raw rubber samples	Dielectric constant at 4 GHz
XNBR(latex)	3.34
SBR (latex)	2.65
NBR (dry)	3.04
SBR (dry)	1.8

Fig.7.1. **Variation of dielectric constant with frequency of (A) XNBR/MWCNT (B) XNBR/graphene (C) SBR/MWCNT (D) SBR/graphene (E) NBR (dry) /MWCNT (F) NBR (dry)/graphene (G) SBR (dry)/MWCNT and (H) SBR (dry)/graphene nanocomposites**

Dielectric loss

The mechanism of occurrence of dielectric loss is related mostly to the nature of dielectric polarization. The dielectric loss E"in XNBR latex and NBR dry rubber nanocomposites increased with concentration and frequency as shown in Fig 7.2. (A) (B) and(E) (F). Interfacial polarization and conductivity contributed to E"value. Addition of MWCNT and graphene containing pi electrons, to the polar XNBR and NBR increased the dipole polarity of the nanocomposite in the interfacial region [18]. Also, the free and mobile electrons in MWCNT and graphene increased with the increase in filler loading. This contributed to conductive chain formation leading to an increase in E" value [19] .When frequency increased the inertia of the molecule and the binding forces became dominant. This also led to an increase in dielectric loss [20].

E" values of SBR dry rubber composites increased with frequency. The increase was due to the conductive nature of pi electrons in MWCNT and graphene.

E"values of SBR latex/MWCNT nanocomposites showed a very small decrease with increase in frequency. While, for SBR latex/graphene nanocomposites the decline in value was more prominent. This might be because of the nonpolar nature of SBR and the presence of non ionic surfactant vulcastabV,L used in the preparation of graphene dispersion. The presence of this nonionic surfactant might have prevented graphene from making direct contact between themselves. So the contribution from conductivity of graphene was very low in SBR nanocomposite.
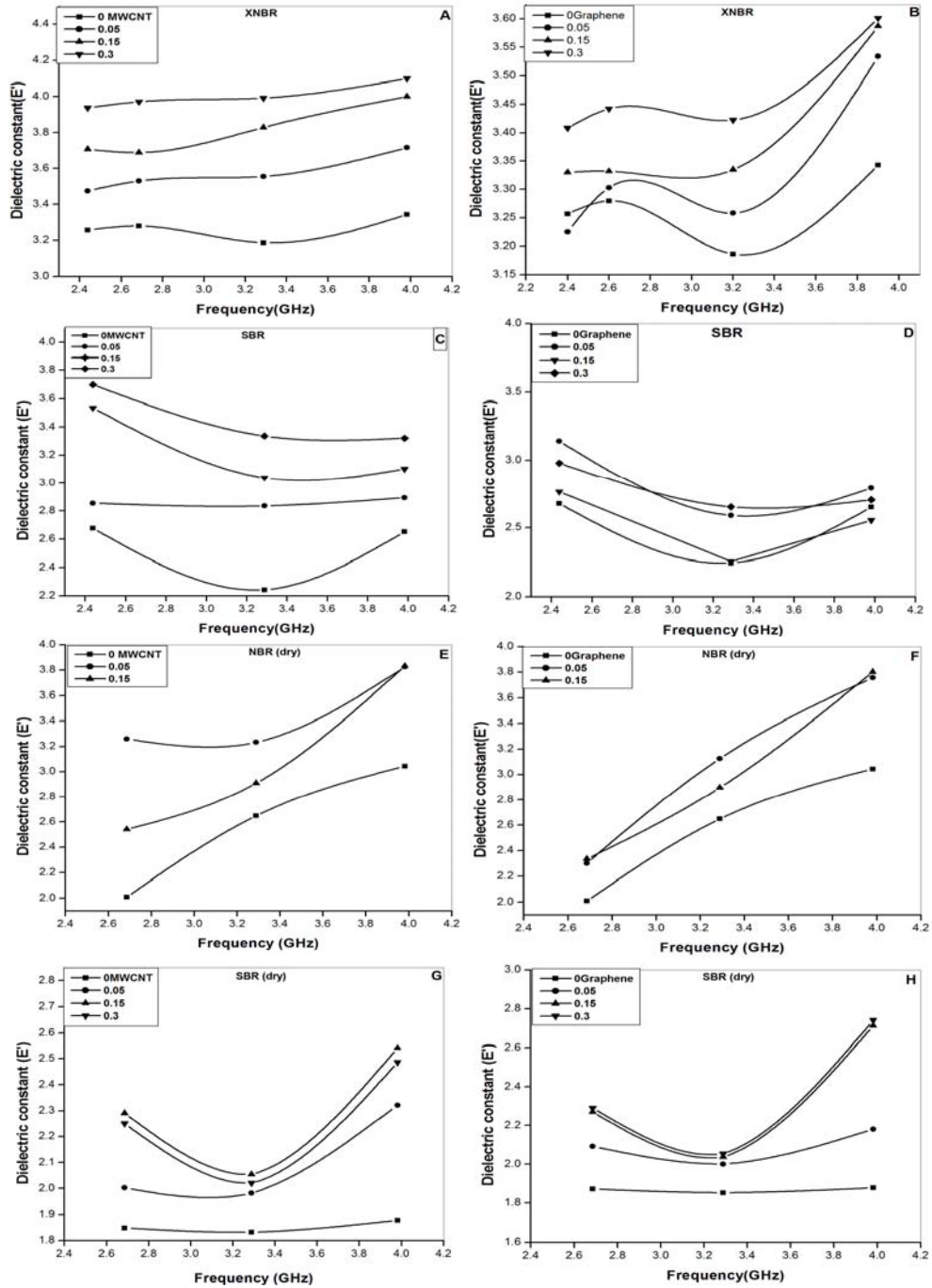
Fig.7.2. Variation of dielectric loss with frequency of (A) XNBR/MWCNT (B)XNBR/graphene (C) SBR/MWCNT (D) SBR/graphene (E) NBR (dry)/MWCNT (F) NBR (dry)/graphene (G) SBR (dry)/ MWCNT and (H) SBR(dry)/graphene nanocomposites

Skin depth

Penetration depth otherwise called skin depth (δf) is basically the effective distance of penetration of an electromagnetic wave ino the material. $\delta f = 1/\alpha f$ where αf is the absorption coefficient. Skin depth can be applied to a conductor carrying high frequency signal. With increase in frequency, skin depth decreases. The self inductance of the conductor limits the conduction of the signal to the outer shell and the shell thickness is the skin depth [21].

The conductivity of nanotube and graphene reduced the depth of penetration of the signal. Fig.7.3 (A)-(H) shows the decrease in skin depth with frequency and filler loading.
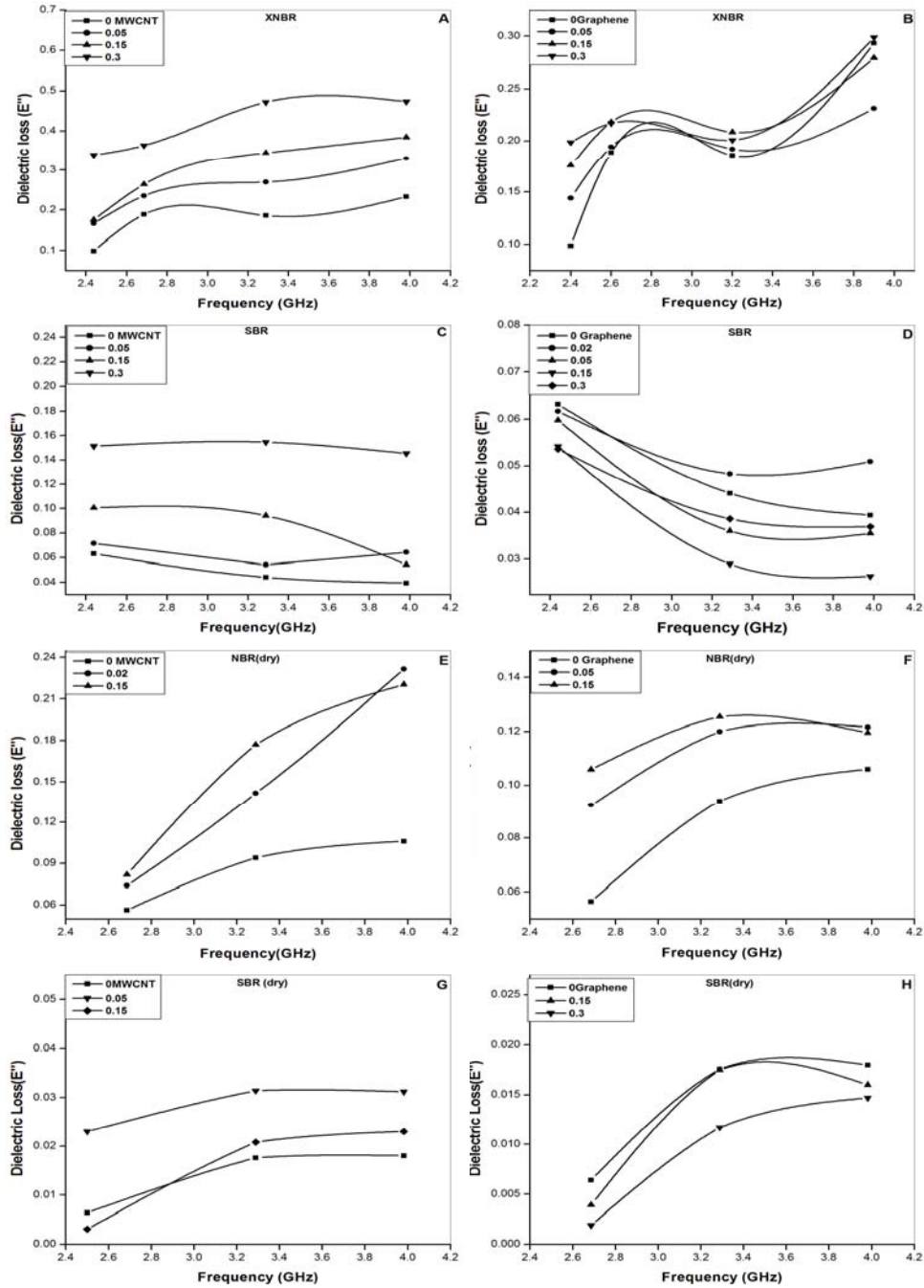
Fig.7.3. Variation of skin depth with frequency of (A) XNBR/MWCNT (B) XNBR/ graphene (C) SBR/MWCNT (D) SBR/graphene (E) NBR (dry)/MWCNT, (F) NBR (dry)/graphene (G) SBR (dry)/ MWCNT and (H) SBR(dry)/ graphene nanocomposites

AC conductivity

The honey comb lattice of graphene consists of a monolayer of sp^2 bonded carbon atoms where each carbon atom is attached to three carbon atoms in the XY plane and a weak pi electron cloud in the Z axis. Carbon nanotubes are cylindrical shells made by rolling graphene sheets. This gives carbon nanotube and graphene its unique electrical properties [22].

Electrical properties of nanocomposites depend primarily on the way the filler particles are distributed throughout the polymer matrix. In the presence of AC field, the growth of the conducting filler takes place from both electrodes. Since the poles change alternatively the formation of filler network does not start immediately on applying the electric field. The properly aligned filler starts moving towards each other and forms network overtime.With increase in filler loading the onset of network formation takes place earlier. Increasing the filler loading also increases the number of networks and decreases the number of dead points [23].

Variation of AC conductivity with frequency at different concentration of nanotubes and graphene are plotted in Fig. 7.4. (A)-(H). In all the nanocomposites, except SBR latex based nanocomposites conductivity increased with increase in filler concentration and with frequency. Since only a very small concentration of nanotube and graphene (0, 0.05, 0.15 and 0.3 phr) were used, increase in conductivity was also moderate. For all nanocomposites (except SBR latex nanocomposites) maximum value of conductivity were obtained at the highest frequency 4 GHz.

At low levels of filler loading, the conductivity of the nanocomposites was slightly higher than that of the base polymer, because filler particles were isolated from each other by the insulating rubber matrix [24]. When the concentration of nanofiller in the composite increased, the contact between the filler particles also increased.This led to the formation of a continuous path for the electrons to travel throug the entire volume of the sample [25].

From the figure it is observed that the conductivity of unfilled and filled XNBR latex was the highest. The presence of polar CN group and carboxyl group contributed to the conductivity of XNBR. When compared to XNBR latex based nanocomposites, conductivity was poor for NBR dry rubber nanocomposites which had only polar CN group and no carboxyl group. Introduction of polar hydroxyl and carbonyl groups on the MWCNT surface during purification had increased its conductivity as compared to graphene nanocomposites

In SBR latex /MWCNT nanocomposites conductivity value remained almost constant at different frequencies. For SBR latex/graphene nanocomposites conductivity decreased with frequency. This showed the absence of a continuous network structure in the nanocomposite.The surfactant used for dispersing graphene might have isolated the graphene particles preventing electrical contact between them.
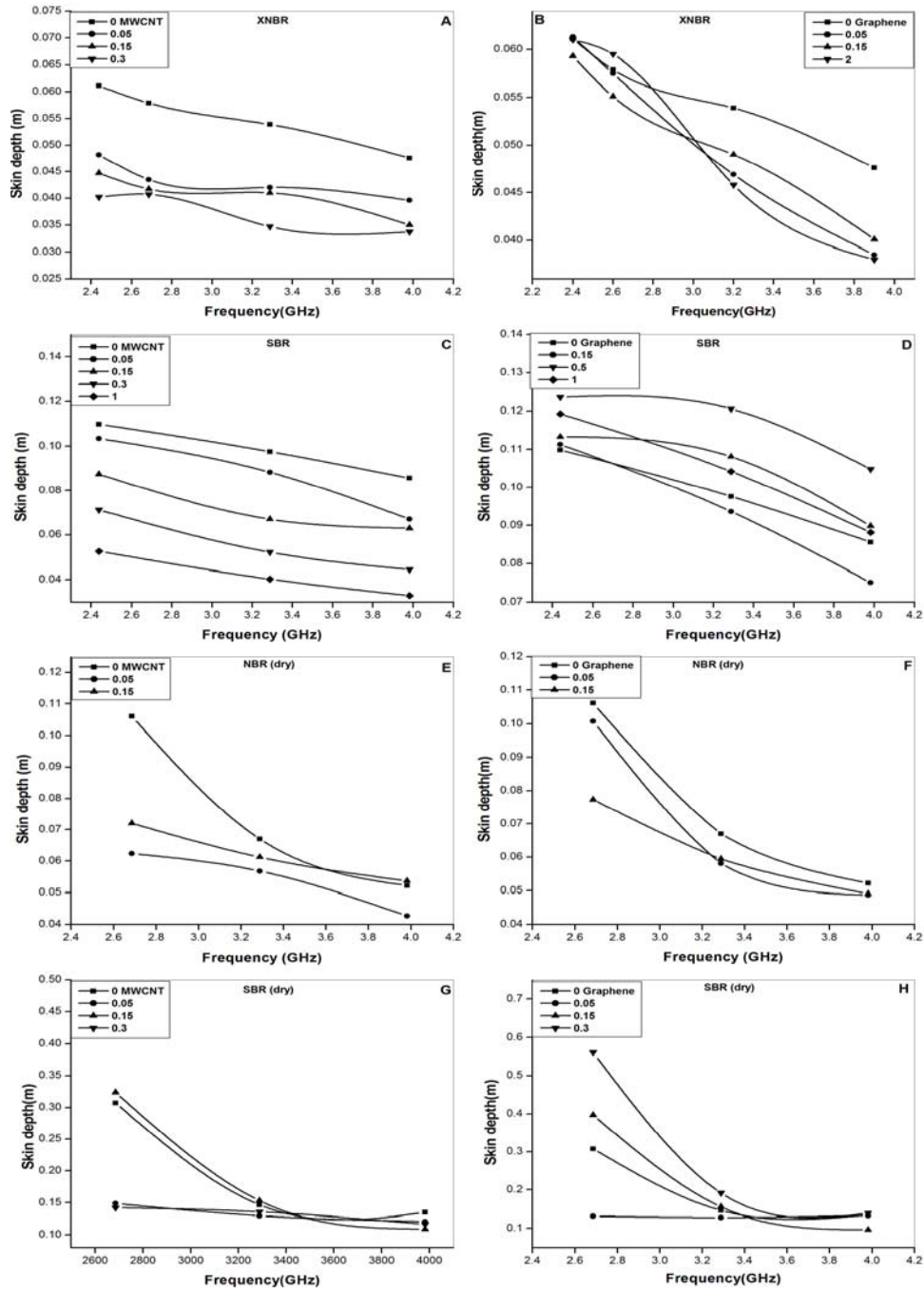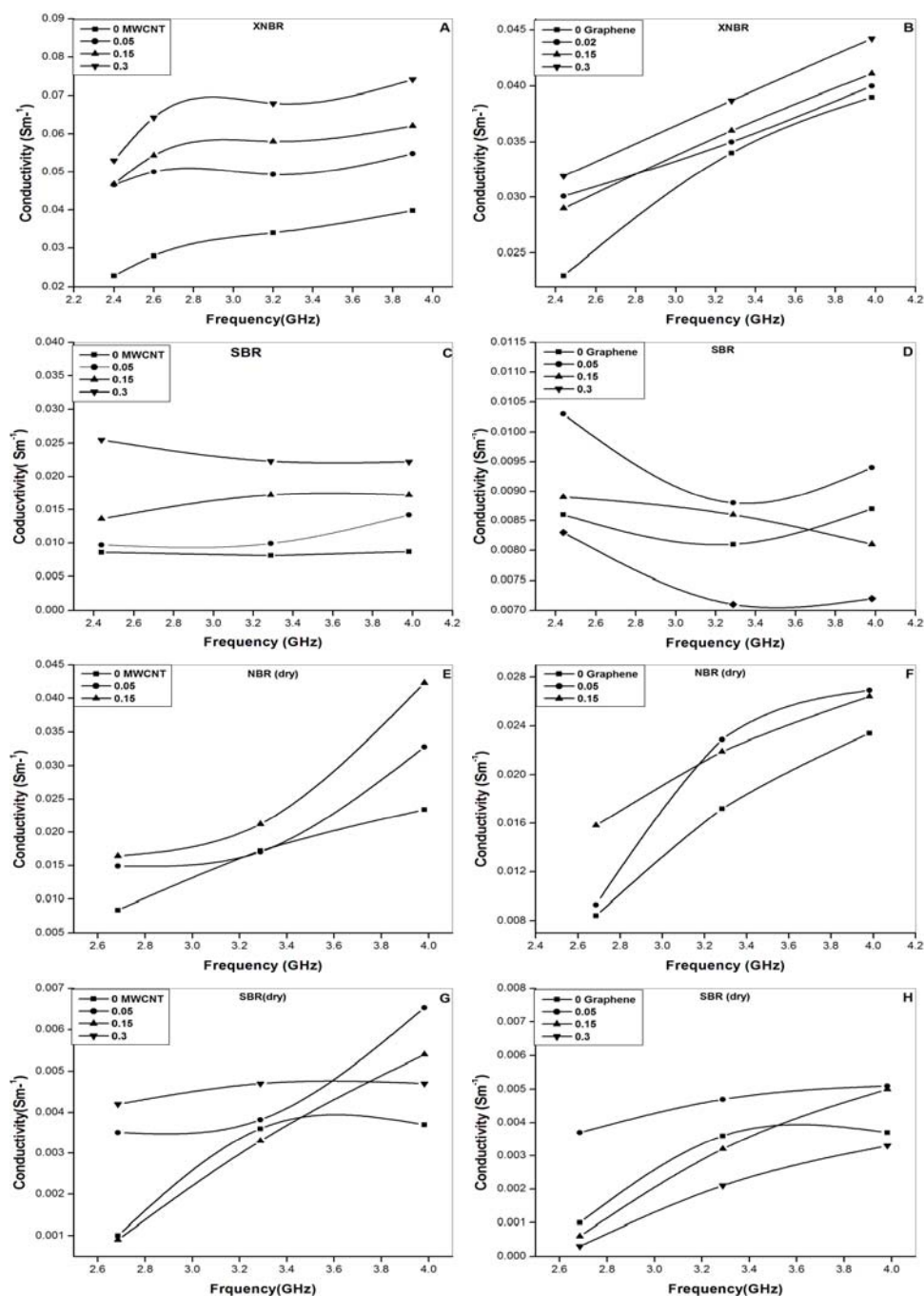
Fig.7.4. Variation of conductivity with frequency of (A) XNBR/MWCNT (B) XNBR/ graphene (C) SBR/MWCNT (D) SBR/graphene (E) NBR (dry)/ MWCNT, (F) NBR (dry)/graphene (G) SBR (dry)/ MWCNT and (H) SBR(dry)/ graphene nanocomposites

7.4 Conclusions

Dielectric permittivity, dielectric loss and AC conductivity of all the nanocomposites (except SBR latex nanocomposite) increased with increase in frequency.Enhancement in properties was marginal, since nanotube and graphene were used only in very small concentration ranging from 0-0.3 phr.

Penetration of electromagnetic waves into the material was reduced by the presence of conducting fillers .Thus there was a decrease in skin depth or penetration depth of all the nanocomposites with increase in frequency. Maximum conductivity and minimum skin depth were observed at a frquency of 4 GHz. Dielectric permittivity, dielecric loss and AC conductivity were maximum for XNBR nanocomposites. The nonpolar SBR latex vulcanizate showed some discrepancy in their behaviour.

Reference

[1] Cottevieille, D. Le Mehaute, A. Challioui, C. Mirebeau, P. Demay, J.N. Synth Met. 1999,101,703.

[2] Mouc̆ka, R. Mravc̆akova, M. Vilc̆akova,J. Omastova ,M. Saha,P. Materials and Design 2011, 32, 2006.

[3] Kim, B. Pfeifer, S. Park, S. Bandaru, P.R. Mater. Res. Soc. Symp. Proc. 2011, 1312,281.

[4] Al-Hartomy, O .A. Al-Ghamdi, A. Dishovsky, N. Shtarkov,R. Iliev,V. Mutlay, I. El-Tantawy, F. doi:10.4236/msa.2012.37064. http://www.SciRP.org/journal/msa) 2012 , 453

[5] Al-Hartomy, O .A. Al-Salamy,F. Dishovsky, N. Shtarkov,R. Iliev,V. Mutlay, I. El- Tantawy, F. Inte rnarional Journal of Materials and Chemistry. 2012, 2, 116.

[6] Al-Hartomy, O .A. Al-Ghamdi, A. Dishovsky, N. Shtarkov,R. Iliev,V. Mutlay, I. El- Tantawy, F.Fullerenes, Nanotubes and Carbon Nanostructures doi:10.1080/1536383x.2012.717555.

[7] Sheen,J. Journal of Applied Physics,2007,102, 014102.

[8] Kumar, A. Sharma,S. Progress In Electromagnetics Research, 2007, 69,47.

[9] John, H.Thomas, R.M. Jacob,J. Joseph,R. Mathew, K. T. Microwave and Optical Technology Leters. 2006,48,1324.

[10] Venkatesh, M.S. Raghavan,G.S.V. Canadian Biosystems Engieneering. 2005, 47,7.15

[11] Kumar,B.S. John, H. Joseph,R. Hajian, M. Ligthart,L.P. Mathew,K.T. Journal of the European Ceramic Society. 2001, 21, 2677.

[12]   Lakshmi,K.Ph.D Thesis, Cochin University of Science and Technology, Cochin, India, 2007.

[13]   John, H. Thomas,R. M. Mathew, K. T. Joseph, R. Journal Of Applied Polymer Science, 2004, 92, 592 .

[14]   John, H. Bijukumar, S.Mathew, K.T. Joseph, R. Plastics, Rubber and Composites. 2003, 32, 306.

[15]   Hamdam,S. Hashim,D. Yusop,M. Asian Journal for Science and Technology Development. 2004, 21, 69.

[16]   Moon,K.S. Choi,H.D. Lee,A. K. Cho, K.Y. Yoon, H. G. Suh, K. S. J. Appl. Polym. Sci. 2000, 77, 1294.

[17]   Van Beek, LmIieo.K.H. Physica, 1960, 26, 66-68.

[18]   Nair, A.B. Kurian, P. Joseph, R. European Polymer Journal, 2013, 49, 247.

[19]   Bishay, I. K. EI-Messieh, A.S.L. Mansour, S.H. Materials and Design . 2011, 32, 62.

[20]   Chandran, S. Ph.D Thesis, Cochin University of Science and Technology, Cochin, India, 2008.

[21]   Stephen, C.W. Frederic, H.L. Microwaves made simple: Principles and applications, United States Bookcrafters. Chelsea, 1985

[22]   Bose. Khare, R.A. Moldenaers, P. Polymer. 2010, 51, 975.

[23]   Larijani, M.M. Khamse, E.J. Asadollahi, Z. Asadi, M. Bull. Mater. Sci. 2012, 35, 305.

[24]   Marianella, H. Maria del Mar, B. Raquel, V. Tiberio, A.E. Miguel, A.L. Composites Science and Technology. 2012, 73, 40.

[25]   Connor, M.T. Roy, S. Ezquerra,T.A, Calleja, F.J.B. Phys Rev B .1998, 57, 2286.

.....౸౸.....

Chapter 8

PREPARATION OF LAYERED SILICATES, ITS CHARACTERIZATION AND USE IN XNBR/SBR LATICES AND NBR/SBR DRY RUBBER

Part 1
Preparation of Layered Silicates and Its Characterization

Part 2
Use of prepared layered silicates, in XNBR / SBR latices and NBR/SBR dry rubber

Contents

Part 1

PREPARATION OF LAYERED SILICATES AND ITS CHARACTERIZATION

8.1 Introduction

The use of different types of nanofillers in the preparation of polymer nanocomposites (PNC) is emerging as a new class of industrially important material. Of particular interest is the recently devoleped nanocomposites containing polymer and a layered silicate. Polymer/layered silicate nanocomposite often exhibit remarkable improvement in properties when compared to virgin polymer or conventional micro and macro composites [1].

The most commonly used layered silicates are montmorillonite, hectorite and saponite [2, 3] having different chemical formula.

Montmorillonite- $M_x (Al_{4-x} Mg)Si_8O_{20} (OH)_4$

Hectorite - $M_x (Mg_{6-x} Li_x)Si_8O_{20} (OH)_4$

Saponite- $M_x Mg_6 (Si_{8-x} Al) O_{20}(OH)_4$
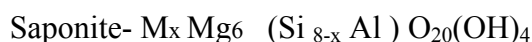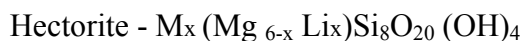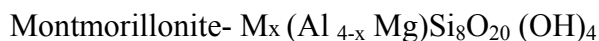
These materials are found abundanly in nature, but are contaminated with impurities. They are usually synthesised in the pure form under hydrothermal conditions [4,5]. Hydrothermal method involves conventional heating with agitation under reflux at atmospheric pressure or heating at high temperature and pressure. This is a time consuming process and requires specialized and costly equipments for the reaction to take place. Moreover the method has the disadvantage of non uniform heating. The surfaces, edges and corners of the particles are heated more than the inside of the material.

The major advantages of this method are uniform heating, reduction in heating time, reduction in capital and operating costs. Further the silicates are obtained in a substantially pure form, so that further purification process can be avoided.

The starting materials usually used in the preparation of layered silicates include silica sources like silica gel, silica powder and colloidal silica. The cheapest raw material among the silica sources is sodium silicate solution.

In this work layered silicates were prepared by microwave heating technique. Three metal chlorides of Mg, Li and Al were primarily selected

for the synthesis of layered silicates. A combination of magnesium and aluminium metal chlorides selected for synthesis of layered silicate was designated as LS1 and the layered silicate designated as LS2 was prepared by replacing aluminium chloride with lithium chloride. Further the layered silicate, LS2 was modified after synthesis, with CTAB and it was designated as MLS2.

8.2 Experimetal

8.2.1 Materials

Lithium chloride (AR), Aluminium chloride (AR), Magnesium chloride (AR) and CTAB (Hexadecyl triethyl ammonium bromide) were purchased from Alpha Chemicals, Ernakulam

Sodium silicate was purchased from Minar Chemicals, Edayar, Cochin.

All other chemicals were of commercial grade.

8.2.2 Methods Used
8.2.2.1 Preparation of layered silicate (1): LS1

To an aqueous solution of sodium silicate (60%), HNO_3 was added dropwise, followed by a well stirred mixture of $MgCl_2$ (71.1g) and $AlCl_3$ (5.66g). To the thus obtained silicicacid-magnesium-aluminium aqueous solution 2N NaOH solution was added over a period of 5 minutes with vigorous agitation until pH=10. The precipitate formed was immediately removed by filtration and after repeated washing with water, 1N NaOH was added and the pH of the slurry was made to 11.6. It was then heated in a microwave oven at a frequency 2450 MHz for 40 minutes. The resulting product was washed with water, dried at room temperature and very finely powdered [6, 7]

8.2.2.2 Preparation of layered silicate (2):LS2

69g $MgCl_2$ (99% purity) and 2.12g LiCl (99% purity) were homogeneously stirred in 500 ml water and added dropwise to a 60% sodium silicate solution. The solution was continuously stirred for 2 hrs. 0.1 M NaOH was added dropwise to the above solution to raise the pH to 9.5 [4, 8, 9]. After vigorous stirring the mixture was kept in a microwave oven with operating frequency 2450 MHz for 40 minutes. The product obtained was washed with water, filtered and dried at 250^0C for 8hrs.

8.2.2.3 Modification of Layered silicate (2)

$MgCl_2$ and LiCl were added to Na_2SiO_3 soluion as per the above discussed procedure. To this solution a mixture of 25% aqueous solution of CTAB and ethylene glycol were added under vigorous stirring at room temperature for 1hour. By adding NaOH, pH of the mixture was adjusted to 9.5. The mixture was kept in a microwave for 40 minutes. The product was washed with water, filtered and dried at 250^0C for 8 hrs. Modified layered silicate thus obtained was designated as MLS2

Microwave heating of all the samples were done on a NG microwave appliance (Model number MS 1911HE) having a frequeny 2450MHz (RS output 7000W, micro wave 1000W).

8.2.3 Characterization

The silicates were characterized by XRD (2.4.10), FTIR (2.4.11), HRTEM (2.4.12). SEM (2.4.13), EDS (2.4.14) and ICPAES (2.4.15) analysis.

8.3 Results and Discussion

8.3.1 X- ray diffraction analysis (XRD)

X-ray diffraction pattern of layered silicate (LS1) is given in Fig 8.1. The diffraction patterns were obtained at d spacing $2.51A^0$ and $1.54 A^0$ corresponding to the 2θ value 35.63^0 and 60^0 respectively.
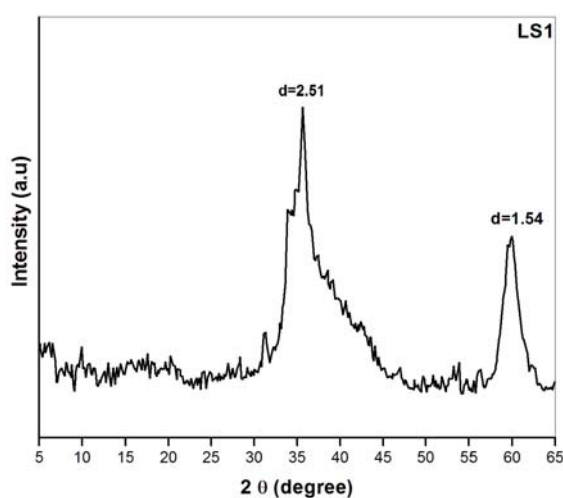
Fig.8.1. X-ray diffraction pattern of layered silicate (LS1)

Fig.8.2 shows the XRD pattern of the layered silicate (LS2).The measured diffraction peaks were at $2\theta=6.3^0$ and 35.6^0 corresponding to an interlayer spacing of $13.91 A^0$ and $2.52 A^0$ respectively. Other peaks resulted from the multiple reflections as predicted by Bragg's law. [10]. The typical pattern of a synthetic hectorite gave peaks at $14.3 A^0$ ($2\theta = 6.18^0$) and $2.56A^0$ ($2\theta=35.6^0$) for (001) and (130) reflection planes respectively [11, 12].Thus the XRD interpretations confirmed that the structure of the prepared silicate resembled closely the hectorite class silicates. The miscellaneous peaks at 27^0 and 32^0 showed some deviation from definition. Particle size as calculated using Debye Scherrer equation

was 36.1nm. As evidenced from TEM pictures both silicates had particle size in the range of nanometers. Also the interlayer spacing which is the beneficial factor on which the performance of a silicate depends; increased for LS2, compared to LS1.Though both had a d-spacing of 2.5 A^0, at $2\theta = 35.6^0$ the d-spacing was good with LS2 as indicated by the peak at $2\theta = 6.3^0$ with d=13.91A^0
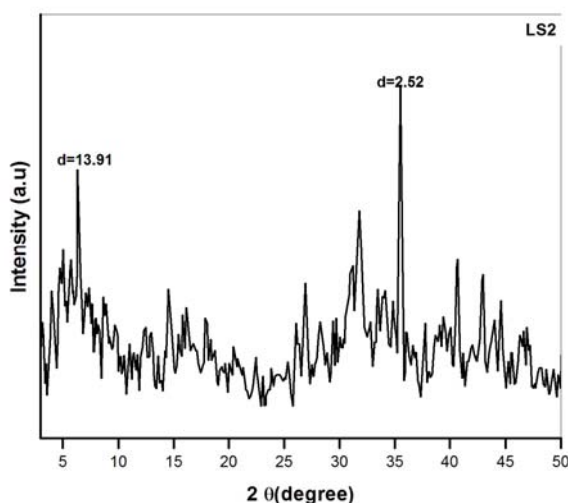
Fig.8.2. X-ray diffraction pattern of layered silicate (LS2)

Fig.8.3 shows the XRD pattern of the layered silicate LS2 modified with CTAB (MLS2).

On modification with CTAB, the peak at 6.3^0 was shifted to a lower angle 5.5^0 with an increase in the inter layer spacing (from 13.91A^0 to 16A^0). The peak at 35.6^0 broadened and shifted slightly to the smaller angle.This broadening of the peak indicated that modification caused some degree of disorder of the crystallites. Thus the intercalation of CTAB into the gallery space was confirmed by this broadening characteristic observed in XRD. Helena palkova et al. [13] exchanged sodium for HDTMA (hexa decyl tri

methyl ammonium) cations in Laponite (Laponite is a synthetic layered hydrous magnesium silicate resembling hectorite) and observed an expansion of clay layers with a shift in the basal reflection to lower 2θ value (estimated value is in the range 17-22 A^0). Lagaly and Weiss had suggested that such a value points to the bilayer or pseudo tri molecular layer arrangement of surfactant cations in the inter gallery space [13]
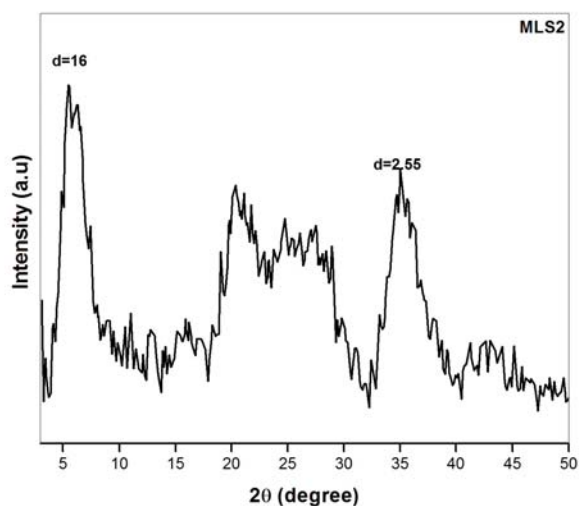
Fig. 8.3. X-ray diffraction pattern of modified layered silicate (MLS2)

8.3.2 Fourier transform infrared spectroscopy (FTIR)

IR spectrum of the layered silicate (LS1) prepared by microwave heating is given in Fig. 8.4. The peaks at $3454cm^{-1}$ represents the stretching vibration of OH groups. The peak at 1017 cm^{-1} was due to the adsorbed water molecules and the band at ~$1644cm^{-1}$ represented the stretching of Si-O-R group
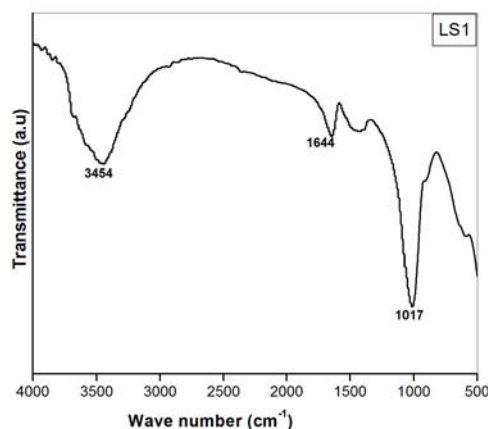
Fig.8.4. FTIR spectrum of layered silicate LS1

Fig.8.5 is the IR spectrum of layered silicate (LS2). The presence of hydroxyl groups at $3445cm^{-1}$ might be formed by the overlapping of stretching vibrations due to Si-OH and Mg-OH groups [14]. Band at $1029cm^{-1}$ represents Si-O and Si-O-Si stretching vibration and the one at $666cm^{-1}$ resulted from the weak OH bending vibration from adsorbed water. Physically adsorbed water in the form of association of molecules gave an absorption band at $1639cm^{-1,}$ [15, 16] .The IR spectrum obtained once again reminded us of a synthetic hectorite.
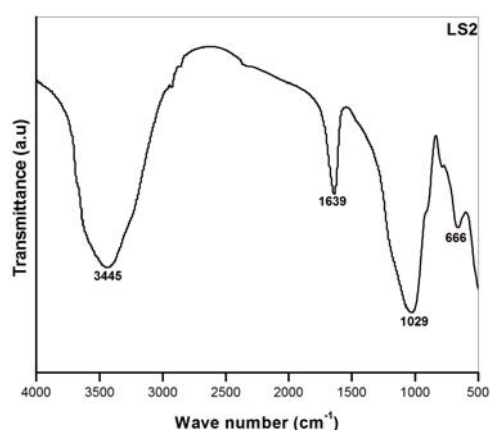
Fig.8.5. FTIRspectrum of layered silicate LS2.

Modification of clay with CTAB introduced peaks at 2920 and 2855 cm^{-1} corresponding to asymmetric and symmetric C-H stretch vibrations of the modifying group. Band at 1470 cm^{-1} was assigned to the ammonium salt [17]. The relatively lower intensity of the band centered around 3440 cm^{-1} and the deformation band at 1640cm^{-1} indicated a reduction in the adsorbed water content. These bands indicate that, modification made clay hydrophobic [16]. Fig. 8.6. is the IR spectrum of modified silicate MLS2
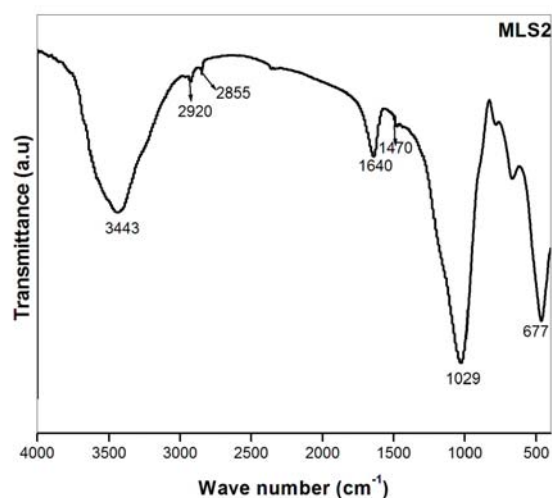
Fig.8.6. FTIR spectrum of modified layered silicate MLS

8.3.3 Scanning electron microscopy (SEM)

Fig.8.7 shows the SEM image of layered silicates LS1. A layer like structure was evident from the photograph. Fig.8.8 is the SEM image of LS2. The images clearly indicates the strong tendency of particles to form agglomerates of irregular shapes
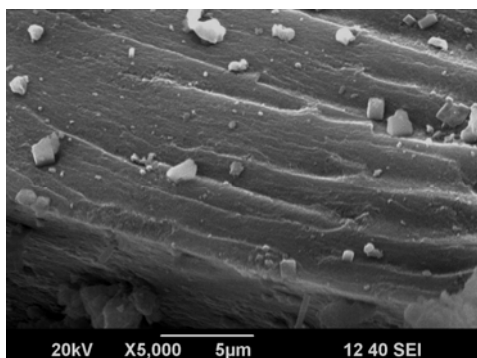
Fig.8.7. SEM images of layered silicate (LS1)
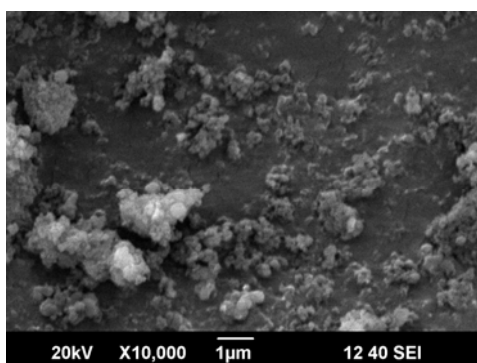
Fig.8.8. SEM image of layered silicate (LS2)

8.3.4 Energy dispersive spectrometry (EDS)

The EDS spectra assisted to some extent the confirmation of compositional purity of silicates prepared. EDS of layered silicates given in Fig 8.9 and Fig 8.10 confirmed the presence of all the elements in the silicates LS1 and LS2. EDS of layered silicate LS1 (Fig 8.9) showed the presence of Na, Mg, Al, Si and O. Fig 8.10 is the EDS of layered silicate LS2. It gave the presence of Mg, Si, O and Na. The presence of Li cannot be detected by EDS, since the EDS source was based on Beryllium.
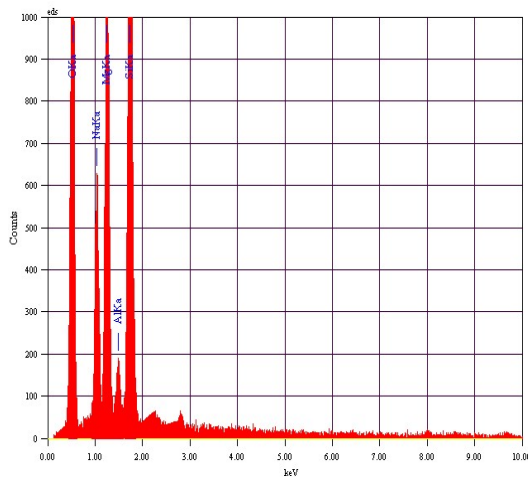
Fig.8.9. EDS of layered silicateLS1   **Fig.8.10. EDS of layered silicateLS2**
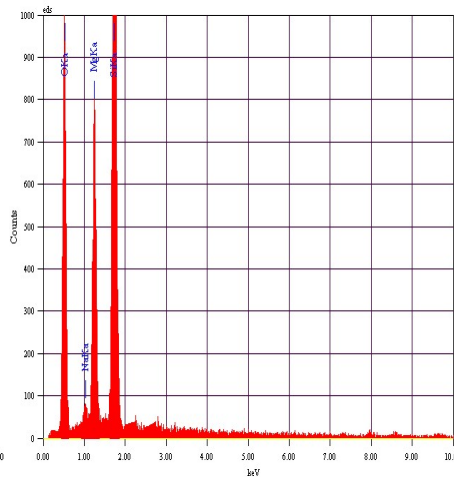
8.3.5 Inductively coupled plasma atomic emission spectrometery (ICP-AES)

Presence of Li in LS2, along with Mg and Na was futher confirmed by ICPAES analysis.Table 8.1 gives the result of ICPAES analysis conducted on LS2

Table 8.1. ICP-AES analysis of LS2

Sample name	Li6707	Mg 2852	Na 5889
LS2	17.6	0.054	1.365

8.3.6 High resolution transmission electron microscopy (HRTEM)

Fig.8.11 and Fig.8.12 shows the TEM images of the layered silicates (LS2) and modified layered silicate (MLS2). The dark areas were the aggregated silicate layers. From the lighter shades seen in the images it was clear that the particle sizes of both silicates were in the nanometer range. It appeared that modified silicate was fully enveloped by the surfactant CTAB.
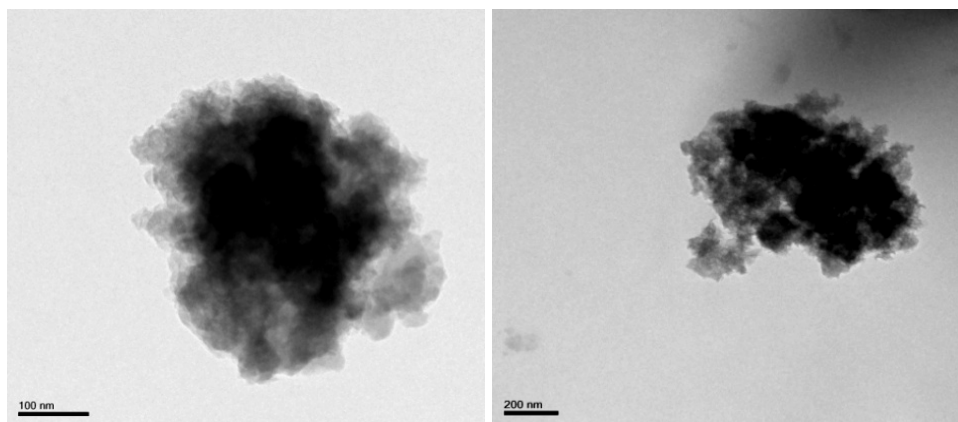
Fig. 8.11. TEM image of layered silicate (LS2)
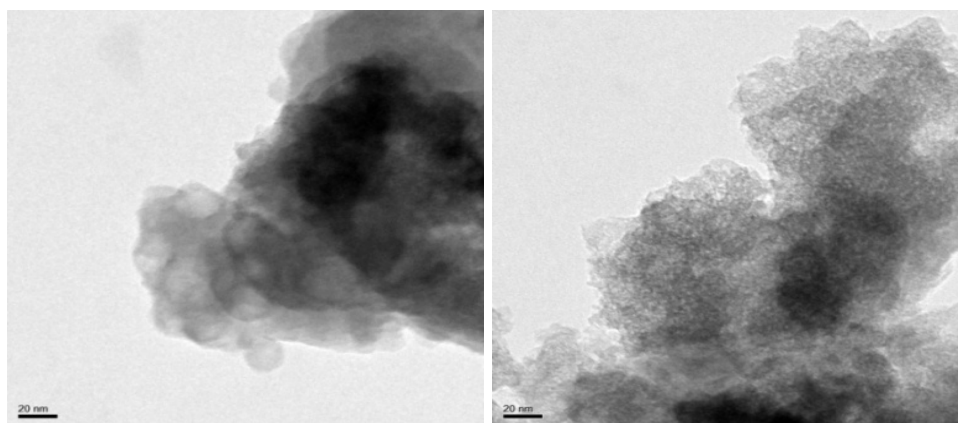
Fig. 8.12. TEM image of modified layered silicate (MLS2)

8.4 Conclusions

Microwave technique proved to be an effective method for the production of layered silicates. The presence of lithium instead of aluminium affected the overall performance of the silicates. XRD analysis of LS2 was similar to that of hectorite. Modification of LS2 by CTAB was confirmed by IR analysis. XRD analysis of MLS2 showed an increase in interlayer spacing. SEM images of LS1 showed layered structure. TEM images of LS2 and MLS2 showed agglomeration of particles.

Part 2

USE OF PREPARED LAYERED SILICATES, IN XNBR / SBR LATICES AND NBR/SBR DRY RUBBER

8.5 Introduction

Layered silicate based nanocomposites have received considerable interest recently, owing to the simple and cost effective method of enhancing polymer properties by the incorporation of fillers at the nanometer level. Naturally occuring layered silicates are usually impure and is undesirable in many industrial applications. Synthetic silicates on the other hand are considered environmentally benign, nanoparticulate material with unique electrical, mechanical and rheological properties, which are of interest to a number of industries [12.] Among the various types of layered silicates available, montmorillonite is the most widely studied [18, 19]

One of the main problems encountered in the preparation of polymer/layered silicate nanocomposite consists in providing complete delamination of the silicate layers and a uniform dispersion of the filler particles over the polymer marix. Fischer et al. [20] have suggested that complete delamination is not a necessary condition for preparing nanocomposites with improved properties.

In this part the layered silicates LS1, LS2 and MLS2 were incorporated in XNBR /SBR latices as well as NBR / SBR dry rubber, to assess their reinforcing effect. The mechanical properties of the composites were studied.

8.6 Experimental

8.6.1 Materials

XNBR-Carboxylated NBR latex, CLX 530, was purchased from Eliokem India Pvt. Ltd. Bombay. Specification is given in Table 2.1.

SBR-Encord 204 latex is styrene butadiene copolymer latex, supplied by Jubilant Organosys Limited. Gujarat Specification is given in Table 2.2.

NBR-Nitrile rubber–KNB 35L with acrylonitrile content (% by weight) 34 and Mooney viscosity ML (1+4) at 100^0C=41, supplied by Kumho Petrochemicals Co., Ltd.

SBR- Kumho SBR (SBR-1502) with bound styrene content 24 and Mooney viscosity ML (1+4) at 100^0C= 56 was supplied by Kumho Petrochemicals Co., Ltd.

8.6.2 Preparation of composites

The silicates were finely powdered and 50% dispersions were made by ball milling for 24 hrs.The compounding ingredients were added to XNBR and SBR latices as per the formulation given in Table 3.3 and Table3.4 respectively. 5phr each of the prepared silicates were added in XNBR and SBR. Composites were prepared according to the procedure given in section 3.11.1. NBR sheets were cured at 30 min (100^0C) and SBR sheets were cured for 40 min (110^0C).

Compounding of NBRand SBR (dry rubber) was done on a two roll mill (Section 3.11.4) according to the formulation given in Table 3.5 and Table 3.6. Mixing of NBR and SBR were done as per ASTM D 3187-001 and 3185-99 respectively. 5phr each of the prepared silicates were added in

NBR and SBR. The nip gap was set at 0.2 mm and temperature maintained a 50+/- 5^{0}C.The mixed compounds were matured for a period of 24 hrs and cure characteristics were determined using rubber process analyzer (RPA 2000 Alpha Technologies, 2.4.3) at a temperature of 160^{0}C.

8.6.3 Methods

The test specimens for determining the physical properties were prepared in standard moulds by compression moulding on an electrically heated press. Details of the process are given in Section 2.4.4.

Mechanical properties of the composites were studied as per ASTM D 412-2002 on a Shimadzu Model AGI Universal Testing Machine using test specimens punched out from the molded sheet using the C-type die. The measurements were carried out at a cross head speed of 500 mm/min.

8.7 Results and Discussion
8.7.1 Mechanical Properties

Fig.8.13.(A)-(D) shows the variation of tensile strength, elongation at break, modulus and tear strength of the silicates in the various elastomeric matrices. Of the three types of layered silicates prepared LS2 showed the maximum reinforcing effect. The layered silicate (LS2), must be a porous fibrous clay, like hecorite [10]. The nanosize of LS2 as determined by XRD and SEM analysis and the presence of water in the inter layer region (confirmed from IR studies) allowed the penetration of rubber molecules into the inter layer spacing. The reinforcing effect of MLS2 was less than that expected. This might be due to the agglomeration of the particles as seen in the TEM images
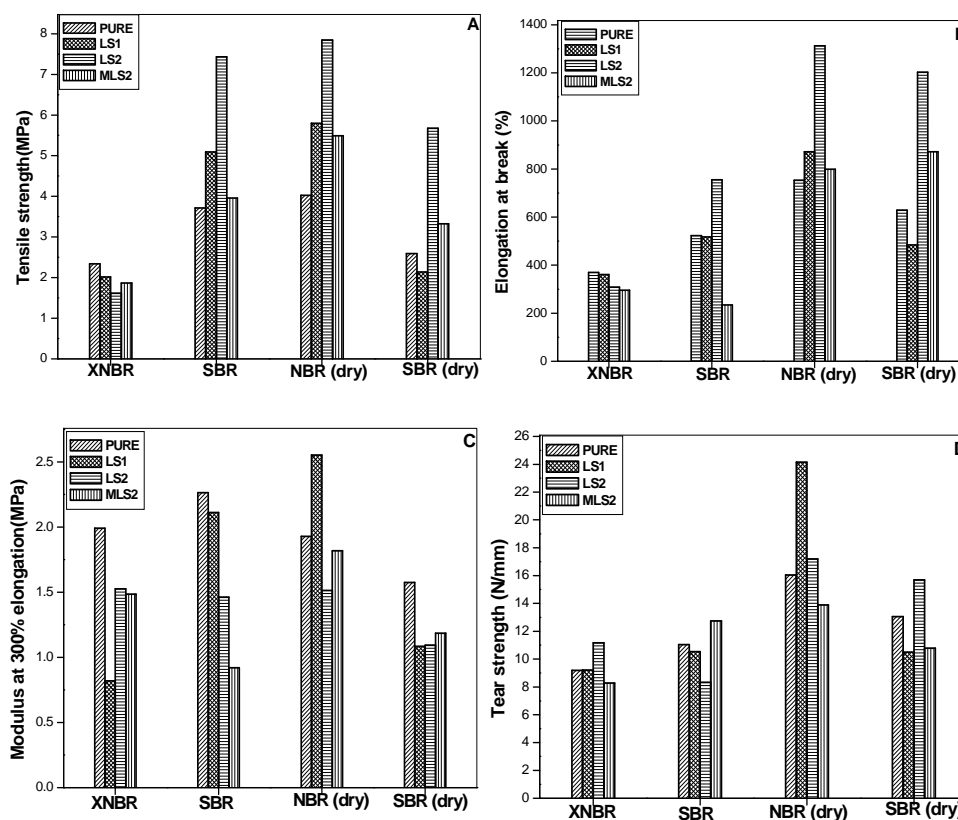
Fig. 8.13. **Variaition in (A) Tensile strength (B) Elongation at break (C) modulus at 300% elongation and (D) tear strength by the addition of LS1, LS2 and MLS2 in XNBR latex,SBR latex ,NBR (dry) and SBR (dry) rubber**

Dry rubber composites showed superior properties than the latex based composites. Tendency of the silicates to agglomerate might have contributed to the decline in properties of the latex based composites. Stephen, R. et al. have suggested that absence of mastication step in the preparation of latex composites lead to the decline in properties. Mastication helped in the formation of free radical sites in rubber molecules and these labile free radicals could interact with the surface of filler particles resulting in a bonded structure [21], enhancing the properties of the dry rubber composites.

Table8.2 gives the percentage increase in the mechanical properties of NBR produced by the incorporation of LS1and LS2. The polar nature of NBR contributed to strong rubber-filler interaction leading to stress transfer from rubber matrix to filler particles. On the basis of the increase in the tensile strength and elongation at break it could be inferred that an organic /inorganic net work structure existed throughout the composite, eventhough the layered silicates were not covalently bonded to the polymer matrix. The increase in tear strength of NBR by the addition of layered silicate LS1 might be due to the special layer structure of the silicate in the composite leading to interfacial sliding between the silicate layers and NBR matrix.

Table 8.2. Percentage increase in the mechanical properties of NBR produced by the incorporation of the layered silicate LS1and LS2.

NBR	Layered silicate(LS1)	Layered silicate(LS2)
Tensile srength	95	44
Elongation at break	74	16
Modulus	-	32
Tear strength	7	50

8.8 Conclusions

Incorporaion of LS2 enhanced the tensile strength of NBR by 100% and SBR by119%. Elongation at break increased by 74% with NBR and 91% with SBR respectively.Thus the silicate LS2 was found to be good reinforcing filler in NBR and SBR. Organomodified silicate did not give an expected result, might be due to the agglomeration of the silicate formed. The incorporation of all these fillers declined the properties of latice composites especially XNBR latex. Lack of proper dispersion of filler and the tendency for the silicates to agglomerate in latex medium might have contributed to the decline in properties of the latex composites.

References

[1]   Ray, S. S. Okamoto, M. Prog.Polym.Sci. 2003, 28, 1539.

[2]   Alexandre, M. Dubois, P. Materials Science and Engineering R: Reports. 2000, 28, 1.

[3]   Pavlidou, S. Papaspyrides, C.D. Prog. Polym. Sci. 2008, 32, 1119.

[4]   Neumann,B.S. et al. Synthetic Hectorite –Type Clay Minerals. United States Patent. 3586478. 1971.

[5]   Granquist, W.T. Synthetic smectite compositions, their preparation,and their use as thickeners in aqueous systems. United States Patent 3855147, 1974.

[6]   Torii, K. Iwasaki, T. Onodera, Y. Sythetic mixed-layer silicate and method for the preparation there of. United States Patent 5595716. 1997.

[7]   Yamada,H. Tamura,K. Yokoyama,S. Mixed –Layered Phyllosilicate and process for producing the same. Patent Application No: 2009/0233107A1. 2009.

[8]   Patel, M .D. Process for the synthesis of clay particles. US 2010/0098614 A1 Pub., 2010

[9]   Neumann, B. S. Sansom, K.G. Composition and Process for Making Stable Aqueous Sol of Synthetic silicates. United Sates Patent 3,654,176.1972.

[10]   Paul, D.R. Robeson, L.M. Polymer. 2008, 49 3187.

[11]   Carrado, K.A. Thiyagarajan, P. Elder,D. L. Clays and Clay Mineral. 1996, 44, 506.

[12]   Blanton, T. N. Majumdar, D. Melpolder,S.M. Micro structure of clay polymer composites. Copyright (C) JCPDS-International Centre for Diffraction data 2000, Advances in X-ray analysis. 42, 562

[13] Pálková, H. Madejová,J. Zimowska,M. Bielańska,E. Olejniczak,Z.et al. Microporous and Mesoporous Materials, 2010,127,228.

[14] Kuzniarska-Biernacka, I. Silva, A. R. Carvalho, A. P. Pires, J. Friere, C. Langmuir.2005, 21,10825.

[15] Vlaev, L. Damyanov, D. Mohamed, M.M. Infrared spectroscopy study of the nature and reactivity of hydrate coverage on the surface of γ-Al2O3. http://dx.doi.org/10.1016/0166- 6622(89)80257-4

[16] Angela de Mello Ferreira Guimaraes; Virgina Sampaio Teixeira Ciminelli; Wander Luiz Vasconcelos. Mat.Res.2007,10. http://dx.doi.org/10.1590/ S1516-14392007000100009.

[17] Jacob, A. Ph.D Thesis Cochin University of Sciencs and Technology. 2008

[18] Kim, J. Oh,T. Lee, D .Polym Int.2003, 52,1058.

[19] Kader, M. A. Kim, K. Lee. Y.S. Nah, C. J. Mater Sci. 2006 41, 7341.

[20] Fisher, H.R. Gielgens, L.H. Kostger, T.P. ActaPolym. 1999, 50, 122.

[21] Stephen,R. Alex,R. Cherian,T. Varghese,S. Joseph,K. Thomas ,S. Journal of Applied Polymer Science. 2006, 101, 2355.

.....ജ്ഞ.....

STUDIES ON THE MECHANICAL PROPERTIES OF NANOCLAY FILLED XNBR LATEX GLOVES

9.1 Introduction

Nanofillers, at low concentration, improve the mechanical and physical properties, electrical conductivity and flame retardancy of the rubber vulcanizates. Improvement in air impermeability and good filler dispersion gives more surface finish and fewer rejections in large scale production of thin walled goods like thin films, gloves, balloons, medical items etc. [1]. Thin walled polymer products are usually produced by dipping process. Latex dipping processes are classified as simple or straight dipping, coagulant dipping, heat-sensitized dipping and electro deposition. Natural rubber latex is the major raw material for dipped goods. Synthetic latices are used for some special properties. Due to the protein allergy of natural rubber latex, examination gloves are manufactured in XNBR latex. Fillers are usually used in gloves to reduce the manufacturing cost. Fillers upto 15% are usually tolerable, anything above that can become detrimental to the performance and quality of the glove.

In the foregoing sections of this work, reinforcing effect of nanokaolin and vinylsilane grafted nanokaolin in XNBR and SBR latices were studied by casting latex films in glass trays. In this Chapter nano clay

reinforced nitrile gloves were made by dipping process, in the normal production line. The work was done at Primus, a well reputed glove manufacturing company in Cochin. Mechanical properties of the latex gloves were studied and the samples were characterized by SEM analysis.

Brief description of glove manufacturing process.

The manufacturing process is a multi stage process and includes mainly latex compounding, maturation, dipping, testing and packing

Latex compounding:

Concentrated latex as per BIS standards, was mixed with all the ingredients including accelerators, antioxidants etc. The compounded latex was then maintained undisturbed for maturation and then sent to the dipping tank through pipes.

Dipping Process

The process of coagulant dipping took place in a continuous chain dipping line. The pre heated, cleaned, hand shaped formers were first dipped in a coagulant tank containing dry coagulant based on calcium nitrate tetrahydrate and then in the latex compound. Dwell time was adjusted to get the required thickness for the product. Then it was send to the drying chamber were the temperature was maintained at 85^0C. When half dried, bead rolling was done, while the article was still on the former. Thus a serrated edge was formed on the open end of the glove which helped in better fitting. Then the latex coated former was immersed in a water bath to wash out all water leachable materials. This is called 'wet gel leaching' or 'pre vulcanization leaching'. Vulcanization temperature was in the range 120^0C. The vulcanized sample was then given a dry leaching,

also called 'post vulcanizaion leaching'. The gloves were then dusted with corn starch to prevent adhesion and to faciliate the sripping of gloves from the former. Then the gloves were stripped from the former manually and turned inside out. After stripping they were fed into tumble driers where complete drying took place. Then they were given lot numbers for identification, sent for inspection and later to the packaging unit. A flow chart of the dipping process is given in Fig. 9.1.
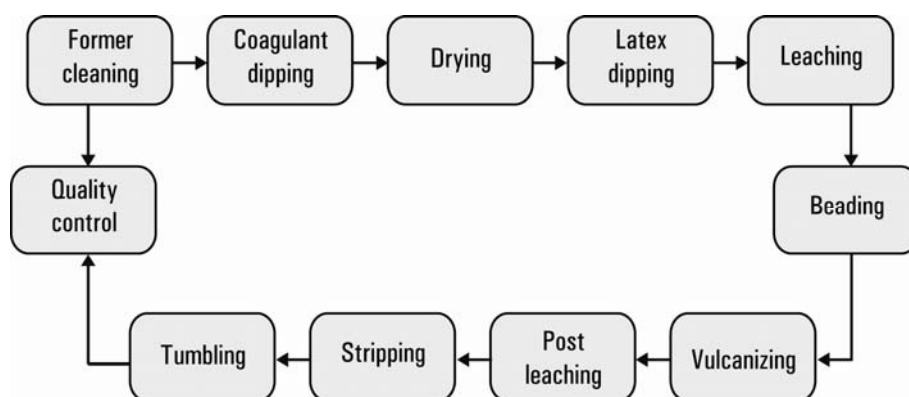
Fig. 9.1. Flow chart of the dipping process

9.2 Experimental

Materials

XNBR latex is Synthomer 6311. Specifications are given in Table 9.1

Total solids	45%
pH	8.5
Viscosity @ 23°C, Brookfield LVT	75 mPa.s
Particle size	130nm
Specific Gravity @ 25 ^{0} C	1.00
Surface Tension LVT	31mN/m
Acrylonitrile Content Level	Medium

Nanokaolin is Nanocaliber100, supplied by English Indian Clays Ltd., Veli, Thiruvananthapuram. Vinylsilane grafted nano kaolin is Nanocalibre - 100V, supplied by English Indian Clays Ltd., Veli, Thiruvananthapuram. Nanokaolin is referred as 'C' and vinylsilane grafted nanokaolin as 'V'

Method

The compounding ingredients S, ZDC, ZnO and TiO_2 along with nanokaolin /vinylsilane grafted nanokaolin were added to XNBR latex by continuous stirring. The fillers were added in varying concentration, ranging from 1-10 phr. This compounded latex was used in the production of gloves. Further studies were done using ball billed and sonicated samples of clay. Mechanical properties of the gloves were determined using Shimadzu Model AGI Universal Testing Machine and SEM analysis of the tear fractured surface of gloves were determined using JEOL Model JSM - 6390LV.

9.3   Results and Discussion
9.3.1 Mechanical properties

Effect of nanoclays ('C' and 'V') on the mechanical properties of XNBR latex was studied. Variations of tensile strength/elongation at break and modulus/tear strength of XNBR-C and XNBR-V nanocomposites are given in Fig 9.2.and 9.3 respectively. Tensile strength increased upto 20% for XNBR-C nanocomposite (3phr) and after that decreased. XNBR-V nanocomposite gave 32% increase in tensile strength at 5phr. Tensile strength is a measure of the force required to stretch a glove sample until it breaks. So higher the tensile strength, greater will be the strength of the glove.
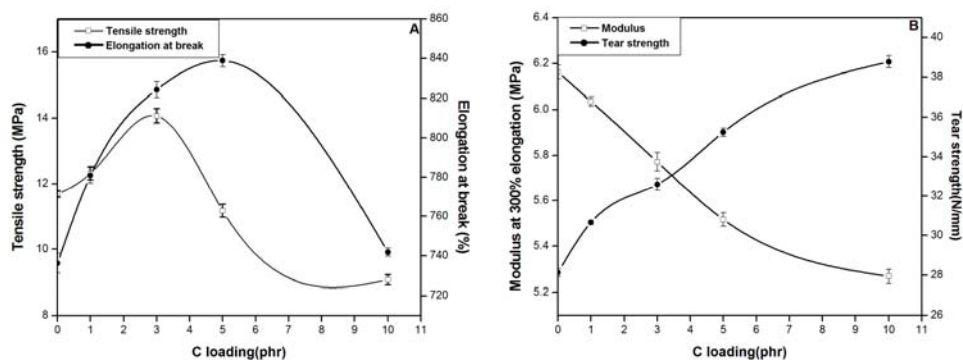
Fig.9.2. Variation of (A) Tensile strength /Elongation at break and (B) Modulus /tear strength of nirile glove containing varying concentration of 'C'.
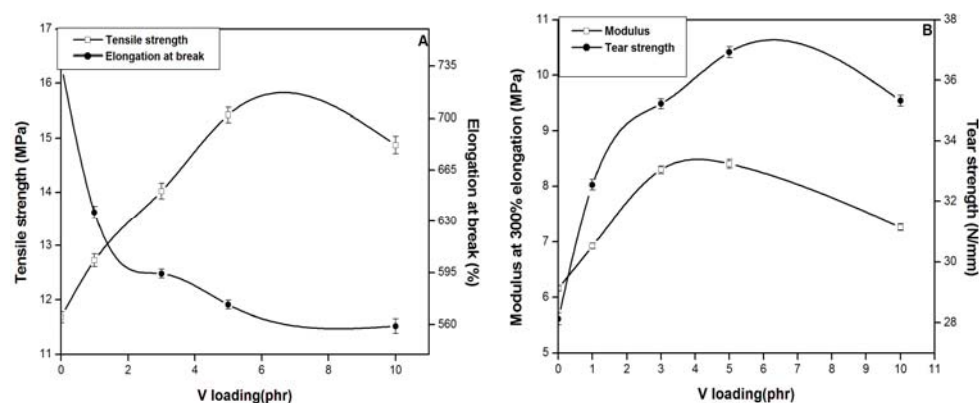
Fig.9.3. Variation of (A) Tensile strength/Elongation at break and (B) Modulus /tearstrength of nirile glove containing varying concentration of 'V'.

Elongation at break gives a measure of how long the glove stretches, as percentage of origial sample length, before it breaks. Elongation at break increased for XNBR-C nanocomposite and showed 14% increase at 5phr concentration. Modulus is a measure of the comfort. Lower modulus reflects softer, more comfortable gloves. Comfort depends on proper fit and to some extent on the glove thickness. Here incorporation of nanokaolin increased the tensile strength, elongation at break and reduced the modulus at 300% elongation. Tear strength of both the samples, were greater than that of the nitrile gloves without filler.

Fine particle size and uniform distribution of filler in XNBR latex contributed to the reinforcement. Increase in properties indicated improved product performance.

Further sudies were conducted using sonicated and ball milled nanokaolin. Fig.9.4. gives a comparison of mechanical properties of gloves made with sonicated nanokaolin and ball milled nanokaolin. From the figure it was observed that the sonicated nanokaolin gave better increase in mechanical properties when compared to the ball milled sample.
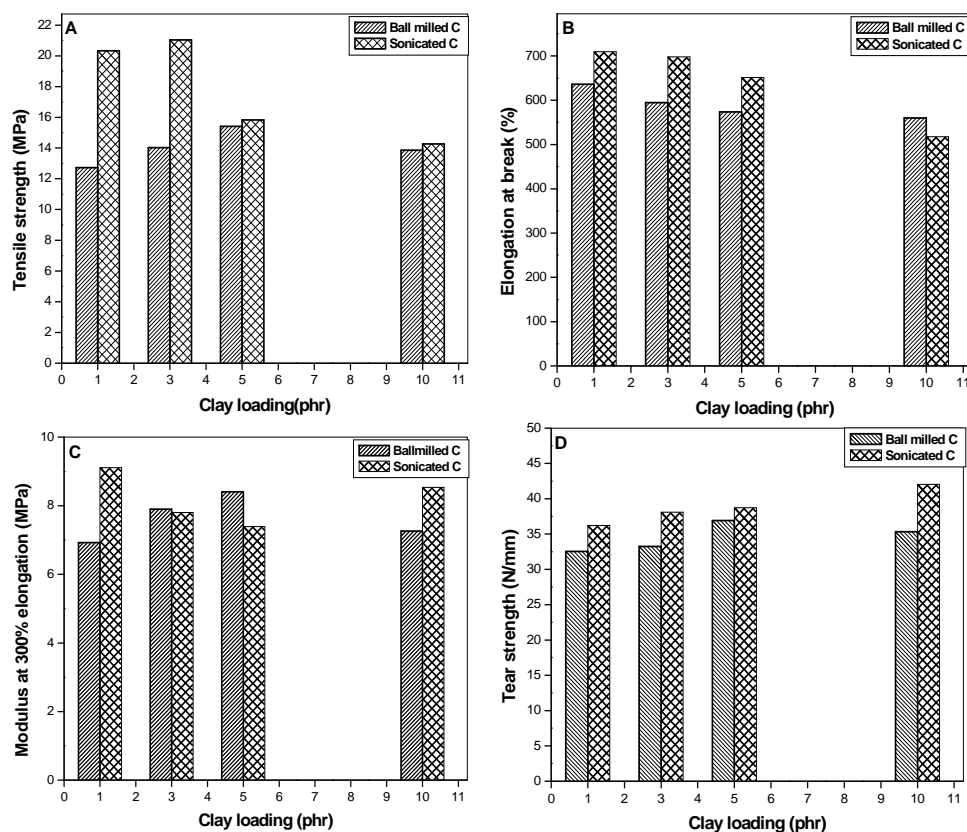
Fig.9.4. **Variation of A. Tensile strength, B. Elongation at break, C.Modulus and D.Tear strength of ball milled and sonicated clay filled nitrile gloves against clay concentration.**

Table9.2. gives the percentage increase in properties of sonicated clay filled gloves compared to the ball milled samples. The property improvement for samples with sonicated clay might be attributed to the reduction in the size of the aggregates by sonication.

Table 9.2. Percentage increase in mechanical properties of sonicated nanokaolin filled nitrile gloves in comparison to the ball milled samples.

Clay loading(phr)	Tensile strength (MPa)	Elongation at break (%)	Modulus at 300% elongation (MPa)	Tear strength(N/mm)
1	74	12	31	11
3	65	17	-	15
5	3	14	-	15
10	2	-	18	9

9.3.2 Scanning electron microscopy (SEM)

Fig.9.5. A and B. shows the SEM micrographs of the tear fractured surfaces of gloves containing sonicated and ball milled nanokaolin (3phr) respectively. Sample containing sonicated clay showed multiple crazing along different directions. More roughness on the tear fractured surface showed greater resistance to crack propogation. This proved better stress transfer from the rubber matrix to the nanoclay and greater adhesion of the sonicated clay to the rubber matrix [2] .The reduction in the size of the clay particles on sonication increased the surface area of the particles and might have helped in better interaction. But in the ball milled samples the clay flakes were more conspicuous and were sparecely distributed. They seem to be thrown out of the matrix. This might be the reason for the

reduction in the property of the ball milled nanokaolin when compared to the sonicated sample.
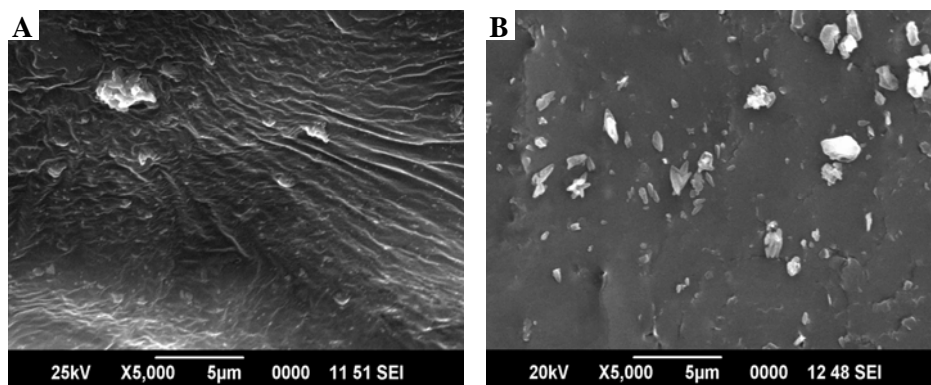
Fig.9.5. SEM images of tear fractured surface of gloves containing   A. 3phr sonicated nanokaolin and B. 3phr ball milled nanokaolin

9.4   Conclusions

Mechanical properties of nitrile gloves could be improved by the addition of nanokaolin and vinylsilane grafted nanokaolin. Gloves made with sonicated clay showed greater increase in mechanical properties compared to those made with ball milled clay.

References

[1]   Thomas,S. Stephen, R. Editors. Rubber Nanocomposites.Preparation, Properties and Application. (Chapter 9). John Wiley&Sons .1985.231

[2]   Tavakoli, M. Katbab, A. A. Nazockdast, H. Journal of Applied Polymer Science.2011,123,1853.

.....ౚౙ.....

Chapter **10**

SUMMARY AND CONCLUSIONS

Elastomers are generally reinforced with particulate fillers like carbon black, silica etc. The full reinforcing effect from these fillers is not observed due to their tendency for agglomeration. Thus the use of nanofillers in polymers to obtain beneficial mechanical and physical properties is becoming crucial. Use of organic and inorganic fillers has become ubiquitous in polymer systems. Parallel to the development of polymer layered silicate composites, there has been rapid growth in the use of other nanofillers like carbon nanotubes, nanosilica etc. in polymers.

First part of the study is the characterization of fillers used, optimisation of the cure time of latex compounds, and the methods used for the preparation of rubber nanocomposites.

XRD analysis of nanokaolin gave characteristic peaks at $2\theta = 12^0, 20^0$ and 25^0 corresponding to the interlayer spacing 7.05, 4.41 and $3.55A^0$ respectively. Grafting of vinylsilane did not increase the interlayer spacing of modified nanokaolin. Diffraction peak of MWCNT was obtained at 25.7^0 and the XRD curve of graphene showed its similarity to graphite in interlayer spacing. From XRD analysis, particle sizes of nanokaolin, vinyl silane grafted nanokaolin, MWCNT and graphene were found as 16, 21, 40 and 15 nm respectively.

Peaks of same intensity were observed for nanokaolin and vinyl grafted nanokaolin (FTIR spectrum). It showed that grafting of vinylsilane groups had taken place only to some of the OH groups in nanokaolin. Eventhough virgin MWCNT showed no characteristic peak, acid treated MWCNT showed the presence of hydroxyl and carbonyl groups on MWCNT surface. Presence of these groups assisted in the formation of MWCNT dispersions.

SEM analysis of these fillers showed agglomeration. Grafting seemed to reduce agglomeration in nanokaolin. MWCNT showed less purity and the samples remained as bundles. But after purification they remained as entangled lose curly thread like entities. SEM images of graphene had a wavy or wrinkled appearace and consisted of thin stacks anchored with each other at the edge of the platelets.

Cure time of the latex compounds were optimised by measuring the variation in mechanical properties of XNBR and SBR vulcanizates. Cure time of XNBR based nanocomposites were taken as 30min at 100^0C and that of SBR nanocomposites as 40min at 110^0C. Both ball milled and sonicated clay were used in the preparation of latex composites and it was found that sonicated clay gave better properties than the ball milled sample. Examination of the dispersions of ball milled and sonicated clays showed that ball milled sample had a higher tendency to settle down than the sonicated clay. Cure time of dry rubber composites were determined by using RPA 2000.

Different methods were used for the preparation of filler dispersions and the methods adopted for the preparation of latex based and dry rubber

composites were included in Chapter 3, Part 3. MWCNT dispersions were made in SDBS and graphene dispersions in Vulcastab VL .

Chapters 4 and 5 gave a detailed study of the effect of these fillers on the mechanical and thermal properties of XNBR and SBR latices and the different methods for the characterization of the nanocomposites.

Enhancement in the mechanical properties of XNBR and SBR latices by the incorporation of clay showed that nanokaolin and vinylsilane grafted nanokaolin could be used as good reinforcing fillers in XNBR and SBR. Eventhough there was enhancement in mechanical properties; nano effect was not observed in the composites. Tendency of the clay particles to agglomerate and the non swellable nature of nanokaolin contributed to the decrease in nano effect.

Compared to SBR latex based composites, XNBR composites showed good improvement in properties. This might be due to the higher interaction of the polar CN and COOH groups in XNBR with the OH groups of clay. Non polar nature of SBR and the presence of bulky styrene group reduced the compatability of clay in SBR latex. In latex nanokaolin composite there was greater interaction between the hydrophilic clay and the aqueous latex medium. But in modified nanokaolin, the introduction of organic moiety in nanokaolin made it hydrophobic and reduced the interaction with the latex. So for XNBR and SBR latex composites mechanical properties were lower for vinyl modified clay composite. Tensile strength, elongation at break, modulus at 300% elongation and tear strength, showed a similar trend in XNBR and SBR. The only variation was found for elongation at break of SBR–vinyl grafted nanocomposite. The

value declined with clay loading showing poor adhesion of the modified clay to SBR matrix.

Incorporation of MWCNT and graphene at low concentration ranging from 0-1.5 phr increased the mechanical properties of XNBR and SBR latex based nanocomposites. Compared to XNBR/graphene, XNBR/MWCNT nanocomposites gave good enhancement in properties due to the polar interaction of XNBR with the OH and CO groups introduced in MWCNT during purification. SBR/graphene and SBR/MWCNT nanocomposites showed similar change in mechanical properties.

Grafting of bulky, vinyl groups increased the tortuosity of path leading to greater reduction in swelling for XNBR/vinyl grafted nanokaolin composites. But for SBR latex nanocomposites, the lower compatability of organophilic vinyl grafted nanokaolin increased swelling.

Greater reduction in swelling for XNBR/MWCNT might be due to the greater adhesion between XNBR and MWCNT. A discrepancy was shown in the swelling studies of graphene nanocomposites in SBR. Here filled nanocomposites gave higher swelling than the unfilled sample.This might be due to the weak interface created by vulcastab which allowed greater penetration of solvent.

Thermal studies conducted on the nanocomposites showed an increase in thermal stability of XNBR and SBR containing clays. Usually the incoporation of inorganic components into organic materials improve thermal stability.

Thermal studies of all MWCNT and graphene nanocomposites showed an increase in the thermal stability, except for SBR graphene

nanocomposite where the decrease in thermal stability was an evidence of composite heterogenity and lack of filler protective action.

DSC studies showed T_g of XNBR clay nanocomposites remained a constant while there was small increase in T_g for SBR clay nanocomposites. Incorporation of MWCNT and graphene showed marginal increase in T_g for XNBR nanocomposites while T_g decreased for SBR nanocomposites. Literature reports that chain mobility depends on polymer cohesive forces and in non polar elastomers the cohesive forces are low and therefore no change in Tg was expected for SBR/MWCNTand SBR /Graphene nanocomposites.

XRD analysis confirmed the intercalation/exfoliation of polymer chains. The increase in interlayer spacing was small for the vinyl modified clay composites showing the reduced compatability of hydrophobic organophilic clay with the hydrophilic polymer.

FTIR studies showed the interaction of OH groups in nanokaolin with the polar CN and COOH group in XNBR, and styrene units in SBR. In vinyl grafted nanokaolin composites the interaction was between the vinyl groups of clay and butadiene double bonds in XNBR and SBR. In MWCNT and graphene nanocomposites there were interaction of the pi electrons with the butadiene double bond of XNBR and SBR. Morphological studies of the composites showed good dispersion of fillers in the latices. In the SEM image of SBR-vinyl grafted nanocomposite the clay particles projected out from the matrix showing the low compatability of organophilic clay with non polar SBR.

Clay showed a cure retarding effect in NBR. The adsorption of curatives on the surface OH groups of clay decreased the effective

concentration of curatives leading to an increase in cure time and scorch time. Presence of thermally conducting MWCNT and graphene accelerated the curing reaction and decreased the scorch time and cure time. Thermal stability increased slightly for clay nanocomposites but for low concentration of MWCNT and graphene the increase was negligible. DSC analysis showed that there was no change in T_g for all the nanocomposites. XRD of clay nanocomposite showed a slight increase in interlayer space, showing intercalation of polymer chain into the clay gallery. FTIR of NBR/clay nanocomposites showed interaction of OH groups and vinyl group in clay with the butadiene double bond of polymer chain, while FTIR of NBR/MWCNT/graphene nanocomposites showed the interaction of pi bonds with the butadiene double bond of polymer chain.

One of the most referred applications of MWCNTand graphene is in electronic devices. Although rubbers were known to be thermal and electrical insulators, incorporation of conductive fillers would produce composite materials with some electrical properties. Potential applications of rubber nanocomposites might vary from industrial application to electrical shielding and electrical heating. The dielectric properties of XNBR/MWCNT/graphene, SBR/MWCNT/graphene, NBR(dry)/MWCNT/graphene and SBR (dry)/ MWCNT/graphene were evaluated by Cavity Perturbation technique in the microwave frequency (Sband 2-4GHz). Dielectric permittivity, dielectric loss and AC conductivity of all the nanocomposites increased with increase in frequency and in most cases with increase in concentration. Maximum values were obtained for XNBR based nanocomposites. Presence of conducting fillers reduced the penetration of electromagnetic waves into the material and skin depth decreased with

increase in frequency. Maximum value of conductivity and minimum value of skin depth were obtained at a frquency of 4 GHz. The nonpolar SBR latex showed some discrepancy in their behaviour.

In Chapter 8, the preparation of layered silicates by microwave technique using Na_2SiO_3 as the precursor was reported. The prepared silicates were designated as LS1 (containing Mg and Li), LS2 (containing Mg and Al) and MLS2 (LS2 modified with CTAB). XRD analysis of LS2 gave the typical pattern of a synthetic hectorite and it showed greater interlayer spacing than LS1. Particle size of LS2 was 36.1nm as determined by Debye Scherrer equation. SEM image of LS1 showed a layer sructure and LS2 showed small particles in an agglomerated state. Modification of LS2 by CTAB was confirmed by IR analysis. TEM images of LS2 and MLS2 also showed agglomeration of particles

The effect of these fillers on the mechanical properties of XNBR/SBR latices, and NBR/SBR dry rubber, revealed, that the best performance was obtained with LS2 in dry rubber. Incorporation of LS2 enhanced the tensile strength of NBR by 100% and SBR by 119% and elongation at break increased by 74% and 91% for NBR and SBR respectively. Organomodified silicate did not give expected result, might be due to the agglomeration of the silicate particles. The incorporation of these fillers declined the properties of latice composites especially in XNBR. Lack of a proper dispersion of filler and the tendency for the silicates to agglomerate in latex medium might have contributed to the decline in properties of the latex composites.

Although nanofillers have a myriad of applications, the use of nanokaolin and vinyl grafted nanokaolin in the production of gloves is part

of the research work. Increase in tensile strength, elongation at break, modulus at 300% elongation and tear strength of the gloves showed that nanokaolin and vinyl grafted naokaolin could be used as a good reinforcing filler in glove production.

Usually compatabilizers are introduced in nanocomposites to reduce the surface tension between the immiscible polymers and fillers as well as to improve the surface adhesion of filler. The simple latex stage mixing adopted for the preparation of nanocomposites and the effectiveness of ultra sonication for preparing filler dispersion contributed to optimum filler dispersion and improvement in the properties of the nanocomposite.

Exceptional physical properties associated with CNTs, their highly graphitic structure and very high aspect ratio holds good for applications requiring unique electrical and mechanical properties. As a robust, yet flexible material, graphene also provides infinite applications. Cost effective composites could be fabricated using MWCNT and graphene as they alter properties at very low concentration.

.....ജ്ഞ.....

Response to Comments

1. Equation 6 on page No: 51 may need correction .Do you need molar mass of solvent? If needed why not maolar mass of polymer?

   - Solvent uptake $Qt \% = \dfrac{\text{Mass of solvent sorbed /Molar mass of solvent}}{\text{Mass of polymer}} \times 100$

   Solvent uptake Qt % is expressed as the molar % uptake of solvent per gram of polymer.

References

[1] Stephen, R. Joseph, K. Oommen, Z. Thomas, S. Composites Science and Technology.2007, 67, 1187.

[2] Obasi, H.C. Ogbobe, O. Igwe, I.O. International Journal of Polymer Science.2009, 2009, http://dx.doi.org/10.1155/2009/140682

2. Page 28, line 3. Mentions, endless industrial applications. Please mention a few.
   - Industrial applications of polymer nanocomposites: In packaging industry, automobiles, aerospace, as coatings, fuel tanks, stoppers for medical containers, sensors etc.

3. Several spelling mistakes may be corrected. Page 6 and some other places.
   - Corrections are made.

4. Page 45. Do the plate thickness / particle size match with BET surface area? Or what would be the theoretical surface area?
   - Plate thickness, particle size and BET surface area of nanokaolin and vinylsilane grafted nanokaolin given in Table 2.3. is taken from specification given in literature.

   As per literature there is a difference between the theoretical surface area and surface area obtained by BET equation. BET surface area depends on many factors like particle size, plate thickness, porosity, density etc. So the particle size and plate thickness are not entirely responsible for the given BET surface area.

Abbreviations and Symbols

ACN	Acrylo Nitrile
AC	Alternating Current
ASTM	American Society of Testing of Materials
AFM	Atomic Force Microscopy
BET	Brunauer–Emmett–Teller
BIS	Bureau of Indian Standards
CBS	N-cyclohexyl 2- Benzothiazol Sulphenamide
CCVD	Catalytic Chemical Vapour Deposition
CNTs	Carbon nanotubes
c P	Centi Poise
cpm	cycles per minute
CRI	Cure rate index
CTAB	Hexa decyl Triethyl Ammonium Bromide
DC	Direct Current
DMRT	Dynamic Mechanical Rheological Tester
DTAB	Dodecyl Trimethyl Ammonium Bromide
DTG	Differential thermogravimetry
EB	Elongation at break
EDS	Electron Dispersive Spectrometer
EG	Ethylene glycol
EMI	Electro magnetic Interference
EPDM	Ethylene Propylene Diene Rubber
FGS	Functionalised graphene sheets
FTIR	Fourier Transform Infra Red
FWHM	Full Width at Half Maximum
G*	Complex modulus
G"	Loss modulus
G'	Storage modulus
HAO	Hydroxyl aluminium oxalate
HS	1,2 dihydro2,2,4 tri methyl quinoline
HR-TEM	High Resolution Transmission Electron Microscope
ICPAES	Inductively Coupled Plasma Atomic Emission Spectrometer
LDH	Layered double hydroxide

LDPE	Low density poly ethylene
Ma	Milli ampere
MEK	Methyl ethyl ketone
M_H	Maximum Torque
M_L	Miimum Torque
min	Minutes
MMT	Montmorillonite
MPa	Mega Pascal
MWCNT	Multiwalled carbon nanotube
nm	Nanometer
N/mm	Newton/millimeter
NR	Natural rubber
OHP	Olive Husk Powder
phr	Parts per hundred parts of rubber
RPA	Rubber Process Analyzer
rpm	rotations per minute
SBR	Styrene butadiene rubber
SDBS	Sodium dodecyl bezene sulphonate
SDS	Sodium dodecyl sulphonate
SEM	Scanning electron microscope
TEM	Transmission electron microscope
TMTD	Tetra methyl thiuram disulphide
T_g	Glass transition temperature
TGA	Thermogravimetric analysis
THF	Tetrahydrofuran
TMTD	Tetramethyl thiuram disulphide
UTM	Universal testing machine
XNBR	Carboxylated nitrile butadiene rubber
XRD	X-ray diffraction
ZDC	Zinc diethyldithiocarbamate
A	Area
A^0	Angstrom
σ	Conductivity
dΩ	Complex frequecy shift
^0C	Degree Celsius

d	Interlayer space
D	Particle size
E	Electric field
f	Frequecy
α_f	Filler specific constant/Absorption coefficient
β	Full width at half maximum
2θ	Diffraction angle
n	Order of reflection
Hz	Hertz
ε"	Imaginary part of complex permittivity
T_5	Induction time
l	Length
T_{90}	Optimum cure time
%	Percentage
Q	Quality factor
ε'	Real part of complex permittivity
T_{10}	Scorch time
δ_f	Skin depth
Qt	Solvent uptake
V	Voltage
Vc	Volume of the cavity
Vs	Volume of the sample
Ws	Weight of swollen sample
Wi	Weight of sample before swelling
λ	Wave length of light

List of Publications

Publications in International Journals

[1] Nanokaolin clay as reinforcing filler in nitrile rubber. Preetha Nair K, Dr. Rani Joseph.
International Journal of Scientific & Engineering Research . ISSN 2229-5518. 2012, 3(3), 1-10

[2] Latex stage blending of multiwalled carbon nanotube in carboxylated acrylonitrile butadiene rubber: Mechanical and electrical properties . K. Preetha Nair, Paulbert Thomas, Rani Joseph Materials and Design.2012, 41, 23–30.

[3] Kaolin/Carboxylated acrylonitrile butadiene rubber nanocomposites Preetha Nair K, Ajalesh B Nair and Rani Joseph—Applied Clay Science Elsevier (communicated)

Publications in Conferences

[4] Reinforcing effect of kaolin clay on SBR latex. Preetha Nair K, Dr. Rani Joseph. International Conference on Advancements in Polymeric Materials- APM. Chennai 2011

[5] Effect of nanokaolin clay on the mechanical properties of nitrile rubber. Preetha Nair K and Dr. Rani Joseph. Challenges in Nano science and Technology-CNT. Ernakulam 2011

[6] Effect of vinyl silane grafted nanokaolin clay on the mechanical properties of styrene butadiene rubber. Preetha Nair K and Dr. Rani Joseph. Emerging trends in nanotechnology, Kottayam 2011

.....ಬಂ.....

Curriculum Vitae

Preetha Nair K
'Abhiramam'
Vishal Nagar
Ayyanthole
Thrissur

Ph : 9526021023
E mail: preethaknair@gmail.com

Date of Birth	:	28-04-1962
Qualification	:	M.Sc. Chemistry
Teaching Experience	:	27 years
Official Address	:	Associate Professor Department of Chemistry Sree Kerala Varma College Thrissur, Kerala
Research Publications	:	2 Published, 1 communicated

.....ॐ.....